THE UNIVERSITY OF MICHIGAN

INDUSTRY PROGRAM OF THE COLLEGE OF ENGINEERING

PREDICTION OF GAS STORAGE RESERVOIR BEHAVIOR

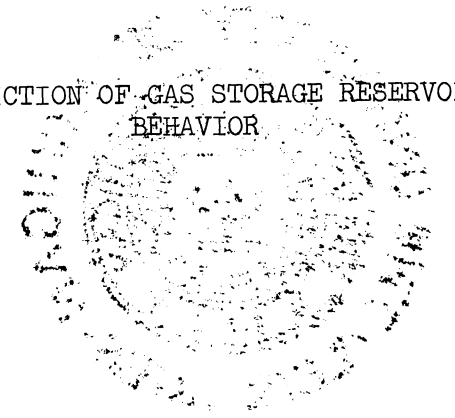

Keith H. Coats

April, 1959

IP-367

ersm
UMR1275

Doctoral Committee:

Assistant Professor M. Rasin Tek, Chairman
Associate Professor John W. Carr, III
Professor Donald L. Katz
Professor Robert R. White
Professor Chia-Shun Yih

ACKNOWLEDGMENTS

The author wishes to express his appreciation to the following individuals and organizations for their contributions to the research which was the basis of this dissertation:

Assistant Professor M. Rasin Tek, chairman of the doctoral committee, for his sincere interest, useful advice, and most generous donation of time to discussion of the problems which arose in the course of the research.

Professor Donald L. Katz for his invaluable suggestions concerning important and appropriate problems for consideration in the research, for his aid in securing gas field data, and for his advice regarding the application of the research results in practical reservoir problems.

The other members of the doctoral committee for their advice and encouragement.

Assistant Professor Bernard A. Galler of the University of Michigan Math Department and Mrs. Shirley Callahan of General Motors for their aid in securing use of the General Motors' IBM 704 computer and in the processing of calculations on that machine.

The Michigan Consolidated Gas Company and the Natural Gas Storage Company of Illinois for their donations of gas storage reservoir data. The National Science Foundation and MGA fellowship programs for their financial assistance.

Glen C. Smith for valuable assistance in many phases of the calculations.

The University of Michigan Industry Program personnel for their efficient and accurate rendering of the dissertation in its final form.

TABLE OF CONTENTS

TABLE OF CONTENTS (CONT'D)

TABLE OF CONTENTS (CONT'D)

LIST OF TABLES

LIST OF TABLES (CONT'D)

LIST OF FIGURES

LIST OF FIGURES (CONT'D)

LIST OF FIGURES (CONT'D)

NOMENCLATURE

A_j	pressure drop, at time $t = j\Delta t$, due to initial non-uniform pressure distribution, psia
c	sum of aquifer water and formation compressibilities, vol/vol-psia
d	distance between centers of oil or gas fields, feet
DEV	average fractional deviation between predicted and observed pressures
f	foci of ellipse in x-y plane are at $x = \pm f$, $y=0$
$f_{m,n}$	$\frac{(\Delta u)^2}{\Delta t_{DE}} [\cosh^2 (m\Delta u) - \cos^2 (n\Delta v)]$
h	thickness of aquifer formation, or of flow model, feet
J_0, J_1	Bessel functions of the first kind and of 0^{th} and 1^{st} order, respectively
k	permeability, millidarcies or ft-lb_m/sec^2-psi
k/μ	mobility, ft^2/sec-psi
k_R	ratio of permeability in vertical direction to permeability in horizontal direction, dimensionless
K_1	$\pi h \phi c r_b^2$, ft^3/psi
K_2	$k/\mu\phi c r_b^2$, 1/seconds
K_2'	$(k/\mu\phi c)(\pi\phi/600RT)^{2/3}$
K_3	$\mu/2\pi hk\Delta t$, psi/ft^3
K	constant determined from gas compressibility data, $z = 1+KP$, 1/psia
n_t	gas in reservoir at time t, lb. moles
n_i or n_j	n_t at $t = i\Delta t$ or $j\Delta t$, respectively
N	total number of time increments included in period for which performance of reservoir is to be calculated
P	pressure, psia

NOMENCLATURE (CONT'D)

P_t	pressure at time t, psia
P_j or P_i	P_t at $t = j\Delta t$ or $i\Delta t$, respectively
$\overline{P}$	pressure drop, $P_o - P$, psia
P_o	initial pressure, psia
$\underline{P}_{t_D}$	dimensionless pressure drop quantity, tabulated vs t_D in the literature[1][2], at dimensionless time t_D
$P_{a_{i\Delta t}}$	observed gas bubble pressure at time $t = i\Delta t$, psia
Q_t	cumulative influx of water into circular gas field at time t, ft^3
Q_{t_E}	cumulative influx of water into elliptic gas field at time t, ft^3
$\overline{Q}_{t_D}$	dimensionless production quantity for radial flow case, tabulated in the literature[1][2] vs t_D, at dimensionless time t_D
$\overline{Q}_{t_{DE}}$	dimensionless production quantity for elliptic flow case
q	rate of water movement, ft^3/second
q'_i	average rate of water influx into gas bubble during time increment from $(i-1)\Delta t$ to $i\Delta t$, ft^3/second
$\Delta q'_i$	$q'_{i+1} - q'_i$
r	radius, feet
r_b	gas reservoir radius, feet
r_e	aquifer exterior radius, feet
r_D	dimensionless radius $= r/r_b$
r_{D_e}	dimensionless exterior radius, r_e/r_b
R	gas constant, 10.73 psia-ft^3/lb.mole-°R, or (in elliptic flow section) $(\frac{\Delta u}{\Delta v})^2$
S_j	slope of predicted pressure-time curve, psi/sec.
T	temperature, °R

t	time, seconds
t_D	dimensionless time = $(k/\mu\varphi c r_b^2)t = K_2 t$
t_{DE}	dimensionless time for elliptic flow, $(k/\mu\varphi c f^2)t$
τ_D	dimensionless time for moving boundary method, $\tau_D = (k/\mu\varphi c)\int_0^t \frac{dt}{r_b^2(t)}$
Δt	time increment, seconds
Δt_D	dimensionless time increment
u,v,w	elliptic cylinder coordinates (u,v dimensionless, w in feet)
u_b	value of u on interior ellipse (gas field), dimensionless
u_e	value of u on exterior ellipse (aquifer exterior boundary), dimensionless
$U_o(\lambda_n r_D)$	$Y_o(\lambda_n r_{D_e})\ J_o(\lambda_n r_D) - J_o(\lambda_n r_{D_e})\ Y_o(\lambda_n r_D)$
$\vec{V}$	velocity vector, ft/sec.
V_x, V_y, V_z	velocity vector components in x, y, and z directions, ft/sec.
V_t	gas field pore volume at time t, ft^3
V_i or V_j	V_t at $t = i\Delta t$, or $j\Delta t$, respectively, ft^3
$V_{a_{i\Delta t}}$	actual gas field pore volume at time $t = i\Delta t$, ft^3
V_o	initial pore volume, ft^3
ΔV_i	$2V_i - V_{i-1} - V_{i+1}$
x, y, z	cartesian coordinates, ft
Y_0, Y_1	Bessel functions of second kind, and of 0^{th} and 1^{st} order, respectively
z	cartesian coordinate, ft, or gas compressibility factor, dimensionless
ρ	density, lbs mass/ft^3
φ	porosity, fraction

I. INTRODUCTION

Natural gas producing reservoirs often occur in close proximity to large water bearing formations called aquifers. When a gas reservoir is adjacent to an aquifer, the gas-water interface becomes mobile under the effect of pressure gradients resulting from gas production. The rate of water movement is a function of the aquifer formation and fluid properties and the pressure-time relationship at this interface. The purpose of the research herein described is the development and application of general methods of predicting the performance (e.g., volume-time and pressure-time relationships) of gas storage reservoirs situated adjacent to aquifers.

The storage of natural gas in underground reservoirs is referred to as either "depleted-field storage" or "aquifer storage". The former term designates gas storage operations in oil or gas fields which are converted to gas storage use after a period of natural depletion. The latter term denotes storage operations in a gas reservoir which was initiated and grown by injection of gas into an aquifer formation originally containing no gas. Gas is usually injected into a storage reservior during the summer months when consumer demand is low and is withdrawn during the winter months when the demand is high. This cyclic gas injection and withdrawal results in cyclic periods of high and low gas reservoir pressure, which in turn result in aquifer water movement out of and into the gas field. This water movement results in a variable gas reservoir volume and it becomes very desirable to be able to predict the gas field volume-time and pressure-time behavior for a postulated gas injection-production schedule.

The prediction of the effect of aquifer water movement on the volume and pressure variations of an adjacent gas storage reservoir can provide information valuable in the study of several reservoir engineering problems. The prediction of the pressure behavior is important in relation to the deliverability potential of the gas storage reservoir. For a fixed number of wells, the deliverability (or gas production rate) of a storage field is a function of the field pressure. A prediction of the pressure during the high demand winter months thus allows calculation of the deliverability potential for this period and comparison of this potential with the estimated demand. The economics of gas storage operations are directly influenced by the influx of aquifer water since a shrinking storage reservoir results in increasing pressures for the same quantity of gas in storage. Material balance and reserve or recovery calculations obviously require knowledge of the reservoir volume-time relationship. Various other reservoir engineering calculations such as interpretation of well interference data, evaluation of physical characteristics of porous media, water coning and pressure maintenance studies are typical problems where variations of reservoir volume due to edge or bottom-water encroachment becomes important.

The available literature relating to the performance of gas storage reservoirs situated adjacent to aquifers consists primarily of the papers by Van Everdingen and Hurst[1] and Chatas[2] which present dimensionless, tabular solutions to the partial differential equation governing unsteady state liquid flow through porous media. A paper by Katz, Tek, and Coats[3] describes the results of the initial stages of

the research reported in this thesis. Certain design aspects of the development of gas storage fields are treated by Katz, Vary, and Elenbaas.[4]

The general purpose of this research has been the development of fundamental theory relating to the performance of gas storage field-aquifer systems and evaluation of this theory by application to actual gas field studies. Several sub-problems were studied in order to attain this general purpose. Thus the specific objectives of this research were the development and application of the following theory and methods of calculation to actual gas storage reservoirs:

1) A general digital computer method to predict the pressure and volume behavior of a gas storage reservoir from any postulated gas injection-production schedule. This method should employ the assumptions of a constant gas bubble radius, a constant initial pressure throughout the aquifer, circular geometry of the gas field, negligible vertical flow effects, and absence of interfering, neighboring gas fields.

2) A method of determination of the "effective" values of reservoir physical constants, i.e., those values which result in best agreement between the calculated and actual field performance during the initial period for which data is available from the field.

3) A gas field-aquifer system model which will account for the effect of vertical pressure penetration into the aquifer.

4) A numerical method of solving the unsteady state diffusion equation in elliptic coordinates. Use of this method should make possible certain conclusions concerning the effect of the gas storage reservoir areal geometry on the reservoir performance.

5) A digital computer method of treating pressure interference between two or more gas storage reservoirs situated on a common aquifer.

6) A predictive method which will take into account any non-uniform initial pressure distribution throughout the aquifer.

7) A method of predicting the performance of an "aquifer storage" reservoir which accounts for the fact that the gas bubble radius is not constant but increases continuously from 0 feet as the gas bubble is grown.

II. LITERATURE REVIEW

With the exception of Reference 3, the literature contains no material relating directly to methods of predicting the performance of gas storage reservoirs situated on aquifers. Schilthuis in a 1935 article[5] described calculations, relating to unsteady state aquifer motion, which reproduced quite well the observed pressure performance of the East Texas oil field. As mentioned above, Van Everdingen and Hurst[1] and Chatas[2] presented tables of dimensionless quantities obtained by solution of the partial differential equation governing isothermal, radial, unsteady state liquid flow through porous media (hereafter designated as the diffusivity equation). Their solution was obtained for the two cases of "constant terminal rate" (the rate of water movement across the gas-water interface is assumed constant) and "constant terminal pressure" (the pressure at the gas-water interface is assumed constant). They also indicated a method of combining the superposition principle with their solution to treat a variable rate or variable pressure case. Neither Reference 1 nor Reference 2 includes any application of the developed theory to an actual field study.

Mortada[6] presented a method of treating interference between two or more oil fields situated on a common aquifer which requires use of the solutions presented by Van Everdingen and Hurst or Chatas. He presented illustrative calculations but did not apply the method to an actual field study. Warren[7] presented a numerical solution to the partial differential equation governing linear, unsteady state gas flow through a porous medium. He considered his results applicable to the

case of a linear gas storage reservoir bounded on all sides by an impermeable rock. Books by Muskat[8], Carslaw and Jaeger[9], Churchill[10], and Sneddon[11] contain analytical solutions to the diffusivity equation for a variety of boundary conditions which cover a wide spectrum of practicality in reservoir engineering problems.

Muskat and Woods[12] showed that, in the case of oil reservoirs, a minimum deviation between the actual or known oil in place and the values calculated from the material balance equation (including an aquifer water influx term) is a poor basis for choice of reservoir physical constants. Their conclusion was that if core, logging, or other data were available to fix the values of all but one of the reservoir parameters, then agreement between observed and calculated field behavior serves as a good basis for selection of this one remaining unknown parameter.

III. FUNDAMENTALS OF GAS STORAGE RESERVOIR PERFORMANCE

The performance of gas storage fields can be investigated by either a mathematical or an empirical approach. The latter approach, which would consist of determining empirical relationships between the performance and certain operational variables of a specific storage reservoir, might prove useful in predicting the performance of the reservoir concerned but would very likely fail to be useful in other cases. The mathematical approach, however, has the potential of providing a general method capable of predicting the performance of many reservoirs. From an academic as well as a practical point of view, the achievement of a general predictive method is certainly preferable to the development of a myriad of empirical correlations, each of which is developed for and applicable to only one field. However, mathematical analysis of storage reservoir behavior requires certain assumptions concerning the reservoir geometry and formation and fluid properties. The generality of the methods obtained by the mathematical approach will therefore be restricted insofar as the storage fields fail to conform to these assumptions. The present section (III) of this thesis treats the storage reservoirs which satisfy, in general, the flow model chosen and assumptions given in Section III-A below. Realizing that the methods developed from these assumptions will not be applicable to all cases, the author has treated in Section IV certain important storage cases which definitely fail to satisfy certain of the assumptions in Section III-A.

A. Mathematical Relations

Calculation of aquifer water movement and its effect on the performance of a gas storage reservoir requires adoption of a flow model, certain assumptions concerning aquifer formation and fluid properties, and formulation and solution of the appropriate differential equation. Three typical gas field-aquifer system configurations are shown in Figure 1 where r_b denotes the gas bubble radius, h the aquifer thickness, and r_e the aquifer exterior radius. The aquifer exterior boundary is assumed at infinity if the boundary is so far removed from the gas bubble that its effect on the gas bubble performance will be negligible for any practical length of time. The flow model adopted for the present study approximates the systems shown in Figures 1a and 1b and is shown in Figure 2; a model which will approximate the system of Figure 1c will be discussed in Section III-D-1 of this thesis. Figure 2a shows the assumed position of the gas bubble relative to the aquifer and Figure 2b indicates the radial nature of the aquifer water flow.

The following assumptions are made concerning the flow model and aquifer formation and fluid properties:

1) The rate of water influx into the gas bubble is equal to the rate of water movement in the negative r direction across the vertical dotted line boundary at $r = r_b$ indicated in Figure 2a.
2) Uniform aquifer formation permeability and porosity.
3) Negligible capillary, gravity, and vertical flow effects.
4) Single phase, isothermal, radial, unsteady state aquifer water flow.

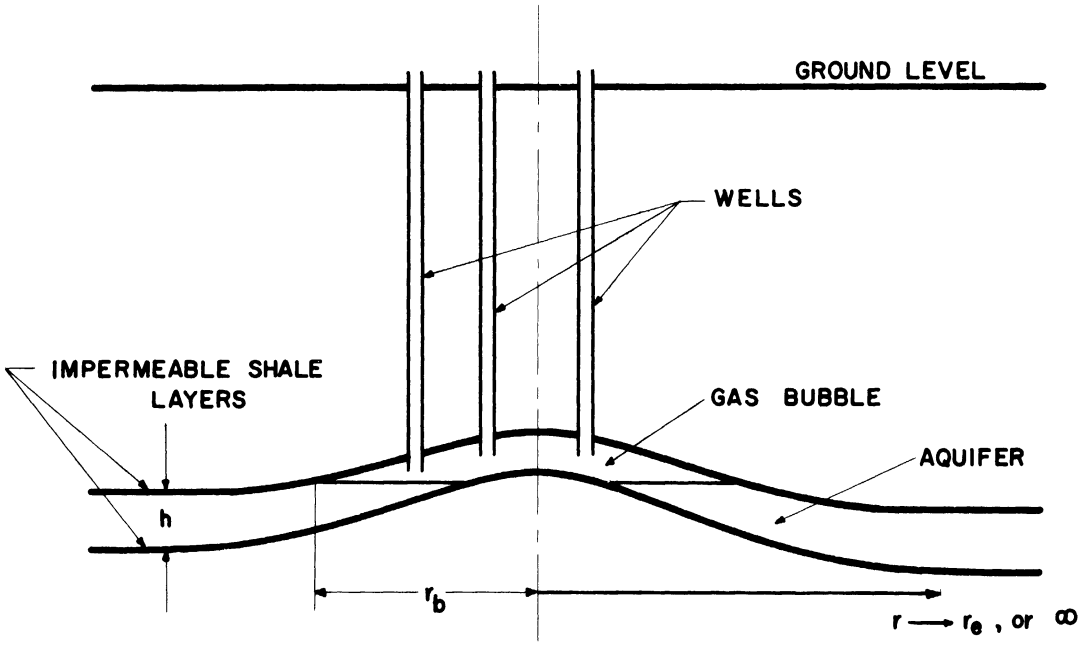

1a. Edge-Water Drive System.

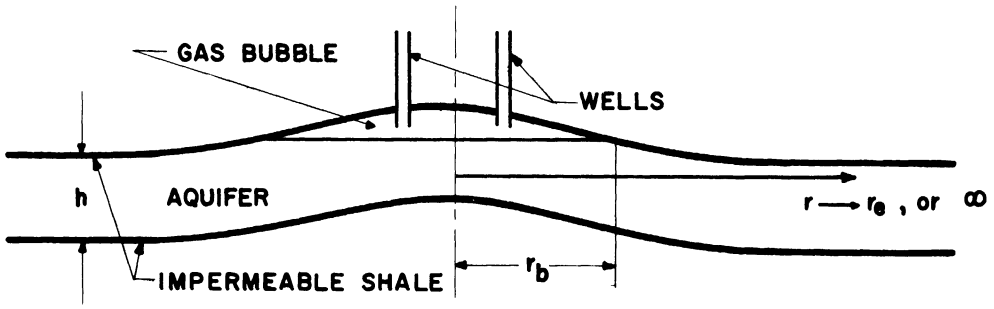

1b. Bottom-Water Drive System with Definite Aquifer Thickness.

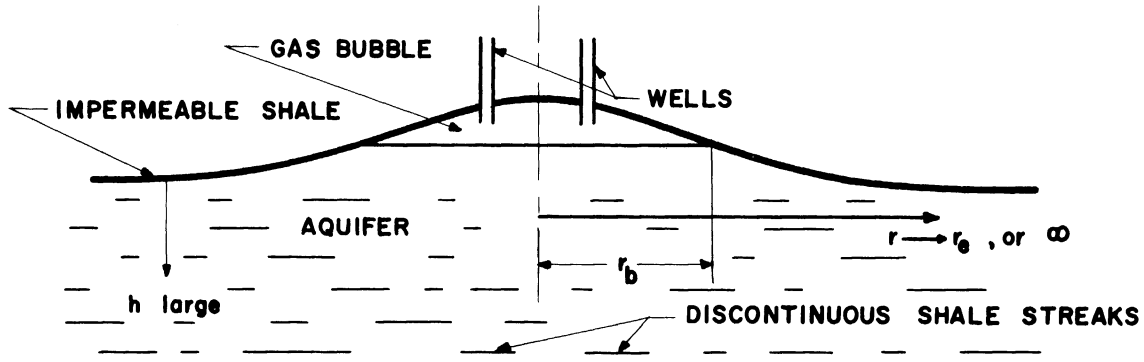

1c. Bottom-Water Drive System with Large Aquifer Thickness.

Figure 1. Typical Gas Storage Reservoir-Aquifer System Configurations.

Figure 1

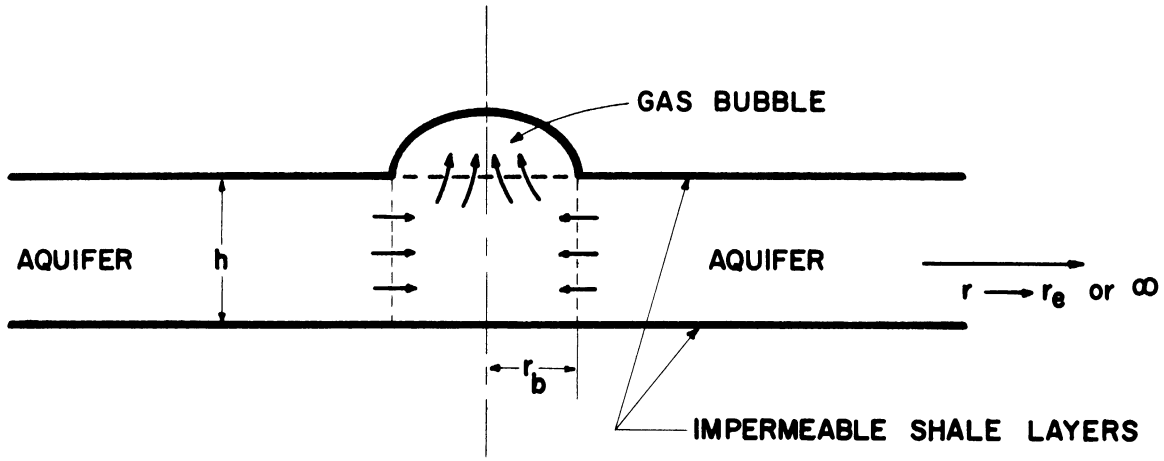

2a

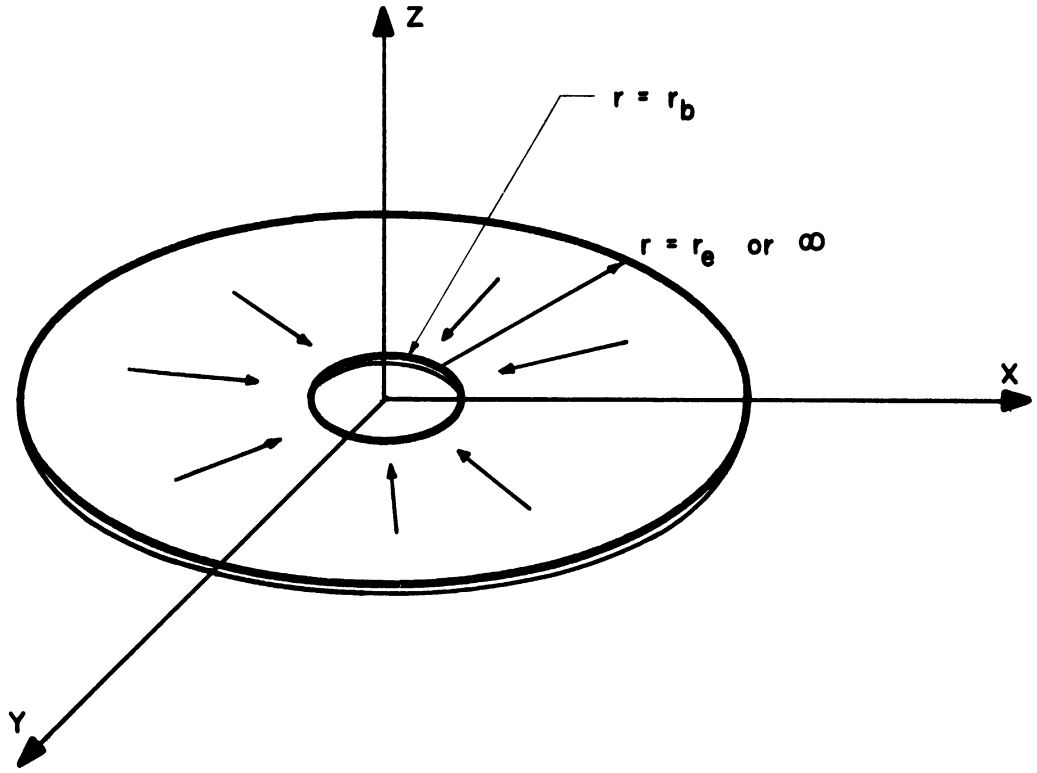

2b

Figure 2. Representation of Assumed Flow Model.

5) r_b, the gas bubble radius, is constant with respect to time.

6) Absence of pressure interference effects from neighboring gas (or oil) fields.

The above assumptions and described flow model now allow formulation of the partial differential equation governing the aquifer water flow. This equation is derived by combination of the continuity Equation (III-1), which is obtained by a mass balance about an infinitesimal volume element, with Darcy's flow Equation (III-2) and an equation of state (III-3) for the aquifer liquid.[1,8]

$$\frac{\partial}{\partial x}(\rho V_x) + \frac{\partial}{\partial y}(\rho V_y) + \frac{\partial}{\partial z}(\rho V_z) = div(\rho \vec{V}) = -\phi \frac{\partial \rho}{\partial t} \qquad \text{(III-1)}$$

$$\vec{V} = -\frac{k}{\mu}\left(\frac{\partial P}{\partial x}\vec{i} + \frac{\partial P}{\partial y}\vec{j} + \frac{\partial P}{\partial z}\vec{k}\right) = -\frac{k}{\mu} grad\, P \qquad \text{(III-2)}$$

$$\rho = \rho_o e^{c(P-P_b)} \cong \rho_o[1 + c(P-P_b)] \text{ for } c \text{ small} \qquad \text{(III-3)}$$

c = sum of aquifer water and formation compressibilities, vol/vol-psi

e = base of natural logarithm

k/μ = aquifer formation mobility, ft^2/sec-psi

P = aquifer water pressure, psi

P_b = arbitrary pressure base, psi

t = time, seconds

$\vec{V}$ = velocity vector, ft/sec

x,y,z = cartesian coordinates, ft

ρ = aquifer water density, lbs/ft^3

ρ_o = aquifer water density at $P = P_b$, lbs/ft^3

φ = aquifer formation porosity, dimensionless

Substitution of $\vec{V}$ and ρ from (III-2) and (III-3) into (III-1) yields Equation (III-4) below.

$$\nabla^2 P = \frac{\partial^2 P}{\partial x^2} + \frac{\partial^2 P}{\partial y^2} + \frac{\partial^2 P}{\partial z^2} = \frac{\mu \phi c}{k} \frac{\partial P}{\partial t} \qquad \text{(III-4)}$$

Equation (III-4) can now be expressed in cylindrical coordinates[8] with the terms $\partial^2 P/\partial \theta^2$ (θ = polar angle) and $\partial^2 P/\partial z^2$ set equal to 0 since the flow is assumed radial with negligible vertical flow effects. Thus (III-4) can be rewritten as in (III-5)

$$\frac{\partial^2 \bar{P}}{\partial r_D^2} + \frac{1}{r_D} \frac{\partial \bar{P}}{\partial r_D} = \frac{\partial \bar{P}}{\partial t_D} \qquad \text{(III-5)}$$

where $\bar{P} = P_o - P$, pressure drop (P_o is the initial aquifer pressure, psia), $r_D = r/r_b$, dimensionless radius, and $t_D = kt/\mu\varphi c r_b^2$, dimensionless time.

Equation (III-5) has been solved by Van Everdingen and Hurst[1] for the two cases of 'constant terminal pressure' and 'constant terminal rate'; the details of the solution are therefore omitted here. The initial and boundary conditions employed in the constant pressure and constant rate cases are given below in Equations (III-6) and (III-7), respectively.

$$\left.\begin{aligned} &\bar{P}(r_D, 0) = 0 \\ &\bar{P}(1, t_D) = 1 \\ &\lim_{r_D \to \infty} \bar{P}(r_D, t_D) = 0 \end{aligned}\right\} \qquad \text{(III-6)}$$

$$\left.\begin{aligned} &\bar{P}(r_D, 0) = 0 \\ &\left(\frac{\partial \bar{P}}{\partial r_D}\right)_{1, t_D} = 1 \\ &\lim_{r_D \to \infty} \bar{P}(r_D, t_D) = 0 \end{aligned}\right\} \qquad \text{(III-7)}$$

Thus the initial condition in both cases specifies a uniform pressure, P_o, throughout the aquifer at time 0. The constant pressure case specifies that the pressure is decreased by unity at the inner aquifer boundary at time 0 and held constant at that value for all time. The constant rate case assumes a constant rate of aquifer water movement across the inner aquifer boundary, $r = r_b$. The condition $\lim_{r_D \to \infty} \bar{P}(r_D, t_D) = 0$ is equivalent to the assumption of an infinite aquifer. Van Everdingen and Hurst also presented some solutions for the case of limited aquifers. Their solution for the constant pressure case consists of dimensionless production quantities, $\bar{Q}_{t_D}$, given in tables as a function of dimensionless time t_D. The $\bar{Q}_{t_D}$ values are employed in the calculation of Q_t as shown in Equation (III-8),

$$Q_t = 2\pi h \phi c r_b^2 \Delta P \bar{Q}_{t_D} \qquad \text{(III-8)}$$

where Q_t = cumulative influx of aquifer water into the gas bubble at time t, ft^3

$\Delta P = P_o - (P)_{r_D=1}; (P)_{r_D=1}$ = constant pressure maintained at edge of gas bubble ($r=r_b$), psia

$\bar{Q}_{t_D}$ = dimensionless production quantity at dimensionless time $t_D = \frac{kt}{\mu\phi c r_b^2}$

The constant rate solution consists of dimensionless pressure drop quantities related to the pressure drop in the gas bubble as shown in Equation (III-9).

$$\bar{P}_t = P_o - P_t = \frac{\mu}{2\pi hk} q P_{t_D} \qquad \text{(III-9)}$$

P_t = pressure at gas bubble boundary $r = r_b$, at time t, psia

P_o = initial aquifer pressure, psia

q = specified constant rate of water influx into the gas bubble, ft^3/sec

P_{t_D} = dimensionless pressure drop quantity, tabulated as a function of dimensionless time by Van Everdingen and Hurst[1], at dimensionless time $t_D = \frac{kt}{\mu\phi c r_b^2}$

The restrictions of constant gas bubble pressure or constant water influx rate severely limit the usefulness of Equations (III-8) and (III-9). Duhamel's super-position principle[10], however, can be employed in conjunction with these two equations to yield solutions valid for a varying gas bubble pressure or water influx rate.[1] This principle states that if $\bar{P}_1(r_D, t_D)$ is the solution to Equation (III-5) for a condition $\bar{P}_{(1,t_D)} = 1$, if $y_1(r_D, s)$ is the La Place transform of $\bar{P}_1(r_D, t_D)$, if $\bar{P}_2(r_D, t_D)$ is the solution to Equation (III-5) for a condition $\bar{P}_{(1,t_D)} = f(t_D)$,

and if $y_2(r_D,s)$ is the La Place transform of $\bar{P}_2(r_D,t_D)$, then

$$y_2(r_D,s) = s\bar{f}(s)\,y_1(r_D,s) \qquad \text{(III-10)}$$

where $\bar{f}(s)$ is the La Place transform of $f(t_D)$. $\bar{Q}_{t_D}$, the dimensionless function tabulated by Van Everdingen and Hurst, is defined as[1]

$$\bar{Q}_{t_D} = -\int_0^{t_D} \left(\frac{\partial \bar{P}_1(r_D,\tau)}{\partial r_D}\right)_{r_D=1} d\tau$$

Employing the property of the La Place transformation

$$\mathcal{L}\left[\int_0^t f(\tau)d\tau\right] = \frac{1}{s}\,\mathcal{L}[f(t)]$$

[where $\mathcal{L}[f(t)] = \int_0^\infty e^{-st}f(t)dt$ = the La Place transform of $f(t)$]

one finds that $\bar{Q}(s)$, the La Place transform of $\bar{Q}_{t_D}$, is

$$\bar{Q}(s) = -\frac{1}{s}\left[\frac{\partial}{\partial r_D}\,y_1(r_D,s)\right]_{r_D=1}$$

Now, $(\bar{Q}_{t_D})_2$, the dimensionless production quantity corresponding to the 'time varying reservoir pressure' solution, $\bar{P}_2(r_D,t_D)$, is

$$(\bar{Q}_{t_D})_2 = -\int_0^{t_D}\left[\frac{\partial \bar{P}_2(r_D,\tau)}{\partial r_D}\right]_{r_D=1} d\tau$$

and the transform of $(\bar{Q}_{t_D})_2$ is

$$(\bar{Q}(s))_2 = -\frac{1}{s}\left[\frac{\partial}{\partial r_D}\,y_2(r_D,s)\right]_{r_D=1}$$

Since $y_2(r_D,s) = s\bar{f}(s)\,y_1(r_D,s)$ (Equation III-10),

$$(\bar{Q}(s))_2 = -\bar{f}(s)\left[\frac{\partial}{\partial r_D}\,y_1(r_D,s)\right]_{r_D=1}$$

$$= -\bar{f}(s)\,s\left[\frac{1}{s}\frac{\partial}{\partial r_D}\,y_1(r_D,s)\right]_{r_D=1}$$

$$= \mathcal{L}[f(t_D)] \times \mathcal{L}\left[\frac{\partial \bar{Q}_{t_D}}{\partial t_D}\right]$$

and $(\bar{Q}_{t_D})_2$ is found, by application of the convolution theorem in La Place transform theory, to be

$$(\bar{Q}_{t_D})_2 = -\int_0^{t_D} f(\tau) \frac{\partial}{\partial \tau} [\bar{Q}(t_D - \tau)] d\tau \qquad \text{(III-11)}$$

Now, Q_t, the cumulative influx into the gas bubble at time t, is related to $\bar{Q}_{t_D}$ as shown in Equation (III-12).

$$Q_t = 2\pi h \phi c r_b^2 \bar{Q}_{t_D} \qquad \text{(III-12)}$$

Q_t for the varying reservoir pressure case is then obtained by insertion of $(Q_{t_D})_2$, the dimensionless solution for the varying pressure case, into Equation (III-11) to yield

$$\begin{aligned} Q_t &= -2\pi h \phi c r_b^2 \int_0^{t_D} f(\tau) \frac{\partial}{\partial \tau} \bar{Q}(t_D - \tau) d\tau \\ &= -2\pi h \phi c r_b^2 \left[\int_0^{t_{D_1}} f(\tau) \frac{\partial}{\partial \tau} \bar{Q}(t_D - \tau) d\tau \right. \qquad \text{(III-13)} \\ &\left. + \int_{t_{D_1}}^{t_{D_2}} f(\tau) \frac{\partial}{\partial \tau} \bar{Q}(t_D - \tau) d\tau + \cdots\cdots + \int_{t_{D_{j-1}}}^{t_{D_j}} f(\tau) \frac{\partial}{\partial \tau} \bar{Q}(t_D - \tau) d\tau \right] \end{aligned}$$

If, now, the pressure drop at the gas bubble boundary $r = r_b$, $\bar{P}(1, t_D)$, is some function of time and is approximated by a step function as shown in Figure 3, then $f(\tau)$ [$f(\tau) = \bar{P}(1, \tau)$] in each of the integrals of Equation (III-13) can be taken as a constant equal to $\frac{\bar{P}(1, t_{D_i}) + \bar{P}(1, t_{D_{i-1}})}{2}$.

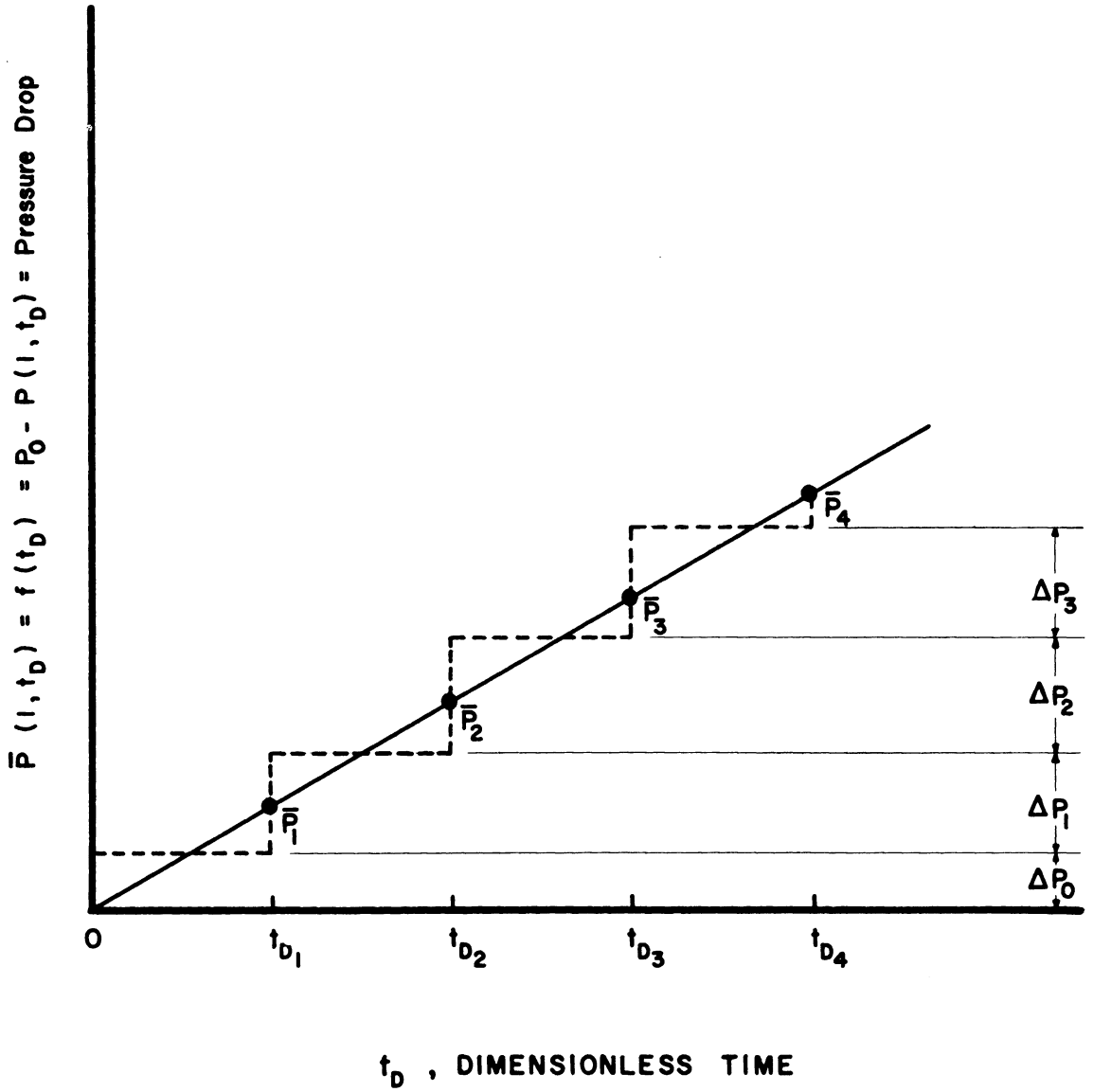

Figure 3. Approximation of Pressure Drop at Gas Bubble Boundary by a Step Function.

Equation (III-13) then becomes

$$Q_t = -2\pi h\phi c r_b^2 \left[\frac{\bar{P}_0 + \bar{P}_1}{2} \left(\bar{Q}_{t_D - t_{D_1}} - \bar{Q}_{t_D} \right) \right.$$

$$\left. + \frac{\bar{P}_1 + \bar{P}_2}{2} \left(\bar{Q}_{t_D - t_{D_2}} - \bar{Q}_{t_D - t_{D_1}} \right) + \cdots\cdots + \frac{\bar{P}_j + \bar{P}_{j-1}}{2} \left(\bar{Q}_0 - \bar{Q}_{t_D - t_{D_{j-1}}} \right) \right] \qquad \text{(III-14)}$$

where $\bar{P}_i = \bar{P}(1, t_{D_i}) = P_o - P(1, t_{D_i}) = P_o - P_i$

$t_{D_i} = i\Delta t_D$

$t_D = j\Delta t_D$

$t = j\Delta t$

Rearrangement of Equation (III-14) yields (III-15), a result which appears in Reference 1.

$$Q_t = 2\pi h\phi c r_b^2 \left[\frac{P_o - P_1}{2} \bar{Q}_{t_D} + \frac{P_o - P_2}{2} \bar{Q}_{t_D - t_{D_1}} \right.$$

$$\left. + \frac{P_1 - P_3}{2} \bar{Q}_{t_D - t_{D_2}} + \cdots\cdots \frac{P_{j-2} - P_j}{2} \bar{Q}_{t_D - t_{D_{j-1}}} \right] \qquad \text{(III-15)}$$

$$= 2\pi h\phi c r_b^2 \left[\Delta P_0 \bar{Q}_{t_D} + \Delta P_1 \bar{Q}_{t_D - t_{D_1}} + \cdots\cdots + \Delta P_{j-1} \bar{Q}_{t_D - t_{D_{j-1}}} \right]$$

$$= 2\pi h\phi c r_b^2 \sum_{i=0}^{i=j-1} \Delta P_i \bar{Q}_{(j-i)\Delta t_D}$$

where $\Delta P_i = \dfrac{P_{i-1} - P_{i+1}}{2}$; $P_{-1} = P_o$, psi

P_i = pressure at gas bubble boundary $r = r_b$ at time $t = i\Delta t$, psia

$\bar{Q}_{t_D - t_{D_i}} = \bar{Q}_{j\Delta t_D - i\Delta t_D} = \bar{Q}_{(j-i)\Delta t_D}$ = dimensionless production quantity evaluated at dimensionless time $t_D = (j-i)\Delta t_D$

$\Delta t_D = \dfrac{k\Delta t}{\mu\phi c r_b^2}$

Δt = chosen time increment, seconds

$t = j\Delta t$, seconds

A similar application of the superposition principle to the constant rate solution, Equation (III-9), yields Equation (III-16) as the varying rate case solution.(1)

$$P_o - P_t = \frac{\mu}{2\pi hk} \sum_{i=0}^{i=j-1} \Delta q'_i \, P_{(j-i)\Delta t_D} \qquad \text{(III-16)}$$

where $\Delta q_i = q'_{i+1} - q'_i$

q'_i = average rate of water influx into gas bubble during time increment from $(i - 1)\,\Delta t$ to $i\Delta t$, ft^3/sec.

1. Pressure-Explicit Equation for Gas Storage Reservoir Situated on an Aquifer

The gas law can be combined with a simple material balance and Equation (III-15) or (III-16) to give an equation explicit in the gas bubble pressure. The material balance Equation (III-17) simply expresses the fact that the gas storage reservoir pore volume is equal to the original volume minus the cumulative influx of aquifer water.

$$V_t = V_c - Q_t \qquad \text{(III-17)}$$

V_t = gas bubble pore volume at time t, ft^3

V_o = original gas bubble pore volume, ft^3

The gas compressibility factor z can be substituted from Equation (III-18) into the gas law (III-19) to give Equation (III-20) by rearrangement.

$$z = 1 + KP \tag{III-18}$$

$$P_t V_t = z n_t R T \tag{III-19}$$

$$V_t = n_t R T \left(K + \frac{1}{P_t} \right) \tag{III-20}$$

K = a constant determined from gas compressibility data, 1/psia

z = gas compressibility factor

R = universal gas constant, 10.73 psia-ft^3/lb.mole - °R

T = gas reservoir formation temperature, °R

P_t = static gas storage reservoir pressure, psia

n_t = lb. moles gas in place in storage reservoir at time t

The representation of z as a linear function of pressure is in general valid for pressures less than 700 psia. For pressures greater than 700 psia, additional terms should be present on the right side of Equation (III-18). In most practical cases, however, z can be approximated as a linear function of pressure over the limited pressure range encountered in the gas storage operations, regardless of whether the average pressure is above or below 700 psia.

Equations (III-15), (III-17), and (III-20) are now three equations in the three unknowns P_t, V_t, and Q_t. The role played by P_t in Equation (III-15) can be seen more clearly by removing the last term from the summation as shown in (III-15a) below.

$$Q_t = 2\pi h \phi c r_b^2 \left[\sum_{i=0}^{i=j-2} \Delta P_i \, \bar{Q}_{(j-i)\Delta t_D} + \frac{P_{j-2} - P_j}{2} \bar{Q}_{\Delta t_D} \right] \qquad \text{(III-15a)}$$

where $P_j = P_t$ and $t = j\Delta t$

Eliminating V_t and Q_t from Equations (III-15a), (III-17), and (III-20), one obtains (III-21).

$$P_t = \frac{K_4 + \sqrt{K_4^2 + K_5}}{2} \qquad \text{(III-21)}$$

where $$K_4 = \frac{K n_t R T + K_1 P_{j-2} \bar{Q}_{\Delta t_D} - V_0 - 2K_1 \sum_{i=0}^{i=j-2} \Delta P_i \, \bar{Q}_{(j-i)\Delta t_D}}{K_1 \bar{Q}_{\Delta t_D}}$$

$$K_1 = \pi h \phi c r_b^2$$

$$K_5 = \frac{4 n_t R T}{K_1 \bar{Q}_{\Delta t_D}}$$

$$\sum_{i=0}^{i=j-2} \Delta P_i \, \bar{Q}_{(j-i)\Delta t_D} \equiv 0 \quad \text{for } j = 1$$

Equation (III-21) is an explicit relation for P_t, the gas bubble pressure at time $t = j\Delta t$, provided the calculations for P_t are begun at $t = \Delta t$ and continued in order $t = 2\Delta t$, $3\Delta t$, ..., $(j-1)\Delta t$. For if P_t has been calculated at all time steps prior to $t = j\Delta t$, then all the pressures appearing on the right side of (III-21) are known at time step j (at $t = j\Delta t$).

The water influx rate terms, q_i', in Equation (III-16) can be combined with (III-20) to yield a pressure explicit equation. Since q_i' is (as defined above) the average rate of water influx into the gas bubble during the time interval from $(i-1)\Delta t$ to $i\Delta t$, q_i' can be defined as

$$q_i' = \frac{V_{i-1} - V_i}{\Delta t}$$

where V_i is the gas bubble pore volume at time $t = i\Delta t$. Substituting this expression for q_i' into (III-16) and removing the

last term from the summation, one obtains (III-16a), below.

$$P_o - P_t = \frac{\mu}{2\pi hk\Delta t}\left[\sum_{i=0}^{i=j-2}(2V_i - V_{i-1} - V_{i+1})P_{(j-i)\Delta t_D} + (2V_{j-1} - V_{j-2} - V_j)P_{\Delta t_D}\right] \qquad \text{(III-16a)}$$

Eliminating V_t (= V_j) from Equations (III-20) and (III-16a), one obtains (III-22).

$$P_t = \frac{-K_6 + \sqrt{K_6^2 + K_7}}{2} \qquad \text{(III-22)}$$

where $$K_6 = K_3\left[\sum_{i=0}^{i=j-2}(2V_i - V_{i-1} - V_{i+1})P_{(j-i)\Delta t_D} + P_{\Delta t_D} \cdot (2V_{j-1} - V_{j-2} - n_j RTK)\right] - P_o$$

$$K_7 = 4K_3 P_{\Delta t_D} n_j RT$$

$$K_3 = \mu/2\pi hk\Delta t$$

P_o = original aquifer pressure, psia

n_j = lb. moles gas in storage reservoir at time $t = j\Delta t$

$t = j\Delta t$

All the pressures on the right side of (III-22) are known at time step j if calculations are started at $t = \Delta t$ and continued at $t = 2\Delta t$, $3\Delta t$, ..., $(j-1)\Delta t$.

Equations (III-21) and (III-22) are useful only when the gas in place quantities, n_i, are known or specified and the gas bubble pressure-time relationship is desired. When the gas storage reservoir pressure is specified as a function of time, then the two Equations (III-21) and (III-22) must be rearranged to allow calculation of the unknown gas in place quantities.

(III-23) and (III-24), below, are such arranged versions of (III-21) and (III-22), respectively.

$$n_j = n_{(t=j\Delta t)} = \frac{2K_1 \sum_{i=0}^{i=j-1} \Delta P_i \, \bar{Q}_{(j-i)\Delta t_D}}{RT\left(K + \frac{1}{P_j}\right)} \qquad \text{(III-23)}$$

$$n_j = \frac{P_j - P_0 + K_3\left[\sum_{i=0}^{i=j-2}(2V_i - V_{i-1} - V_{i+1})P_{(j-i)\Delta t_D} + P_{\Delta t_D}(2V_{j-1} - V_{j-2})\right]}{K_3 P_{\Delta t_D} RT\left(K + \frac{1}{P_j}\right)} \qquad \text{(III-24)}$$

B. Application of the Developed Equations to the Prediction of Gas Storage Reservoir Performance

Application of the equations developed in Section III-A is now made in order to (1) determine the effect of the shape of the gas field pressure-time cycle on the gas reservoir volume behavior, and (2) evaluate the applicability of the equations to actual gas storage reservoir studies. The first application should yield answers to some of the following important questions concerning the pressure cycle-volume variation relationship: For the same number of gas field pound-days above and below discovery or initial pressure and at the end of one or several complete cycles, does the gas reservoir volume return to its original or discovery value? Is there a definite phase difference between the time of change in the reservoir pressure and the time corresponding to the response in the aquifer movement? How does shape of the gas field pressure-time curve affect the water movement? Does the time at which a gas reservoir is converted from production to storage operations appreciably affect the size or

subsequent size-variation of the gas reservoir? Answers to these and other important questions can best be obtained by simulating some idealized cases by digital computations based on the equations of Section III-A.

The second application of the developed equations involves comparison of the predicted performance of an actual gas field with available observed data. An IBM 650 digital computer program has been written to facilitate the calculations involving use of Equation (III-21). This program is described and listed in Appendix I.

1. Predicted Volume Variation of a Gas Storage Reservoir for Idealized Pressure Cycles

Equations (III-15) and (III-17) have been employed in calculating on an IBM 650 computer the gas storage reservoir volume behavior effected by nine different pressure cycles. The pressure cycles are specified in a manner which will facilitate answers to certain of the above questions concerning pressure cycle-volume behavior relationships. The pressure cycles are intended to represent the static gas bubble pressure, i.e., the gas (or water) pressure at the boundary $r = r_b$.

Calculations for pressure cycles 1, 2, and 3 (see Figure 4) allow certain conclusions concerning the effect of amplitude and duration of the pressure drawdown portion of the pressure cycle on the reservoir volume behavior. Each of the three pressure cycles has an equal number of pound-days above and below the reference $P/P_o = 1.0$ and has a period of one year.

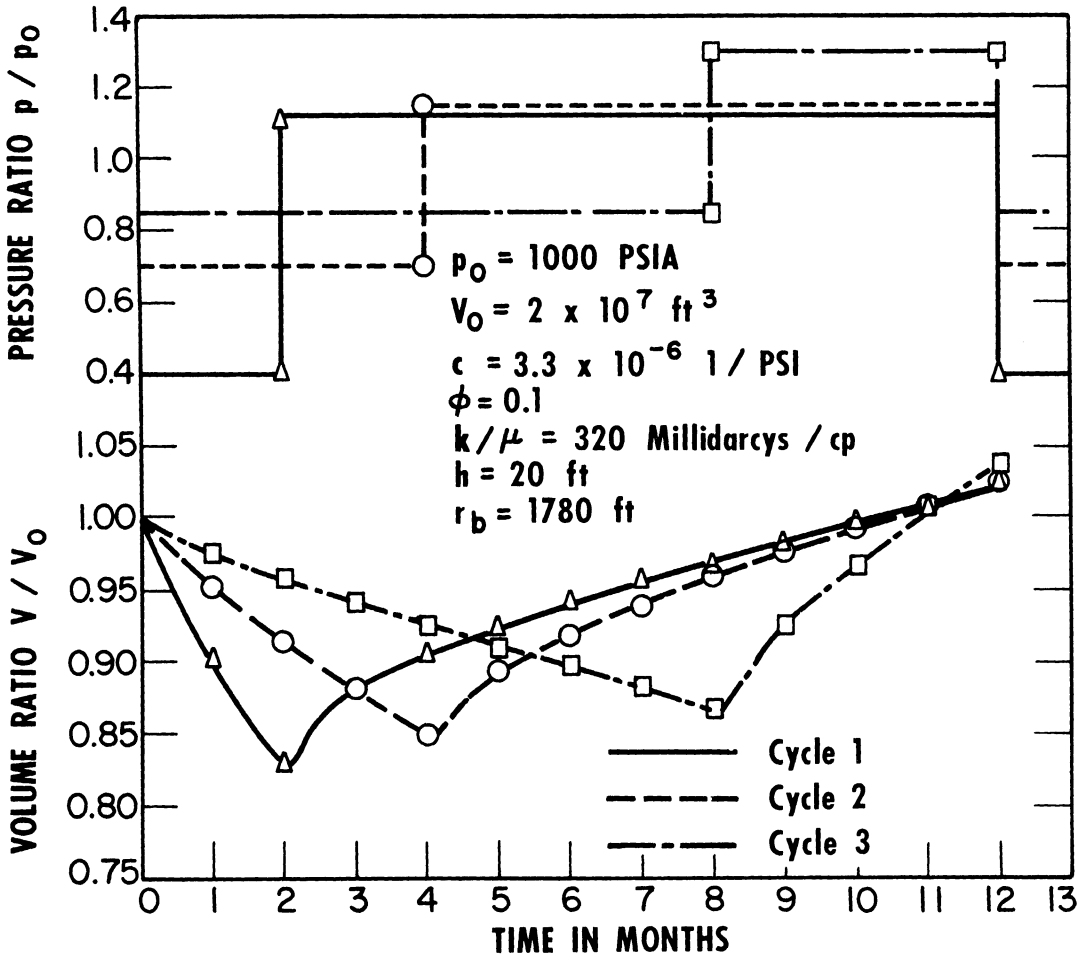

Fig. 4 Effect of pressure-time cycle on gas reservoir volume

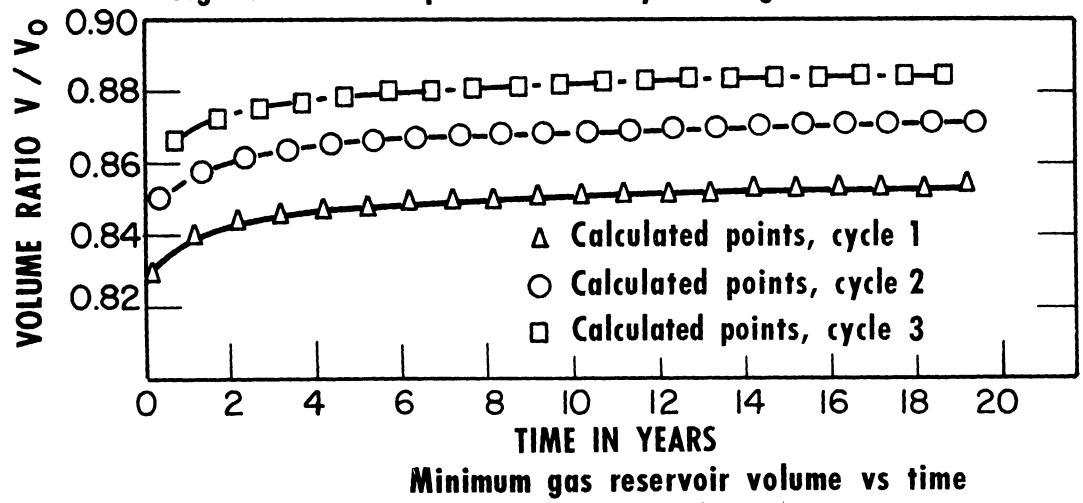

Minimum gas reservoir volume vs time

Figure 5

Pressure cycle 1 represents a large amplitude, short duration pressure drawdown followed by a mild, extended gas injection period. Cycle 3, on the other hand, represents a low-amplitude extended duration pressure drawdown followed by a relatively large-amplitude short duration gas injection period. Cycle 2 represents the intermediate case. The formation and fluid properties used in calculations for pressure cycles 1, 2, and 3 are noted on Figure 4. The aquifer fluid is assumed to be water of one centipoise viscosity and compressibility noted on Figure 4. Calculated volume ratio curves (Figure 4) clearly indicate that pressure cycle 1 results in the maximum gas reservoir shrinkage. Another result of interest is that the gas reservoir volume does not assume its original value after one complete pressure cycle but exceeds that value by 2 - 4%, although the net pound-days after one cycle is the same above and below discovery pressure ratio for all three cases. Perhaps the most interesting observation is that although each of the three pressure cycles has as many pound-days above the original pressure as below, the corresponding calculated V/V_0 curves show that the net gas reservoir volume is less than its discovery value for 10-11 months of the 12-month cycle. This fact is of practical interest because of possibility of water coning and direct proportionality of amount of gas stored to gas reservoir volume. If the pressure cycle curves in Figure 4 are reversed about the axis $P/P_0 = 1.0$ to

represent a gas injection period followed by a gas withdrawal period, the corresponding V/V_o curves will simply be symmetrical about the axis $V/V_o = 1.0$. Equation (III-15) shows this since reversal of the pressure cycle curves will simply change the algebraic sign of each ΔP_i in Equation (III-15). Thus, if the gas reservoir is converted to storage operations upon discovery by injecting gas at the beginning of the cycle and withdrawing gas at the end of the cycle, net gas reservoir volume will be greater than the original value for 10-11 months of the 12-month cycle. Figure 7 compares the number of moles of gas stored in the reservoir for the two pressure cycles shown.

Yearly minimum gas reservoir volumes corresponding to pressure cycles 1, 2, and 3, are plotted versus time in Figure 5. The pressure cycles were repeated for 20 years to allow calculation of points plotted in the latter figure. The points or curves clearly indicate growth of the gas reservoir with time. This increase in the average reservoir size is also shown on Figure 6 where curves of the relative volume ratio V/V_o of the gas field were plotted versus time corresponding to pressure cycles 1, 2, and 3, repeated for 20 years. This gas reservoir growth will later be seen to be dependent upon the fact that the pressure cycle curve represents an initial period of gas withdrawal followed by gas injection.

Pressure cycles 4, 5, and 6, shown in Figure 8, again have the same number of pound-days above and below the reference

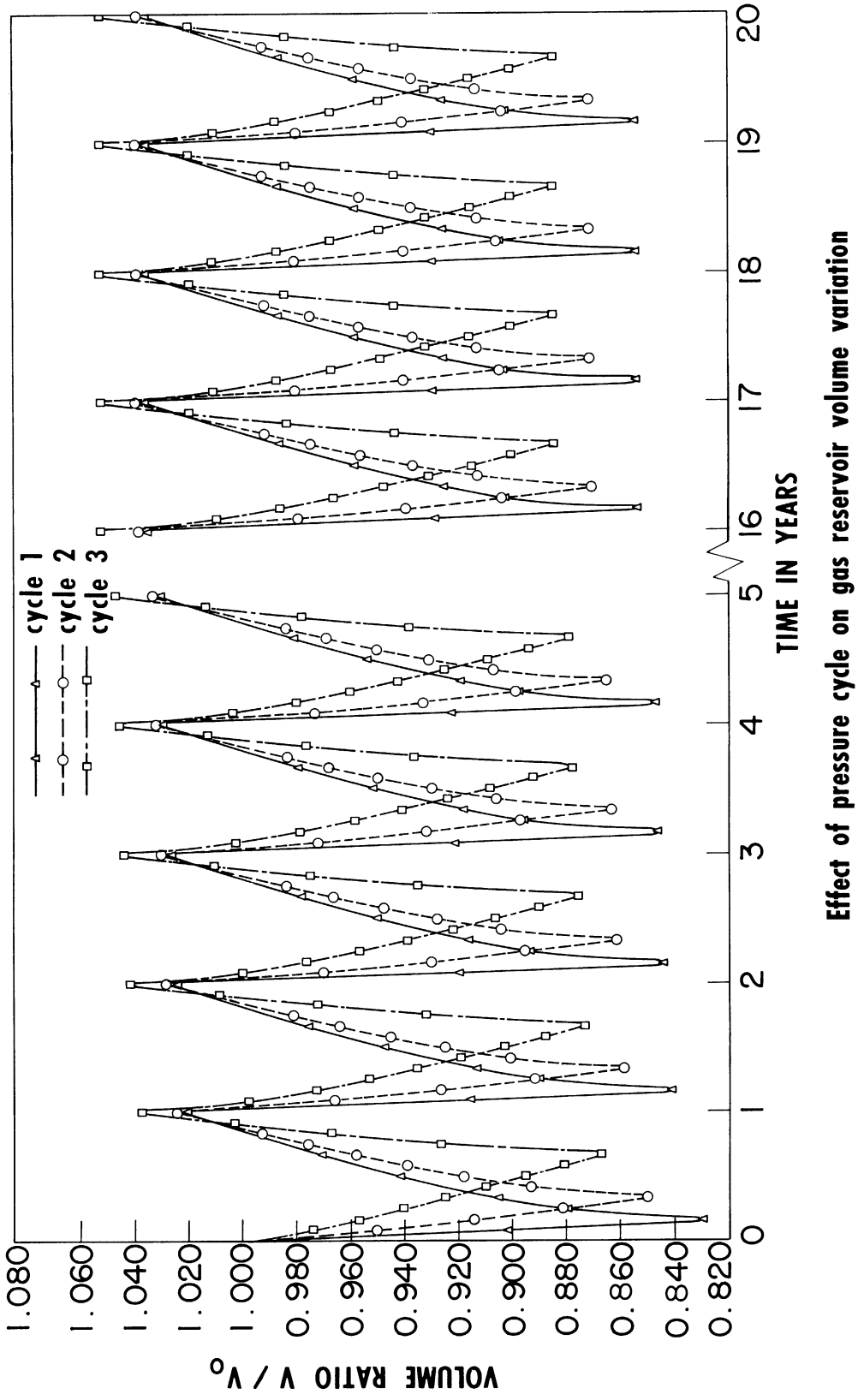

Effect of pressure cycle on gas reservoir volume variation

Figure 6

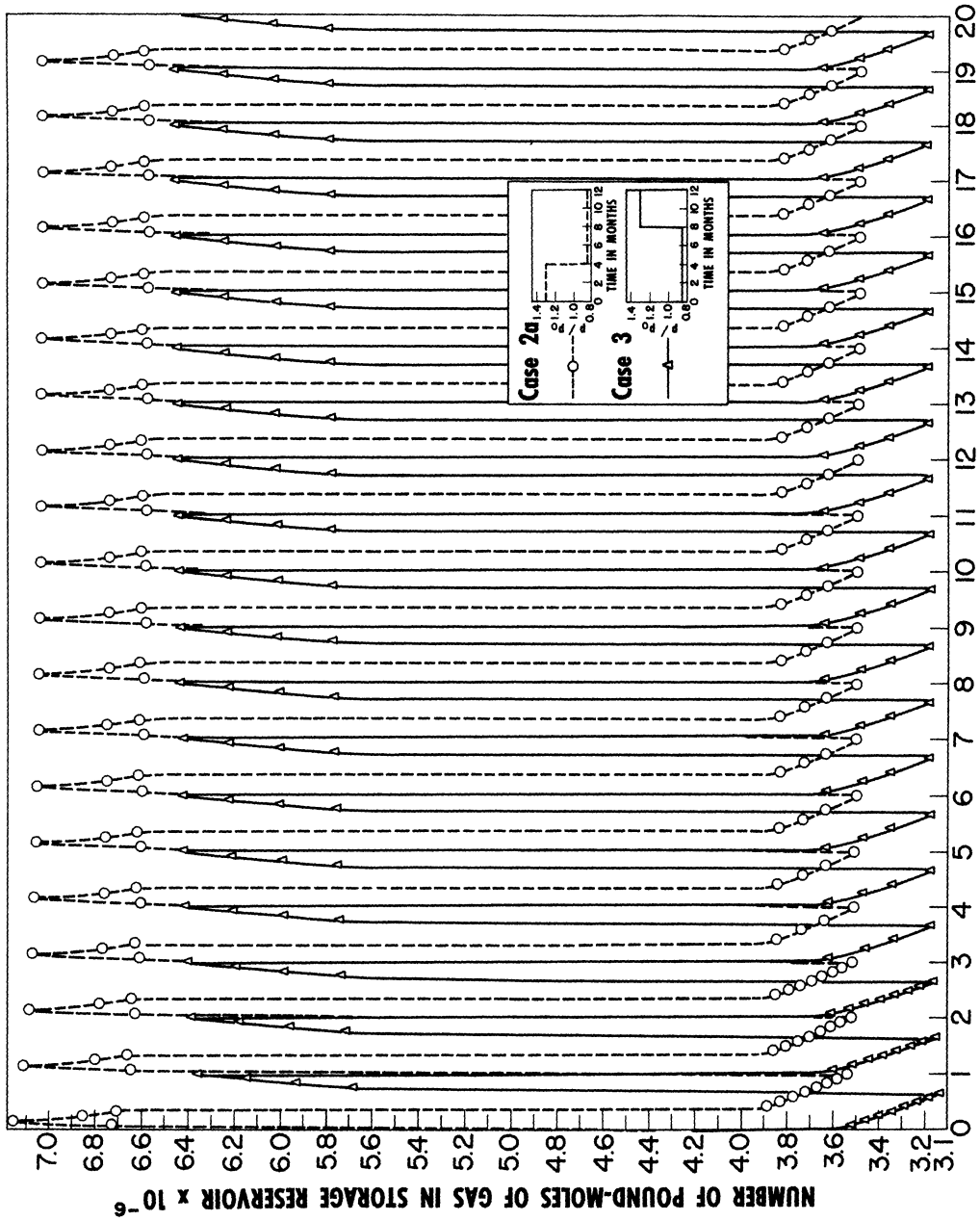

Effect of pressure cycle on quantity of gas stored

Figure 7

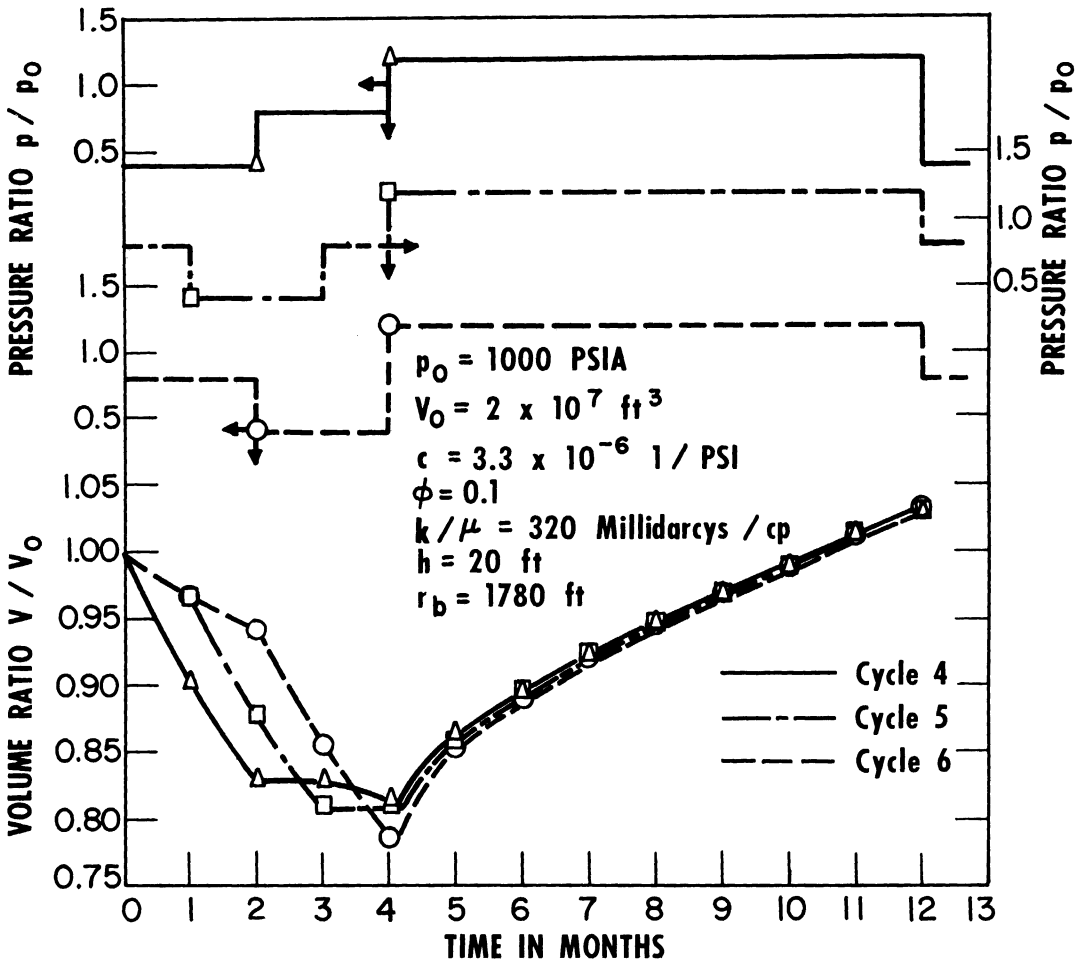

Fig. 8 Effect of pressure-time cycle on gas reservoir volume

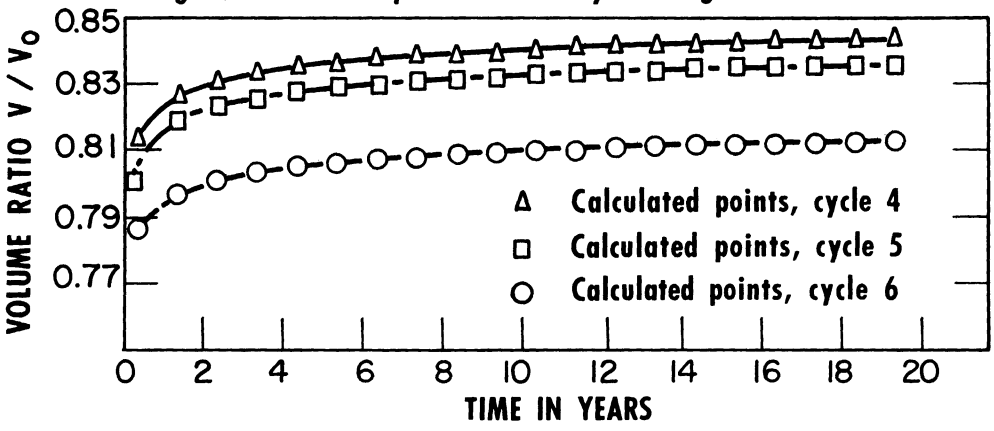

Minimum gas reservoir volume vs time

Figure 9

$P/P_o = 1.0$. Upper and lower pressure limits are the same for all cycles, and the latter two-thirds of each cycle is identical. Cycle 4 shows steep pressure drawdown to the minimum cycle pressure and gradual buildup to maximum cycle pressure. Cycle 6 represents gradual pressure drawdown followed by steep pressure buildup. Cycle 5 shows the intermediate case. Formation and fluid properties used in the calculations are the same as those employed for pressure cycles 1, 2, and 3, and are again given in Figure 8. The calculated V/V_o curves of Figure 8 corresponding to cycles 4, 5, and 6, show that cycle 6 gives maximum water encroachment into the gas field, and cycle 4 causes least amount of water encroachment. Again, results show failure of the gas reservoir volume to assume its original value at the end of the cycle, the decreased volume for 10-11 months of the 12-month cycle, and growth of the yearly average gas reservoir volume with time (Figures 9 and 10).

Figure 12 shows the effect of the time of conversion from production to storage operations and of injection of gas as opposed to withdrawal of gas during the initial portion of the storage cycle. Figure 10 gives pressure cycles 7, 8, and 9, showing initiation of storage operations after a four-year production period, initiation of storage operations immediately upon discovery with a production-injection cycle, and initiation of storage operations upon discovery with an injection-production cycle, respectively. The periodic gas field pressure

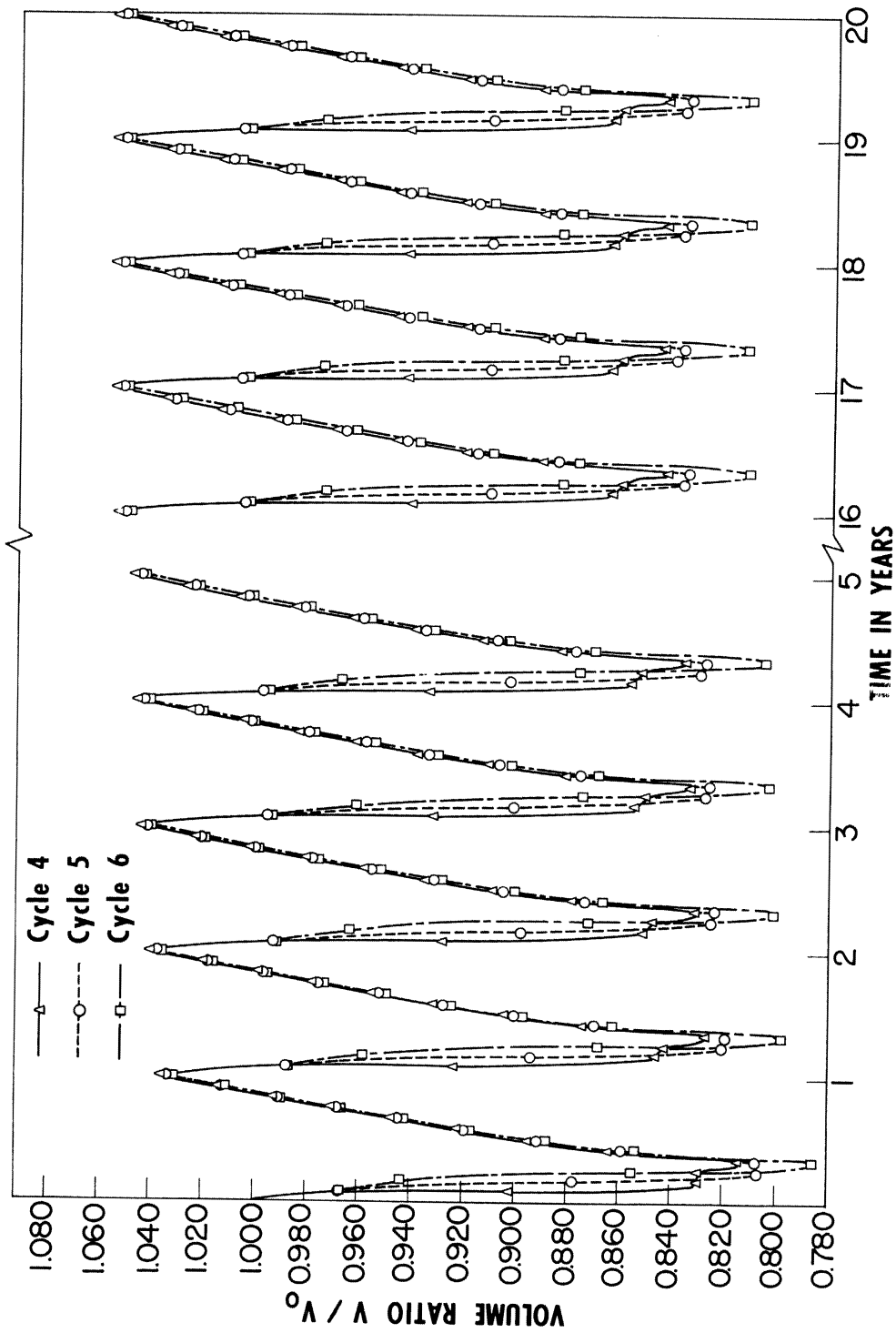

Effect of pressure cycle on gas reservoir volume variation

Figure 10

in order to allow mathematical treatment of aquifer water movement, they are seldom realized in an actual gas reservoir-aquifer system. Actual aquifer formations have varying degrees of non-uniformity and gas field boundaries rarely conform closely to circular geometry. Thus the predictive accuracy of the equations of Section III-A, based on assumptions of uniform aquifer sand porosity and permeability and radial aquifer water flow, might well be questioned. The only practical method of evaluation of the usefulness of these equations is comparison of the observed behavior of an actual gas field with that predicted from the equations.

The Section III-A Equations (III-20) and (III-21) have been applied in predicting the performance of a Michigan gas field ("Field A") which was discovered in 1941 and produced for six years prior to conversion to storage operations. The pressure and gas production-injection data from Field A and other data used in the calculations are listed in Table 1. The monthly wellhead pressures are shut-in pressures and are intended to represent an average uniform gas field pressure. Figure 13 is a sketch of the gas field boundary and shows the non-circular geometry of the gas sand.

The gas injection-production data from Table I and Equation (III-21) were employed in calculating the predicted gas bubble pressures, P_t. These pressures were then employed in Equation (III-20) to obtain the predicted volume ratio V_t/V_o.

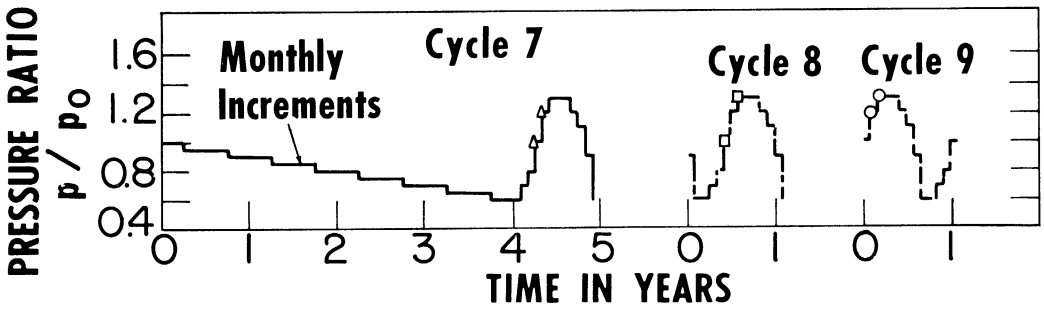

Fig. 11 Gas Reservoir Pressure-Time Cycles

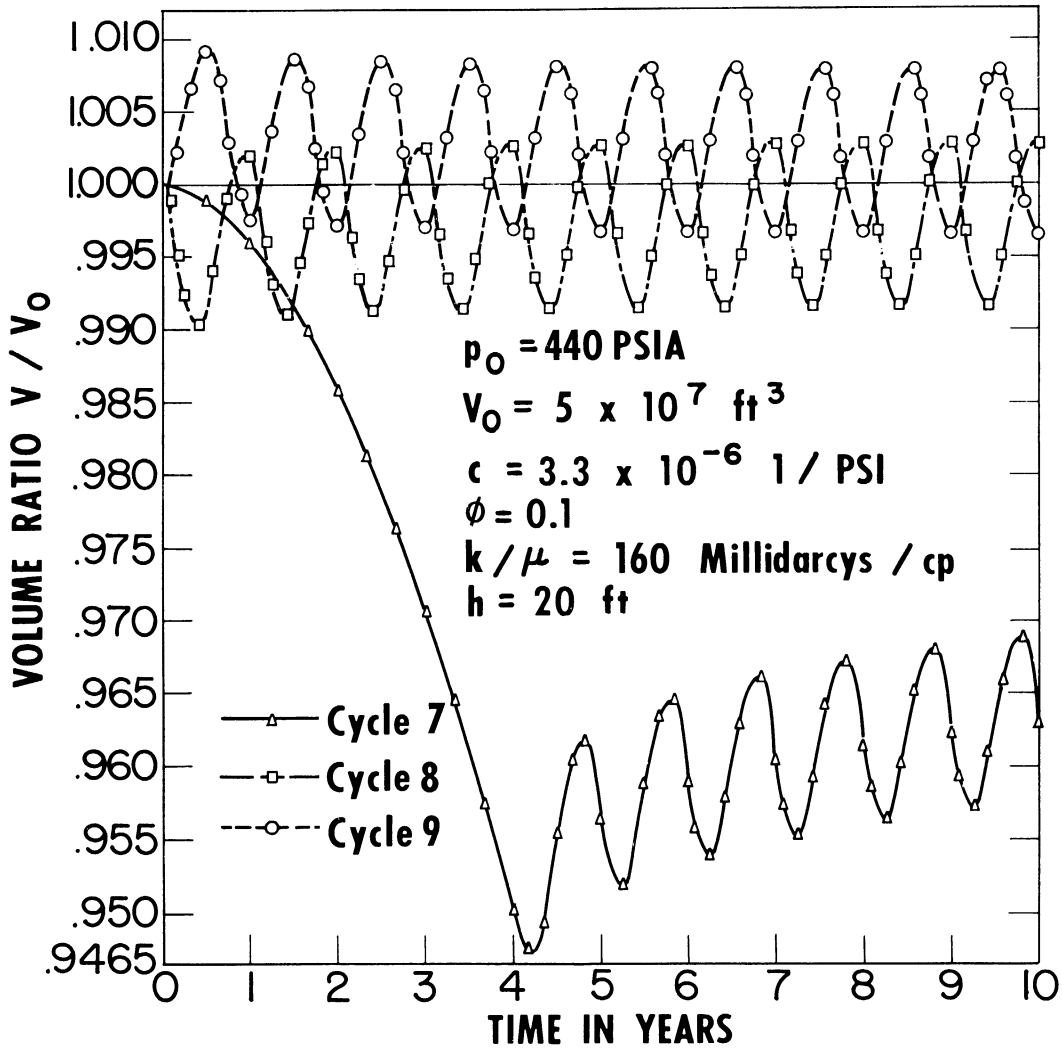

Gas field volume variation with time

Figure 11

in order to allow mathematical treatment of aquifer water movement, they are seldom realized in an actual gas reservoir-aquifer system. Actual aquifer formations have varying degrees of non-uniformity and gas field boundaries rarely conform closely to circular geometry. Thus the predictive accuracy of the equations of Section III-A, based on assumptions of uniform aquifer sand porosity and permeability and radial aquifer water flow, might well be questioned. The only practical method of evaluation of the usefulness of these equations is comparison of the observed behavior of an actual gas field with that predicted from the equations.

The Section III-A Equations (III-20) and (III-21) have been applied in predicting the performance of a Michigan gas field ("Field A") which was discovered in 1941 and produced for six years prior to conversion to storage operations. The pressure and gas production-injection data from Field A and other data used in the calculations are listed in Table 1. The monthly wellhead pressures are shut-in pressures and are intended to represent an average uniform gas field pressure. Figure 13 is a sketch of the gas field boundary and shows the non-circular geometry of the gas sand.

The gas injection-production data from Table I and Equation (III-21) were employed in calculating the predicted gas bubble pressures, P_t. These pressures were then employed in Equation (III-20) to obtain the predicted volume ratio V_t/V_o.

Table 1

GAS FIELD A DATA

Pressure Base = 15.025 psia

Date	Cumulative Gas Production Mcf	$P_{wellhead}$, psig at End of Month
Initial		438
1941 Sept.	152,222	
Oct.	305,413	
Nov.	504,643	
Dec.	783,967	
1942 Jan.	1,043,989	419
Feb.	1,281,223	410
Mar.	1,517,966	402
Apr.	1,708,094	397
May	1,814,486	394
June	2,001,371	391
July	2,199,592	389
Aug.	2,401,853	
Sept.	2,679,791	
Oct.	2,964,208	
Nov.	3,237,656	361
Dec.	3,388,508	359
1943 Jan.	3,541,680	
Feb.	3,671,511	349
Mar.	3,804,659	349
Apr.	3,976,316	336
May	4,187,552	
June	4,372,740	328
July	4,511,098	325
Aug.	4,652,784	318
Sept.	4,803,284	315
Oct.	4,991,379	313
Nov.	5,171,583	311
Dec.	5,306,024	308
1944 Jan.	5,417,306	304
Feb.	5,534,524	298
Mar.	5,662,943	289
Apr.	5,732,432	293
May	5,842,514	294
June	5,950,056	290
July	6,022,813	280
Aug.	6,032,458	286
Sept.	6,047,028	288
Oct.	6,076,636	290½
Nov.	6,115,460	283½
Dec.	6,137,991	
1945 Jan.	6,138,991	280
Feb.	6,139,991	
Mar.	6,140,991	
Apr.	6,141,991	
May	6,141,991	
June	6,141,991	
July	6,141,991	

Pressure Base = 15.025 psia

Date	Cumulative Gas Production Mcf	$P_{wellhead}$, psig at End of Month
1945 Aug.	6,141,991	294
Sept.	6,180,187	300
Oct.	6,348,855	
Nov.	6,510,325	279
Dec.	6,679,127	
1946 Jan.	6,849,875	272
Feb.	7,001,380	
Mar.	7,149,025	
Apr.	7,290,974	289
May	7,438,005	255½
June	7,573,120	253
July	7,689,770	248½
Aug.	7,821,790	247
Sept.	7,927,062	239½
Oct.	8,007,537	239
Nov.	8,010,657	241
Dec.	8,013,657	243
1947 Jan.	8,015,657	240
Feb.	8,017,657	237
Mar.	8,019,657	236
Apr.	8,021,657	236
May	8.022,657	243
June	8,023,657	245½
July	8,024,657	249
Aug.	8,025,657	252
Sept.	8,026,657	251

Pressure Base = 14.735 psia

Date	Net Gas* Stored, Mcf	$P_{wellhead}$, psig at End of Month
		252
1947 Sept.	20,898	251
Oct.	90,950	253
Nov.	130,547	252
Dec.	146,190	252
1948 Jan.	156,194	255
Feb.	200,560	254
Mar.	265,049	258.5
Apr.	540,097	273.0
May	618,588	275.8
June	723,296	279.2
July	943,431	287.5
Aug.	1,127,794	293.5
Sept.	1,211,634	296.2
Oct.	1,265,670	297.7
Nov.	1,294,407	298.6
Dec.	1,296,357	298.8

Table 1 (CONT'D)

GAS FIELD A DATA

Pressure Base = 14.735 psia

Date	Net Gas* Stored, Mcf	$P_{wellhead}$, psig at End of Month
1949 Jan.	1,250,493	297.3
Feb.	1,148,212	293.4
Mar.	1,106,796	291.8
Apr.	1,079,034	291.1
May	1,094,647	291.9
June	1,116,795	293.9
July	1,149,263	295.1
Aug.	1,186,690	297.1
Sept.	1,214,451	297.8
Oct.	1,171,066	296.1
Nov.	1,093,240	292.3
Dec.	1,011,018	289.4
1950 Jan.	927,795	286.9
Feb.	854,447	283.5
Mar.	768,385	280.6
Apr.	686,403	277.9
May	823,811	284.6
June	1,005,054	292.6
July	1,114,710	296.3
Aug.	1,151,136	299.5
Sept.	3,316,323	360.5
Oct.	5,802,859	436.2
Nov.	5,999,237	444.4
Dec.	5,786,152	434.4
1951 Jan.	3,555,830	367.5
Feb.	2,730,345	338.3
Mar.	2,509,993	331.7
Apr.	3,771,416	369.1
May	5,546,526	424.7
June	8,551,702	504.5
July	10,037,144	543.3
Aug.	12,143,655	596.1
Sept.	13,356,328	622.4
Oct.	13,985,542	634.4
Nov.	12,237,623	584.2
Dec.	11,158,958	549.8
1952 Jan.	8,869,235	492.4
Feb.	7,832,494	463.4
Mar.	7,673,820	457.4
Apr.	8,201,524	470.2
May	10,217,490	524.8
June	12,439,120	582.5
July	14,909,489	641.9
Aug.	15,801,603	661.0
Sept.	16,178,353	664.9
Oct.	15,525,408	644,7
Nov.	14,671,019	621.1
Dec.	13,381,302	587.7

Pressure Base = 14.735 psia

Date	Net Gas* Stored, Mcf	$P_{wellhead}$, psig at End of Month
1953 Jan.	10,821,652	521.0
Feb.	8,969,990	473.0
Mar.	7,821,885	441.6
Apr.	7,725,988	440,0
May	8,316,359	454.3
June	8,538,477	465.4
July	11,222,572	533.1
Aug.	13,574,474	594.0
Sept.	14,554,598	616.6
Oct.	15,176,916	627.0
Nov.	14,321,056	605.5
Dec.	12,264,235	549.4
1954 Jan.	9,381,780	476.3
Feb.	7,816,040	433.1
Mar.	6,923,033	407.6
Apr.	7,229,710	417.2
May	8,425,373	449.8
June	9,943,134	494.4
July	11,417,386	531.2
Aug.	13,298,400	577.6
Sept.	14,383,519	603.2
Oct.	14,309,735	598.0
Nov.	12,699,370	558.5
Dec.	9,132,326	467.0
1955 Jan.	6,519,597	396.2
Feb.	4,771,604	332.4
Mar.	3,809,960	333.0
Apr.	3,735,442	329.0
May	3,695,422	329.0
June	6,922,929	409.8
July	10,426,744	497.7
Aug.	13,208,806	565.2
Sept.	13,816,648	581.4
Oct.	13,813,026	580.8
Nov.	10,923,240	520.0
Dec.	7,422,351	431.4
1956 Jan.	5,212,311	375.5
Feb.	2,923,306	312.8
Mar.	1,866,177	275.0
Apr.	1,978,250	277.4
May	2,333,641	276.6
June	3,626,166	329.2
July	5,434,820	380.4
Aug.	7,592,736	434.5
Sept.	9,301,879	502.3
Oct.	9,431,169	483.2
Nov.	10,140,934	497.8
Dec.	8,693,064	466.8
1957 Jan.	5,640,184	392.4
Feb.	4,336,604	356.8

TABLE I (CONT'D)

GAS FIELD A DATA

Pressure Base = 14.735 psia

Date		Net Gas* Stored, Mcf	$P_{wellhead}$, psig at End of Month
1957	Mar.	4,862,678	360.9
	Apr.	5,987,497	389.7
	May	7,381,146	427.5
	June	9,291,480	476.6
	July	12,303,629	546.8
	Aug.	15,526,498	622.8
	Sept.	15,582,213	625.2
	Oct.	15,309,240	616.0
	Nov.	14,353,834	595.7
	Dec.	12,104,393	542.0

Depth of Gas Field Below Surface	1100 ft
Gas Field Initial Volume	4.6×10^8 ft.^{3}
Aquifer Thickness, ft	20
Formation (Gas Field and Aquifer) Porosity	.20
Gas Gravity	0.70
Total Aquifer Compressibility, Vol/Vol-Psi	7×10^{-6}
Permeability of Formation, md	956
Water Viscosity, cp	1
Formation Temperature, °F	70
Gas Bubble Radius, ft	3020

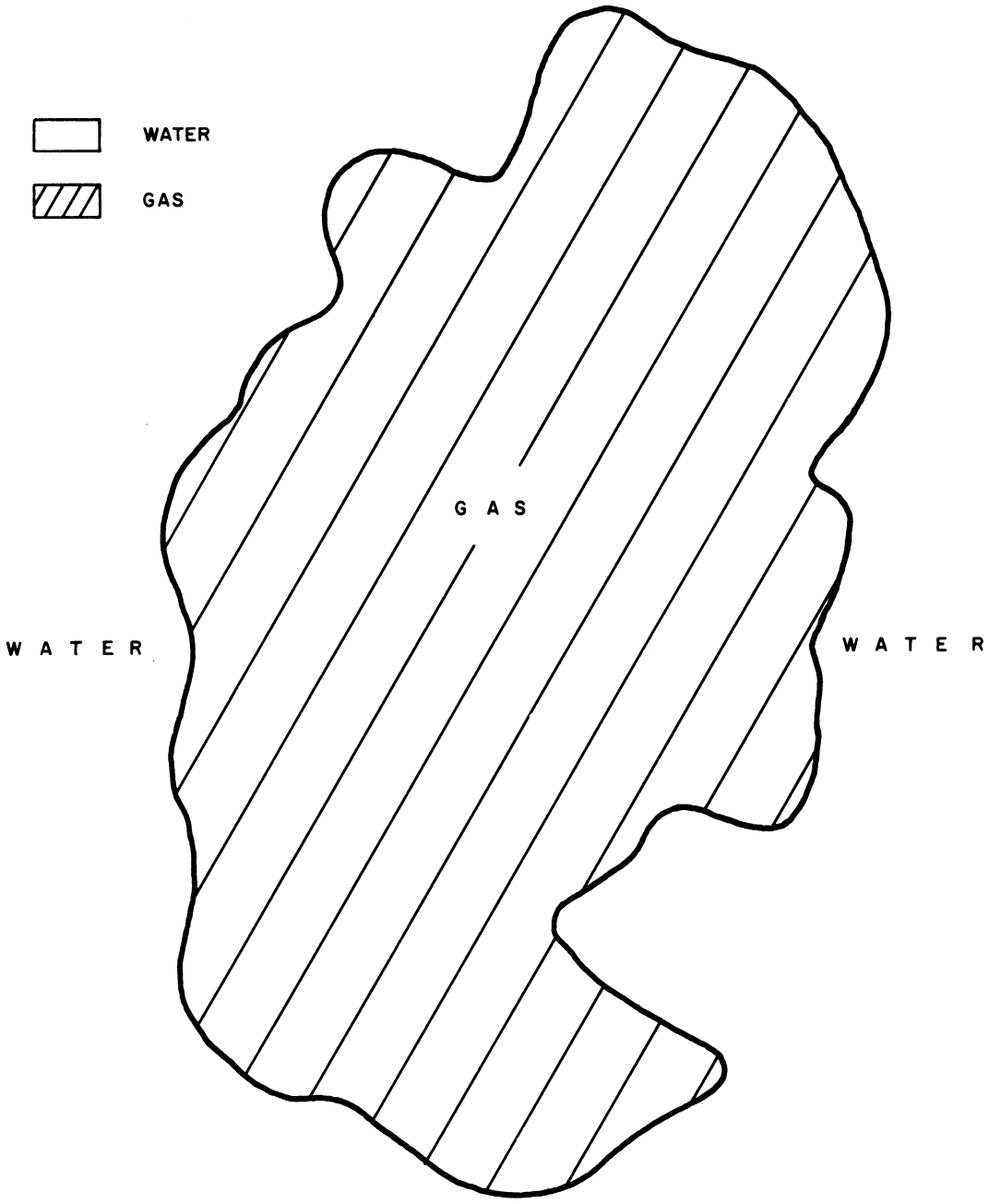

Plan Sketch of Gas Field A Boundary.

Figure 13

The observed pressures of Table I, converted to psia and corrected for depth, were employed in Equation (III-20) to calculate the actual gas field volume ratio. The calculations employed reservoir constants noted in Table I and were programmed on the IBM 650 digital computer. Monthly time increments were used in the calculation.

Figure 14 shows the agreement between the predicted and observed gas field pressure ratios, P/P_c. Figure 15 permits a comparison between observed (calculated from observed pressures) and predicted volume ratios, V_t/V_c, each plotted as a function of time. Calculations were performed for several different assumed values of r_{De}, the ratio of the aquifer exterior radius, r_e, to interior radius, r_b. Results for $r_{De} = 20$ are shown in Figure 14, and results for $r_{De} = 10$ and $r_{De} = 20$ are shown in Figure 15. The value of r_{De} is assumed to be 'approximately' 20 because the dimensionless production quantities, $\bar{Q}_{t_D}$, given by Van Everdingen and Hurst[1] are not tabulated for $r_{De} > 10$ for their 'constant terminal pressure' case of unsteady state radial liquid flow. Thus the values of $\bar{Q}_{t_D}$ employed in Equation (III-21) for an $r_{De} > 10$ had to be extrapolated from the $\bar{Q}_{t_D}$ values given for values of $r_{De} < 10$. Equation (III-21) was also solved for the case of an infinite aquifer, but results were in poorer agreement with data than were the results for a finite aquifer with $r_{De} = 20$.

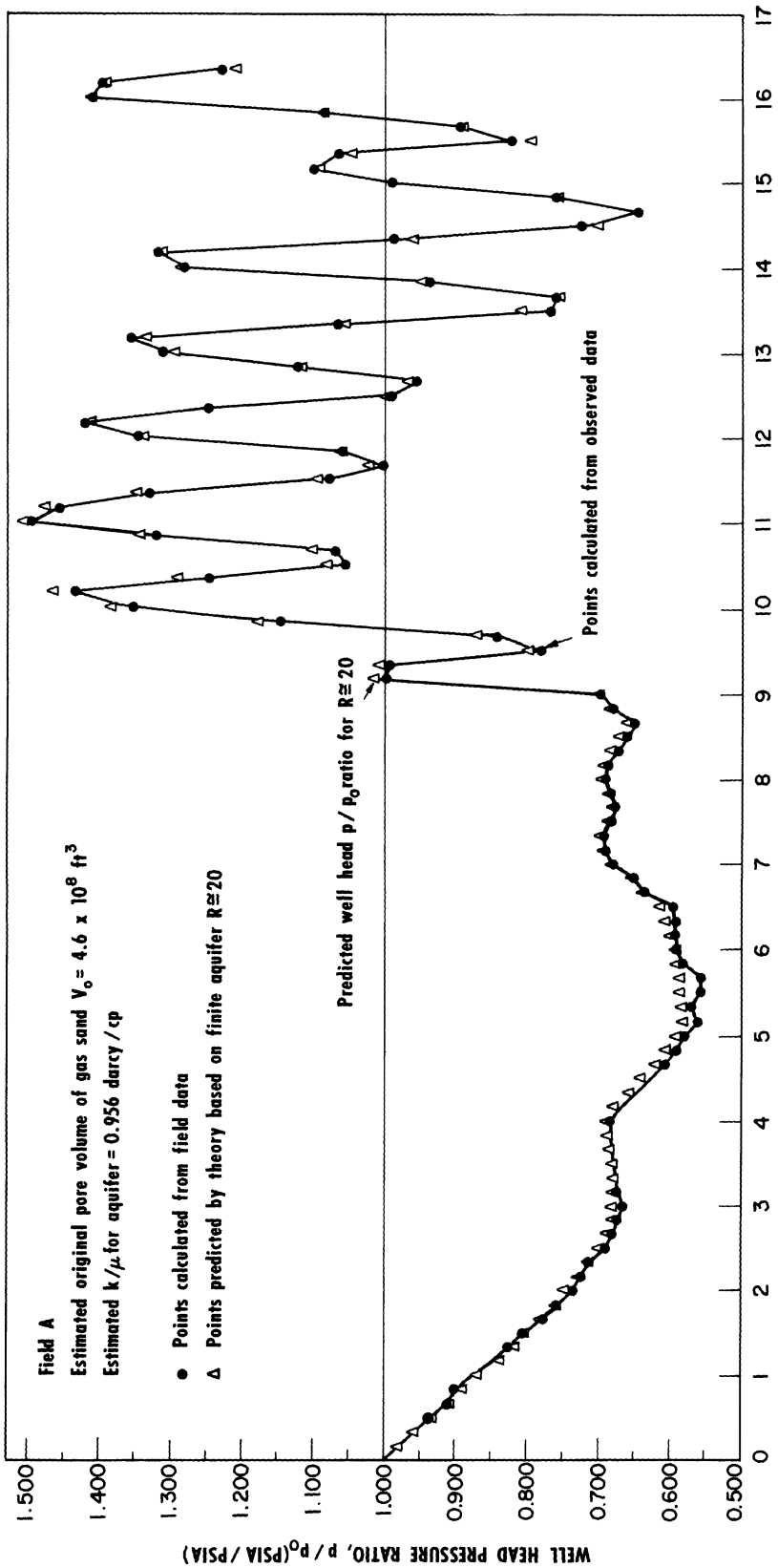

Comparison Between Observed and Predicted Gas Storage Reservoir Well Head Pressures

Figure 14

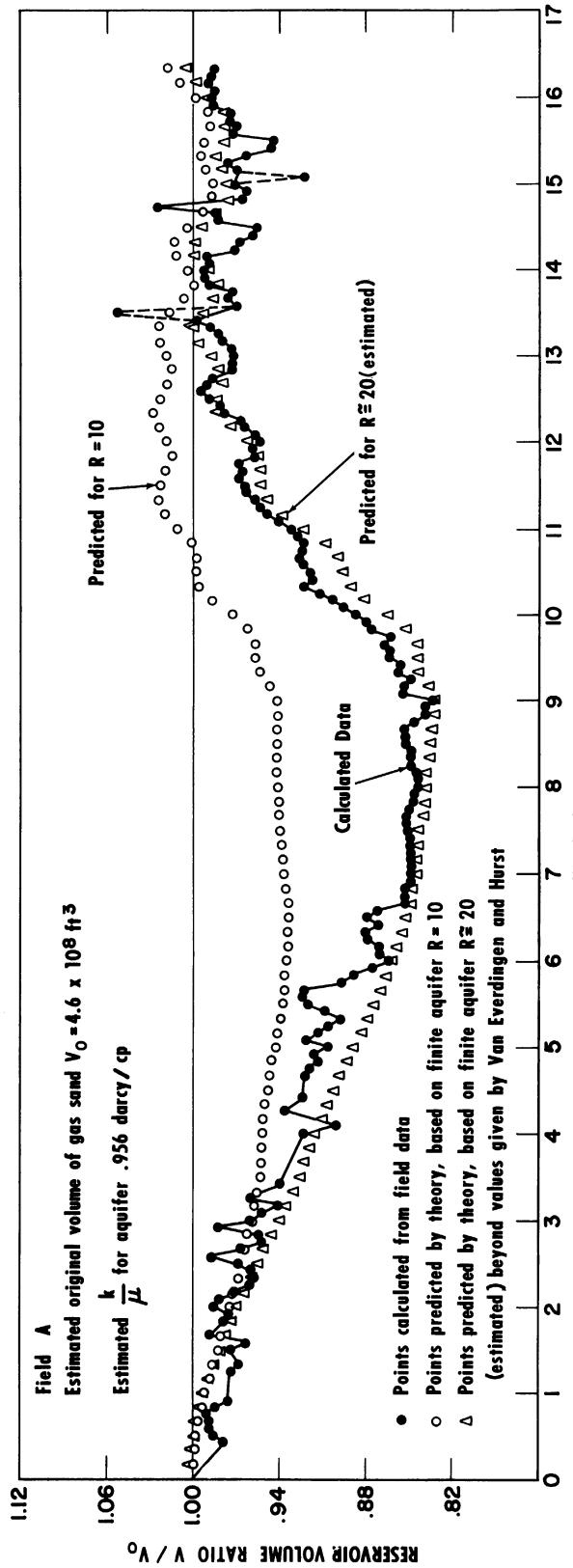

Comparison Between Observed data and Predicted Gas Storage Reservoir Volume Variations

Figure 15

C. Determination of Effective Reservoir Parameter Values from Gas Field Pressure-Production Data

The parameters appearing in the equations of Section III are the aquifer formation thickness h, porosity φ, and mobility k/μ, the aquifer compressibility c, and the gas bubble radius r_b. The 'effective' values of these parameters are defined as those values which result in closest agreement between the predicted and actual gas reservoir performance over the period of time for which pressure-production-injection data is available.

Examination of the expression relating t_D to t (page 12) and the previously presented Equations (III-21) and (III-22) shows that the reservoir parameters appear only in the combinations $K_1 = \pi h \varphi c r_b^2$ (in Equation III-21), $K_2 = k/\mu\varphi c r_b^2$, (in expression for t_D) and $K_3 = \mu/2\pi hk\Delta t$ (in Equation III-22). Thus the values of K_1 or K_3 and K_2, not the individual values of h, k/μ, φ, c, and r_b, are unique for a gas reservoir-aquifer system. One could, for example, obtain mathematically identical P_t values from Equation (III-21) by employing infinitely many different combinations of h, φ, c, r_b, and k/μ values provided one kept constant the values of K_1 and K_2. Therefore the determination of the effective reservoir parameter values reduces to the evaluation of K_1 and K_2 [if Equation (III-21) is employed] or K_3 and K_2 [if Equation (III-22) is employed].

The condition that the assumptions on pages 8 and 9 are satisfied by a specific reservoir-aquifer system is, of course, implicit in the claim of uniqueness of the K_1 (or K_3) and K_2 values for that system. Difficulty might be expected in attempts to determine the effective

K_1 or K_3 and K_2 values for an 'aquifer storage' gas reservoir since the assumption of constant r_b is certainly not satisfied in this case. Thus the method of K_1 or K_3 and K_2 determination is discussed below first in relation to reservoir-aquifer systems which, in general, satisfy the assumptions on pages 8 and 9, and second in relation to 'aquifer storage' gas reservoirs. Section III-C-3 below presents an analysis of the errors in the calculated P_t or V_t values caused by errors in the values of the reservoir parameters.

1. Case 1 - Gas Storage Reservoir-Aquifer Systems Which Satisfy the Assumptions in Section III-A

The phrase 'satisfaction of assumptions' is not to be taken literally in the present context since no actual gas field-aquifer system will conform perfectly to the assumptions made in the development of the equations of Section III-A. No precise statement can be made concerning the extent to which a given reservoir-aquifer system can deviate from the assumptions and yet be amenable to analysis by the method described below. Certain extreme cases such as aquifer storage reservoirs and reservoirs undergoing interference effects can certainly be excluded from the category of systems amenable to treatment by the method discussed below.

The term DEV, defined in Equation (III-25) below, serves as a measure of the agreement between the actual and predicted pressure behavior of a gas storage reservoir; DEV is the average fractional deviation between the observed and predicted

gas bubble pressure over the time period for which field pressure data is available. Its value will, of course, decrease with increasing agreement between these pressures.

$$DEV = \frac{\sum_{i=1}^{i=N} \left(\left| P_{i\Delta t} - Pa_{i\Delta t} \right| / Pa_{i\Delta t} \right)}{N} \qquad \text{(III-25)}$$

$P_{i\Delta t}$ = P_t = predicted gas bubble pressure at time $t = i\Delta t$, calculated from Equation (III-21) or (III-22), psia

$P_{a_{i\Delta t}}$ = observed gas bubble pressure from field data at time $t = i\Delta t$, psia

Δt = time increment chosen for calculations, seconds

N = number of time increments comprising time period for which a comparison between predicted and observed pressures is desired

The effective K_1 (or K_3) and K_2 values for a reservoir-aquifer system can now be determined by analysing the results of the following sequence of calculations:

1) assume a value of K_2
2) assume a value of K_1 (or K_3)
3) calculate $P_{i\Delta t}$ (i = 1, 2, 3, ..., N) from Equation (III-21) or (III-22)
4) calculate DEV from the observed gas bubble pressures and the pressures calculated in step 3)
5) assume a different value of K_1 (or K_3)
6) repeat steps 3), 4), and 5) until a plot of the DEV values calculated in step 4) versus K_1 (or K_3) shows a minimum DEV value

7) choose a different K_2 value and repeat steps 2) - 6)

The effective reservoir parameter values are now the K_1 (or K_3) and K_2 values corresponding to the minimum DEV of the several minimum DEV values referred to in step 6).

The above-outlined calculations are illustrated by application to an ideal gas field-aquifer system having the following characteristics:

infinite aquifer

$K_1 = \pi h \phi c r_b^2 = 10$ ft^3/psia

$K_2 = k/\mu\phi c r_b^2 = 10^{-5}$ seconds^{-1}

V_o = initial gas bubble pore volume = 220,000 ft^3

A time increment of one month was chosen (Δt = one month = 2.628×10^6 seconds) and the calculations were performed for 13 time increments (N = 13). The gas field pressure at $t = \Delta t, 2\Delta t, \ldots, 13\Delta t$ was specified as shown in Table II. The pore volumes of the gas bubble were calculated on the IBM 650 computer from Equations (III-15) and (III-17) for $K_1 = 10$, $K_2 = 10^{-5}$ and are listed in Table II. These pore volumes were then considered as reflecting the actual or observed behavior of the gas field and the effective values of K_1 and K_2 were considered unknown. Since the pressures were specified and the pore volumes were calculated, DEV in this case was defined as in Equation (III-25a) below.

$$DEV = \frac{\sum_{i=0}^{i=13} \left(| V_{iot} - V_{aiat} | / V_{aiat} \right)}{13} \qquad \text{(III-25a)}$$

TABLE II

PRESSURE-VOLUME BEHAVIOR OF IDEALIZED GAS STORAGE RESERVOIR

Month	Specified Gas Reservoir Pressure, Psia	"Observed" Pore Volume (Calculated for $K_1 = 10$, $K_2 = 10^{-5}$), MMcf
0	500	.22000
1	460	.21395
2	420	.19755
3	380	.17296
4	430	.15437
5	480	.15178
6	530	.16066
7	600	.18291
8	600	.20944
9	540	.22213
10	480	.21765
11	440	.20281
12	500	.19606
13	600	.21382

$V_{i\Delta t}$ = predicted gas bubble pore volume at time $t = i\Delta t$, ft^3

$V_{a_{i\Delta t}}$ = actual gas bubble pore volume at time $t = i\Delta t$, ft^3

For each of several assumed values of K_2, the predicted pore volumes $V_{i\Delta t}$ and the corresponding DEV values were calculated for several assumed K_1 values. These calculations were performed in the manner outlined in steps 1) - 7), above. The calculated DEV values corresponding to the various combinations of K_2 and K_1 values are listed in Table III and DEV is plotted versus K_1 with K_2 as a parameter in Figure 16. Figure 17 shows the observed pore volumes [calculated from Equations (III-15) and (III-17) with $K_1 = 10$, $K_2 = 10^{-5}$] and predicted pore volumes [calculated from (III-15) and (III-17) for $K_1 = .0229$, $K_2 = 10^{-2}$, and for $K_1 = 60$, $K_2 = 10^{-6}$] plotted versus time.

Figure 16 reveals that, for a fixed K_2 value, DEV is sensitive to the assumed K_1 value. However, DEV is less sensitive to the assumed value of K_2 provided that for each K_2 value the gas field pore volumes and DEV are calculated for the optimum K_1 value, i.e., the K_1 value corresponding to points a, b, c, and d noted on Figure 16. If one performed the calculations indicated in steps 1) - 7) by fixing a K_1 value and then calculating the pore volumes and DEV values for a sufficient number of K_2 values to obtain a minimum on a plot of DEV versus K_2, then the results would show that DEV is very sensitive to the assumed K_2 value for a fixed K_1 but is relatively insensitive to the

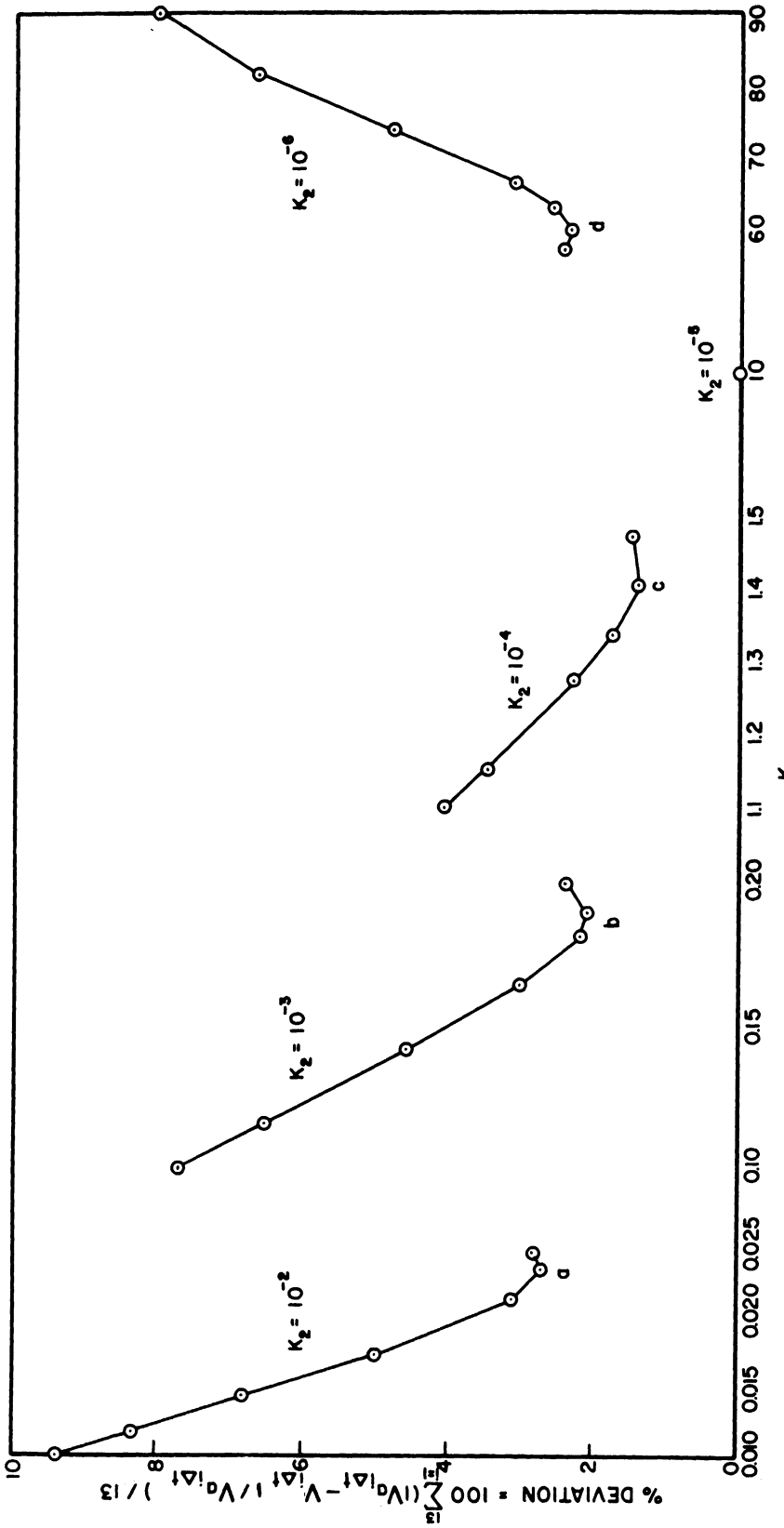

Effect of Assumed K_1 and K_2 Values on Agreement Between Predicted and Observed Gas Bubble Volumes.

Figure 16

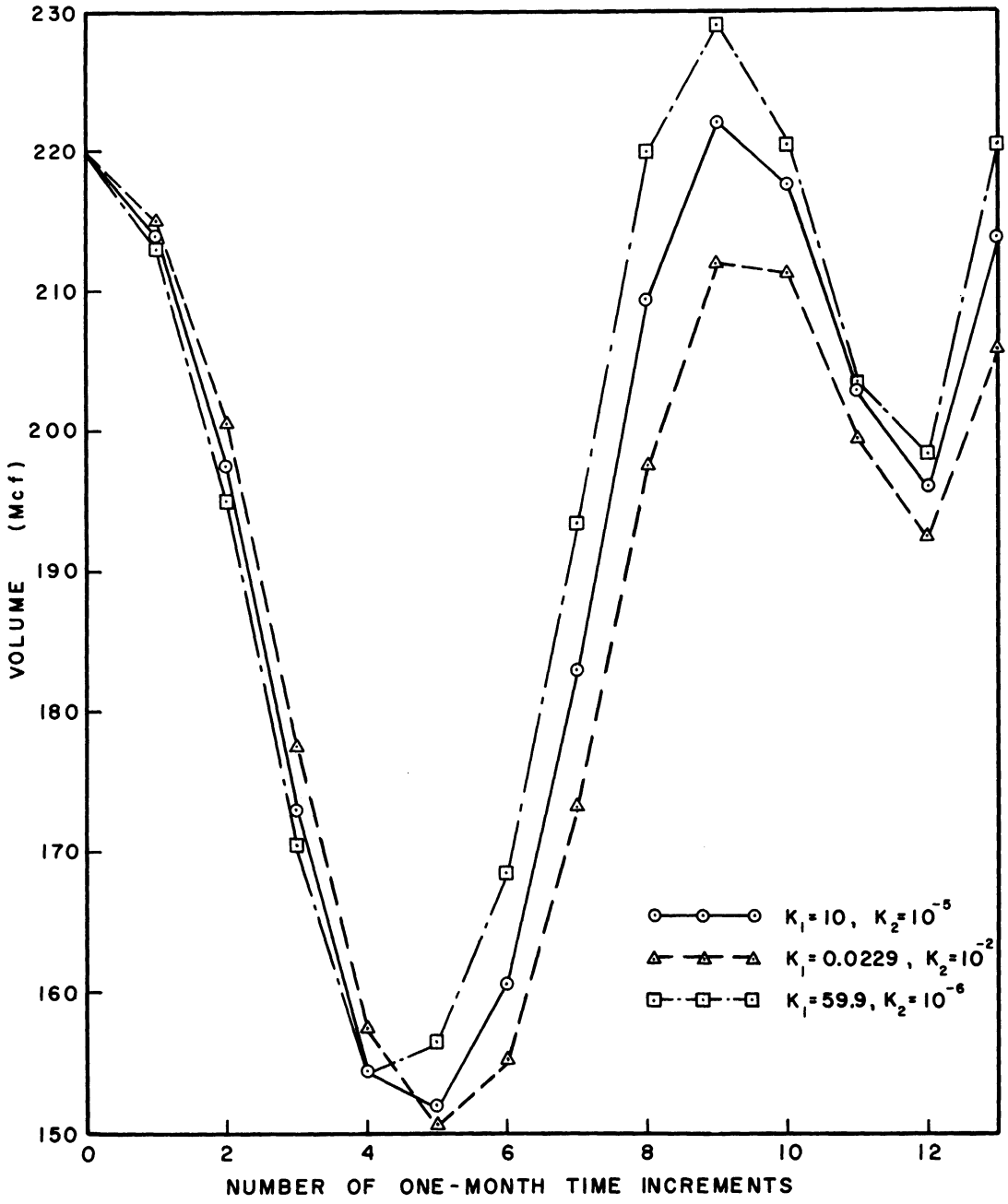

'Observed' and Predicted Gas Bubble Pore Volumes for Idealized Reservoir-Aquifer System.

Figure 17

TABLE III

EFFECT OF K_1 AND K_2 ON DEV VALUE

FOR IDEALIZED GAS RESERVOIR - AQUIFER SYSTEM

$K_2 = k/\mu\phi c r_b^2$	$K_1 = \pi h\phi c r_b^2$	DEV
10^{-2}	2.292×10^{-2}	2.71%
10^{-3}	1.886×10^{-1}	2.12%
10^{-4}	1.407	1.37%
10^{-5}	1.000×10	0
10^{-6}	5.987×10	2.33%
10^{-7}	1.748×10^{2}	9.59%

assumed K_1 value provided K_2 is taken equal to its optimum value for the assumed K_1. Thus, in short, DEV is relatively sensitive to the assumed value of K_1 (or K_2) when K_2 (or K_1) is fixed but is relatively insensitive to the fixed value of K_2 (or K_1) provided the optimum K_1 (or K_2) is chosen for each of the latter fixed values.

2. Case 2 - 'Aquifer Storage' Gas Reservoirs

The validity of the method of K_1 (or K_3) and K_2 determination discussed in Section III-C-1 above depends upon 'randomness' in the errors in the $V_{a_{i\Delta t}}$ and $V_{i\Delta t}$ or $P_{a_{i\Delta t}}$ and $P_{i\Delta t}$ values. That is, differences between the observed and predicted performance of the gas field should be due to some non-homogeniety in the aquifer formation, perhaps slight deviation of the field boundary from a circular shape, slight variation in r_b, and errors in the reservoir pressure and gas flow rate measurements. Differences due to these factors can be reasonably expected to be much more random than the difference between $P_{a_{i\Delta t}}$ and $P_{i\Delta t}$ in the case of an 'aquifer storage' gas reservoir where, while $P_{i\Delta t}$ is calculated from equations derived from the assumption of a constant r_b, r_b actually increase from a value of 0 to values of several thousand feet as the gas bubble is grown.

Analyses involving the Section III-A equations will now be made to (1) determine the effect of an increasing r_b on the actual or observed performance of an aquifer storage gas

reservoir, (2) determine the manner in which K_3 and K_2 must be chosen when employing the method discussed in Section III-C-1, above, in order to produce the same trend in the predicted field performance as the increasing r_b produces in the actual field performance. The results of these analyses are checked by applying the method of Section III-C-1 to an actual aquifer storage reservoir.

The variable rate Equation (III-16a) is employed in these analyses and the assumption is made that the term $(2V_i - V_{i+1} - V_{i-1})$ in this equation is constant and less than 0. [The following analyses would yield the same results if this term were allowed to take on <u>varying</u> negative values; however the analyses are much simpler if $(2V_i - V_{i+1} - V_{i-1})$ is assumed constant.] This is equivalent to asserting that the second derivative of the pore volume with respect to time is greater than 0. This latter assertion is in general valid for an aquifer storage reservoir during the initial growth stage; Figure 21 shows that the actual pore volume-time curve for aquifer storage reservoir B conforms very well to this assumption during the first 31 weeks of the gas bubble growth.

The following analysis shows that the effect of a growing r_b on the performance of an aquifer storage reservoir is a less rapid increase of gas bubble pressure with time than would occur in a reservoir of constant radius. The last term of Equation (III-16a) can be included in the summation term to

yield

$$P_e - P_j = K_3 \sum_{i=0}^{i=j-1} \Delta V_i \, \underline{P}_{(j-i)\Delta t_D} \qquad \text{(III-26)}$$

where $\Delta V_i = 2V_i - V_{i+1} - V_{i-1}$, a negative constant, from the above assumption. The effect of an increasing r_b on P_j can be determined by differentiating both sides of (III-26) with respect to r_b.

$$\frac{\partial P_j}{\partial r_b} = -K_3 \sum_{i=0}^{i=j-1} \Delta V_i \left(\frac{d\underline{P}_{t_D}}{dt_D} \frac{dt_D}{dr_b} \right)_{t_D=(j-i)\Delta t_D} \qquad \text{(III-27)}$$

Now, since $t_D = K_2 t = k/\mu\phi c r_b^2 \Delta t$,

$$\frac{dt_D}{dt} = \frac{-2kt}{\mu\phi c r_b^3} = -\frac{2}{r_b} t_D$$

and (III-27) becomes

$$\frac{\partial P_j}{\partial r_b} = \frac{2K_2K_3}{r_b} \sum_{i=0}^{i=j-1} \Delta V_i \left(t_D \frac{d\underline{P}_{t_D}}{dt_D} \right)_{t_D=(j-i)\Delta t_D} \qquad \text{(III-28)}$$

The term $t_D \; d\underline{P}_{t_D}/dt_D$ is positive for all values of t_D[1,2]. $\partial P_j/\partial r_b$ is therefore negative since ΔV_i is negative and K_2 and K_3 are positive. Thus as r_b increases, P_j will assume lower values than those corresponding to the case of a constant r_b.

Now, since the actual gas bubble pressures reflect the water movement away from a <u>growing</u> gas bubble and the predicted pressures are obtained by calculations in which r_b is assumed constant, one might expect the actual pressures to assume smaller values (smaller than the predicted pressures) as time increases, since $\partial P_j/\partial r_b < 0$. Thus application of the method of Section III-C-1, above, to an aquifer storage

reservoir should yield increased agreement between the reservoir observed and predicted performance for combinations of K_3 and K_2 values which effect a smaller slope of the predicted pressure-time curve.

The statement that the predicted pressure-time curve slope will be decreased by increasing K_2 and decreasing K_3 will now be proven. The slope, S_j, of the predicted pressure-time curve can be obtained by differentiating both sides of (III-26) with respect to time and noting that $\partial/\partial t = K_2 \ \partial/\partial t_D$ (since $t_D = K_2 t$).

$$S_j = \frac{\partial P_j}{\partial t} = -K_3 K_2 \sum_{i=0}^{i=j-1} \Delta V_i \left(\frac{dP_{t_D}}{dt_D} \right)_{t_D = (j-i)\Delta t_D} \qquad \text{(III-29)}$$

The total differential of S_j with respect to K_3 and K_2 is

$$dS_j = \frac{\partial S_j}{\partial K_3} dK_3 + \frac{\partial S_j}{\partial K_2} dK_2 \qquad \text{(III-30)}$$

or, dealing with finite increments,

$$\Delta S_j = \frac{\partial S_j}{\partial K_3} \Delta K_3 + \frac{\partial S_j}{\partial K_2} \Delta K_2 \qquad \text{(III-31)}$$

The terms $\partial S_j/\partial K_3$ and $\partial S_j/\partial K_2$ can be obtained by differentiating (III-29) to yield

$$\Delta S_j = \left(-K_3 K_2 \Delta V_i \sum_{i=0}^{i=j-1} \left(\frac{dP_{t_D}}{dt_D} \right)_{(j-i)\Delta t_D} \right) \frac{\Delta K_3}{K_3}$$

$$- \left(K_3 K_2 \Delta V_i \sum_{i=0}^{i=j-1} \left(\frac{dP_{t_D}}{dt_D} \right)_{(j-i)\Delta t_D} + K_3 K_2 \Delta V_i \sum_{i=0}^{i=j-1} \left(t_D \frac{d^2 P_{t_D}}{dt_D^2} \right)_{(j-i)\Delta t_D} \right) \frac{\Delta K_2}{K_2} \qquad \text{(III-32)}$$

or, upon rearrangement,

$$\Delta S_j = -K_3 K_2 \Delta V_i \left[\left(\sum_{i=0}^{i=j-1} \left(\frac{dP_{t_D}}{dt_D} \right)_{(j-i)\Delta t_D} \right) \frac{\Delta K_3}{K_3} + \left(\sum_{i=0}^{i=j-1} \left(\frac{d}{dt_D} \left(t_D \frac{dP_{t_D}}{dt_D} \right) \right)_{(j-i)\Delta t_D} \right) \frac{\Delta K_2}{K_2} \right] \qquad \text{(III-33)}$$

The reader might interject at this point that a negative ΔS_j (decreased slope) is easily obtained by simply decreasing K_3 (negative $\Delta K_3/K_3$) or K_2 (negative $\Delta K_2/K_2$). However, the answer is not that simple since if K_3 is decreased then K_2 must be increased, and vice-versa, to maintain close agreement between the predicted and actual gas bubble pressures. For suppose that for a certain K_3 and a certain K_2, a close agreement is achieved between actual and predicted pressures and it is desired to change K_3 and K_2 so as to achieve closer agreement. Then by decreasing K_3 and leaving K_2 unchanged, or vice-versa, one will simply effect decreased values of all the predicted pressures, as is obvious from Equation (III-26). But, in general, one desires to change the slope of the predicted pressure-time curve, at the same time keeping the general magnitude of the predicted pressures the same. Actually, if K_3 is decreased by a certain factor then K_2 must be increased by a larger factor in order to maintain close agreement between the predicted and actual pressures. This fact can be seen from Figure 18 and Table VI, which present the results of application of the method of Section III-C-1 to an actual aquifer storage reservoir.

These results will be discussed below. (Table VI shows that as K_3 is decreased, the product $K_3 \times K_2$ is increased; that is, K_2 is increased in greater proportion than that in which K_3 is decreased.)

Equation (III-33) indicates that a negative ΔS_j (decreased slope) can be obtained by decreasing K_3. Since the product $-K_2K_3\Delta V_i$ in (III-33) is positive ($\Delta V_i < 0$) the term in the square brackets must be negative for ΔS_j to be negative. Approximate values of the terms dP_{t_D}/dt_D and $d/dt_D \ (t_D \ dP_{t_D}/dt_D)$ are tabulated in Table IV. These values show that if $t_D > 90$, the latter term is negligible compared to the former. Since these two terms are the coefficients of $\Delta K_3/K_3$ and $\Delta K_2/K_2$ in (III-33), the sign of ΔS_j is primarily dependent upon the sign of $\Delta K_3/K_3$. Thus if K_3 is decreased, ΔS_j will be negative; a decreased predicted pressure-time curve slope is therefore obtained by decreasing K_3 and increasing K_2. The agreement between predicted and actual aquifer storage reservoir performance (during initial growth stage) should therefore increase as K_3 is chosen smaller and K_2 larger.

The method described in Section III-C-1 has been applied to aquifer storage reservoir B in order to check the above conclusions concerning the effects of an increasing r_b and the manner of K_3 and K_2 variation on the field observed and predicted performance. Field B is an aquifer storage reservoir which was initiated in 1957 by injection of natural gas into an

TABLE IV

VALUES OF $\underline{P}_{t_D}$ AND RELATED DERIVATIVES VS t_D

t_D	$\underline{P}_{t_D}$	$\frac{d\underline{P}_{t_D}}{dt_D}$	$t_D \frac{d\underline{P}_{t_D}}{dt_D}$	$\frac{d}{dt_D}\left(t_D \frac{d\underline{P}_{t_D}}{dt_D}\right)$
8	1.556			
9	1.604	.048	.432	
10	1.651	.047	.470	.038
40	2.282			
50	2.388	.0106	.53	
60	2.476	.0088	.528	-.0002
80	2.615			
90	2.762	.0057	.513	
100	2.723	.0051	.510	-.0003
400	3.406			
500	3.516	.0011	.550	
600	3.608	.0092	.5515	.000015
1000*	3.860*	.0005*	.5*	0*

* For $t_D \geq 1000$, $\underline{P}_{t_D} \tilde{=} 1/2\ [.8090 + \ell n\ t_D]$ (reference 1)

$\therefore \frac{d\ \underline{P}_{t_D}}{dt_D} = \frac{1}{2t_D} = .0005$ for $t_D = 1000$,

$t_D \frac{d\ \underline{P}_{t_D}}{dt_D} = .5$ and $\frac{d}{dt_D}\left(t_D \frac{d\ \underline{P}_{t_D}}{dt_D}\right) = 0.$

aquifer formation having an initial uniform pressure of 1060 psia. This field is an excellent example of a gas storage reservoir which does not satisfy the assumption of a constant r_b, since Field B's radius increased from 0 feet on November 30, 1957 to approximately 2600 feet in early summer of 1958.

Available pressure-injection data for the period November 30, 1957 - July 5, 1958 were employed in the determination of the K_3 and K_2 values which would result in closest agreement between the observed and predicted gas bubble pressures. The predicted pressures were calculated from Equation (III-22), with the required n_t values obtained from the data tabulated in Table V. These predicted pressures and the n_t data were employed in Equation (III-20) to calculate the predicted pore volumes. The actual pore volumes were calculated by inserting P_t and n_t from the data into Equation (III-20). A measure of the agreement between the actual and predicted field B performance was provided by the value of DEV, defined in Equation (III-25) (with N = 31). The calculations of the predicted pressures were performed with a time increment of 7 days and with various combinations of K_3 and K_2 values chosen as outlined in the method of Section III-C-1. Table V lists the observed field B data and the actual and predicted pressures and pore volumes (for $K_3 = 2.3 \times 10^{-5}$, $K_2 = 1000$) for the period November 30, 1957 - July 5, 1958 (31 weeks).

Figure 18 shows DEV plotted versus K_3 with K_2 as a parameter. These curves show that the agreement between the

TABLE V

SUMMARY OF FIELD B ACTUAL AND PREDICTED

PERFORMANCE FOR PERIOD NOVEMBER 30, 1957 - JULY 5, 1958

Date	MMcf In-Situ Gas* @ 14.65 Psia & 60°F	Reservoir Pressure*, Psia		Gas Bubble Pore Volume*, MMcf	
1957 Nov. 30	0	1060 d		0	
Dec. 7	5.092d	1075 d	1074.3p	.059d	.059p
Dec. 14	8.831d	1075.4d	1071.1p	.1025d	.103p
Dec. 21	15.747d	1088.2d	1079.7p	.180d	.182p
Dec. 28	20.722d	1084.9d	1075.2p	.238d	.241p
1958 Jan. 4	21.697d	1078.8d	1064.6p	.251d	.255p
Jan. 11	29.254d	1093.2d	1080.9p	.333d	.338p
Jan. 18	39.080d	1098.5d	1087.9p	.442d	.448p
Jan. 25	50.330d	1100.7d	1092.3p	.568d	.574p
1958 Feb. 1	69.512d	1206.9d	1111.2p	.702d	.776p
Feb. 8	109.747d	1222.4d	1157.5p	1.09 d	1.17 p
Feb. 15	110.990d	1103.9d	1089.9p	1.25 d	1.27 p
Feb. 22	110.990d	1088.5d	1070.9p	1.27 d	1.30 p
1958 Mar. 1	146.886d	1193.3d	1136.2p	1.50 d	1.60 p
Mar. 8	191.112d	1204.6d	1165.9p	1.93 d	2.01 p
Mar. 15	235.7 d	1202.8d	1174.9p	2.39 d	2.46 p
Mar. 22	254.715d	1166.8d	1140.2p	2.68 d	2.76 p
Mar. 29	310.842d	1203.6d	1181.1p	3.15 d	3.22 p
1958 Apr. 5	316.410d	1202.4d	1189.1p	3.67 d	3.72 p
Apr. 12	403.439d	1191.4d	1182.5p	4.14 d	4.18 p
Apr. 19	459.657d	1201.7d	1196.3p	4.67 d	4.69 p
Apr. 26	481.326d	1145 d	1165.1p	5.18 d	5.07 p
1958 May 3	497.766d	1143.2d	1143.5p	5.37 d	5.37 p
May 10	558.301d	1181.2d	1178.0p	5.79 d	5.81 p
May 17	617.3 d	1193.4d	1194.7p	6.32 d	6.31 p
May 24	657.215d	1180.8d	1186.4p	6.82 d	6.78 p
May 31	714.131d	1194.7d	1196.9p	7.30 d	7.29 p
1958 June 7	784.039d	1208.8d	1214.1p	7.90 d	7.86 p
June 14	850.387d	1207. d	1221.5p	8.59 d	8.46 p
June 21	925.87 d	1190.3d	1233.1p	9.51 d	9.11 p
June 28	1024.42 d	1238.9d	1256.6p	10.02 d	9.84 p
1958 July 5	1116.565d	1242.7d	1267.2p	10.88 d	10.62 p

* d denotes guantity obtained from field data.

* p denotes quantity predicted for $K_3 = 2.3 \times 10^{-5}$, $K_2 = 1000$.

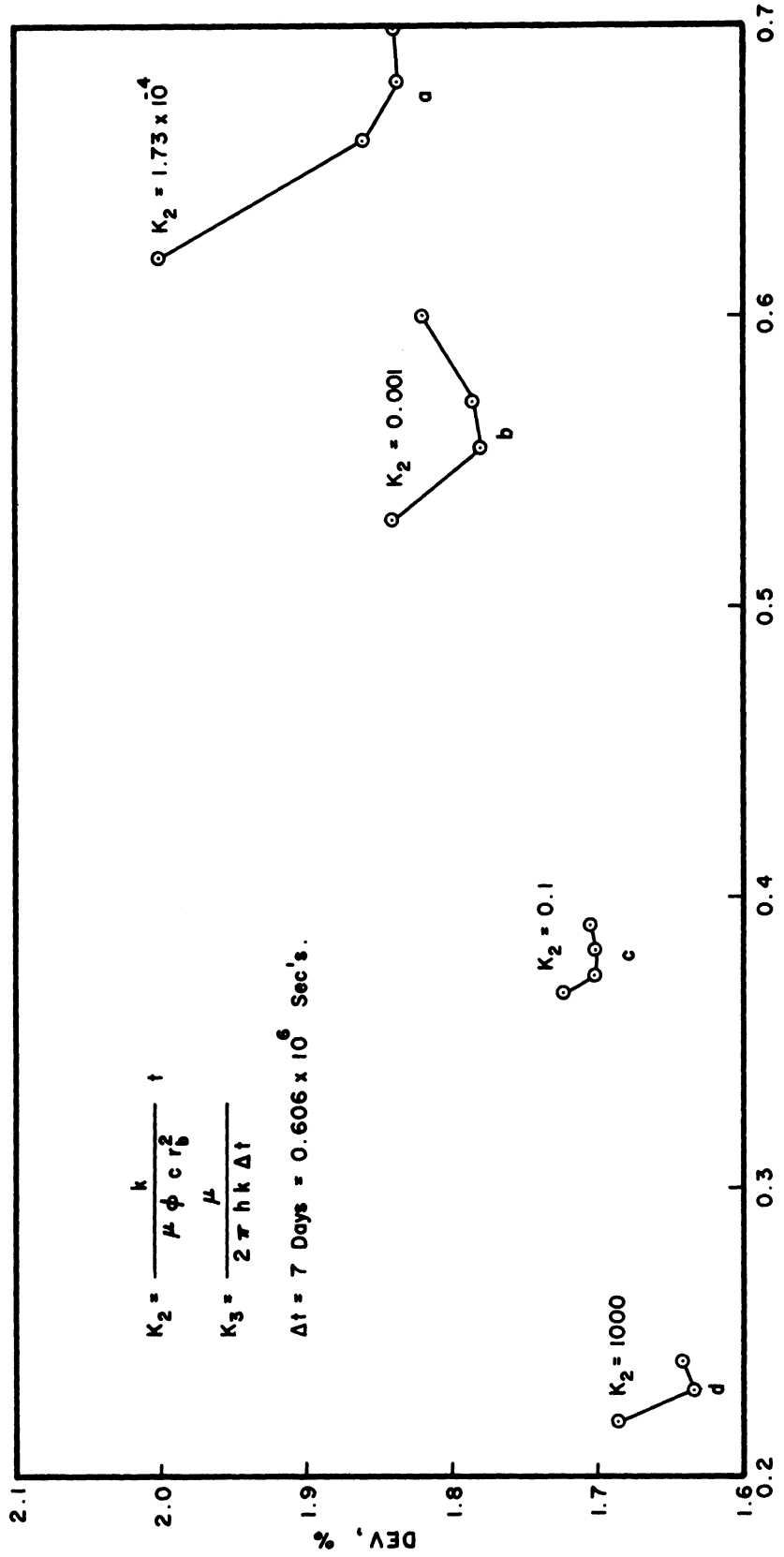

Dev vs. K_3 for Aquifer Storage Reservoir B.

Figure 18

predicted and observed field B pressures improves as K_3 is decreased and K_2 is increased. Thus application of the method of Section III-C-1 to field B does not yield a unique pair of K_3 and K_2 values corresponding to closest agreement between predicted and actual performance but yields increasingly better agreement as K_3 is decreased and K_2 increased.

Table VI lists the K_3, K_2, $K_3 \times K_2$, and DEV values corresponding to the points a, b, c, and d noted on Figure 18. It is of interest to compare the K_3 and K_2 values in Table VI with the following approximate K_3 and K_2 calculated from available data relating to h, φ, c, k/μ, and r_b:

$$K_3 = \frac{\mu}{2\pi hk\Delta t} = 9.55 \times 10^{-5} \text{ psia/ft}^3 \quad (\Delta t = 0.606 \times 10^6 \text{ sec's})$$

$$K_2 = \frac{k}{\mu \varphi c r_b^2} = 1.09 \times 10^{-5} \text{ sec's}^{-1}$$

The product $K_3 \times K_2$, tabulated in Table VI, varies widely with K_2 (or K_3). If $K_2 \times K_3$ were equal to a constant A, then the calculations involved in the method of Section III-C-1 would be greatly reduced since for every value of K_2 assumed, DEV would have to be calculated for only one K_3 value, namely $K_3 = A/K_2$.

Figures 19 and 20 compare the actual and predicted field B pressures as a function of time for pairs of K_3 and K_2 values corresponding to points d and b of Figure 18. The actual pressures are seen to fall below the predicted pressures as time increases; that is, the 'average' slope of the predicted pressure-time curve becomes greater than the 'average' slope

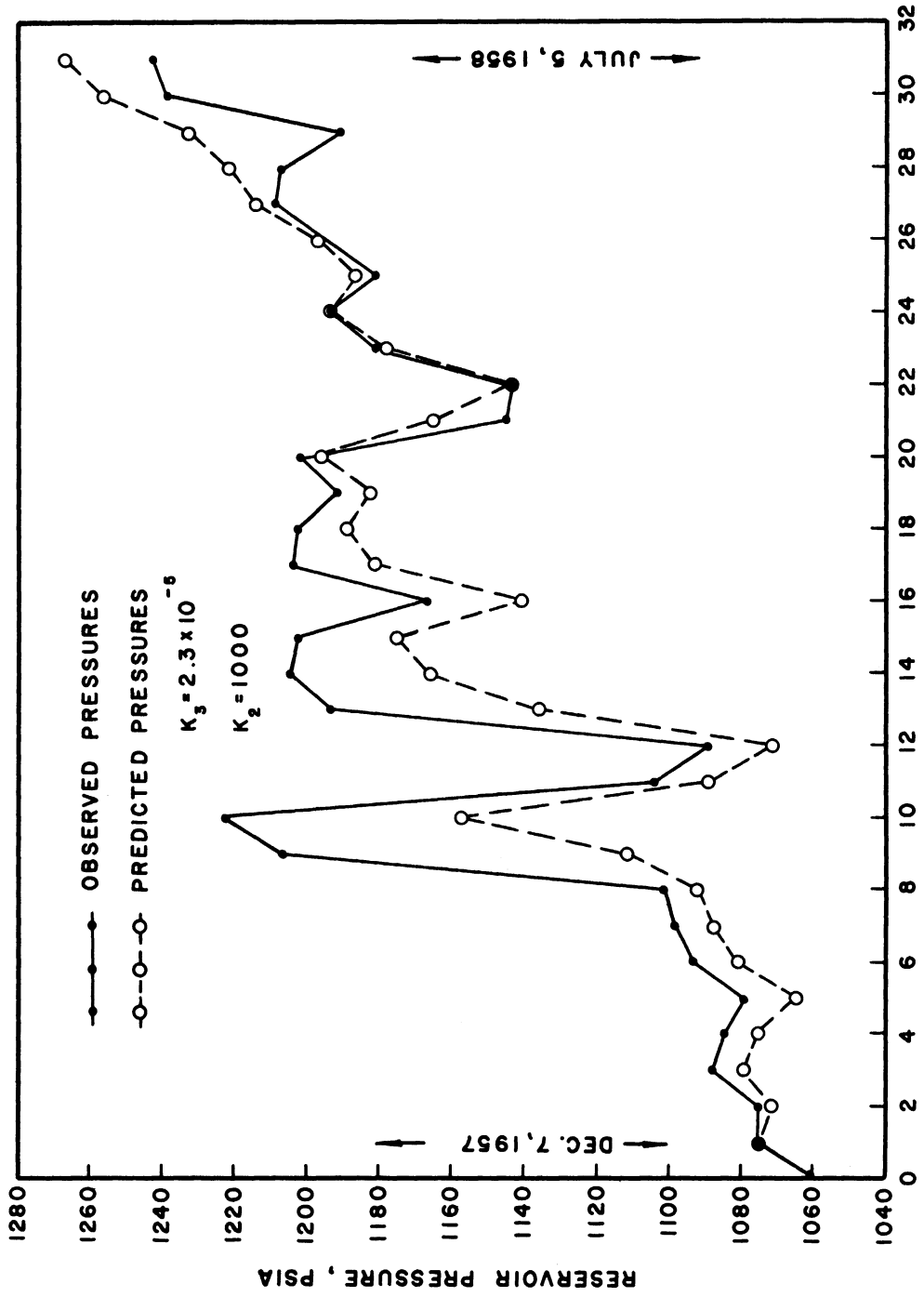

Field B Observed and Predicted Pressures vs. Time, November 30, 1957-July 5, 1958.

Figure 19

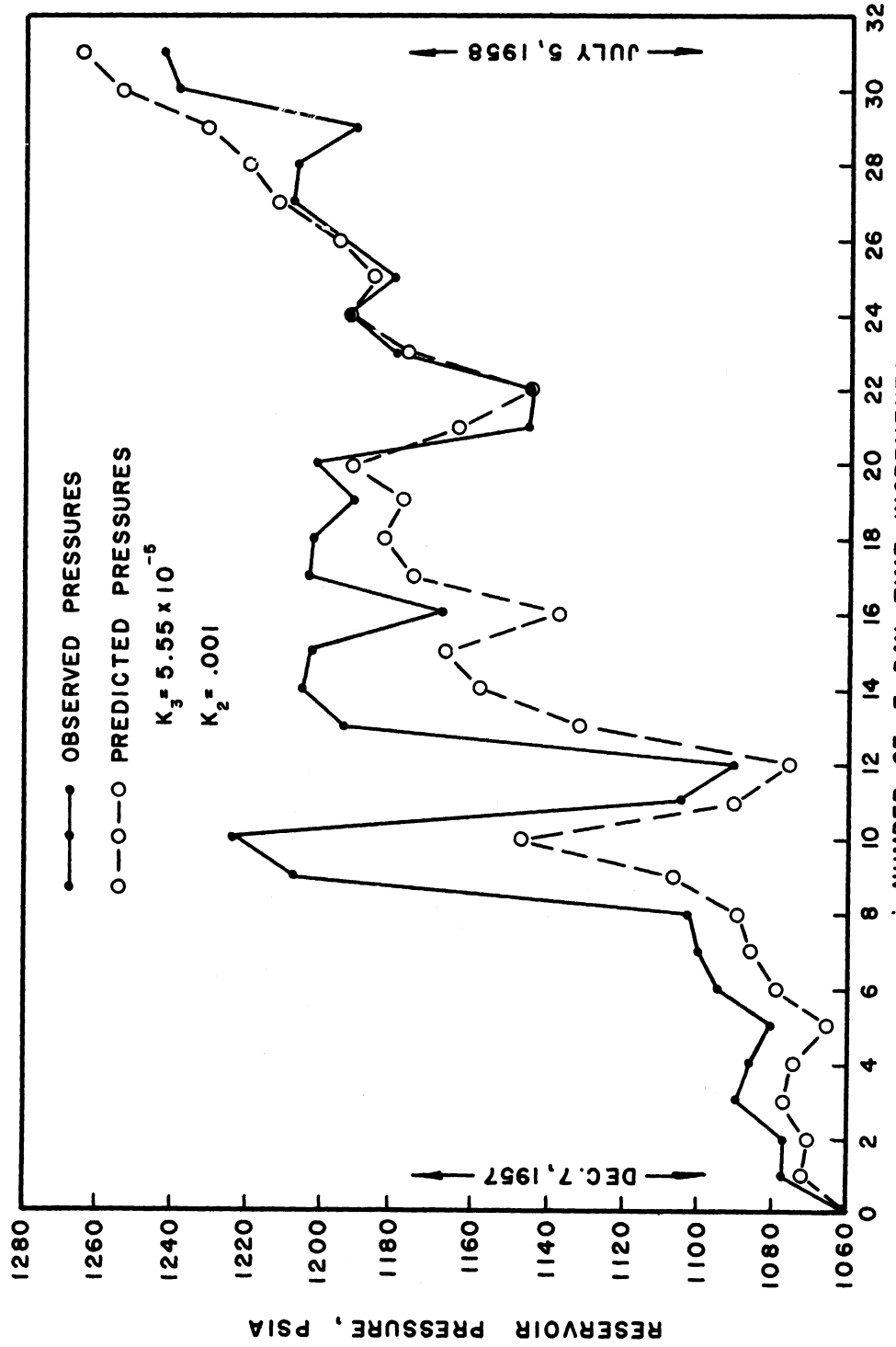

Field B Observed and Predicted Pressures vs. Time, November 30, 1957-July 5, 1958.

Figure 20

TABLE VI

$K_3 \times K_2$ AND DEV TABULATED AS A FUNCTION OF K_2 FOR FIELD B

Point on Fig. 18	K_2	K_3	$K_2 \times K_3$	DEV, %
a	1.73×10^{-4}	$.680 \times 10^{-4}$	1.18×10^{-8}	1.837
b	.001	$.555 \times 10^{-4}$	5.55×10^{-8}	1.782
c	.1	$.382 \times 10^{-4}$	3.82×10^{-6}	1.702
d	1000	$.230 \times 10^{-4}$	.023	1.633

of the actual pressure-time curve. All the pairs of K_3 and K_2 values employed resulted in an average predicted curve slope greater than the actual curve slope, although the former slope approached the latter more closely as K_3 was decreased and K_2 was increased. Figures 21 and 22 show the actual and predicted pore volumes as a function of time for combinations of K_3 and K_2 values corresponding to points d and b of Figure 18.

Thus the results of application of the method of Section III-C-1 to field B confirm the earlier conclusions (obtained above by analysis of the predictive equations) that the effect of an increasing gas bubble radius is a less rapid increase of the field pressure with time (relative to a gas field of constant radius) and that the predicted pressures of an aquifer storage reservoir increase more rapidly with time as K_3 is decreased and K_2 is increased.

The important conclusion to be obtained from the results reported in Figures 18 - 21 and Table VI is that application of the method described in Section III-C-1 to aquifer storage reservior B does not yield a unique pair of K_3 and K_2 values but yields increasingly better agreement between predicted and actual field performance as K_3 is decreased and K_2 is increased. The results plotted in Figure 18 show, however, that if the value of K_2 is fixed, application of the method of Section III-C-1 yields a unique K_3 value corresponding to a minimum DEV or best agreement between actual and predicted gas bubble performance.

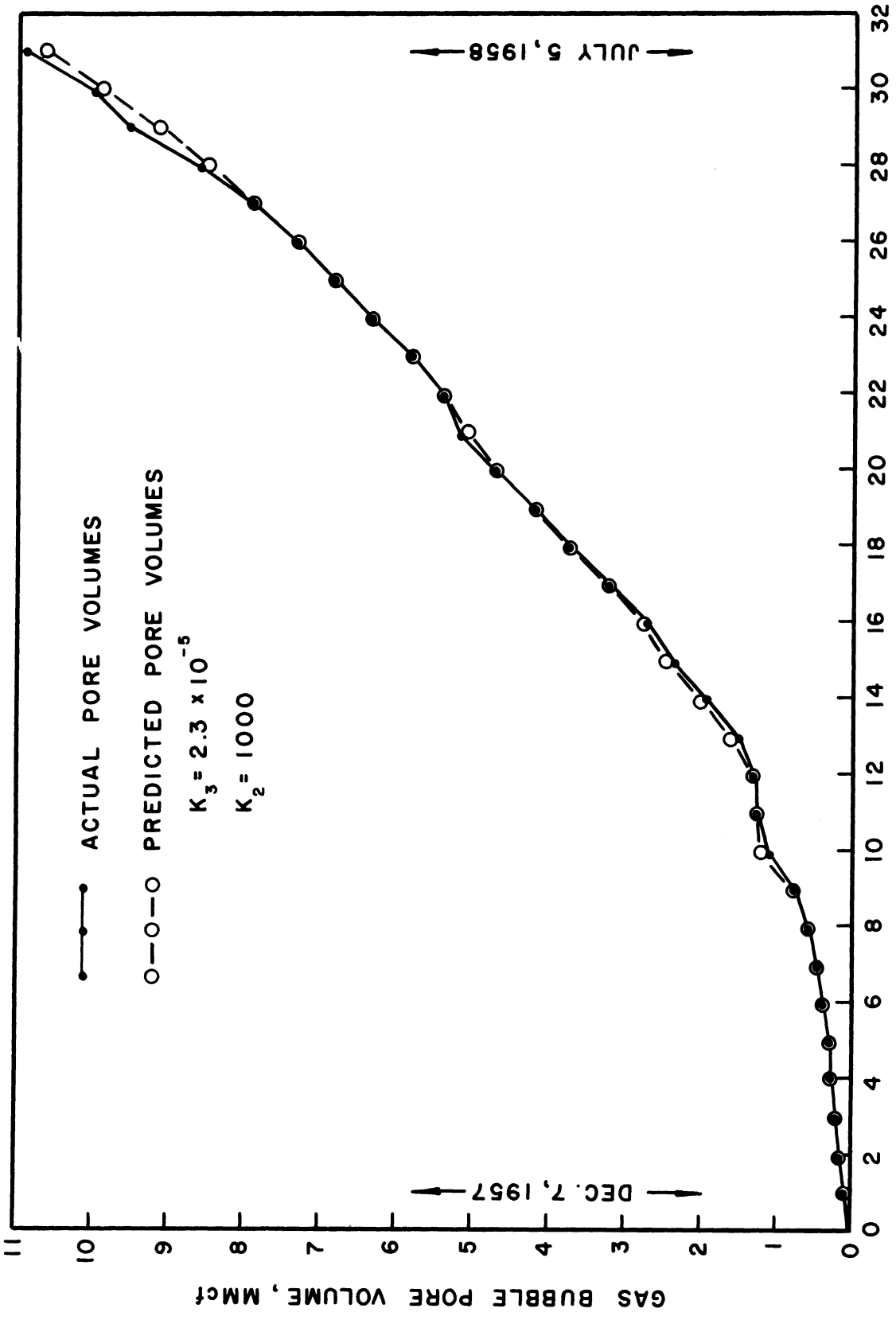

Figure 21. Field B Actual and Predicted Pore Volumes vs. Time, November 30, 1957-July 5, 1958.

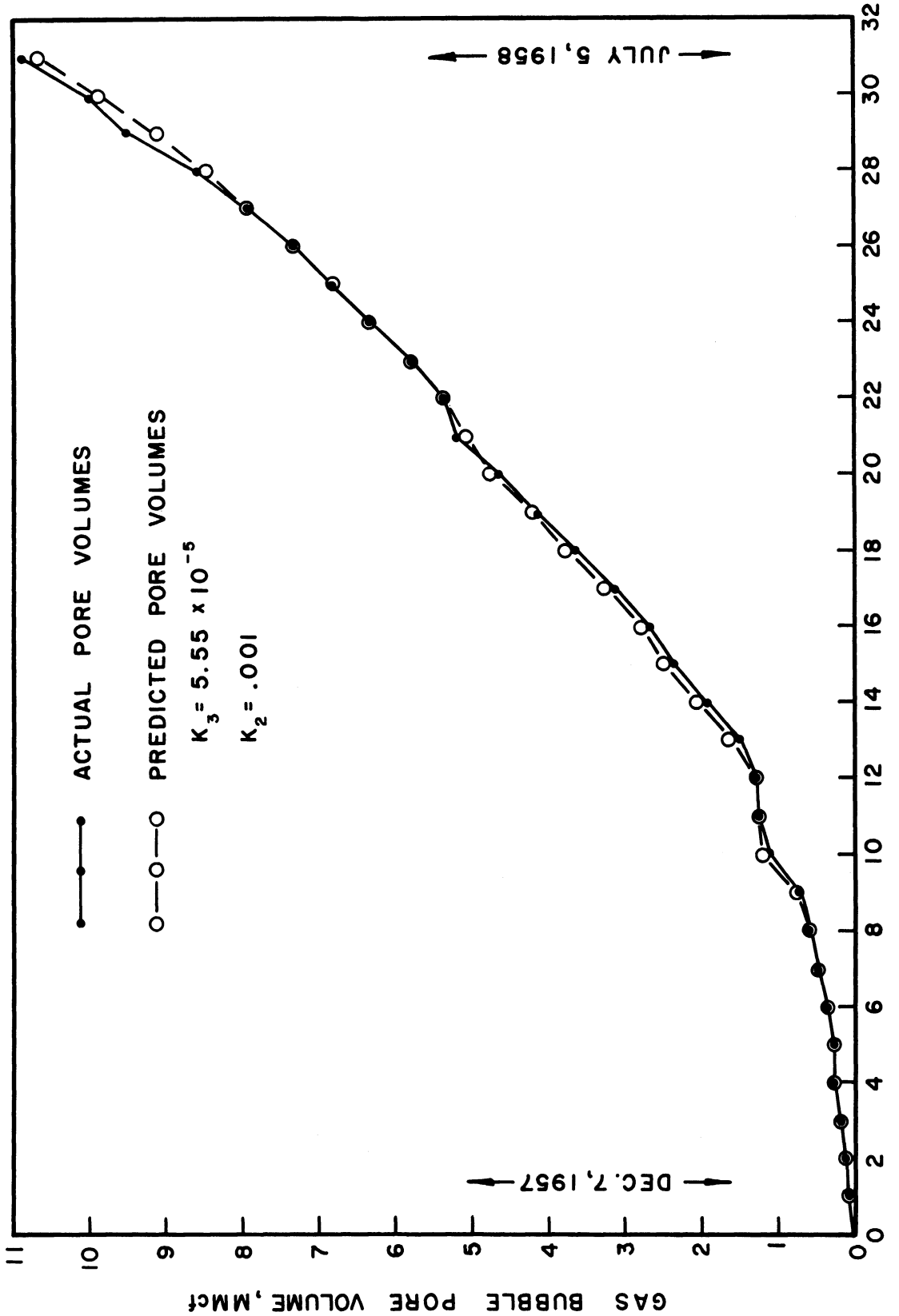

Figure 22. Field B Actual and Predicted Pore Volume vs. Time, November 30, 1957-July 5, 1958.

3. Errors in Predicted Water Influx and Pressure Drop Values Resulting from Errors in Reservoir Parameter Values

An ideal reservoir-aquifer system, satisfying all the assumptions on pages 8 and 9, is considered in this section. Errors associated with use of the variable pressure Equation (III-15) are first considered. The correct or actual values of the parameters K_1 ($= \pi h \phi c r_b^2$) and K_2 ($= k/\mu\phi c r_b^2$) for the ideal system are denoted by $(K_1)_c$ and $(K_2)_c$. $(Q_t)_c$ denotes the cumulative water influx calculated by inserting the $(K_1)_c$, $(K_2)_c$, and pressure schedule ΔP_i (considered known) values into the previously presented Equation (III-15);

$$Q_t = 2K_1 \sum_{i=0}^{i=j-1} \Delta P_i \, \bar{Q}_{(j-i)\Delta t_D} \qquad \text{(III-15)}$$

where $(j-i)\Delta t_D = (j-i)K_2\Delta t$ and $t = j\Delta t$. If $(Q_t)_e$ denotes the erroneous Q_t value calculated by inserting erroneous K_1 and K_2 values into Equation (III-15), then the fractional error in Q_t, E_{Q_t}, is

$$E_{Q_t} = \frac{|(Q_t)_c - (Q_t)_e|}{(Q_t)_c} = \frac{\Delta Q_t}{(Q_t)_c}$$

Now, since Q_t is directly proportional to K_1, the fractional error in Q_t caused by an erroneous K_1 value, $(K_1)_c + \Delta K_1$, is simply

$$(E_{Q_t})_{K_1} = \frac{\Delta K_1}{(K_1)_c} \qquad \text{(III-34)}$$

where $(E_{Q_t})_{K_1}$ denotes the fractional error in Q_t caused by use of an erroneous K_1 value and the correct K_2 value $(K_2)_c$.

For small errors in K_2, the fractional error in Q_t caused by an error in K_2 can be obtained from the truncated Taylor series form

$$(Q_t)_e - (Q_t)_c = \left(\frac{\partial Q_t}{\partial K_2}\right)_{(K_2)_c} \Delta K_2 \qquad \text{(III-35)}$$

where the erroneous K_2 value = $(K_2)_c + \Delta K_2$. $\partial Q_t/\partial K_2$ can be determined by differentiating both sides of Equation (III-15) with respect to K_2 to yield

$$\frac{\partial Q_t}{\partial K_2} = 2 \sum_{i=0}^{i=j-1} \Delta P_i \left(t_D \frac{d\bar{Q}_{t_D}}{dt_D}\right)_{(j-i)\Delta t_D} \qquad \text{(III-36)}$$

One thus obtains

$$(E_{Q_t})_{K_2} = \frac{|(Q_t)_c - (Q_t)_e|_{K_2}}{(Q_t)_c} = \frac{\sum_{i=0}^{i=j-1} \Delta P_i \left(t_D \frac{d\bar{Q}_{t_D}}{dt_D}\right)_{(j-i)\Delta t_D}}{\sum_{i=0}^{i=j-1} \Delta P_i \, \bar{Q}_{(j-i)\Delta t_D}} \frac{\Delta K_2}{(K_2)_c} \qquad \text{(III-37)}$$

where $(E_{Q_t})_{K_2}$ denotes the fractional error in Q_t caused by use of an erroneous K_2 value and the correct K_1 value $(K_1)_c$. Since $t_D \; d\bar{Q}_{t_D}/dt_D$ ranges from $0.7\bar{Q}_{t_D}$* for small t_D to $0.9\bar{Q}_{t_D}$* for large t_D, the percentage error in Q_t effected by an error in K_2 is 0.7 to 0.9 the percentage error in K_2.

The fractional errors in Q_t effected by erroneous h, k/μ, and $\varphi c r_b^2$ values can be determined, by proceeding in the manner employed above, as

$$(E_{Q_t})_h = \frac{\Delta h}{(h)_c} \qquad \text{(III-38)}$$

* These figures are calculated from tables of $\bar{Q}_{t_D}$ vs t_D given in References 1 and 2.

$$(E_{Q_t})_{k/\mu} = \frac{\sum_{i=0}^{i=j-1} \Delta P_i \left(t_D \frac{d\bar{Q}_{t_D}}{dt_D}\right)_{(j-i)\Delta t_D}}{\sum_{i=0}^{i=j-1} \Delta P_i \, \bar{Q}_{(j-i)\Delta t_D}} \frac{\Delta(k/\mu)}{(k/\mu)_c} \qquad \text{(III-39)}$$

$$(E_{Q_t})_{\phi c r_b^2} = \left[1 - \frac{\sum_{i=0}^{i=j-1} \Delta P_i \left(t_D \frac{d\bar{Q}_{t_D}}{dt_D}\right)_{(j-i)\Delta t_D}}{\sum_{i=0}^{i=j-1} \Delta P_i \, \bar{Q}_{(j-i)\Delta t_D}}\right] \frac{\Delta(\phi c r_b^2)}{(\phi c r_b^2)_c} \qquad \text{(III-40)}$$

The Equations (III-38) - (III-40) reveal that an x per cent error in h causes an x per cent error in Q_t, an x per cent error in k/μ causes an 0.7x (for small t_D) to 0.9x (for large t_D) per cent in Q_t, and an x per cent error in $\phi c r_b^2$ effects an 0.3x (for small t_D) to 0.1x (for large t_D) per cent error in Q_t. Thus an error in h causes the greatest error in Q_t while the same percentage error in k/μ causes a slightly smaller error in Q_t and the same error in $\phi c r_b^2$ effects a significantly smaller error in Q_t.

An approximate upper limit ('approximate' since all second and higher derivatives in the Taylor series are ignored) on the total fractional error in Q_t caused by errors in K_1 and K_2 is

$$E_{Q_t} \leq \left|(E_{Q_t})_{K_1}\right| + \left|(E_{Q_t})_{K_2}\right| = \frac{\Delta K_1}{(K_1)_c} + 0.9\frac{\Delta K_2}{(K_2)_c} \qquad \text{(III-41)}$$

The corresponding approximate upper limit on the total fractional error in Q_t caused by errors in h, k/μ, and $\phi c r_b^2$ is

$$E_{Q_t} \leq \frac{\Delta h}{(h)_c} + 0.9\frac{\Delta(k/\mu)}{(k/\mu)_c} + 0.3\frac{\Delta(\phi c r_b^2)}{(\phi c r_b^2)_c} \qquad \text{(III-42)}$$

Errors associated with use of the variable rate Equation (III-26) are now considered. The correct or actual value of K_3 ($= \mu/2\pi hk\Delta t$) is denoted by $(K_3)_c$ and $(\bar{P}_j)_c$ ($= (P_o - P_j)_c$) denotes the pressure drop calculated by inserting the $(K_3)_c$, $(K_2)_c$, and growth schedule ΔV_i values (considered specified or known) into Equation (III-26).

$$\bar{P}_j = P_o - P_j = K_3 \sum_{i=0}^{i=j-1} \Delta V_i \, \underline{P}_{(j-i)\Delta t_D} \qquad \text{(III-26)}$$

$$\Delta V_i = 2V_i - V_{i-1} - V_{i+1}$$

If $(\bar{P}_j)_e$ denotes the erroneous $\bar{P}_j$ value calculated by inserting erroneous K_3 and K_2 values into (III-26), then the fractional error in $\bar{P}_j$, $E_{\bar{P}_j}$, is

$$E_{\bar{P}_j} = \frac{|(\bar{P}_j)_c - (\bar{P}_j)_e|}{(\bar{P}_j)_c}$$

Now, since $\bar{P}_j$ is directly proportional to K_3, the fractional error in $\bar{P}_j$ caused by an erroneous K_3 value, $(K_3)_c + \Delta K_3$, is simply

$$(E_{\bar{P}_j})_{K_3} = \frac{\Delta K_3}{K_3} \qquad \text{(III-43)}$$

where $(E_{\bar{P}_j})_{K_3}$ denotes the fractional error in $\bar{P}_j$ caused by use of an erroneous K_3 value and the correct K_2 value $(K_2)_c$.

For small errors in K_2, the truncated Taylor series form similar to that given in (III-35) can be employed to

relate $(\bar{P}_j)_e$ to $(\bar{P}_j)_c$. The term $\partial\bar{P}_j/\partial K_2$ required in this Taylor series form can be obtained from Equation (III-26) as

$$\frac{\partial \bar{P}_j}{\partial K_2} = K_3 \sum_{i=0}^{i=j-1} \Delta V_i \left(\frac{d\underline{P}_{t_D}}{dt_D} \frac{dt_D}{dK_2} \right)_{(j-i)\Delta t_D}$$

$$= \frac{K_3}{K_2} \sum_{i=0}^{i=j-1} \Delta V_i \left(t_D \frac{d\underline{P}_{t_D}}{dt_D} \right)_{(j-i)\Delta t_D} \qquad \text{(III-44)}$$

Thus

$$(E_{\bar{P}_j})_{K_2} = \frac{\sum_{i=0}^{i=j-1} \Delta V_i \left(t_D \frac{d\underline{P}_{t_D}}{dt_D} \right)_{(j-i)\Delta t_D}}{\sum_{i=0}^{i=j-1} \Delta V_i \, \underline{P}_{(j-i)\Delta t_D}} \frac{\Delta K_2}{K_2} \qquad \text{(III-45)}$$

where $(E_{\bar{P}_j})_{K_2}$ denotes the fractional error in $\bar{P}_j$ caused by use of an erroneous K_2 value and the correct K_3 value $(K_3)_c$; the erroneous K_2 value = $(K_2)_c + \Delta K_2$. Now, since $t_D \; d\underline{P}_{t_D}/dt_D$ ranges from 0.5 $\underline{P}_{t_D}$* for small t_D (t_D .01) to less than .187 $\underline{P}_{t_D}$ for large t_D ($t_D \; d\underline{P}_{t_D}/dt_D$ = .187 $\underline{P}_{t_D}$ for t_D = 100, $t_D \; d\underline{P}_{t_D}/dt_D$ < .187 $\underline{P}_{t_D}$ for t_D > 100), the percentage error in $\bar{P}_j$ effected by an error in K_2 is 0.5 to .19 (or less) times the percentage error in K_2. Thus an approximate ('approximate' since all second and higher derivatives in the Taylor series are ignored) upper limit on the total error in $\bar{P}_j$ caused by errors in K_3 and K_2 is

$$E_{\bar{P}_j} \leq \frac{|\Delta K_3|}{(K_3)_c} + 0.5 \frac{|\Delta K_2|}{(K_2)_c} \qquad \text{(III-46)}$$

* This figure and the .187 $\underline{P}_{t_D}$ following were calculated from tables of $\underline{P}_{t_D}$ vs t_D given in Reference 1.

The fractional errors in $\bar{P}_j$ caused by erroneous h, k/μ, and $\phi c r_b^2$ values can be easily determined as

$$(E_{\bar{P}_j})_h = -\frac{\Delta h}{(h)_c} \qquad \text{(III-47)}$$

$$(E_{\bar{P}_j})_{k/\mu} = \left[\frac{\sum_{i=0}^{i=j-1} \Delta V_i \left(t_D \frac{dP_{t_D}}{dt_D}\right)_{(j-i)\Delta t_D}}{\sum_{i=0}^{i=j-1} \Delta V_i \, P_{(j-i)\Delta t_D}} - 1 \right] \frac{\Delta(k/\mu)}{(k/\mu)_c} \qquad \text{(III-48)}$$

$$(E_{\bar{P}_j})_{\phi c r_b^2} = -\left[\frac{\sum_{i=0}^{i=j-1} \Delta V_i \left(t_D \frac{dP_{t_D}}{dt_D}\right)_{(j-i)\Delta t_D}}{\sum_{i=0}^{i=j-1} \Delta V_i \, P_{(j-i)\Delta t_D}} \right] \frac{\Delta(\phi c r_b^2)}{(\phi c r_b^2)_c} \qquad \text{(III-49)}$$

Thus an x per cent error in h causes a -x per cent error in $\bar{P}_j$, an x per cent error in k/μ causes a -.5x per cent (for small t_D) to -x per cent (for very large t_D) error in $\bar{P}_j$, and an x per cent error in $\phi c r_b^2$ effects a -.5x per cent (for small t_D) or smaller (for large t_D) error in $\bar{P}_j$.

D. Effect of Reservoir Geometry on the Calculation of Water Encroachment Into the Gas Field

Water influx calculations reported in the literature invariably employ the two assumptions of planar (i.e., two-dimensional) liquid flow and circular geometry of the oil or gas reservoir. These assumptions are perhaps more necessary in formulating governing mathematical equations which can be solved analytically than they are justified by the geometry

or characteristics of actual reservoirs. For example, relatively few reservoirs conform closely to circular geometry. However, no solutions to the diffusivity equation, analogous to Van Everdingen and Hurst's tabular solutions for the radial flow case[1], have been presented in the literature for the case of a square or elliptic sink (or source) surrounded by a large liquid bearing porous medium. Mathematicians have in fact been unable to solve analytically the diffusivity equation, in one time and two space coordinates, in a planar region bounded internally and externally by concentric rectangles or in a region bounded internally by a rectangle and unbounded externally.

Perhaps the most practical and important question is not "Do actual reservoirs conform closely to the assumptions of planar flow or circular geometry?" but is "Does the actual performance of a reservoir which does not conform to these assumptions differ appreciably from the performance predicted by equations derived from the assumptions?". The calculations described in Section III-D-2, below, represent an attempt to answer this latter question with respect to the assumption of circular, reservoir geometry. The performance of an elliptically shaped reservoir, determined by numerical solution of the diffusivity equation in elliptic coordinates, is compared to the performance calculated by approximating the elliptic reservoir boundary as an 'equivalent' (e.g., equal area or equal perimeter) circle and employing the radial flow equations. Section III-D-1 presents an analytical solution to the diffusivity equation governing three dimensional liquid flow in an aquifer, i.e., governing the case where the aquifer formation is very thick and vertical flow effects may be significant.

1. Method of Treating Vertical Pressure Penetration into Aquifer

The previously presented Equation (III-5) governs the radial aquifer water flow in the reservoir-aquifer systems sketched in Figures 1a and 1b. Water flow in the neighborhood of a gas bubble situated on top of a very thick aquifer formation, as sketched in Figure 1c, however, will not be strictly radial, or horizontal, and will be governed by an equation accounting for a vertical as well as a horizontal pressure distribution.

a. Diffusivity Equation Including Vertical Pressure Distribution

The diffusivity equation in cylindrical coordinates, with the term $\partial^2 P/\partial z^2$ included to account for the vertical pressure distribution, appears as follows:

$$\frac{\partial^2 P}{\partial r^2} + \frac{1}{r}\frac{\partial P}{\partial r} + k_R \frac{\partial^2 P}{\partial z^2} = \frac{\mu \phi c}{k}\frac{\partial P}{\partial t} \qquad \text{(III-50)}$$

where k = permeability in horizontal direction, ft-lb_m/sec^2-psi

k_R = permeability in vertical direction/permeability in horizontal direction

z = vertical distance coordinate, ft.

Definition of the new variables

$$t_D = \frac{kt}{\mu \phi c r_b^2}$$

$$r_D = \frac{r}{r_b}$$

$$y = \frac{z}{r_b \sqrt{k_R}}$$

$$\bar{P}(r_D, y, t_D) = \frac{1}{r_b}\left[P_o(y) - P(r_D, y, t_D)\right] \qquad \text{(III-51)}$$

$P_o(y)$ = initial pressure with vertical gradient due to gravity alone, psia

transforms Equation (III-50) into (III-52) below.

$$\frac{\partial^2 \bar{P}}{\partial r_D^2} + \frac{1}{r_D}\frac{\partial \bar{P}}{\partial r_D} + \frac{\partial^2 \bar{P}}{\partial y^2} = \frac{\partial \bar{P}}{\partial t_D} \qquad \text{(III-52)}$$

The flow model represented by Equation (III-50) is shown in Figure 23. The vertical distance variable z is set equal to 0 at the upper impermeable plane covering the aquifer and set equal to h, the aquifer thickness, at the lower impermeable plane. The assumptions implicit in Equation (III-52) and made in formulating the boundary conditions, below, necessary for its solution, are

1) constant value of the gas bubble radius, r_b
2) uniform aquifer formation directional permeabilities in the horizontal and vertical directions of k and k_z ft-lb_m/sec^2-psi, respectively
3) uniform aquifer formation porosity
4) isothermal, unsteady state aquifer water flow
5) uniform rate of water influx into gas bubble over circular plane portion z = 0, $0 \leq r_D \leq 1$ (the rate may vary with time)

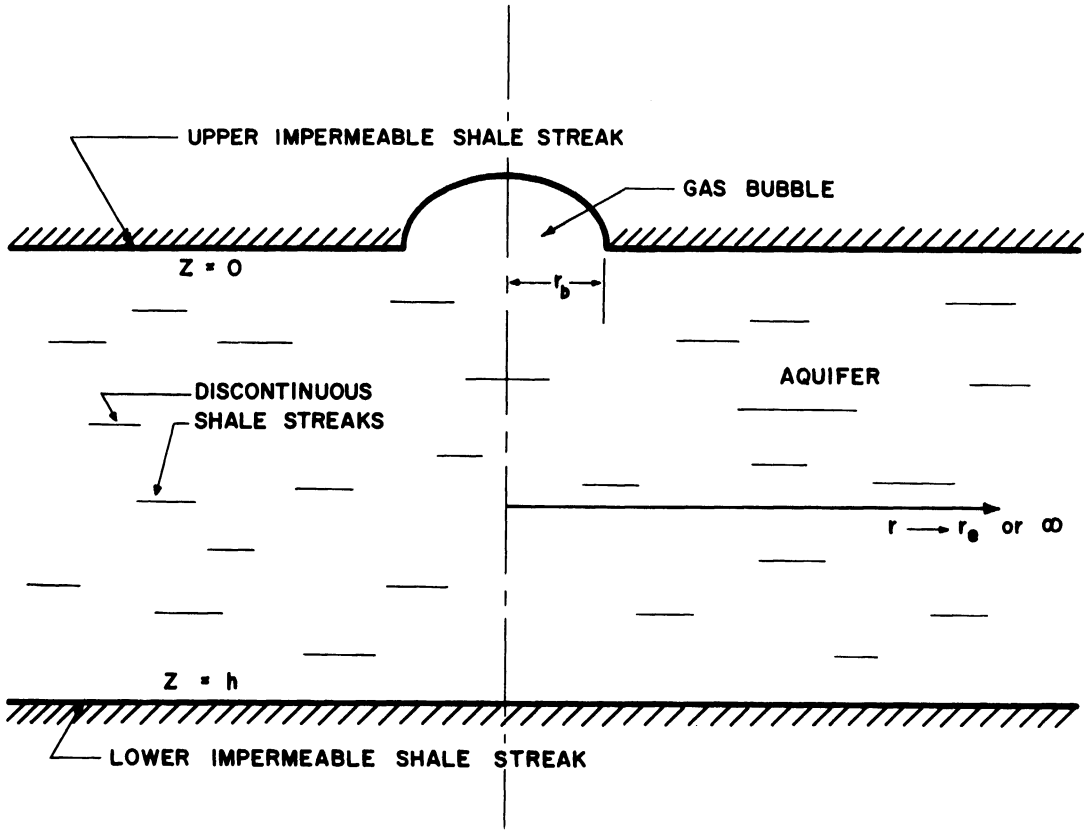

Vertical Pressure Penetration Flow Model.

Figure 23

6) initial aquifer pressure is a function of z only, in accordance with the pressure variance with depth induced by gravity.

b. Equation Governing Water Influx into Gas Bubble

Darcy's flow law relates the aquifer water velocity across the horizontal boundary $z = 0$, $0 \leq r_D \leq 1$, to the vertical pressure gradient as shown in Equation (III-53).

$$V = \frac{k_z}{\mu}\left[\frac{\partial}{\partial z}\left(P - \frac{\gamma}{144} z\right)\right]_{z=0} \qquad \text{(III-53)}$$

where k_z = aquifer formation permeability in vertical direction

The volumetric rate of water influx into the gas bubble, q, is then

$$q = VA = \pi r_b^2 V = \frac{\pi r_b^2 k_z}{\mu}\left[\frac{\partial}{\partial z}\left(P - \frac{\gamma}{144} z\right)\right]_{z=0} \qquad \text{(III-54)}$$

Now, from Equation (III-51),

$$\frac{\partial \bar{P}(r_D, y, t_D)}{\partial y} = -\frac{1}{r_b}\left[\frac{\partial P(r_D, y, t_D)}{\partial y} - \frac{\partial P_o(y)}{\partial y}\right]$$

and, employing the relations

$$\frac{\partial P}{\partial y} = r_b \sqrt{k_R}\,\frac{\partial P}{\partial z}$$

$$\frac{\partial P_o}{\partial y} = r_b \sqrt{k_R}\,\frac{\partial P_o}{\partial z} = r_b \sqrt{k_R}\,\frac{\gamma}{144}$$

one finds that

$$\frac{\partial \bar{P}(r_D, y, t_D)}{\partial y} = -\sqrt{k_R}\left[\frac{\partial P(r_D, y, t_D)}{\partial z} - \frac{\gamma}{144}\right],$$

or

$$\frac{\partial P(r_D, y, t_D)}{\partial z} = \frac{\gamma}{144} - \frac{1}{\sqrt{k_R}} \frac{\partial \bar{P}(r_D, y, t_D)}{\partial y} \qquad \text{(III-55)}$$

Substitution of $\frac{\partial P(r_D, y, t_D)}{\partial z}$ from (III-55) into (III-54) yields

$$q = -\frac{\pi r_b^2 k_z}{\mu \sqrt{k_R}} \left(\frac{\partial \bar{P}(r_D, y, t_D)}{\partial y} \right)_{y=0}$$

or

$$\left(\frac{\partial \bar{P}(r_D, y, t_D)}{\partial y} \right)_{y=0} = -\frac{q \mu \sqrt{k_R}}{\pi k_z r_b^2} \qquad \text{(III-56)}$$

Thus Equation (III-56) relates the volumetric rate of water influx into the gas bubble to the z-direction gradient of the dependent pressure variable in Equation (III-52).

c. Analytical Solution of the Developed Equations for the Vertical Pressure Penetration Flow Model

An analytical solution has been obtained to Equation (III-52) for the boundary and initial conditions given in Equations (III-57), (III-58), and (III-59) below.

$$\left(\frac{\partial \bar{P}(r_D, y, t_D)}{\partial y} \right)_{y = \frac{h}{r_b \sqrt{k_R}}} = 0 \qquad \text{(III-57)}$$

$$\left(\frac{\partial \bar{P}(r_D, y, t_D)}{\partial y} \right)_{y=0} = f(r_D) \begin{cases} f(r_D) = 0 & 1 < r_D < \infty \\ f(r_D) = -1 & 0 \leq r_D \leq 1 \end{cases} \qquad \text{(III-58)}$$

$$\bar{P}(r_D, y, 0) = 0 \qquad \text{(III-59)}$$

The condition (III-57) expresses the fact that the plane z = h is impermeable to water flow. (III-58) represents the condition that the upper limiting plane of the aquifer formation, z = 0, is impermeable with the exception of the circular portion of that plane covered by the gas bubble (see Figure 23). The gradient $\left(\frac{\partial \bar{P}(r_D, y, t_D)}{\partial y}\right)_{y=0}$ is set equal to -1 at this circular portion of the plane z = 0; Duhamel's superposition principle can be employed to transform the solution to Equation (III-52) satisfying condition (III-58) to a solution satisfying the condition

$$\left(\frac{\partial \bar{P}(r_D, y, t_D)}{\partial y}\right)_{y=0} = g(t_D) \qquad 0 \leq r_D \leq 1 \qquad \text{(III-60)}$$

where $g(t_D)$ is any semi-continuous function of dimensionless time, t_D. The initial condition (III-57) simply equates the initial pressure $P(r_D, y, 0)$ to the uniform (with exception of the gravity variation with z) pressure $P_o(y)$. The analytical solution to Equation (III-52) for the above boundary and initial conditions is given in Equation (III-61):

$$\bar{P}(r_D, 0, t_D) = \int_0^\infty \frac{J_1(\eta)}{\eta}\left[\coth M\eta - \frac{1}{M\eta}e^{-\eta^2 t_D} - \frac{2\eta}{M}\sum_{m=1}^{\infty}\frac{e^{-(\eta^2+\alpha_m^2)t_D}}{\eta^2+\alpha_m^2}\right] J_0(r_D\eta)\, d\eta \qquad \text{(III-61)}$$

where $M = \dfrac{h}{r_b\sqrt{k_R}}$

$\alpha_m = m\pi/M$

The reader is referred to Appendix II for the details of the development of this equation. The presented solution, $\bar{P}(r_D, 0, t_D)$, is related to the aquifer pressure at the upper limiting plane z = 0 by the previously given Equation (III-51).

Duhamel's principle, discussed in Section III of this thesis, can be employed in conjunction with Equation (III-61), above, to yield the gas bubble pressure corresponding to a variable water influx rate into the gas bubble:

$$P(1,0,t_D) = P_0(0) - \frac{\mu \sqrt{k_R}}{\pi k_z r_b} \sum_{i=0}^{i=j-1} \Delta q_i' \bar{P}(1,0,t_D) \qquad \text{(III-62)}$$

where $P_0(0)$ = the initial uniform pressure throughout the plane z = 0, psi

$P(1,0,t_D)$ = the gas bubble pressure at the circular boundary r = r_b, z = 0, psia

$\Delta q_i' = q_{i+1}' - q_i'$

q' = average rate of water influx into gas bubble during the time increment from $(i-1)\Delta t$ to $i\Delta t$, ft^3/sec.

$t_D = kt/\mu\phi c r_b^2$ = dimensionless time

$t = j\Delta t$, seconds

Δt = time increment chosen for purpose of approximating variable water influx rate, q, by a step function, seconds

$\bar{P}(1,0,t_D)$ = given by Equation (III-61) for $r_D = 1$

Numerical evalutation of the term $\overline{P}_{(1,0,t_D)}$ has not been performed owing to the lack of data from a gas field conforming to the vertical pressure penetration flow model described above.

2. Numerical Solution of Diffusivity Equation in Elliptic Coordinates

The studies reported in the literature of water encroachment into oil and gas reservoirs invariably involve approximation of the reservoir boundary by a circle. This approximation allows use of the solutions to the radial flow equations presented in the literature.[1,2] Nevertheless, the areal boundaries of a majority of the oil and gas fields can be better approximated by ellipses of appropriate eccentricity (> 0) than by circles. Thus the question arises as to whether a significant difference exists between the performance of an elliptically shaped reservoir, calculated from solutions to the diffusivity equation in elliptic coordinates, and the performance calculated by approximating the reservoir boundary as a circle and employing the radial flow equations. The present treatment of elliptic flow has been performed to answer this question.

The literature presents neither analytical nor numerical solutions to the diffusivity equation in elliptic coordinates. Several texts[14,15,16] discuss the Mathieu functions, which are involved in analytical solutions to this equation, but the authors do not provide solutions useful in applications of

interest here. Analytical methods are required to obtain general solutions which can be tabulated in dimensionless form as a function of dimensionless time. However, the analytical approach presents greater difficulties than those encountered in the numerical treatment. The developments and calculations described below are therefore performed only to determine whether there exists any need for general solutions to the elliptic flow diffusivity equation. For if the water flow quantities calculated from the elliptic equation can be duplicated closely by the quantities calculated (for an equivalent circle) from the radial flow equation, then analytical treatment of the former equation would be unnecessary.

The results obtained below are plotted in Figure 26 and show that significant error ($\lesssim 7\%$ in Q_t for small t_D) can be introduced into the influx quantity, Q_t, by approximating the elliptic reservoir as an equal area circle and employing the radial flow equations. Q_t is the cumulative water influx (ft^3) into a circular reservoir of area equal to that encompassed by the elliptic boundary considered. Q_{tE} is the influx into the elliptic reservoir, calculated by numerical solution of the elliptic flow diffusivity equation, as described below.

In the development given below, the flow model and assumptions concerning the aquifer formation and fluid properties are identical to the flow model described and assumptions given at the beginning of Section III, with the following exceptions:

Radial flow assumptions in Section III	Corresponding elliptic flow assumptions
The flow model is a thin circular disk having concentric circles as interior and exterior boundaries	The flow model is a thin elliptical disk having confocal ellipses as interior and exterior boundaries
r_b does not change with time	The position of the interior ellipse (gas bubble areal boundary) does not change with time

The diffusivity equation in elliptic coordinates is developed below and the equations describing liquid flow across an elliptic boundary are given. A numerical method of solution is then presented and employed to obtain dimensionless water influx quantities corresponding to the dimensionless quantities given by Van Everdingen and Hurst[1] in their "constant terminal pressure" radial flow case. The tabulated elliptic flow results are finally compared to Van Everdingen and Hurst's solution. Error and stability analyses of the numerical method are presented at the end of this section.

a. The diffusivity Equation in Elliptic Coordinates

The general form of the diffusivity equation governing unsteady state liquid flow through a porous medium is given by the previously presented Equation (III-4).

$$\nabla^2 P = \frac{\mu \phi c}{k} \frac{\partial P}{\partial t} \qquad \text{(III-4)}$$

The terms P, k/μ, φ, c, and t have been defined in Section III. The general expression for the three-dimensional Laplacian of a dependent variable in orthogonal curvilinear coordinates u, v, and w, is[3,7]

$$\nabla^2 P(u,v,w) = \frac{1}{\alpha\beta\gamma}\left[\frac{\partial}{\partial u}\left(\frac{\beta\gamma}{\alpha}\frac{\partial P}{\partial u}\right)+\frac{\partial}{\partial v}\left(\frac{\gamma\alpha}{\beta}\frac{\partial P}{\partial v}\right)+\frac{\partial}{\partial w}\left(\frac{\alpha\beta}{\gamma}\frac{\partial P}{\partial w}\right)\right] \quad \text{(III-63)}$$

where

$$\alpha = \sqrt{\left(\frac{\partial x}{\partial u}\right)^2+\left(\frac{\partial y}{\partial u}\right)^2+\left(\frac{\partial z}{\partial u}\right)^2} \quad \text{(III-64)}$$

$$\beta = \sqrt{\left(\frac{\partial x}{\partial v}\right)^2+\left(\frac{\partial y}{\partial v}\right)^2+\left(\frac{\partial z}{\partial v}\right)^2} \quad \text{(III-65)}$$

$$\gamma = \sqrt{\left(\frac{\partial x}{\partial w}\right)^2+\left(\frac{\partial y}{\partial w}\right)^2+\left(\frac{\partial z}{\partial w}\right)^2} \quad \text{(III-66)}$$

x, y, z = cartesian coordinates

The derivatives required in Equations (III-64), (III-65), and (III-66) can be obtained from the following relations between cartesian and elliptic coordinates

$$x = f \cosh u \cos v \quad \text{(III-67)}$$

$$y = f \sinh u \sin v \quad \text{(III-68)}$$

$$z = w \quad \text{(III-69)}$$

where the foci of the ellipse are at $x = \pm f$, $y = 0$, and u, v, and w are the elliptic cylinder coordinates. The geometric relationships between the cartesian planar

coordinates x and y and the elliptic planar coordinates u and v are shown in Figure 24. The vertical-direction elliptic cylinder coordinate is denoted by w. Differentiating Equations (III-67), (III-68), and (III-69) and inserting the resulting derivatives into (III-64), (III-65), and (III-66), one obtains

$$\left.\begin{aligned} \alpha &= f\sqrt{\cosh^2 u - \cos^2 v} \\ \beta &= \alpha \\ \gamma &= 1 \end{aligned}\right\} \qquad \text{(III-70)}$$

Insertion of these expressions for α, β, and γ into (III-63) then yields

$$\nabla^2 P(u,v,w) = \frac{1}{f^2(\cosh^2 u - \cos^2 v)}\left[\frac{\partial^2 P}{\partial u^2} + \frac{\partial^2 P}{\partial v^2} + f^2(\cosh^2 u - \cos^2 v)\frac{\partial^2 P}{\partial w^2}\right] \qquad \text{(III-71)}$$

This expression for the Laplacian of $P_{(u,v,w)}$ can be simplified by making use of the assumption (page 8) that the flow has no vertical component. This assumption is equivalent to the equality

$$\frac{\partial P(u,v,w)}{\partial w} = -\frac{\gamma}{144} \qquad \text{(III-72)}$$

where γ is the liquid specific weight, pounds force/cubic foot, since there is no liquid velocity component in the vertical direction. Since $\partial P/\partial w$ is equal to a constant $\partial^2 P/\partial w^2$ is equal to 0 and Equation (III-71) simplifies to

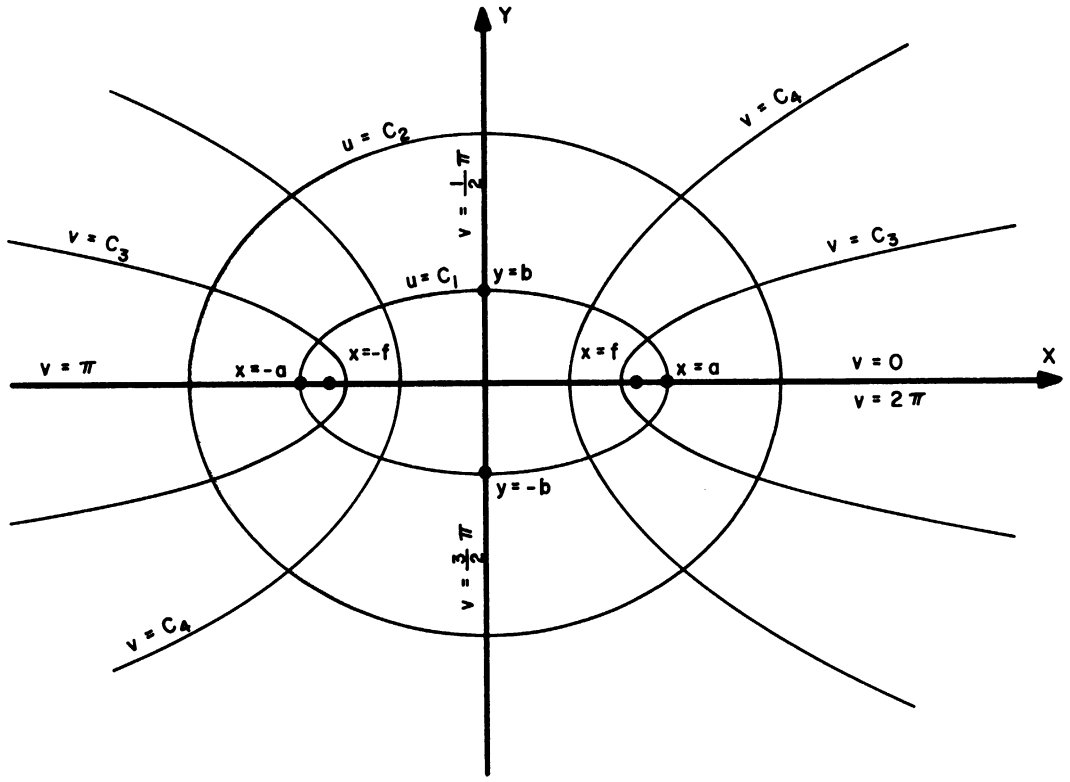

Geometric Relationships Between Cartesian and Elliptic Planar Coordinates.

Figure 24

$$\nabla^2 P(u,v,w) = \frac{1}{f^2(\cosh^2 u - \cos^2 v)}\left[\frac{\partial^2 P}{\partial u^2} + \frac{\partial^2 P}{\partial v^2}\right] \qquad \text{(III-73)}$$

Substituting $\nabla^2 P$ from (III-73) into (III-4), one obtains the diffusivity equation in elliptic coordinates

$$\frac{\partial^2 P}{\partial u^2} + \frac{\partial^2 P}{\partial v^2} = f^2(\cosh^2 u - \cos^2 v)\frac{\mu \phi c}{k}\frac{\partial P}{\partial t} \qquad \text{(III-74)}$$

b. Equations Describing Liquid Flow Across an Elliptic Boundary

Darcy's flow equation relates the superficial fluid velocity in a porous medium to the pressure gradient in the following manner,

$$\vec{V} = -\frac{k}{\mu}\vec{\nabla}\left(P + \frac{\gamma}{144} w\right) \qquad \text{(III-75)}$$

where $\vec{V}$ is the velocity vector, feet/second, γ is the liquid specific weight, and w is the vertical direction space coordinate, feet. The gradient of the dependent variable $P_{(u,v,w)}$ is expressed in the elliptic coordinates u, v, and w as

$$\vec{\nabla} P = \frac{1}{\alpha}\frac{\partial P}{\partial u}\vec{i} + \frac{1}{\beta}\frac{\partial P}{\partial v}\vec{j} + \frac{1}{\gamma}\frac{\partial P}{\partial w}\vec{k} \qquad \text{(III-76)}$$

where $\vec{i}$, $\vec{j}$, and $\vec{k}$ are the unit vectors in the u, v, and w directions, respectively. Substitution of the previously determined expressions for α, β, and γ into (III-76) yields

$$\vec{\nabla} P = \frac{1}{f\sqrt{\cosh^2 u - \cos^2 v}}\left[\frac{\partial P}{\partial u}\vec{i} + \frac{\partial P}{\partial v}\vec{j}\right] + \frac{\partial P}{\partial w}\vec{k} \qquad \text{(III-77)}$$

Equation (III-78) is obtained by inserting $\vec{VP}$, from (III-77), into (III-75).

$$\vec{V} = -\frac{k}{\mu}\left[\frac{1}{f\sqrt{\cosh^2 u - \cos^2 v}}\left(\frac{\partial P}{\partial u}\vec{i} + \frac{\partial P}{\partial v}\vec{j}\right) + \left(\frac{\partial P}{\partial w} + \frac{\gamma}{144}\right)\vec{k}\right] \qquad \text{(III-78)}$$

At any given point on an ellipse u = constant, the term $\partial P/\partial v\ \vec{j}$ is proportional to the velocity vector component in the v direction, or in the direction tangent to the ellipse at that point. This term can therefore be deleted from (III-78) since only the flow <u>across</u> an elliptic boundary is being considered here. Also, the term $(\partial P/\partial w + \gamma/144)\ \vec{k}$ in Equation (III-78) can be set equal to 0 since $\partial P/\partial w = -\gamma/144$, from Equation (III-72). Making these simplifications in (III-78), one obtains

$$V(v,t) = -\frac{k}{\mu}\left[\frac{1}{f\sqrt{\cosh^2 u - \cos^2 v}}\frac{\partial P}{\partial u}\right]_{u=C} \qquad \text{(III-79)}$$

where C = a constant

V = $V_{(v,t)}$ = fluid velocity in positive u direction across the elliptic boundary u = C, feet/second

The volumetric rate of liquid flow across an infinitesimal area element dA at the elliptic boundary is simply VdA or

$$dq = -\frac{k}{\mu}\left[\frac{dA}{f\sqrt{\cosh^2 u - \cos^2 v}}\frac{\partial P}{\partial u}\right]_{u=C} \qquad \text{(III-80)}$$

where dA = hds, feet^2

s = arc length on ellipse u = C, feet

$q = q_{(t)}$ = volumetric liquid flow rate across entire elliptic boundary $u = C$, feet^3/second

h = thickness of aquifer formation, or height of elliptic cylinder flow model, feet

ds is given on an ellipse by

$$ds = \beta dv = f\sqrt{\cosh^2 u - \cos^2 v}\, dv \qquad \text{(III-81)}$$

and substitution of $hf\sqrt{\cosh^2 u - \cos^2 v}$ for dA in Equation (III-80) yields

$$dq = -\frac{kh}{\mu}\left(\frac{\partial P}{\partial u}\right)_{u=C} dv \qquad \text{(III-82)}$$

q is now obtained by integrating dq over the ellipse from $v = 0$ to $v = 2\pi$.

$$q(t) = -\frac{kh}{\mu}\int_{v=0}^{v=2\pi}\left(\frac{\partial P}{\partial u}\right)_{u=C} dv \qquad \text{(III-83)}$$

However, because of obvious flow symmetry about the x and y axes (see Figure 24) the right side of Equation (III-83) can be multiplied by 4 and the integration carried out from $v = 0$ to $v = \pi/2$.

$$q(t) = -\frac{4kh}{\mu}\int_{v=0}^{v=\frac{\pi}{2}}\left(\frac{\partial P}{\partial u}\right)_{u=C} dv \qquad \text{(III-84)}$$

The cumulative volume of water which has flowed across the elliptic boundary up to time t, Q_{tE}, is given by

$$Q_{tE} = \int_0^t q(t)dt = -\frac{4kh}{\mu}\int_0^t\left[\int_0^{\frac{\pi}{2}}\left(\frac{\partial P}{\partial u}\right)_{u=C} dv\right]dt \qquad \text{(III-85)}$$

c. Numerical Method of Solving the Diffusivity Equation in Elliptic Coordinates

The first step in any numerical treatment of the diffusivity equation is the replacement of the derivatives in the equation by proper finite difference forms. The resulting difference equation is called 'explicit' or 'implicit' depending upon the time index attached to the difference forms of the spatial derivatives.[17,18] For example, consider the equation

$$\frac{\partial^2 P(x,t)}{\partial x^2} = \frac{\partial P(x,t)}{\partial t} \qquad \text{(III-86)}$$

The explicit difference form of (III-86) is

$$\frac{P_{m+1,i} - 2P_{m,i} + P_{m-1,i}}{(\Delta x)^2} = \frac{P_{m,i+1} - P_{m,i}}{\Delta t} \qquad \text{(III-87)}$$

where the spatial derivative $\partial^2 P/\partial x^2$ is replaced by a difference form of time index i. Thus the unknown value of P at time $t = (i+1)\Delta t$ can be determined explicitly in terms of known values of P at time $t = i\Delta t$. An implicit difference representation of (III-86) is

$$\frac{P_{m+1,i+1} - 2P_{m,i+1} + P_{m-1,i+1}}{(\Delta x)^2} = \frac{P_{m,i+1} - P_{m,i}}{\Delta t} \qquad \text{(III-88)}$$

Here the derivative $\partial^2 P/\partial x^2$ has been replaced by a difference form of time index i+1 and the unknown values of P at time $t = (i+1)\Delta t$ are bound together by a system of simultaneous equations. Thus the explicit form seems preferable to the

implicit in the respect that the former allows explicit calculation of the unknown P values while the latter form usually requires an iterative procedure to calculate P at time $t = (i+1)\Delta t$. However, the utility of the explicit form is severely restricted by the stability requirement[19] that

$$\Delta t \leqq \frac{(\Delta x)^2}{2}$$

If this restriction is violated then small errors arising at the beginning of the calculations grow and eventually become so large that the results are meaningless. This condition is commonly referred to as 'computational instability'. Thus if Δx is made small to reduce truncation error (i.e., error resulting from approximation of derivatives by finite difference forms) then Δt must be accordingly reduced, often to such small values that an impractical number of time steps must be employed to cover the desired time period. Bruce et al.[18] report that use of an explicit difference representation of the diffusivity equation governing unsteady state gas flow would entail 20,000 time steps to remove half the gas from the system they considered.

The implicit form, (III-88), on the other hand, is stable for any size time increment.[19] The disadvantage associated with the restriction on the size of Δt usually outweighs the disadvantages posed by the greater difficulty of solving the implicit difference equation. Thus the majority of the numerical treatments of the diffusivity equation reported in the literature employ the implicit form.

The numerical procedure presented here is a combination of the alternating-direction implicit method developed by Peaceman and Rachford[20] and a method given by Richtmyer.[21] Definition of the new variables

$$\bar{P}(u,v,t) = P_o - P(u,v,t)$$

$t_{DE} = kt/\mu\phi cf^2$ = dimensionless time for elliptic flow

simplifies Equation (III-74) to

$$\frac{\partial^2 \bar{P}}{\partial u^2} + \frac{\partial^2 \bar{P}}{\partial v^2} = (\cosh^2 u - \cos^2 v) \frac{\partial \bar{P}}{\partial t_{DE}} \qquad \text{(III-89)}$$

The alternating-direction method involves replacing, at odd numbered time steps, the derivative $\partial^2 P/\partial u^2$ by a difference form composed of the unknown values of $\bar{P}$ at time $t = (2i+1)\Delta t$ and the derivative $\partial^2 \bar{P}/\partial v^2$ by a difference form composed of known $\bar{P}$ values at time $t = 2i\Delta t$. At even numbered time steps, $\partial^2 \bar{P}/\partial u^2$ is replaced by a difference term involving known values of $\bar{P}$ at time $t = (2i+1)\Delta t$ and $\partial^2 \bar{P}/\partial v^2$ is replaced by a difference term involving unknown $\bar{P}$ values at time $t = (2i+2)\Delta t$. Thus the difference representation of (III-89) at odd numbered time steps [i.e., $t = (2i+1)\Delta t$] is

$$\frac{\bar{P}_{m+1,n,2i+1} - 2\bar{P}_{m,n,2i+1} + \bar{P}_{m-1,n,2i+1}}{(\Delta u)^2} + \frac{\bar{P}_{m,n+1,2i} - 2\bar{P}_{m,n,2i} + \bar{P}_{m,n-1,2i}}{(\Delta v)^2} \qquad \text{(III-90)}$$

$$= (\cosh^2 m\Delta u - \cos^2 n\Delta v)\left(\frac{\bar{P}_{m,n,2i+1} - \bar{P}_{m,n,2i}}{\Delta t_{DE}}\right)$$

and the representation of (III-89) at even numbered time steps [i.e., $t = (2i+2)\Delta t$] is

$$\frac{\bar{P}_{m+1,n,2i+1} - 2\bar{P}_{m,n,2i+1} + \bar{P}_{m-1,n,2i+1}}{(\Delta u)^2} + \frac{\bar{P}_{m,n+1,2i+2} - 2\bar{P}_{m,n,2i+2} + \bar{P}_{m,n-1,2i+2}}{(\Delta v)^2} \qquad \text{(III-91)}$$

$$= (\cosh^2 m\Delta u - \cos^2 n\Delta v)\left(\frac{\bar{P}_{m,n,2i+2} - \bar{P}_{m,n,2i+1}}{\Delta t_{DE}}\right)$$

where $\bar{P}_{m,n,i}$ = the value of $\bar{P}$ at $u = m\Delta u$, $v = n\Delta v$ and $t = i\Delta t$.

Equations (III-90) and (III-91) can be rearranged to (III-92) and (III-93), respectively, in which all the unknown values of $\bar{P}$ are on the left side of the equations,

$$\bar{P}_{m,n,2i+1}(f_{m,n}+2) - \bar{P}_{m+1,n,2i+1} - \bar{P}_{m-1,n,2i+1} = A_{m,n,2i} \qquad \text{(III-92)}$$

$$\bar{P}_{m,n,2i+2}(f_{m,n}+2R) - R(\bar{P}_{m,n+1,2i+2} + \bar{P}_{m,n-1,2i+2}) = B_{m,n,2i+1} \qquad \text{(III-93)}$$

where

$$f_{m,n} = \frac{(\Delta u)^2}{\Delta t_{DE}}(\cosh^2 m\Delta u - \cos^2 n\Delta v)$$

$$A_{m,n,2i} = \bar{P}_{m,n,2i}(f_{m,n} - 2R) + R(\bar{P}_{m,n+1,2i} + \bar{P}_{m,n-1,2i})$$

$$B_{m,n,2i+1} = \bar{P}_{m,n,2i+1}(f_{m,n} - 2) + \bar{P}_{m+1,n,2i+1} + \bar{P}_{m-1,n,2i+1}$$

$$R = \left(\frac{\Delta u}{\Delta v}\right)^2$$

The non-iternative or explicit method given by Richtmyer[21] for solving implicit difference equations systems involving one spatial variable is easily extended

to the case of Equations (III-92) and (III-93) involving the two spatial variables u and v. Consider, for the moment, Equation (III-92). Let us assume a relationship of the following kind between $\bar{P}_{m,n,2i+1}$ and $\bar{P}_{m+1,n,2i+1}$.

$$\bar{P}_{m,n,2i+1} = C_{m,n}\bar{P}_{m+1,n,2i+1} + D_{m,n} \qquad \text{(III-94)}$$

$C_{m,n}$ and $D_{m,n}$ are supposed to be functions of m and n, i.e., functions of u and v in the u-v planar grid. Then

$$\bar{P}_{m-1,n,2i+1} = C_{m-1,n}\bar{P}_{m,n,2i+1} + D_{m-1,n} \qquad \text{(III-95)}$$

and substitution of this expression for $\bar{P}_{m-1,n,2i+1}$ into Equation (III-92) yields

$$\bar{P}_{m,n,2i+1} = \frac{\bar{P}_{m+1,n,2i+1}}{f_{m,n} + 2 - C_{m-1,n}} + \frac{D_{m-1,n} + A_{m,n,2i}}{f_{m,n} + 2 - C_{m-1,n}} \qquad \text{(III-96)}$$

Comparison of (III-96) with (III-94) shows that

$$\left.\begin{aligned} C_{m,n} &= \frac{1}{f_{m,n} + 2 - C_{m-1,n}} \\ \text{and} \qquad D_{m,n} &= \frac{D_{m-1,n} + A_{m,n,2i}}{f_{m,n} + 2 - C_{m-1,n}} \end{aligned}\right\} \qquad \text{(III-97)}$$

Similarly, assuming that

$$\bar{P}_{m,n,2i+2} = E_{m,n}\bar{P}_{m,n+1,2i+2} + F_{m,n} \qquad \text{(III-98)}$$

one finds

$$\left.\begin{aligned} E_{m,n} &= \frac{1}{\frac{1}{R} f_{m,n} + 2 - E_{m,n-1}} \\ \text{and} \qquad F_{m,n} &= \frac{R F_{m,n-1} + B_{m,n,2i+1}}{f_{m,n} + 2R - R E_{m,n-1}} \end{aligned}\right\} \qquad \text{(III-99)}$$

The recursive relationships (III-97) and (III-99) allow explicit calculation of all $C_{m,n}$ and $D_{m,n}$ at odd numbered time steps [$A_{m,n,2i}$ is known at odd numbered time steps when $\overline{P}$ at $t = (2i+1)\Delta t$ is being determined] and $E_{m,n}$ and $F_{m,n}$ at even numbered time steps ($B_{m,n,2i+1}$ is known at these time steps) if starting values of these coefficients can be obtained. After the values of these coefficients are known, the pressures $\overline{P}_{m,n,2i+1}$ and $\overline{P}_{m,n,2i+2}$ can be calculated explicitly from Equations (III-94) and (III-98), respectively.

Attention is now given to the boundary conditions since these conditions must be employed to obtain the starting values of $C_{m,n}$, $D_{m,n}$, $E_{m,n}$, and $F_{m,n}$. Since the liquid flow is obviously symmetrical about the x and y axes, as seen from Figure 24, only the quadrant of the plane from $v = 0$ to $v = \pi/2$ need be considered. The boundaries of the flow model in this quadrant are characterized by the following m and n index values:

on the gas field ellipse: $u = u_b$ and $m = M_o = u_b/\Delta u$

on the aquifer exterior boundary: $u = u_e$ and $m = M_e = (u_e - 1/2\ \Delta u)/\Delta u$

on the positive x axis, $x > a$ (see Figure 24): $v = 0$ and $n = N_o = 0/\Delta v = 0$

on the positive y axis, $y > b$ (see Figure 24): $v = \pi/2$ and $n = \dfrac{\pi/2}{\Delta v} = N_e$

Because of the flow symmetry about the x and y axes, the gradient of the pressure in the v direction is 0 at v = 0 and v = $\pi/2$. If the aquifer exterior boundary ($u = u_e$) is assumed closed (i.e., no flow across exterior boundary), the initial pressure is assumed equal to P_o, and if the pressure is dropped by unity at $u = u_b$ for $t > 0$, then the initial and boundary conditions become

$$\left(\frac{\partial \bar{P}(u,v,t)}{\partial v}\right)_{v=0} = 0$$

$$\left(\frac{\partial \bar{P}(u,v,t)}{\partial v}\right)_{v=\frac{\pi}{2}} = 0$$

$$\left(\frac{\partial \bar{P}(u,v,t)}{\partial u}\right)_{u=u_e} = 0$$

$$\bar{P}(u,v,0) = P_o - P(u,v,0) = 0$$

$$\bar{P}(u_b,v,t) = 1$$

When expressed in difference form these conditions are

$$\bar{P}_{m,0,i} = \bar{P}_{m,-1,i} \qquad \text{(III-100)}$$

$$\bar{P}_{m,N_e+1,i} = \bar{P}_{m,N_e,i} \qquad \text{(III-101)}$$

$$\bar{P}_{M_e,n,i} = \bar{P}_{M_e+1,n,i} \qquad \text{(III-102)}$$

$$\bar{P}_{m,n,0} = 0 \qquad \text{(III-103)}$$

$$\bar{P}_{M_o,n,i} = 1 \qquad \text{(III-104)}$$

Since $\bar{P}_{M_e,n,i} = \bar{P}_{M_e+1,n,i}$, the effective position of the exterior boundary is at $u = (M_e + 1/2)\Delta u$; this is the reason that M_e was chosen above as $(u_e - 1/2\Delta u)/\Delta u$ rather than as $u_e/\Delta u$.

The starting values of $C_{m,n}$ and $D_{m,n}$ are now obtained in the following manner. Letting $m = M_o + 1$ in Equation (III-92) and inserting the value $\bar{P}_{M_o,n,2i+1} = 1$ [from Equation (III-104)], one obtains

$$\bar{P}_{M_o+1,n,2i+1} = \frac{\bar{P}_{M_o+2,n,2i+1}}{f_{M_o+1,n}+2} + \frac{1 + A_{M_o+1,n,2i}}{f_{M_o+1,n}+2} \qquad \text{(III-105)}$$

Comparison of (III-105) with (III-94) yields

$$\left.\begin{aligned} C_{M_o+1,n} &= \frac{1}{f_{M_o+1,n}+2} \\ D_{M_o+1,n} &= \frac{1 + A_{M_o+1,n,2i}}{f_{M_o+1,n}+2} \end{aligned}\right\} \qquad \text{(III-106)}$$

Equations (III-97), in conjunction with (III-106), now allow explicit calculation of $C_{m,n}$ and $D_{m,n}$ for $m = M_o + 2, M_o + 3, \ldots, M_e$, and for $n = 0, 1, 2, \ldots, N_e$. At the exterior boundary, $u = u_e$, we have from Equations (III-102) and (III-94),

$$\bar{P}_{M_e+1,n,2i+1} = \bar{P}_{M_e,n,2i+1} = C_{M_e,n}\bar{P}_{M_e+1,n,2i+1} + D_{M_e,n}$$

or

$$\bar{P}_{M_e,n,2i+1} = \frac{D_{M_e,n}}{1 - C_{M_e,n}} \qquad \text{(III-107)}$$

After the value of $\bar{P}_{M_e,n,2i+1}$ is calculated from (III-107), the values of $\bar{P}_{m,n,2i+1}$, for $m = M_e - 1, M_e - 2, \ldots, M_o + 1$ (and for $n = 0, 1, 2, \ldots, N_e$), can be explicitly calculated from Equation (III-94).

The starting $E_{m,n}$ and $F_{m,n}$ values can be obtained by letting $n = 0$ in (III-93) and setting $\bar{P}_{m,-1,2i+2}$ equal

to $P_{m,o,2i+2}$ [from Equation (III-100)], to obtain

$$\bar{P}_{m,o,2i+2} = \frac{R}{f_{m,o}+R}\bar{P}_{m,1,2i+2} + \frac{B_{m,o,2i+1}}{f_{m,o}+R}$$

which, by comparison with (III-98), yields

$$\left.\begin{aligned} E_{m,o} &= \frac{R}{f_{m,o}+R} \\ F_{m,o} &= \frac{B_{m,o,2i+1}}{f_{m,o}+R} \end{aligned}\right\} \qquad \text{(III-108)}$$

The starting values $E_{m,o}$ and $F_{m,o}$ and the recursive relationships (III-99) now allow calculation of $E_{m,n}$ and $F_{m,n}$ for $m = M_o + 1, M_o + 2, \ldots, M_e$, and for $n = 0, 1, 2, \ldots, N_e$. At the upper boundary $v = \pi/2$, we have from Equations (III-101), (III-98), and (III-93),

$$\bar{P}_{m,N_e,2i+2} = E_{m,N_e}\bar{P}_{m,N_e+1,2i+2} + F_{m,N_e}$$

and

$$\bar{P}_{m,N_e,2i+2} = \bar{P}_{m,N_e+1,2i+2}$$

Eliminating $\bar{P}_{m,N_e+1,2i+2}$ from these two equations, one obtains

$$\bar{P}_{m,N_e,2i+2} = \frac{F_{m,N_e}}{1-E_{m,N_e}} \qquad \text{(III-109)}$$

After $\bar{P}_{m,N_e,2i+2}$ is calculated from (III-109), the values of $\bar{P}_{m,n,2i+2}$ for all m and $n = N_e - 1, N_e - 2, \ldots, 0$, can be calculated from (III-98).

At each time step the calculated $\bar{P}$ values can be employed in the determination of a quantity, $\bar{Q}_{t_{DE}}$, defined as

$$\bar{Q}_{t_{DE}} = \int_0^{t_{DE}} \bar{q}(t_{DE})\,dt_{DE} \qquad \text{(III-110)}$$

where

$$\bar{q}(t_{DE}) = -\int_0^{\frac{\pi}{2}} \left(\frac{\partial \bar{P}(u,v,t_{DE})}{\partial u}\right)_{u=u_b} dv \qquad \text{(III-111)}$$

Simpson's rule of numerical integration can be employed to yield

$$\bar{q}(t_{DE}) = -\frac{\Delta v}{3}\left[\left(\frac{\partial \bar{P}}{\partial u}\right)_{v=0} + 4\left(\frac{\partial \bar{P}}{\partial u}\right)_{v=\Delta v} + 2\left(\frac{\partial \bar{P}}{\partial u}\right)_{v=2\Delta v}\right. \qquad \text{(III-112)}$$

$$\left. + 4\left(\frac{\partial \bar{P}}{\partial u}\right)_{v=3\Delta v} + \text{-----} + 4\left(\frac{\partial \bar{P}}{\partial u}\right)_{v=(N_e-1)\Delta v} + \left(\frac{\partial \bar{P}}{\partial u}\right)_{v=N_e\Delta v}\right]_{u=u_b}$$

or, expressing the derivatives $\partial\bar{P}/\partial u$ by differences,

$$\bar{q}(t_{DE}) = \frac{\Delta v}{3\Delta u}\left[(1-\bar{P}_{M_o+1,0,i}) + 4(1-\bar{P}_{M_o+1,1,i}) + \text{- - - -} + (1-\bar{P}_{M_o+1,N_e,i})\right] \qquad \text{(III-113)}$$

since $\left(\frac{\partial \bar{P}}{\partial u}\right)_{u=u_b} = -\frac{\bar{P}_{M_o,n,i} - \bar{P}_{M_o+1,n,i}}{\Delta u}$ and $\bar{P}_{M_o,n,i} = 1$, from the boundary condition (III-104).

The values of $\bar{q}$ at successive time steps, determined by inserting the calculated values of $\bar{P}_{M_o+1,n,i}$ into (III-113) can then be employed to determine $\bar{Q}_{t_{DE}}$ by a Simpson's integration as

$$\bar{Q}_{j\Delta t_{DE}} = \frac{\Delta t_{DE}}{3}\left[\bar{q}(0) + 4\bar{q}(\Delta t_{DE}) + 2\bar{q}(2\Delta t_{DE})\right. \qquad \text{(III-114)}$$

$$\left. + 4\bar{q}(3\Delta t_{DE}) + \text{---} + 4\bar{q}((j-1)\Delta t_{DE}) + \bar{q}(j\Delta t_{DE})\right]$$

The term $\bar{Q}_{t_{DE}}$ or $\bar{Q}_{j\Delta t_{DE}}$ is the dimensionless production quantity, for elliptic flow, corresponding to the dimensionless production quantity $\bar{Q}_{t_D}$, for radial flow, tabulated by Van Everdingen and Hurst.[1]

d. Comparison Between Elliptic and Radial Flow

The above described numerical method has been employed to calculate the water influx into an elliptic cylinder sink having an eccentricity of 0.925 or a ratio of 2.63 between the major and minor axes. The exterior boundary of the flow model was specified as a confocal ellipse encompassing an area equal to 101.3 times the area of the inner ellipse. The boundary conditions employed in the solution are given in Equations (III-100) - (III-104).

The variable u ranged from a value of 0.4 (corresponding to an eccentricity of 0.925) on the interior ellipse to 2.6 on the exterior boundary. Since the area of an ellipse is πab, where

$$a = \text{semi-major axis} = f(\cosh(u))$$

$$b = \text{semi-minor axis} = f(\sinh(u)),$$

the ratio between the areas of the exterior and interior ellipses is $\frac{\cosh(2.6)\sinh(2.6)}{\cosh(.4)\ \sinh(.4)}$ or 101.3. (The ratio of the area included within the exterior boundary of a flow model to that included within the interior boundary is designated hereafter as the 'area ratio'.) The variable v ranged from 0 to $\pi/2$, covering the first quadrant, (see Figure 24), and dimensionless time, t_{DE}, was varied from 0 to 426 in increments of the following values:

t_{DE}	Δt_{DE}
0-1	.01
1-9	.05
9-26	.1
26-106	.5
106-426	1

A Δu increment of .08 and a Δv of .098175 were employed in the numerical solution. The calculations were programmed in the FORTRAN code and carried out by an IBM 704 digital computer.

The calculated values of $\overline{Q}_{t_{DE}}$ [see Equation (III-110)] are listed in Table VII and plotted in Figure 25 as a function of dimensionless time. The latter figure shows that, for all practical purposes, a steady state or asymptotic value of $\overline{Q}_{t_{DE}}$ is attained at $t_{DE} = 200$.

Figure 25 also shows $\overline{Q}_{t_D}$, the dimensionless influx quantity tabulated in the literature[1,2] for the constant pressure radial flow case, plotted versus time. These $\overline{Q}_{t_D}$ values were calculated[1] for a circular cylinder flow model having an exterior radius 10 times the interior radius; that is, the area ratio for the flow model is 100. The difference between the 100 and 101.3 area ratios for the radial and elliptic flow models is taken into account in the comparison developed below. The boundary conditions employed by Van Everdingen and Hurst[1] in obtaining the $\overline{Q}_{t_D}$ values are identical to those used here in solving

TABLE VII

$\bar{Q}_{t_{DE}}$ AS A FUNCTION OF DIMENSIONLESS TIME t_{DE}

$$t_{DE} = \frac{kt}{\mu\phi c f^2}$$

$\Delta v = .098175$

Δt_{DE} = given on page 103 of Thesis

$\Delta u = .08$

t_{DE}	$\bar{Q}_{t_{DE}}$	$\left(100 \times \frac{\Delta\bar{Q}_{t_{DE}}}{\bar{Q}_{t_{DE}}}\right)^*$	t_{DE}	$\bar{Q}_{t_{DE}}$	$\left(100 \times \frac{\Delta\bar{Q}_{t_{DE}}}{\bar{Q}_{t_{DE}}}\right)^*$
0	0		90	32.58599	
.1	.47584	4.4	95	32.92836	
.5	1.29198	1.9	100	33.22521	
1	1.98924	.99	110	33.70573	
2	3.16138		120	34.06693	
3	4.18009	.51	130	34.33840	
4	5.11626	.50	140	34.54244	
6	6.83881	.43	150	34.69578	.33
8	8.42793		160	34.81102	
10	9.91663	.36	170	34.89761	
15	13.27534		180	34.96267	.33
20	16.18515	.31	190	35.01154	
25	18.70798		200	35.04821	
30	20.89547		220	35.09638	
35	22.79213		240	35.12344	
40	24.43662	.30	260	35.13860	.33
45	25.86248		280	35.14701	
50	27.09876	.30	300	35.15162	
55	28.17068		320	35.15404	
60	29.10009		340	35.15523	.33
65	29.90592		360	35.15574	
70	30.60462		380	35.15587	
75	31.21043		400	35.15587	.33
80	31.73569	.31	420	35.15587	.33
85	32.19112				

* $100 \times \frac{\Delta\bar{Q}_{t_{DE}}}{\bar{Q}_{t_{DE}}}$ = maximum % error in $\bar{Q}_{t_{DE}}$, calculated from Equation (III-124)

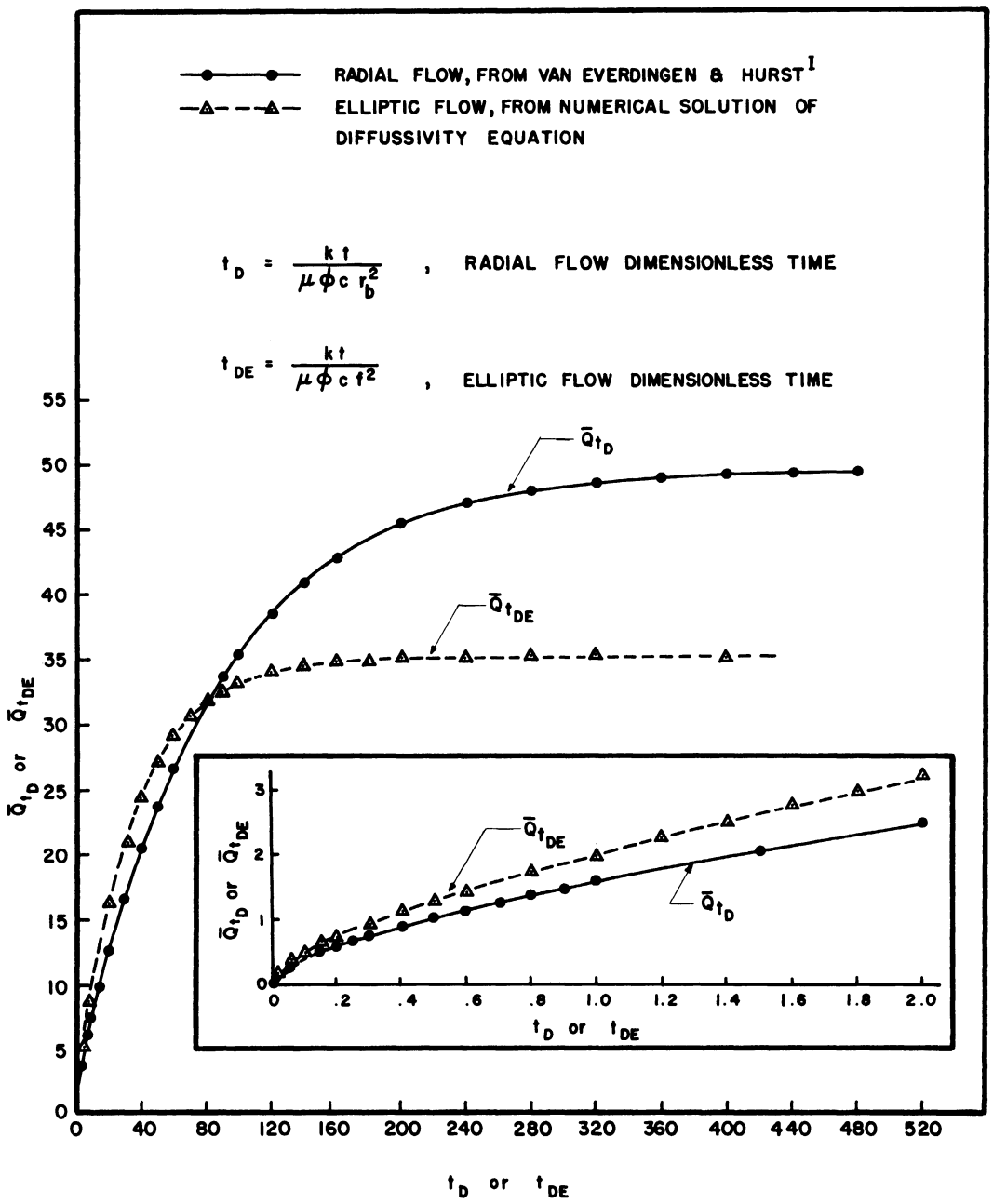

$\bar{Q}_{t_D}$ and $\bar{Q}_{t_{DE}}$ vs Dimensionless Time.

Figure 25

the elliptic flow diffusivity equation, namely an initial pressure drop of 0, a closed exterior boundary, and a pressure drop of 1 for all time at the interior boundary.

In order to compare the radial flow with elliptic flow, one must establish some basis of comparison. This basis cannot be the distance between the exterior and interior flow model boundaries since the elliptic model has no single characteristic dimension analogous to the radius of the circular model. The comparison has therefore been made on a basis of equal areas encompassed by the exterior ellipse and the exterior circle and equal areas included within the interior ellipse and the interior circle. Thus each flow model contains the same volume (or mass) of water. The equality between the areas included within the interior boundaries yields the relationship

$$\pi r_b^2 = \pi f^2 \cosh u_b \sinh u_b$$

where r_b = radius of inner boundary of circular cylinder flow model

u_b = value of u on inner ellipse of elliptic cylinder flow model.

Since $u_b = .4$, one obtains

$$r_b^2 = f^2 \cosh(.4) \sinh(.4) = 0.445 f^2 \qquad \text{(III-115)}$$

Equation (III-115) is employed in relating t_{DE} to t_D as

$$t_D = \frac{kt}{\mu\phi c r_b^2} = \frac{kt}{.445\mu\phi c f^2} = 2.245 \frac{kt}{\mu\phi c f^2} = 2.245\, t_{DE} \qquad \text{(III-116)}$$

Thus corresponding $\bar{Q}_{t_D}$ and $\bar{Q}_{t_{DE}}$ values should be taken at $t_D = 2.245\ t_{DE}$ rather than at $t_D = t_{DE}$.

The actual cumulative water influx across the inner elliptic boundary is related to $\bar{Q}_{t_{DE}}$ in the following manner.

$$Q_{tE} = 4h\phi c f^2 \Delta P \bar{Q}_{t_{DE}} \qquad \text{(III-117)}$$

Q_{tE} = total volume of water influx across inner elliptic boundary at time t, ft^3

ΔP = pressure drop at inner elliptic boundary, psi

h = thickness or height of elliptic cylinder flow model, ft.

f foci of ellipse are at $x = \pm f$, $y = 0$ (see Figure 24)

The actual volume of water influx into the inner circular sink of the radial flow model is related to $\bar{Q}_{t_D}$ as[1]

$$Q_t = 2\pi h\phi c r_b^2 \Delta P \bar{Q}_{t_D} \qquad \text{(III-118)}$$

Q_t = total volume of water influx into circular sink of radius r_b, at time t, ft^3

h = thickness or height of circular cylinder flow model, ft.

Thus a comparison between the actual water flow into the elliptic sink and that calculated by approximating the

ellipse as an equal area circle and employing the radial flow equation is afforded by the ratio

$$\frac{Q_t}{Q_{tE}} = \frac{\pi r_b^2}{2f^2} \frac{\bar{Q}_{t_D}}{\bar{Q}_{t_{DE}}} = 0.699 \frac{\bar{Q}_{t_D}}{\bar{Q}_{t_{DE}}} \qquad \text{(III-119)}$$

where $t_D = 2.245 t_{DE}$. The relation $Q_t/Q_{tE} = 1$ would denote exact duplication of the elliptic flow results by radial flow quantities calculated for an inner circular boundary including an area equal to that included by the inner elliptic boundary.

The ratio Q_t/Q_{tE} is listed in Table VIII and plotted in Figure 26 as a function of dimensionless time t_{DE}. This plot is actually a band rather than a line because of errors in the calculated $\bar{Q}_{t_{DE}}$ values and in the $\bar{Q}_{t_D}$ values. Error in the latter quantity arises from the fact that the literature does not contain $\bar{Q}_{t_D}$ values corresponding to an area ratio of 101.3. Thus available $\bar{Q}_{t_D}$ for a ratio of 100 were employed in calculating the points plotted as circles in Figure 26; a band of sufficient width to include the difference between the $\bar{Q}_{t_D}$ for ratios of 100 and 101.3 was then drawn through the points. The determination of the various errors which are included within this band is discussed below.

Figure 26 shows that application of radial flow calculations to the elliptic cylinder flow model described above results in errors of the order of 7% in Q_t for small dimensionless time t_{DE}. The error decreases as dimensionless time increases and approaches 0 (i.e., Q_t/Q_{tE} approaches

TABLE VIII

Q_t/Q_{t_E} AS A FUNCTION OF DIMENSIONLESS TIME t_{DE}

$$\frac{Q_t}{Q_{t_E}} = .699 \frac{\bar{Q}_{t_D}}{\bar{Q}_{t_{DE}}}$$

$$t_D = 2.245\ t_{DE}$$

t_{DE}	$\bar{Q}_{t_{DE}}$	t_D	$\bar{Q}_{t_D}$*	Q_t/Q_{t_E}	Max. Neg. Error $\left(\frac{-100 \times}{\Delta Q_{t_{DE}}/Q_{t_{DE}}}\right)$**	Max. Pos. Error	$\left(\frac{\Delta \bar{Q}_{t_D}}{\bar{Q}_{t_D}}\right)$* x 100
1	1.9892	2.245	2.636	.928	- .185	+ .99	
3	4.1800	6.75	5.598	.936	- .185	+ .51	
6	6.8388	13.5	9.213	.944	- .185	+ .43	
10	9.9166	22.45	13.416	.948	- .185	+ .36	.04
20	16.1852	45	22.09	.955	- .185	+ .31	.09
50	27.0988	112.1	37.31	.965	- .185	+ .30	.28
80	31.7357	180	44.21	.975	- .185	+ .31	.46
110	33.7057	247	47.12	.98	- .185	+ .32	.62
140	34.5424	314.3	48.45	.982	- .185	+ .33	.84
170	34.8976	382	49.03	.984	- .185	+ .33	.99
200	35.0482	450	49.30	.985	- .185	+ .33	1.17
230	35.1119	516	49.5	.986	- .185	+ .33	1.31
400	35.1559	900	50.15***	.999	- .185	+ .33	0

* The listed $\bar{Q}_{t_D}$ values were calculated[1] for an area ratio of 100;
$\Delta\bar{Q}_{t_D} = (\bar{Q}_{t_D})_{101.3} - (\bar{Q}_{t_D})_{100}$

** $\Delta\bar{Q}_{t_{DE}}$ was calculated from Equation (III-124).

***This $\bar{Q}_{t_D}$ value corresponds to an area ratio of 101.3.

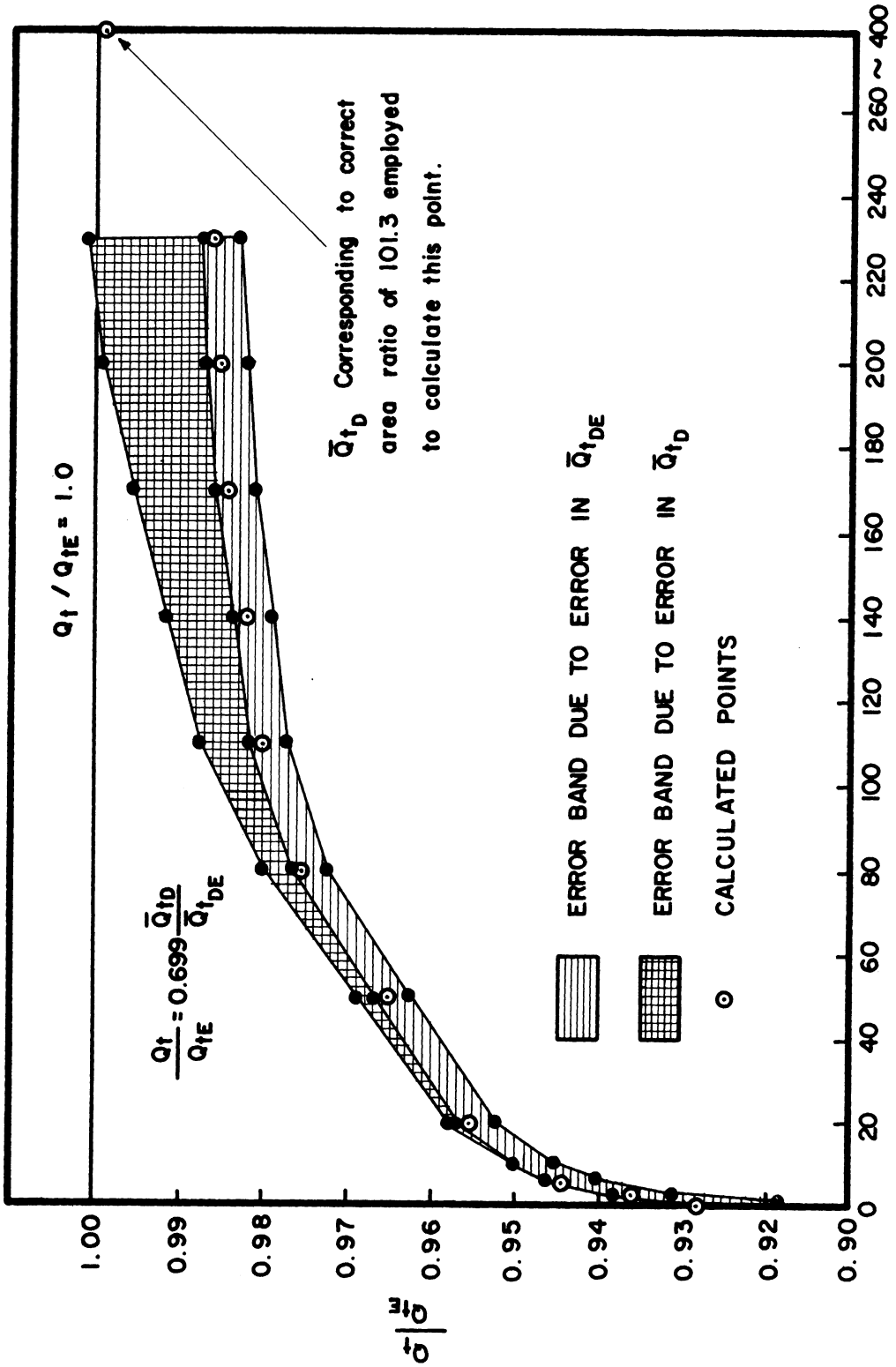

Figure 26. Comparison Between Elliptic and Radial Flow.

1.0) for large time. This approach of Q_t/Q_{tE} to 1 as t_D or t_{DE} grows large is a good check on the accuracy of the calculated $\bar{Q}_{t_{DE}}$ values, since for large time the pressure drop approaches a steady-state uniform value of 1 and the total expansion of the (equal) volumes of water in both flow models (i.e., the cumulative influx Q_t or Q_{tE} into the inner sinks) should be identical. The circle plotted on Figure 26 at the far right ($t_{DE} = 400$) is the only point in this figure calculated from a $\bar{Q}_{t_D}$ value corresponding to an area ratio of 101.3 (the other points are calculated from $\bar{Q}_{t_D}$ values corresponding to an area ratio of 100). The reason for this fact is that the large-time or asymptotic $\bar{Q}_{t_D}$ value can be exactly determined for any given area ratio as[1]

$$(\bar{Q}_{t_D})_{asymptotic} = \frac{(r_e/r_b)^2 - 1}{2}$$

Thus $(\bar{Q}_{t_D})$ asymptotic equals 50.15 for an area ratio $(r_e/r_b)^2$ of 101.3 and employment of this value in the ratio $Q_t/Q_{tE} = .7\bar{Q}_{t_D}/\bar{Q}_{t_{DE}}$ yields the plotted (Figure 26) value of 0.999.

From Figure 26 the conclusion can be drawn that the error incurred by applying radial flow calculations to elliptic gas storage reservoirs is inversely proportional to the magnitude of the t_D values employed in the calculations (for $t_D \geq 1$). For example, suppose an elliptically shaped reservoir (with a finite, impervious exterior boundary) is approximated by an equal area circle and

Equation (III-15a) is employed to calculate the water influx, Q_t, for 20 time steps. Then the error in Q_t will be larger if the range of t_D values, for the time period concerned, is 0 - 20, with a Δt_D of 1, than if the range is 0 - 1000, with a Δt_D of 50. This fact is evidenced by the curve plotted in Figure 26, since the error in the calculated Q_t value is larger for small t_D than for large t_D. The fact that the error in Q_t ranges approximately from 7% to 2% for intermediate t_D from 2.245 ($t_{DE} = 1$) to 224.5 ($t_{DE} = 100$) indicates that a need exists for analytical solution of the elliptic flow diffusivity equation for larger (i.e., more practical) aquifer/reservoir volume ratios.

e. Error Analysis

Error in the ratio $Q_t/Q_{tE} = .699\ \bar{Q}_{t_D}/\bar{Q}_{t_{DE}}$ is caused by errors in the $\bar{Q}_{t_D}$ values employed and in the $\bar{Q}_{t_{DE}}$ values calculated as described above. Thus if $\Delta\bar{Q}_{t_{DE}}$ denotes the error in $\bar{Q}_{t_{DE}}$ and $\Delta\bar{Q}_{t_D}$ the error in $\bar{Q}_{t_D}$, the error in the ratio Q_t/Q_{tE} will be

$$\Delta\left(\frac{Q_t}{Q_{tE}}\right) = .699\left[\frac{\bar{Q}_{t_D}}{\bar{Q}_{t_{DE}}} \times \frac{\Delta\bar{Q}_{t_D}}{\bar{Q}_{t_D}} - \frac{\bar{Q}_{t_D}}{\bar{Q}_{t_{DE}}} \times \frac{\Delta\bar{Q}_{t_{DE}}}{\bar{Q}_{t_{DE}}}\right]$$

Thus the percentage error in Q_t/Q_{tE} is

$$\frac{\Delta(Q_t/Q_{tE})}{Q_t/Q_{tE}} \times 100 = \left(\frac{\Delta\bar{Q}_{t_D}}{\bar{Q}_{t_D}} - \frac{\Delta\bar{Q}_{t_{DE}}}{\bar{Q}_{t_{DE}}}\right) \times 100 \qquad \text{(III-120)}$$

or the difference between the percentage errors in $\bar{Q}_{t_D}$ and $\bar{Q}_{t_{DE}}$. The error components $\Delta\bar{Q}_{t_D}/\bar{Q}_{t_D}$ and $\Delta\bar{Q}_{t_{DE}}/\bar{Q}_{t_{DE}}$ have

been calculated, as described below, and are listed separately in Table VIII.

Errors in the calculated $\bar{Q}_{t_{DE}}$ values arise from truncation and computer round-off error. Truncation error is introduced by approximation of the differential Equation (III-74) by the difference Equations (III-90) and (III-91). Round-off error is caused by the fact that the computer carries only a finite number of digits. An upper limit on the round-off error is estimated in Appendix III as .00185 $\bar{Q}_{t_{DE}}$. A truncation error analysis based on a method given by Scarborough[22] is also described in Appendix III. This analysis yields the relation

$$\bar{Q}^{**}_{t_{DE}} - \bar{Q}_{t_{DE}} = A(\Delta u)^2 + B\Delta v + C\Delta t_{DE} \qquad \text{(III-121)}$$

where $\bar{Q}^{**}_{t_{DE}} - \bar{Q}_{t_{DE}}$ denotes the truncation error in $\bar{Q}_{t_{DE}}$ and A, B, and C are numbers which may vary with t_{DE}. If $(\bar{Q}^{**}_{t_{DE}} - \bar{Q}_{t_{DE}})$ is denoted by $(\Delta\bar{Q}_{t_{DE}})_{Trunc.}$ and if $A\Delta u^2$, $B\Delta v$, and $C\Delta t_{DE}$ are denoted by $(\Delta\bar{Q}_{t_{DE}})_{\Delta u}$, $(\Delta\bar{Q}_{t_{DE}})_{\Delta v}$, and $(\Delta\bar{Q}_{t_{DE}})_{\Delta t_{DE}}$, respectively, then Equation (III-121) becomes

$$(\Delta\bar{Q}_{t_{DE}})_{Trunc.} = (\Delta\bar{Q}_{t_{DE}})_{\Delta u} + (\Delta\bar{Q}_{t_{DE}})_{\Delta v} + (\Delta\bar{Q}_{t_{DE}})_{\Delta t_{DE}} \qquad \text{(III-122)}$$

The value of $(\Delta\bar{Q}_{t_{DE}})_{\Delta u}$ can be determined by calculating $\bar{Q}_{t_{DE}}$ for two different sets of increment values, each set having identical Δv increments and identical Δt_{DE} increments but different Δu increments. For example, if $\bar{Q}_i$ $(i = 1,2)$ denotes the value of $\bar{Q}_{t_{DE}}$ calculated with a set

of increments (Δu_i, Δv, Δt_{DE}), then the value of A can be obtained from (III-121) as

$$A = \frac{\bar{Q}_2 - \bar{Q}_1}{(\Delta u_1)^2 - (\Delta u_2)^2}$$

The value of $(\Delta \bar{Q}_{t_{DE}})_{\Delta u}$, the truncation error in $\bar{Q}_{t_{DE}}$ due to Δu, is then

$$(\Delta \bar{Q}_{t_{DE}})_{\Delta u} = A(\Delta u)^2 = \frac{\bar{Q}_2 - \bar{Q}_1}{(\Delta u_1)^2 - (\Delta u_2)^2} (\Delta u)^2$$

This method of determining the error terms on the right side of Equation (III-122) has been employed to obtain the results listed in Table IX. These results show that, for $t_{DE} > 1$, the error in $\bar{Q}_{t_{DE}}$ due to Δv and Δt_{DE} is small compared to that due to Δu. The combined errors due to Δv and Δt_{DE} are ignored here since they cause an error in Q_t/Q_{t_E} of less absolute value than the radius of the circles used to plot Q_t/Q_{t_E} in Figure 26. Thus Equation (III-122) is rewritten

$$(\Delta \bar{Q}_{t_{DE}})_{Trunc.} \cong (\Delta \bar{Q}_{t_{DE}})_{\Delta u} = A(\Delta u)^2 \qquad \text{(III-123)}$$

where $A(\Delta u)^2$ is always positive (see Table IX) and therefore causes only a negative error in Q_t/Q_{t_E}, as shown by Equation (III-120).

The total error in $\bar{Q}_{t_{DE}}$ is equal to the sum of the round-off and truncation errors. Thus if $\bar{Q}^*_{t_{DE}}$ denotes the true solution and $\bar{Q}_{t_{DE}}$ is, as before, the machine solution, then

$$\Delta \bar{Q}_{t_{DE}} = A(\Delta u)^2 \pm 0.00185 \bar{Q}_{t_{DE}} \qquad \text{(III-124)}$$

TABLE IX

INDIVIDUAL EFFECTS OF Δu, Δv, AND Δt_{DE} ON THE TRUNCATION ERROR IN $\bar{Q}_{t_{DE}}$

Effect of Δu

$\Delta v = .098175$

Δt_{DE} = given on page 103

t_{DE}	$\bar{Q}_{t_{DE}}$ $\Delta u = .08$	$\bar{Q}_{t_{DE}}$ $\Delta u = .133333$	$(\Delta\bar{Q}_{t_{DE}})_{\Delta u} = A(.08)^2$
1	1.98924	1.96054	.0162
5	5.99779	5.96793	.0168
9	9.18374	9.15236	.0176
26	19.17078	19.12799	.0240
50	27.09876	27.03897	.0336
106	33.52980	33.44528	.0474
276	35.14570	35.05145	.0529
426	35.15587	35.06323	.0520

Effect of Δv

$\Delta u = .133333$

Δt_{DE} = given on page 103

t_{DE}	$\bar{Q}_{t_{DE}}$ $\Delta v = .0715$	$\bar{Q}_{t_{DE}}$ $\Delta v = .098175$	$(\Delta\bar{Q}_{t_{DE}})_{\Delta v} = B(.098175)$
1	1.96063	1.96054	.000337
5	5.96797	5.96793	.000147
9	9.15240	9.15236	.000147
26	19.12804	19.12799	.000184
50	27.03904	27.03897	.000258
106	33.44539	33.44528	.000405
276	35.05122	35.05145	-.000846
426	35.06275	35.06323	-.00177

TABLE IX (CONT'D)

Effect of Δt_{DE}

$\Delta u = 0.1$

$\Delta v = .098175$

t_{DE}	Δt_{DE} given on page 103	Δt_{DE} = twice values on page 103	$(\Delta \bar{Q}_{t_{DE}})_{\Delta t_{DE}} = C(\Delta t_{DE})_{\text{page 103}}$
1	1.97852	1.97859	-.00007
5	5.98696	5.98684	.00012
9	9.18149	9.18128	.00021
26	19.48793	19.48742	.00051
50	28.24847	28.24800	.00047
106	36.25795	36.2567	.00125
276	38.82800	38.82292	.00508
426	38.86234	38.85430	.00804

where $\Delta\bar{Q}_{t_{DE}}$ is $\bar{Q}_{t_{DE}}^{*}$ - $\bar{Q}_{t_{DE}}$ and $\pm$ .00185 $\bar{Q}_{t_{DE}}$ is the maximum round-off error, as mentioned above and estimated in Appendix III. $\Delta\bar{Q}_{t_{DE}}$ has been calculated from (III-124) for a range of t_{DE} values and is listed in Table VII as a percentage of $\bar{Q}_{t_{DE}}$ [the maximum value of the right side of (III-124) was employed].

Attention is now given to the error caused in Q_t/Q_{tE} by use of erroneous $\bar{Q}_{t_D}$ values. The term Q_t/Q_{tE} is claimed here to be a comparison between elliptic and radial flow for equal areas included by the inner boundaries and for equal areas included by the outer boundaries of the respective flow models. The equality of the areas enclosed by the inner ellipse and the inner circle is assured by the relationship (III-115). However, the $\bar{Q}_{t_{DE}}$ values were calculated for an external boundary area 101.3 times the inner area while $\bar{Q}_{t_D}$ was obtained from the literature[1] for an external circular area 100 times the inner area. If $(\bar{Q}_{t_D})_{101.3}$ and $(\bar{Q}_{t_D})_{100}$ denote the values calculated for the subscripted area ratios, then

$$(\bar{Q}_{t_D})_{101.3} = (\bar{Q}_{t_D})_{100} + \Delta\bar{Q}_{t_D} \qquad \text{(III-125)}$$

where $\Delta\bar{Q}_{t_D}$ is the error of interest here. The maximum error, $(\Delta\bar{Q}_{t_D})_{max.}$, as well as the maximum $\Delta\bar{Q}_{t_D}/(\bar{Q}_{t_D})_{100}$ occurs in the asymptotic value of $\bar{Q}_{t_D}$. This fact is apparent from tables of $\bar{Q}_{t_D}$ versus t_D given in the literature[1] for various area ratios, as well as from the observation that for

sufficiently small t_D, $\bar{Q}_{t_D}$ will be independent of the potition of the exterior boundary. This maximum $\Delta\bar{Q}_{t_D}$ can be exactly determined since the asymptotic value of $\bar{Q}_{t_D}$ is the following explicit function[1] of the area ratio:

$$(\bar{Q}_{t_D})_{asymptotic} = \frac{(r_e/r_b)^2 - 1}{2}$$

The term $(r_e/r_b)^2$ is the area ratio, i.e., the ratio of the area encompassed by the exterior circle to that encompassed by the inner circular boundary. Thus, from (III-125),

$$\frac{101.3-1}{2} - \frac{100-1}{2} = (\Delta\bar{Q}_{t_D})_{max.} = 0.65$$

and

$$\left[\frac{\Delta\bar{Q}_{t_D}}{(\bar{Q}_{t_D})_{100}}\right]_{max.} = \frac{.65}{49.5} = .0131$$

This $\Delta\bar{Q}_{t_D}/(\bar{Q}_{t_D})_{100}$ ratio is 0 for dimensionless time $t_D = 15$[1] and increases to 0.0131 at $t_D = 500$, where the asymptotic $(\bar{Q}_{t_D})_{100}$ value of 49.5 is reached. The manner in which $\Delta\bar{Q}_{t_D}/\bar{Q}_{t_D}$ [$= \Delta\bar{Q}_{t_D}/(\bar{Q}_{t_D})_{100}$] varies from 0 to .0131 has been estimated from tables of $\bar{Q}_{t_D}$ vs t_D, for various area ratios, given in the literature.[1]

The $\Delta\bar{Q}_{t_D}/\bar{Q}_{t_D}$ values, estimated as described immediately above, and $\Delta\bar{Q}_{t_{DE}}/\bar{Q}_{t_{DE}}$, calculated from Equation (III-124), have been employed in (III-120) to yield the maximum percentage error in Q_t/Q_{tE}. This calculated error is plotted as a band about Q_t/Q_{tE} in Figure 26.

f. Stability Analysis

The numerical method of calculation employing Equations (III-92) and (III-93) proved to be stable and

convergent for all combinations of Δu, Δv, and Δt_{DE} values used. The question remains, however, as to whether the author was merely fortunate in avoiding combinations which would result in instability or whether the method is actually stable for any combination of increment values. The method is shown by the following analysis to be stable for all increment values.

If the solution for $\bar{P}_{m,n,i}$ is assumed to be of the form

$$\bar{P}_{m,n,i} = \sum_{j=1}^{\infty} \sum_{\ell=1}^{\infty} D_{m,n,i}\, e^{\sqrt{-1}(jm\Delta u + \ell n \Delta v)} \qquad \text{(III-126)}$$

then the condition for stability of the numerical method of solution described above is that $|D_{m,n,2i+2}/D_{m,n,2i}|$ be < 1 for all m, n, and i.(21) This method of stability analysis is strictly valid only for difference or differential equations with constant coefficients. However, as pointed out by Mickley et al.(19) the method can be applied to variable coefficient equations by treating the variable coefficients as fixed constants in the determination of the form of $|D_{m,n,2i+2}/D_{m,n,2i}|$ and then letting them take on their most adverse values when determining whether this latter ratio is < 1 for all m, n, and i.

Substitution of $\bar{P}_{m,n,i}$ from (III-126) into (III-90) yields

$$\frac{D_{m,n,2i+1}}{D_{m,n,2i}} = \frac{f_{m,n} - 2R(1-\cos \ell \Delta v)}{f_{m,n} + 2(1-\cos j \Delta u)} \qquad \text{(III-127)}$$

Similarly, substituting $\bar{P}_{m,n,i}$ from (III-126) into (III-91), one obtains

$$\frac{D_{m,n,2i+2}}{D_{m,n,2i+1}} = \frac{f_{m,n} - 2(1-\cos j\Delta u)}{f_{m,n} + 2R(1-\cos l\Delta v)} \qquad \text{(III-128)}$$

One can readily obtain from Equations (III-127) and (III-128) the desired ratio

$$\frac{D_{m,n,2i+2}}{D_{m,n,2i}} = \frac{f_{m,n} - 2R(1-\cos l\Delta v)}{f_{m,n} + 2(1-\cos j\Delta u)} \times \frac{f_{m,n} - 2(1-\cos j\Delta u)}{f_{m,n} + 2R(1-\cos l\Delta v)} \qquad \text{(III-129)}$$

Now, by inspection, it can be seen that the absolute value of the right side of (III-129) is < 1 for all m, n, j, ℓ, $f_{m,n}$, and R <u>provided</u> $f_{m,n}$ and R are both > 0. Since $f_{m,n}$ is $[(\Delta u)^2/\Delta t_{DE}]\,[\cosh^2(m\Delta u) - \cos^2(n\Delta v)]$ and R is $(\Delta u/\Delta v)^2$, both are greater than 0 and $D_{m,n,2i+2}/D_{m,n,2i}$ is less than 1 in absolute value for all Δu, Δv, and Δt_{DE}. Thus the numerical method developed above, employing Equations (III-90) and (III-91), is stable for any combination of Δu, Δv, and Δt_{DE} increment values.

IV. INDIVIDUAL PROBLEMS ENCOUNTERED IN THE PREDICTION OF GAS STORAGE RESERVOIR BEHAVIOR

The equations of Section III-A would allow a completely general method of predicting gas storage reservoir performance if all reservoirs satisfied the assumptions on pages 8 and 9 of this thesis. Several cases arise, however, in which certain of these assumptions are completely invalid. For example, the assumption of a constant gas bubble radius is certainly not satisfied during the initial period of growth of an aquifer storage reservoir since the radius increases from a value of 0 at the time of initiation of the gas bubble to values of several thousand feet. Also, the solutions to the diffusivity equation presented in Section III-A are valid neither for cases in which the initial aquifer pressure distribution is a non-uniform function of radius nor for cases involving two or more gas fields situated on a common aquifer. Methods are developed below to treat the cases of gas field interference, non-uniform aquifer initial pressure distribution, and aquifer storage; the methods are then evaluated by application to actual gas storage reservoirs.

A. Treatment of Pressure Interference Between Two or More Gas Fields Situated on a Common Aquifer

The absence of pressure interference effects from neighboring reservoirs was one of the assumptions employed in developing the Section III-A equations governing gas storage reservoir behavior. In cases where this assumption is not valid, a modification is required in the previously described and illustrated (Section III-B) method of application of these equations to the prediction of gas field performance. Mortada[6] described such a modification which allows prediction of the performance of several oil fields situated on a common aquifer but he did not apply his method in an actual

case study. His interference theory is discussed below and an adaptation of his method, applicable to interfering gas fields, is then presented. This adapted method is finally applied in the performance prediction of two interfering fields and a comparison is made between their predicted and actual performances. The validity of both the adapted method presented below and Mortada's method depends upon satisfaction of all the assumptions listed in Section III-A excepting the one specifying absence of interference effects.

1. Existing Theory Relating to Interference Between Oil Reservoirs

M. Mortada[6] presented a method of aquifer water influx calculation which accounts for interference between two or more oil fields situated on a common aquifer. His calculations involve primarily Equation (IV-1), below, which is obtained by application of Duhamel's superposition principle to Van Everdingen and Hurst's "constant terminal rate case" solution to the previously presented diffusivity Equation (III-5). Equation (IV-1) is identical with Equation (III-16) except for the retention in (IV-1) of the independent variable r_D in the aquifer pressure $P_{(r_D,t)}$ and in the dimensionless pressure drop term $\underline{P}_{(r_D,t_D)}$.

$$P_o - P_{(r_D,t)} = \frac{\mu}{2\pi hk} \sum_{i=0}^{i=j-1} (q'_{i+1} - q'_i)\, \underline{P}_{(r_D,(j-i)\Delta t_D)} \qquad \text{(IV-1)}$$

P_o = initial uniform aquifer pressure, psia

$P_{(r_D,t)}$ = aquifer pressure at $r_D x r_b$ feet from center of oil field and at time t, psia

r_b = oil field radius, feet

$\underline{P}_{(r_D,(j-i)\Delta t_D)}$ = dimensionless pressure drop term, obtained as solution to Equation (III-5), at dimensionless radius r_D and dimensionless time $(j-i)\Delta t_D$

t = time = $j\Delta t$, seconds.

Mortada equates the pressure drop in each oil field to the sum of a number of individual pressure drop components, where each component represents the effect of one of the interfering oil fields on the pressure drop in the field considered. Thus, in the case of two interfering oil fields denoted by field R and field T,

$$\bar{P}_{R(j\Delta t)} = P_o - P_{R(j\Delta t)} = \bar{P}_{RR(j\Delta t)} + \bar{P}_{RT(j\Delta t)} \qquad \text{(IV-2)}$$

$$\bar{P}_{T(j\Delta t)} = P_o - P_{T(j\Delta t)} = \bar{P}_{TT(j\Delta t)} + \bar{P}_{TR(j\Delta t)} \qquad \text{(IV-3)}$$

$\bar{P}_{R(j\Delta t)}$ = total pressure drop in field R at time t = $j\Delta t$, psia

$\bar{P}_{T(j\Delta t)}$ = total pressure drop in field T at time t = $j\Delta t$, psia

P_o = initial pressure in reservoir-aquifer system, psia

$\bar{P}_{RR(j\Delta t)}$ = pressure drop in field R caused by R's production, psia

$\bar{P}_{RT(j\Delta t)}$ = pressure drop in field R caused by T's production, psia

$\bar{P}_{TT(j\Delta t)}$ = pressure drop in field T caused by T's production, psia

$P_{TR(j\Delta t)}$ = pressure drop in field T caused by R's production, psia

If n interfering oil fields are involved, then the pressure drop in field i is

$$\bar{P}_{i(j\Delta t)} = \sum_{m=1}^{m=n} \bar{P}_{im(j\Delta t)} \qquad \text{(IV-4)}$$

where $\bar{P}_{im(j\Delta t)}$ is the pressure drop in field i caused by field m's production.

The terms $\bar{P}_{R(j\Delta t)}$ and $\bar{P}_{T(j\Delta t)}$ are calculated as shown in Equations (IV-5) and (IV-6), below.

$$\bar{P}_{R(j\Delta t)} = \frac{\mu}{2\pi hk}\left[\sum_{i=0}^{i=j-1}(q'_{R\,i+1} - q'_{Ri})\underline{P}(1,(j-i)\Delta t_{D_R}) + \sum_{i=0}^{i=j-1}(q'_{T\,i+1} - q'_{Ti})\underline{P}(r_{D_{RT}},(j-i)\Delta t_{D_T})\right] \qquad \text{(IV-5)}$$

where $\Delta t_{D_R} = \dfrac{k\Delta t}{\mu\phi c(r_b)_R^2}$, and $(r_b)_R$ is the field R radius in feet

$\Delta t_{D_T} = \dfrac{k\Delta t}{\mu\phi c(r_b)_T^2}$, and $(r_b)_T$ is the field T radius in feet

q'_{Ri} = the average rate of water influx into field R during the time increment from $(i-1)\Delta t$ to $i\Delta t$, ft.^{3}/second

q'_{Ti} = the average rate of water influx into field T during the time increment from $(i-1)\Delta t$ to $i\Delta t$, ft.^{3}/second

$\underline{P}(1,j-i)\Delta t_D) = \underline{P}_{t_D}$, the dimensionless pressure drop quantity tabulated as a function of dimensionless time t_D by Van Everdingen and Hurst[1] and Chatas[2].

$r_{D_{RT}}$ = distance between centers of fields R and T divided by field T radius, $(r_b)_T$, dimensionless

$\underline{P}(r_{D_{RT}},(j-i)\Delta t_D)$ = dimensionless pressure drop quantity presented graphically by Mortada[6] as a function of r_D and t_D

The first summation of the right side of (IV-5) is $\bar{P}_{RR(j\Delta t)}$ and the second summation is $\bar{P}_{RT(j\Delta t)}$. The expression for $\bar{P}_{T(j\Delta t)}$ is similarly,

$$\bar{P}_{T(j\Delta t)} = \frac{\mu}{2\pi hk}\left[\sum_{i=0}^{i=j-1}(q'_{T\,i+1} - q'_{T\,i})\,\underline{P}(1,(j-i)\Delta t_{D_T}) + \sum_{i=0}^{i=j-1}(q'_{R\,i+1} - q'_{R\,i})\,\underline{P}(r_{D_{TR}},(j-i)\Delta t_{D_R})\right] \qquad \text{(IV-6)}$$

2. Adaptation of Existing Oil Reservoir Interference Theory to the Treatment of Gas Field Interference

Mortada assumes that the rates, q_R and q_T, of aquifer water influx can be equated to the rates of oil production in the corresponding fields or to these latter rates corrected for the expansion of the oil field content. In the case of gas fields, the relationship between the rate of aquifer water influx and the gas production or injection rate is, of course, not a direct proportionality and further attention must therefore be given to the terms q_R and q_T. (Fields R and T are now assumed to be interfering gas fields.)

The aquifer water influx rate q'_i in Equation (IV-1) can be related to the gas field pore volume V_i as outlined in Section III, page 21 of this thesis, to obtain

$$\bar{P}_{(r_D,t)} = P_o - P_{(r_D,t)} = K_3\sum_{i=0}^{i=j-1}(2V_i - V_{i+1} - V_{i-1})\,\underline{P}_{(r_D,(j-i)\Delta t_D)} \qquad \text{(IV-7)}$$

where $P_{(r_D,t)}$ = aquifer pressure, at radius $r_D x r_b$ feet from center of gas field, at time $t = j\Delta t$, psia

r_b = gas field radius, feet

V_i = gas field pore volume at time $t = i\Delta t$, $ft.^3$

$K_3 = \frac{\mu}{2\pi hk\Delta t}$ psi/$ft.^3$.

Δt = time increment, seconds.

The total pressure drop in gas field R is now determined by first calculating the pressure change in R which would occur if no other interfering gas field T were present (i.e., ignoring the presence of field T entirely) and then adding to that calculated pressure drop the pressure change in R caused by T's gas production (or injection). Thus the pressure drop in field R is

$$\bar{P}_{R(j\Delta t)} = (P_o)_R - P_{R(j\Delta t)} = \bar{P}_{RR(j\Delta t)} + \bar{P}_{RT(j\Delta t)} \qquad \text{(IV-8)}$$

and $\bar{P}_{RR(j\Delta t)}$ is first calculated, ignoring field T, as

$$\bar{P}_{RR(j\Delta t)} = K_3 \sum_{i=0}^{i=j-1} (2V'_{Ri} - V'_{Ri-1} - V'_{Ri+1}) P_{(1,(j-i)\Delta t_{D_R})} \qquad \text{(IV-9)}$$

Similarly, $\bar{P}_{TT(j\Delta t)}$ is calculated, ignoring field R, as

$$\bar{P}_{TT(j\Delta t)} = K_3 \sum_{i=0}^{i=j-1} (2V'_{Ti} - V'_{Ti-1} - V'_{Ti+1}) P_{(1,(j-i)\Delta t_{D_T})} \qquad \text{(IV-10)}$$

where V'_{R_i} (or V'_{T_i}) = 'uncorrected' gas field R (or T) pore volume at time $t = i\Delta t$, $ft.^3$.

$P_{R(j\Delta t)}$ (or $P_{T(j\Delta t)}$) = gas field R (or T) pressure at time $t = j\Delta t$, psia

$(P_o)_R$ (or $(P_o)_T$) = initial gas field R (or T) pressure, psia.

The terms V'_{R_i} and V'_{T_i} are 'uncorrected' pore volumes in the respect that they are calculated from the Equations (III-20a and III-20b), below, ignoring the interference effects.

$$V'_{Ri} = n_{Ri} RT \left[1 + \frac{K}{P_{RR(i\Delta t)}} \right] \qquad \text{(III-20a)}$$

$$V'_{Ti} = n_{Ti} RT \left[1 + \frac{K}{P_{TT(i\Delta t)}} \right] \qquad \text{(III-20b)}$$

where n_{R_i} (or n_{T_i}) = pound moles gas in place in field R (or T) at time $t = i\Delta t$, $P_{RR(i\Delta t)}$ (or $P_{TT(i\Delta t)}$) = $(P_o)_R - \bar{P}_{RR(i\Delta t)}$ [or $(P_o)_T - \bar{P}_{TT(i\Delta t)}$]. Elimination of V'_{R_i} between Equations (IV-9) and (III-20a) and of V'_{T_i} between Equations (IV-10) and (III-20b) yields the following equations

$$P_{RR(j\Delta t)} = \frac{-K_{8_R} + \sqrt{K_{8_R}^2 + K_{9_R}}}{2} \qquad \text{(IV-11)}$$

$$P_{TT(j\Delta t)} = \frac{-K_{8_T} + \sqrt{K_{8_T}^2 + K_{9_T}}}{2} \qquad \text{(IV-12)}$$

where

$$K_{8_R} = K_3 \left[\left(\sum_{i=0}^{i=j-2} (2V'_{R_i} - V'_{R_{i-1}} - V'_{R_{i+1}}) \underline{P}(1, (j-i)\Delta t_{D_R}) \right) + \underline{P}(1, \Delta t_{D_R})(2V'_{R_{j-1}} - V'_{R_{j-2}} - n_{R_j} RTK) \right] - (P_o)_R$$

$$K_{9_R} = 4K_3 \underline{P}(1, \Delta t_{D_R}) n_{R_j} RT$$

K_{8_T} and K_{9_T} are same as K_{8_R} and K_{9_R} except all 'R' subscripts are changed to 'T'. Equations (IV-11) and (IV-12) are explicit expressions allowing calculation of $P_{RR(j\Delta t)}$ and $P_{TT(j\Delta t)}$ if the calculations are begun with j = 1 and continued with j = 2,3, ..., etc., since then for a given value of j, all the terms in K_8 and K_9 are known. After all the $P_{RR(j\Delta t)}$ and $P_{TT(j\Delta t)}$ are calculated (j = 1,2,3, ..., N, where N is the total number of time increments for which the predicted gas field performance is required) the terms V'_{R_i} and V'_{T_i} (i = 1,2,3, ..., N) are all known (as calculated from Equations (III-20a) and (III-20b), above). The pressure drops $\bar{P}_{RT(j\Delta t)}$ (pressure change in field R due to T's production) and $\bar{P}_{TR(j\Delta t)}$ (pressure change in field T due to R's production) are then calculated from the equations

$$\bar{P}_{RT(j\Delta t)} = K_3 \sum_{i=0}^{i=j-1} (2V'_{T_i} - V'_{T_{i-1}} - V'_{T_{i+1}}) P(r_{D_{RT}}, (j-i)\Delta t_{D_T}) \qquad \text{(IV-13)}$$

$$\bar{P}_{TR(j\Delta t)} = K_3 \sum_{i=0}^{i=j-1} (2V'_{R_i} - V'_{R_{i-1}} - V'_{R_{i+1}}) P(r_{D_{TR}}(j-i)\Delta t_{D_R}) \qquad \text{(IV-14)}$$

where, letting d = the distance in feet between the centers of gas fields R and T,

$$r_{D_{RT}} = d/(r_b)_T$$

$$r_{D_{TR}} = d/(r_b)_R$$

$(r_b)_R$(or $(r_b)_T$) = gas field R (or T) radius, ft.

Δt_{D_R} (or Δt_{D_T}) = dimensionless time increment for field R (or T).

The total pressure drops in fields R and T are then given by

$$\bar{P}_{R(j\Delta t)} = (P_o)_R - P_{R(j\Delta t)} = \bar{P}_{RR(j\Delta t)} \text{ (from Equation IV-11)} + \bar{P}_{RT(j\Delta t)} \text{ (from Equation IV-13)} \qquad \text{(IV-8)}$$

$$\bar{P}_{T(j\Delta t)} = (P_o)_T - P_{T(j\Delta t)} = \bar{P}_{TT(j\Delta t)} \text{ (from Equation IV-12)} + \bar{P}_{TR(j\Delta t)} \text{ (from Equation IV-14)} \qquad \text{(IV-15)}$$

The correct or predicted gas field pore volumes are finally calculated from the relations

$$V_{R(j\Delta t)} = n_{R_j} RT \left(K + \frac{1}{P_{R(j\Delta t)}} \right) \qquad \text{(IV-16)}$$

$$V_{T(j\Delta t)} = n_{T_j} RT \left(K + \frac{1}{P_{T(j\Delta t)}} \right) \qquad \text{(IV-17)}$$

In order to employ the equations presented here, one must know or specify the values of d, $(P_o)_R$, $(P_o)_T$, $(n_{R_i}, n_{T_i}, i = 1,2,3, \ldots, N)$, K_3, Δt, $K_{2_R} = \frac{K}{\mu\phi c (r_b)_R^2}$, $K_{2_T} = \frac{K}{\mu\phi c (r_b)_T^2}$, K (where

z = 1 + KP = gas compressibility factor), and RT (R = 10.73 $ft.^3$ - psia/# mole - °R, T = gas field formation temperature, °R).

3. Application of the Presented Gas Field Interference Theory to an Actual Case Study

Michigan gas fields C and D were discovered in 1944 with a distance of approximately four miles separating their centers. These fields were originally considered as 'constant volume' fields; as the fields were produced, however, the field pore volumes, calculated from the data, decreased significantly. This pore volume reduction, the production of water from wells near the areal boundary of the gas sand, and the approximately equal values of initial pressure and depth below the surface for the two fields all point toward the existence of a common aquifer underlying both reservoirs. The presence of interference effects between the two fields is evidenced by the failure of many attempts to reproduce the actual volume-time and pressure-time behavior of the fields by the equations and method of calculation given in Sections III-A and III-B.

The 12 year period from 1944 to 1956 was chosen for the purpose of application of the gas field interference theory presented above to the gas reservoirs C and D. A time increment of one month and Equations (IV-11) through (IV-17) were employed in the calculation of the predicted volume and pressure behavior of each of the two fields. The predicted and actual field performance are plotted in Figures 27 and 28 and the values of the reservoir constants employed in the calculations are noted on these figures.

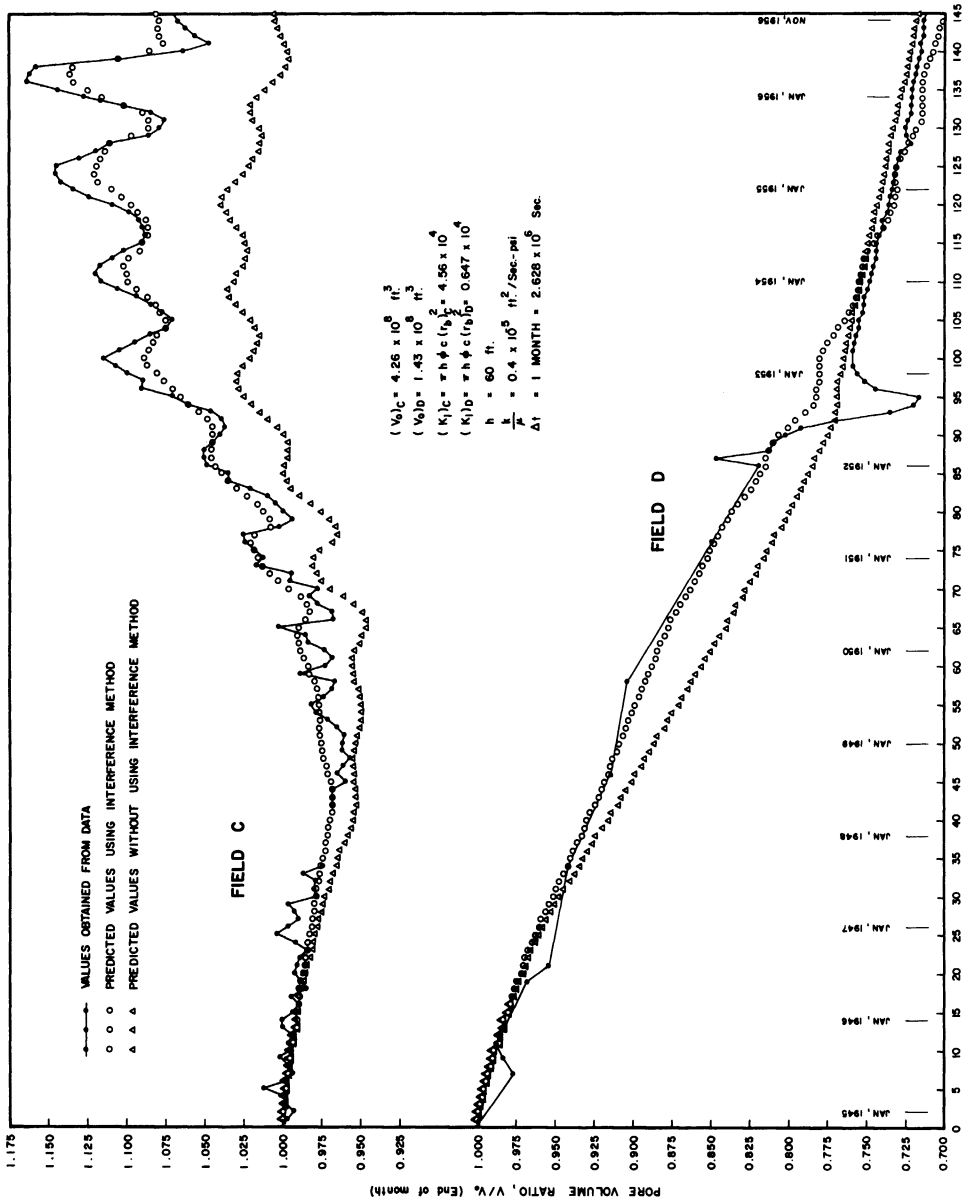

FIELD C AND D PREDICTED AND ACTUAL PORE VOLUME RATIOS VS TIME

Figure 27

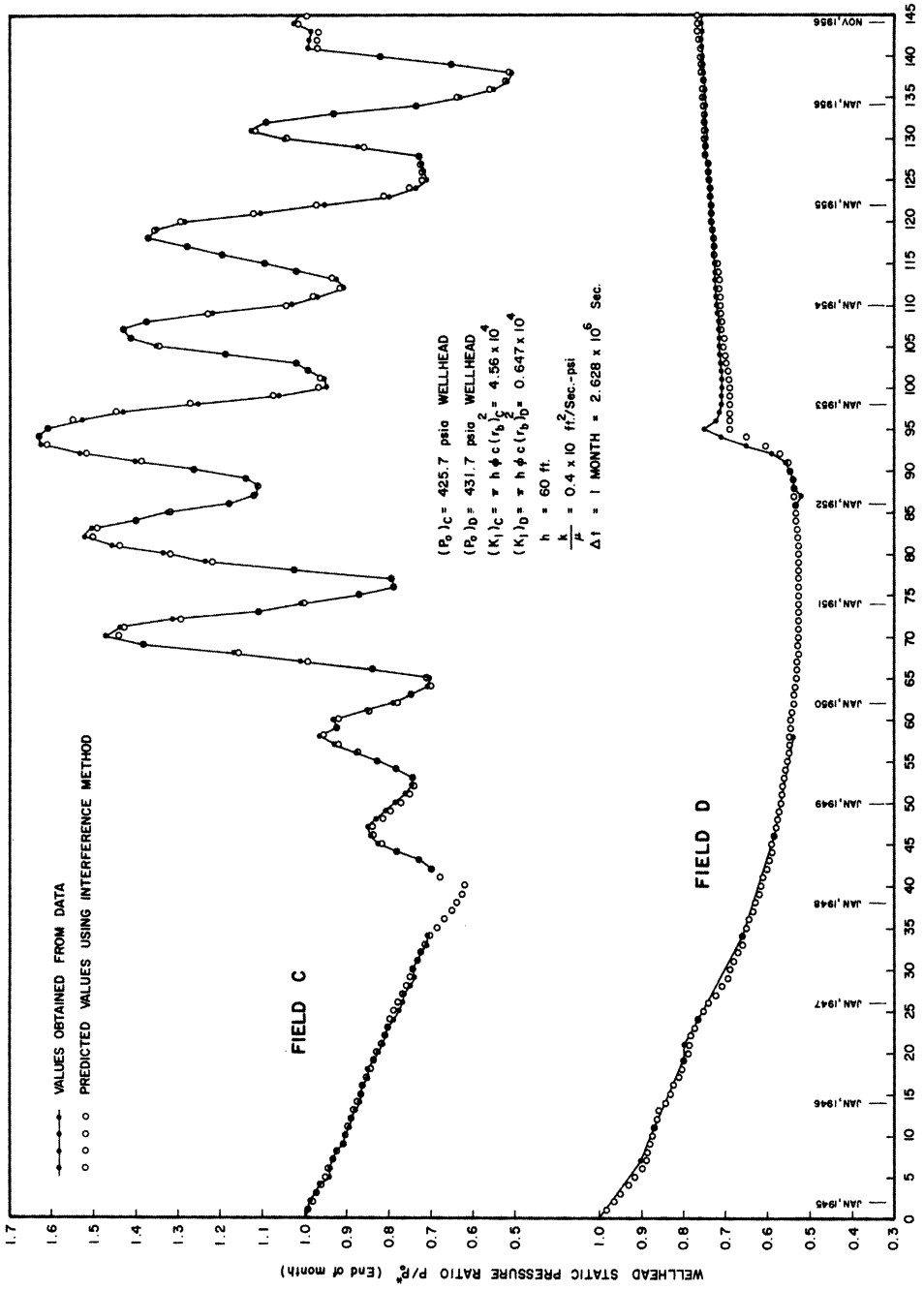

FIELD C AND D PREDICTED AND ACTUAL PRESSURE RATIOS VS TIME

Figure 28

Table X lists the field data and predicted field pressure and volume ratios for the period 1944-1956. The calculations employing Equations (IV-11) through (IV-17) were quite lengthy and were therefore programmed in the FORTRAN code and performed by the IBM 704 digital computer.

An interesting observation is interjected here concerning the necessity for taking the water movement into account. That is, one might question whether the actual field performance might be predicted to sufficient accuracy by simply assuming the field to be of constant volume. An excellent comparison between the 'constant volume' and the 'water influx' methods of prediction is given in Figure 27, since the 'constant volume' performance is represented in this figure by the straight line $V/V_o = 1.0$. Suppose one assumed field C to have a constant volume equal to its original (discovery) value of 4.2×10^8 ft.^{3}. Then the error incurred in the predicted pressure at 136 months after discovery would be approximately 16.2% since an error of 16.2% would be incurred in the predicted volume (see Figure 27) and pressure is approximately inversely proportional to volume ($PV = znRT$). However, Figure 27 shows that the difference between the pore volume predicted by the water influx (interference) method and the actual pore volume at this time is only 2.6% and thus the error in the predicted pressure 136 months after discovery would be approximately 2.6%. An error of approximately 8.7% in the predicted pressure at $t = 136$ months would be incurred by assuming a constant volume only over a period of 5 months since Figure 27 shows that the actual pore volume changes by 8.7% from $t = 131$ to 136

Table X

SUMMARY OF ACTUAL AND PREDICTED PERFORMANCE OF
GAS FIELDS C AND D FOR PERIOD 1944-1956

Initial Field C Pressure = 425.7 psia, static wellhead

Initial Field D Pressure = 431.7 psia, static wellhead

$(K_2)_C = k/\mu\phi c(r_b)_C^2 = 1.65 \times 10^{-8}$ 1/seconds

$(K_2)_D = k/\mu\phi c(r_b)_D^2 = 1.163 \times 10^{-7}$ 1/seconds

$K_3 = \mu/2\pi hk\Delta t = 2.52 \times 10^{-4}$ psia/ft^3

$(V_o)_C = 4.26 \times 10^8$ ft^3

$(V_o)_D = 1.43 \times 10^8$ ft^3

Δt = 1 month = 2.628×10^6 seconds

Month	Cumulative SCF Gas Production* From Data	Wellhead Static Pressure Ratio P/Po* (End of Month) Field C		Field D		Pore Volume Ratio V/Vo* (End of Month) Field C			Field D	
1944										
Initial	0	1		1		1			1	
Dec.	114,787a	.995d	.992p	-	.983p	.997d	.9999e	.9999p	-	.9997e	.9997p
1945										
Jan.	277,423a	.988d	.982p	-	.966p	.992d	.9996e	.9996p	-	.999e	.999p
Feb.	410,887a	.974d	.973p	-	.947p	.998d	.999e	.999p	-	.998e	.998p
Mar.	572,561a	.963d	.963p	-	.931p	.999d	.999e	.999p	-	.997e	.997p
April	727,988a	.941d	.953p	-	.917p	1.012d	.998e	.998p	-	.996e	.996p
May	884,948a	.941d	.943p	-	.900p	.999d	.998e	.998p	-	.994e	.994p
June	1,026,164a	.937d	.933p	.900d	.887p	.993d	.997e	.997p	.944d	.993e	.993p
July	1,187,789a	.923d	.923p	-	.883p	.997d	.996e	.996p	-	.991e	.991p
Aug.	1,342,698a	.909d	.913p	.886d	.880p	1.001d	.996e	.996p	.983d	.990e	.990p
Sept.	1,470,021a	.904d	.905p	-	.877p	.996d	.995e	.995p	-	.988e	.989p
Oct.	1,580,300a	.897d	.898p	.873d	.874p	.996d	.994e	.994p	.988d	.987e	.987p
Nov.	1,680,270a	.892d	.892p	-	.867p	.993d	.993e	.993p	-	.986e	.986p
Dec.	1,786,266a	.880d	.885p	-	.859p	.999d	.992e	.992p	-	.984e	.984p
1946											
Jan.	1,903,416a	.871d	.878p	-	.845p	1.000d	.991e	.991p	-	.983e	.983p
Feb.	2,019,348a	.869d	.871p	-	.834p	.993d	.990e	.991p	-	.981e	.981p
Mar.	2,137,757a	.864d	.863p	-	.825p	.989d	.990e	.990p	-	.979e	.979p
April	2,261,081a	.852d	.855p	-	.815p	.993d	.989e	.989p	-	.977e	.978p
May	2,390,116a	.850d	.846p	-	.805p	.984d	.988e	.989p	-	.975e	.976p
June	2,509,907a	.838d	.839p	.803d	.799p	.989d	.986e	.988p	.968d	.973e	.974p
July	2,645,387a	.826d	.830p	-	.792p	.992d	.985e	.987p	-	.971e	.972p
Aug.	2,795,335a	.817d	.820p	.799d	.786p	.990d	.984e	.986p	.954d	.969e	.970p
Sept.	2,915,190a	.810d	.812p	-	.783p	.998d	.983e	.986p	-	.967e	.969p
Oct.	3,027,398a	.805d	.805p	-	.775p	.984d	.982e	.985p	-	.965e	.967p
Nov.	3,141,836a	.791d	.797p	-	.767p	.992d	.981e	.984p	-	.963e	.965p
Dec.	3,258,882a	.775d	.789p	-	.756p	1.003d	.979e	.983p	-	.961e	.963p
1947											
Jan.	3,399,061a	.770d	.780p	-	.740p	.996d	.978e	.982p	-	.958e	.961p
Feb.	3,533,638a	.765d	.771p	-	.724p	.989d	.977e	.981p	-	.956e	.959p
Mar.	3,676,695a	.753d	.761p	-	.710p	.992d	.975e	.980p	-	.953e	.957p
April	3,796,288a	.742d	.753p	-	.697p	.996d	.974e	.980p	-	.950e	.954p
May	3,931,792a	.746d	.744p	-	.688p	.976d	.973e	.979p	-	.947e	.952p
June	4,072,148a	.734d	.735p	-	.678p	.980d	.971e	.978p	-	.944e	.950p
July	4,204,827a	.725d	.725p	-	.670p	.978d	.970e	.977p	-	.941e	.948p
Aug.	4,347,990a	.709d	.716p	-	.664p	.987d	.968e	.977p	-	.938e	.945p
Sept.	4,507,598a	.706d	.704p	.660d	.659p	.973d	.966e	.976p	.941d	.935e	.943p
Oct.	4,753,088a	-	.687p	-	.654p	-	.965e	.975p	-	.933e	.941p
Nov.	4,984,191a	-	.671p	-	.645p	-	.963e	.974p	-	.930e	.939p
Dec.	5,219,874a	-	.654p	-	.636p	-	.961e	.973p	-	.927e	.937p
1948											
Jan.	5,445,342a	-	.638p	-	.628p	-	.959e	.972p	-	.924e	.934p
Feb.	5,601,993a	-	.627p	-	.621p	-	.957e	.971p	-	.921e	.932p
Mar.	5,672,875a	-	.622p	-	.615p	-	.955e	.970p	-	.917e	.930p
April	752,002b	-	.678p	-	.609p	-	.954e	.969p	-	.914e	.928p
May	1,066,749b	.702d	.701p	-	.603p	.968d	.953e	.969p	-	.911e	.925p
June	1,495,225b	.731d	.731p	-	.596p	.969d	.953e	.969p	-	.908e	.923p
July	2,227,027b	.783d	.783p	-	.592p	.969d	.953e	.969p	-	.905e	.921p
Aug.	2,742,427b	.827d	.818p	-	.589p	.959d	.954e	.970p	-	.902e	.919p
Sept.	3,045,194b	.844d	.838p	.586d	.585p	.965d	.954e	.972p	.915d	.899e	.917p
Oct.	3,043,155b	.847d	.837p	-	.581p	.961d	.955e	.973p	-	.896e	.915p
Nov.	2,774,029b	.831d	.817p	-	.578p	.957d	.955e	.974p	-	.893e	.913p
Dec.	2,495,443b	.808d	.797p	-	.574p	.962d	.954e	.975p	-	.890e	.911p
1949											
Jan.	2,171,643b	.784d	.774p	-	.570p	.962d	.953e	.976p	-	.887e	.909p
Feb.	1,857,267b	.763d	.752p	-	.566p	.960d	.952e	.976p	-	.884e	.907p
Mar.	1,676,078b	.747d	.739p	-	.564p	.965d	.951e	.977p	-	.881e	.905p
April	1,721,350b	.746d	.742p	-	.561p	.971d	.950e	.976p	-	.878e	.904p
May	2,336,595b	.783d	.786p	-	.557p	.979d	.949e	.976p	-	.875e	.902p
June	2,957,088b	.825d	.829p	-	.554p	.982d	.950e	.976p	-	.872e	.899p
July	3,646,471b	.879d	.876p	-	.552p	.973d	.951e	.977p	-	.869e	.897p
Aug.	4,324,981b	.930d	.921p	-	.550p	.968d	.952e	.978p	-	.866e	.895p
Sept.	4,846,694b	.967d	.955p	.542d	.548p	.966d	.954e	.980p	.904d	.863e	.893p
Oct.	4,429,520b	.920d	.924p	-	.546p	.988d	.955e	.983p	-	.860e	.891p
Nov.	4,397,883b	.931d	.921p	-	.544p	.972d	.955e	.984p	-	.857e	.888p
Dec.	3,345,222b	.863d	.847p	-	.542p	.968d	.955e	.987p	-	.854e	.886p
1950											
Jan.	2,417,884b	.793d	.782p	-	.539p	.973d	.953e	.989p	-	.851e	.885p
Feb.	1,952,432b	.753d	.749p	-	.537p	.984d	.951e	.990p	-	.848e	.883p
Mar.	1,294,869b	.706d	.702p	-	.535p	.985d	.949e	.991p	-	.845e	.880p
April	1,400,996b	.702d	.710p	-	.533p	1.002d	.947e	.990p	-	.842e	.878p
May	2,937,336b	.835d	.820p	-	.532p	.967d	.947e	.986p	-	.839e	.876p
June	5,481,165b	1.009d	.994p	-	.531p	.968d	.949e	.983p	-	.836e	.873p
July	8,008,379b	1.166d	1.158p	-	.530p	.977d	.954e	.985p	-	.834e	.870p
Aug.	11,714,392b	1.391d	1.385p	-	.530p	.983d	.962e	.989p	-	.831e	.867p
Sept.	12,867,813b	1.469d	1.444p	-	.530p	.977d	.969e	.996p	-	.828e	.864p
Oct.	12,780,643b	1.441d	1.431p	-	.530p	.995d	.975e	1.003p	-	.825e	.861p
Nov.	10,629,085b	1.313d	1.295p	-	.530p	.994d	.978e	1.009p	-	.822e	.858p
Dec.	7,754,323b	1.110d	1.113p	-	.530p	1.017d	.977e	1.014p	-	.820e	.856p
1951											
Jan.	6,061,630b	1.006d	1.003p	-	.529p	1.012d	.975e	1.016p	-	.817e	.853p
Feb.	4,099,974b	.874d	.873p	-	.529p	1.017d	.972e	1.019p	-	.814e	.851p

Table X (CONT'D)

SUMMARY OF ACTUAL AND PREDICTED PERFORMANCE OF
GAS FIELDS C AND D FOR PERIOD 1944-1956

Month	Cumulative SCF Gas Production* From Data	Wellhead Static Pressure Ratio P/P_o* (End of Month) Field C		Field D		Pore Volume Ratio V/V_o* (End of Month) Field C			Field D		
Mar.	2,857,796b	.786d	.789p	-	.528p	1.024d	.968e	1.021p	-	.811e	.849p
April	2,915,068b	.790d	.794p	-	.528p	1.025d	.965e	1.019p	-	.809e	.846p
May	6,328,301b	1.033d	1.026p	-	.528p	1.002d	.966e	1.009p	-	.806e	.844p
June	9,379,874b	1.236d	1.219p	-	.529p	.993d	.971e	1.009p	-	.803e	.840p
July	11,103,548b	1.335d	1.319p	-	.530p	.999d	.976e	1.013p	-	.801e	.837p
Aug.	13,236,984b	1.457d	1.440p	-	.532p	1.004d	.983e	1.017p	-	.798e	.833p
Sept.	14,468,642b	1.522d	1.504p	-	.532p	1.009d	.989e	1.023p	-	.795e	.829p
Oct.	14,456,835b	1.506d	1.495p	-	.533p	1.021d	.994e	1.030p	-	.793e	.825p
Nov.	12,930,613b	1.403d	1.401p	-	.534p	1.034d	.997e	1.035p	-	.790e	.821p
Dec.	11,612,164b	1.326d	1.320p	-	.535p	1.034d	.999e	1.040p	-	.788e	.819p
1952											
Jan.	9,306,955b	1.175d	1.178p	.535d	.537p	1.048d	.998e	1.044p	.819d	.785e	.816p
Feb.	8,384,215b	1.117d	1.121p	.519d	.538p	1.050d	.997e	1.046p	.847d	.783e	.815p
Mar.	8,249,887b	1.109d	1.112p	.539d	.540p	1.050d	.997e	1.046p	.814d	.780e	.813p
April	8,732,541b	1.141d	1.142p	.542d	.541p	1.046d	.997e	1.046p	.810d	.778e	.811p
May	10,788,594b	1.272d	1.266p	.547d	.544p	1.039d	.999e	1.045p	.802d	.775e	.807p
June	12,962,585b	1.402d	1.390p	.557d	.551p	1.037d	1.003e	1.046p	.792d	.773e	.802p
July	15,331,883b	1.534d	1.520p	.590d	.570p	1.038d	1.009e	1.049p	.769d	.771e	.796p
Aug.	17,165,763b	1.625d	1.614p	.648d	.606p	1.046d	1.015e	1.054p	.735d	.770e	.790p
Sept.	17,581,084b	1.631d	1.628p	.708d	.653p	1.059d	1.021e	1.061p	.720d	.769e	.785p
Oct.	17,400,676b	1.606d	1.611p	.748d	.689p	1.070d	1.025e	1.066p	.716d	.769e	.783p
Nov.	16,333,966b	1.526d	1.548p	.723d	.690p	1.090d	1.028e	1.071p	.744d	.769e	.782p
Dec.	14,570,851b	1.432d	1.446p	.715d	.691p	1.089d	1.030e	1.076p	.752d	.768e	.781p
1953											
Jan.	11,525,577b	1.253d	1.270p	.711d	.691p	1.099d	1.029e	1.081p	.757d	.767e	.780p
Feb.	8,279,304b	1.059d	1.077p	.710d	.691p	1.107d	1.026e	1.087p	.759d	.766e	.780p
Mar.	6,437,259b	.946d	.965p	.710d	.692p	1.114d	1.022e	1.089p	.759d	.765e	.780p
Apr.	6,368,997b	.949d	.963p	.710d	.693p	1.104d	1.019e	1.086p	.759d	.764e	.778p
May	6,812,015b	.984d	.992p	.711d	.696p	1.094d	1.017e	1.083p	.758d	.763e	.776p
June	7,274,647b	1.019d	1.022p	.712d	.699p	1.084d	1.016e	1.081p	.757d	.762e	.772p
July	10,020,604b	1.190d	1.190p	.714d	.702p	1.075d	1.018e	1.075p	.755d	.761e	.769p
Aug.	12,692,443b	1.349d	1.344p	.714d	.705p	1.070d	1.022e	1.075p	.755d	.760e	.765p
Sept.	14,014,979b	1.416d	1.414p	.716d	.708p	1.076d	1.027e	1.078p	.753d	.759e	.762p
Oct.	14,432,099b	1.430d	1.432p	.717d	.711p	1.084d	1.031e	1.082p	.752d	.758e	.759p
Nov.	13,519,224b	1.370d	1.376p	.718d	.713p	1.093d	1.034e	1.087p	.751d	.757e	.757p
Dec.	10,999,458b	1.217d	1.229p	.720d	.714p	1.105d	1.034e	1.093p	.749d	.756e	.756p
1954											
Jan.	7,909,681b	1.030d	1.044p	.721d	.715p	1.116d	1.032e	1.099p	.748d	.755e	.755p
Feb.	6,849,802b	.965d	.981p	.722d	.715p	1.120d	1.029e	1.100p	.747d	.753e	.754p
Mar.	5,774,258b	.904d	.915p	.723d	.716p	1.117d	1.026e	1.102p	.746d	.752e	.753p
Apr.	5,995,596b	.923d	.931p	.725d	.718p	1.109d	1.024e	1.099p	.744d	.751e	.752p
May	7,389,775b	1.012d	1.019p	.725d	.720p	1.102d	1.023e	1.092p	.744d	.750e	.750p
June	8,630,622b	1.096d	1.095p	.726d	.723p	1.088d	1.024e	1.090p	.743d	.749e	.747p
July	10,298,292b	1.194d	1.194p	.727d	.726p	1.088d	1.026e	1.087p	.742d	.748e	.743p
Aug.	11,837,297b	1.281d	1.282p	.729d	.729p	1.089d	1.029e	1.087p	.739d	.747e	.740p
Sept.	13,453,985b	1.367d	1.371p	.729d	.732p	1.092d	1.033e	1.088p	.740d	.746e	.737p
Oct.	13,270,064b	1.350d	1.356p	.732d	.734p	1.098d	1.037e	1.093p	.737d	.745e	.735p
Nov.	12,211,907b	1.282d	1.293p	.735d	.736p	1.108d	1.039e	1.097p	.736d	.743e	.733p
Dec.	9,266,347b	1.102d	1.119p	.734d	.737p	1.124d	1.038e	1.104p	.735d	.742e	.732p
1955											
Jan.	6,746,445b	.950d	.968p	.734d	.737p	1.134d	1.035e	1.110p	.734d	.741e	.731p
Feb.	4,278,932b	.797d	.812p	.736d	.737p	1.142d	1.031e	1.119p	.733d	.740e	.732p
Mar.	3,251,797b	.733d	.748p	.736d	.737p	1.145d	1.026e	1.121p	.732d	.739e	.732p
Apr.	2,820,878b	.708d	.721p	.738d	.738p	1.144d	1.022e	1.120p	.731d	.738e	.731p
May	2,820,449b	.716d	.723p	.739d	.739p	1.129d	1.019e	1.117p	.729d	.737e	.729p
June	2,820,192b	.722d	.725p	.740d	.741p	1.119d	1.016e	1.114p	.728d	.736e	.727p
July	2,820,037b	.725d	.727p	.747d	.744p	1.114d	1.014e	1.111p	.722d	.735e	.724p
Aug.	4,818,371b	.859d	.860p	.744d	.737p	1.085d	1.013e	1.097p	.725d	.734e	.721p
Sept.	7,616,379b	1.045d	1.038p	.744d	.750p	1.078d	1.015e	1.086p	.725d	.733e	.719p
Oct.	8,939,003b	1.127d	1.116p	.745d	.752p	1.075d	1.019e	1.086p	.724d	.732e	.716p
Nov.	8,516,400b	1.094d	1.088p	.747d	.754p	1.084d	1.021e	1.090p	.722d	.731e	.715p
Dec.	6,005,686b	.929d	.930p	.747d	.754p	1.102d	1.021e	1.101p	.722d	.730e	.714p
1956											
Jan.	2,999,464b	.730d	.735p	.748d	.754p	1.125d	1.017e	1.116p	.721d	.728e	.714p
Feb.	1,303,130b	.627d	.637p	.748d	.755p	1.144d	1.012e	1.125p	.721d	.727e	.714p
Mar.	345,285b	.546d	.559p	.748d	.755p	1.163d	1.007e	1.134p	.720d	.726e	.714p
Apr.	- 164,269b	.515d	.526p	.750d	.756p	1.161d	1.002e	1.136p	.719d	.725e	.713p
May	- 367,194b	.504d	.513p	.750d	.757p	1.157d	.998e	1.135p	.718d	.724e	.712p
June	1,521,965b	.648d	.648p	.753d	.759p	1.106d	.996e	1.105p	.716d	.723e	.710p
July	4,004,281b	.833d	.818p	.754d	.761p	1.064d	.997e	1.085p	.715d	.722e	.708p
Aug.	6,294,072b	.991d	.967p	.754d	.763p	1.047d	.999e	1.076p	.715d	.721e	.706p
Sept.	6,345,981b	.987d	.968p	.755d	.765p	1.055d	1.002e	1.079p	.713d	.720e	.704p
Oct.	6,343,531b	.982d	.966p	.756d	.766p	1.061d	1.003e	1.080p	.713d	.719e	.703p
Nov.	7,105,189b	1.023d	1.014p	.756d	.767p	1.067d	1.005e	1.079p	.713d	.718e	.702p
Dec.	6,860,494b	1.007d	.996p	.757d	.768p	1.070d	1.006e	1.082p	.712d	.717e	.701p

* a denotes cumulative gas production, SCF @ 60°F & 15.025 psia

b denotes cumulative gas injected, starting April, 1948, SCF @ 60°F & 14.735 psia

d denotes quantity obtained from field data

e denotes quantity predicted by Equations (III-20a), (III-20b), (IV-11), and (IV-12), which ignore interference effects

p denotes quantity predicted from interference theory - from Equations (IV-8), (IV-15), (IV-16), and (IV-17)

months. The percentage error in predicted field D pressures, effected by use of the constant volume method, would approach 29% at 145 months after discovery since the actual field volume differs from the original volume by 29% at this time.

Figure 27 shows that use of the interference method, described above, produces considerably better agreement between the actual and predicted performances of fields C and D than that achieved by ignoring interference effects. The difference between the two field C predicted pore volume curves represents the decrease in field C's pressure (or increase in pore volume) caused by gas production in field D. The crossing of the two field D predicted pore volume curves at approximately 110 months after discovery is due to the gas injection and subsequent pressurizing of field C during the time period following t = 50 months.

B. Prediction of Gas Storage Reservoir Performance When Initial Aquifer Pressure is a Non-Uniform Function of Radius

The aquifer pressure at the time of discovery or initiation of a gas reservoir is, in general, uniform or constant throughout the aquifer. In some cases, however, it is necessary to predict the performance of a gas bubble situated on an aquifer when the initial aquifer pressure is a non-uniform function of radius. A typical case is a gas field from which little or poor data were obtained during a period immediately following the field discovery or initiation. In such case the predictive calculations must specify as 0 time some date which marks the end of the period during which poor field data were recorded. Another typical case is that of an aquifer storage field, since if the predictive calculations specify the reservoir initiation date as 0 time

then these calculations must take into account the growing radius. If, however, time is considered 0 at some date after the radius has attained a relatively constant value, then the calculations are much simpler since they can employ equations derived from the assumption of a constant gas bubble radius. These equations must, of course, take into account the effect of a non-uniform initial aquifer pressure distribution, since the gas injection during the growth of the aquifer storage field will result in a developed aquifer pressure distribution at the selected date corresponding to 0 time.

The literature contains no solutions to the diffusivity equation corresponding to the case of a source or sink (gas field) of finite radius surrounded by an infinite aquifer in which the initial pressure distribution is a non-uniform function of radius. An approximate solution for this case is developed below and the solution is then employed in predicting the performance of aquifer storage reservoir E.

1. Approximate Solution to the Diffusivity Equation for the Case of a Non-Uniform Initial Aquifer Pressure Distribution

An approximate solution to the previously presented diffusivity Equation (III-5) is presented here for the initial condition (IV-18) and boundary conditions (IV-19) and (IV-20).

$$\frac{\partial^2 \bar{P}(r_D,t_D)}{\partial r_D^2} + \frac{1}{r_D}\frac{\partial \bar{P}(r_D,t_D)}{\partial r_D} = \frac{\partial \bar{P}(r_D,t_D)}{\partial t_D} \qquad \text{(III-5)}$$

$$\bar{P}(r_D,0) = P_o - P(r_D,0) = f(r_D) \qquad \text{(IV-18)}$$

$$\lim_{r_D \to \infty} \bar{P}(r_D,t_D) = 0 \qquad \text{(IV-19)}$$

$$\left(\frac{\partial \bar{P}(r_D,t_D)}{\partial r_D}\right)_{r_D=1} = g(t_D) \qquad \text{(IV-20)}$$

The initial condition (IV-18) equates the initial aquifer pressure $P_{(r_D,0)}$ to $P_o - f(r_D)$, where P_o is the constant aquifer pressure value at large radial distances from the center of the gas bubble. Condition (IV-19) is equivalent to the assumption of an infinite aquifer and (IV-20) specifies a variable water flow rate across the gas field boundary $r_D = r/r_b = 1$.

If the pressure drop $\bar{P}_{(r_D,t_D)}$ is set equal to a sum of two pressure drop components

$$\bar{P}_{(r_D,t_D)} = \bar{P}_{1(r_D,t_D)} + \bar{P}_{2(r_D,t_D)} \qquad \text{(IV-21)}$$

where $\bar{P}_{1(r_D,t_D)}$ satisfies Equation (III-5) and conditions (IV-22) and $\bar{P}_{2(r_D,t_D)}$ satisfies Equation (III-5) and conditions (IV-23), then the sum of $\bar{P}_1$ and $\bar{P}_2$ will satisfy Equation (III-5) and conditions (IV-18), (IV-19), and (IV-20), as desired.

$$\left.\begin{aligned} &\bar{P}_{1(r_D,0)} = 0 \\ &\lim_{r_D \to \infty} \bar{P}_{1(r_D,t_D)} = 0 \\ &\left(\frac{\partial \bar{P}_{1(r_D,t_D)}}{\partial r_D}\right)_{r_D=1} = g(t_D) \end{aligned}\right\} \qquad \text{(IV-22)}$$

$$\left.\begin{aligned} &\bar{P}_{2(r_D,0)} = f(r_D) \\ &\bar{P}_{2(r_{De},t_D)} = 0 \\ &\left(\frac{\partial \bar{P}_{2(r_D,t_D)}}{\partial r_D}\right)_{r_D=1} = 0 \end{aligned}\right\} \qquad \text{(IV-23)}$$

The sum $\bar{P}_1 + \bar{P}_2$ represents only an approximate solution to Equation (III-5) for the conditions (IV-18), (IV-19), and (IV-20) in the respect that $\bar{P}_{2(r_D,t_D)}$ does not approach 0 at increasing radial distances from the gas field center but is identically equal to 0 at $r_D \geq r_{D_e}$.

Solutions to the diffusivity equation (III-5) for boundary conditions similar to (IV-23) have been developed in the literature[9]; the steps involved in the development of the solution $\bar{P}_{2(r_D,t_D)}$ are therefore omitted here and the final solution is given in Equation (IV-24),

$$\bar{P}_2(r_D,t_D) = \sum_{n=1}^{\infty} a_n e^{-\lambda_n^2 t_D} U_0(\lambda_n r_D) \qquad \text{(IV-24)}$$

where

$$a_n = \frac{2\int_1^{r_{De}} x f(x) U_0(\lambda_n x)\,dx}{\frac{4}{\pi^2\lambda_n^2} - U_0^2(\lambda_n)}$$

$$U_0(\lambda_n r_D) = Y_0(\lambda_n r_{De}) J_0(\lambda_n r_D) - J_0(\lambda_n r_{De}) Y_0(\lambda_n r_D)$$

and λ_n are the roots of the equation

$$Y_0(\lambda_n r_{De}) J_1(\lambda_n) - J_0(\lambda_n r_{De}) Y_1(\lambda_n) = 0 \qquad \text{(IV-25)}$$

The solution $\bar{P}_{1(1,t_D)}$ is identical to the solution (Equation III-16a) obtained in Section III-A by application of Duhamel's superposition principle to the 'constant rate case' solution given by Van Everdingen and Hurst[1]; thus

$$\bar{P}_i(r_D,t_D) = K_3 \sum_{i=0}^{i=j-1} (2V_i - V_{i-1} - V_{i+1}) P(r_D,(j-i)\Delta t_D \qquad \text{(IV-26)}$$

where $g(t_D)$ is related to the pore volumes V_i by

$$g((i+1)\Delta t_D) + g(i\Delta t_D) = \frac{\mu}{\pi h k \Delta t}(V_{i+1} - V_i)$$

and $t_D = j\Delta t_D = jK_2\Delta t$

$$K_3 = \frac{\mu}{2\pi h k \Delta t}$$

Setting $r_D = 1$ in (IV-24) and (IV-26), one obtains the following expression for the gas bubble pressure drop at time t_D, $\bar{P}_{(1,t_D)}$,

$$\bar{P}_{(1,t_D)} = P_o - P_{(1,t_D)} = \bar{P}_1(1,t_D) + \bar{P}_2(1,t_D)$$

$$= K_3 \sum_{i=0}^{i=j-1} (2V_i - V_{i-1} - V_{i+1}) P_{(1,(j-i)\Delta t_D)} + \sum_{n=1}^{\infty} a_n e^{-\lambda_n^2 t_D} U_0(\lambda_n) \qquad \text{(IV-27)}$$

Denoting the infinite summation $\sum_{n=1}^{\infty} a_n e^{-\lambda_n^2 t_D} U_0(\lambda_n)$ (or $\sum_{n=1}^{\infty} a_n e^{-\lambda_n^2 j\Delta t_D} U_0(\lambda_n)$) by A_j, and employing the previously presented Equation (III-20) to eliminate the term V_j from (IV-27), one obtains the pressure-explicit equation

$$P_t \equiv P_{(1,t_D)} \equiv P_j = \frac{-K_6' + \sqrt{K_6'^2 + K_7}}{2} \qquad \text{(IV-28)}$$

where $P_t \equiv P_j \equiv P_{(1,t_D)}$ = gas bubble pressure at time $t = j\Delta t$ or $t_D = j\Delta t_D$, psia, $K_6' = K_6 + A_j$, and K_6 and K_7 are defined on page 22 of this thesis.

One fact of interest is readily apparent from Equation (IV-27). The error incurred by neglecting the term $\bar{P}_{2(1,t_D)} = \sum_{n=1}^{\infty} a_n e^{-\lambda_n^2 t_D} U_0(\lambda_n)$ will decrease as the value of t_D, for a fixed value of time t, increases, since a larger t_D results in a smaller value of $e^{-\lambda_n^2 t_D}$ and thus in a smaller value of $\bar{P}_{2(1,t_D)}$ at time t. Therefore, the error incurred by neglecting $\bar{P}_{2(1,t_D)}$ will be smaller as the aquifer formation mobility k/μ or the factor $1/\varphi c r_b^2$ are taken larger, since $t_D = K_2 t = (k/\mu)(1/\varphi c r_b^2)t$.

2. Application to Aquifer Storage Reservoir E - Method A

Gas field E is an aquifer storage reservoir which was initiated in 1953 by injection of gas into an aquifer formation originally containing no gas. Subsequent gas leakage from reservoir

E to shallower formations was indicated by increased gas vent rates from wells completed to small gas pockets in these shallow formations. Calculations performed in 1954 and later years indicated that the effective reservoir E gas content was significantly less than the cumulative inventory gas injected into the storage field.

September 30, 1955 was specified as 0 time in the calculations described below since the gas bubble E radius had attained a relatively constant value at that date and the gas leakage had been significantly reduced in 1955 by the introduction of a gas recirculation system to remove gas from shallow formations and return it to the reservoir E. The calculations were made with the assumption of a 0 gas leakage rate or, in other words, with the assumption that the gas leakage out of the field E was replaced in equal quantity by injection of the shallow formation gas. The initial (September 30, 1955) aquifer pressure distribution was obtained from observation well pressures and is plotted in Figure 29. The reservoir E pressure and gas in place data for the period September 30, 1955 - May 4, 1956 are listed in Table XI. The gas in place data listed in this table are inventory values which represent the net total cumulative gas injected into the reservoir. Calculations performed by the personnel of the operating company have indicated that the effective reservoir content is 4 - 12 billion standard cubic feet less than the inventory volumes listed in Table XI. The following K_2 and K_3 values were calculated from available data relating to the reservoir-aquifer system physical constants:

$$K_2 = k/\mu\phi c r_b^2 = 0.35 \times 10^{-5} \text{ 1/sec.}$$

$$K_3 = \mu/2\pi hk\Delta t = 1.48 \times 10^{-5} \text{ psia/ft}^3$$

Table XI

SUMMARY OF ACTUAL AND PREDICTED PERFORMANCE OF

AQUIFER STORAGE RESERVOIR E FOR PERIOD SEPTEMBER 30, 1955 - MAY 4, 1956

K = -.0001565 1/psia (where $z = 1 + KP$)
P_o = 715 psia
T = Gas Field Formation Temperature = 70°F
$K_2 = k/\mu\phi c r_b^2 = 0.35 \times 10^{-5}$ 1/seconds
$\Delta t = .606 \times 10^6$ seconds = 1 week

Date	Inventory Gas in Place, Mcf (@ 60°F & 14.65 psia)	Observed Reservoir Pressure, Psia	Predicted Pressures, Psia: $A_j \neq 0$, $K_3 = .43 \times 10^{-5}$, "Gas Loss" = 12 M^3cf	Predicted Pressures, Psia: $A_j = 0$, $K_3 = .46 \times 10^{-5}$, "Gas Loss" = 12 M^3cf
1955 Sept. 30	21,718,753	731.5		
Oct. 7	21,921,162	735	726.4	724.2
Oct. 14	22,079,299	736.2	729.8	727.7
Oct. 21	22,271,891	738	733.4	731.7
Oct. 28	22,498,054	738.2	737.2	736.1
1955 Nov. 4	22,728,245	740	740	739.3
Nov. 11	22,806,731	736	735.8	735.3
Nov. 18	22,894,276	732.5	734.1	733.7
Nov. 25	23,155,528	739	740.1	740.1
1955 Dec. 2	23,020,604	728.5	727.9	727.8
Dec. 9	23,123,118	733	730.3	730.2
Dec. 16	22,905,135	721	718.4	718.1
Dec. 23	22,911,443	720	720	719.6
Dec. 30	23,211,928	734	732.2	732.2
1956 Jan. 6	23,404,623	737.4	735.2	735.6
Jan. 13	23,606,872	738.5	737.8	738.4
Jan. 20	23,843,593	742.5	741.2	742
Jan. 27	23,878,525	736	735.8	736.7
1956 Feb. 3	23,996,994	735.5	735.9	736.8
Feb. 10	24,274,831	741	742	743.1
Feb. 17	24,403,826	738	740.3	741.5
Feb. 24	24,594,969	739.6	741.9	743.2
1956 Mar. 2	24,787,774	741.2	743.1	744.5
Mar. 9	23,548,830	692	690.4	690.3
Mar. 16	23,483,865	704	700.1	699.7
Mar. 23	23,614,564	718	712.1	711.8
Mar. 30	23,971,217	733	727.6	727.9
1956 Apr. 6	24,289,732	742	736.1	736.8
Apr. 13	24,416,308	739	735	736
Apr. 20	24,499,116	735	733	734.1
Apr. 27	24,683,076	735	736	737.2
May 4	24,869,274	738	738	739.2

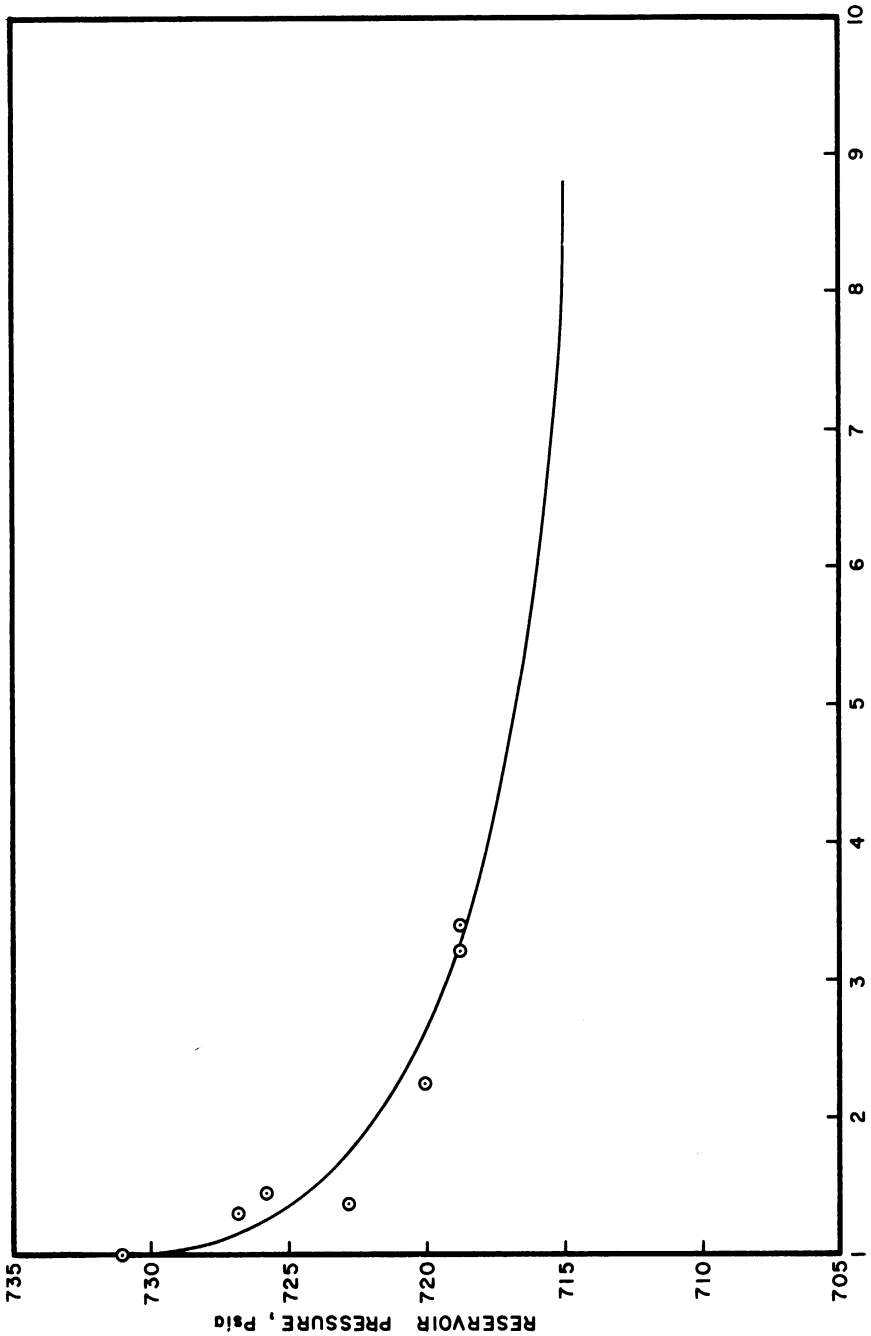

Pressure Distribution in Aquifer Underlying Reservoir E.
September 30, 1955

Figure 29

A time increment Δt of one week or 0.606×10^6 seconds was employed in the calculation of the above K_3 value and in the calculations described below. The value of P_o for reservoir E is 715 psia. The term DEV, defined as in Equation (III-25), serves as a measure of agreement between the field E observed and predicted pressures.

The initial pressure distribution curve given in Figure 29 extrapolates to a value of 0 at an r_D vaule of approximately 9 - 11. An r_{D_e} value of 10 was chosen for the purpose of calculating the value of the term $\sum_{n=1}^{\infty} a_n e^{-\lambda_n^2 t_D} U_o(\lambda_n)$ as a function of dimensionless time t_D. The calculations were programmed in the IBM 704 FORTRAN code and performed by the 704 computer; the results are listed in Table XII and plotted in Figure 32. The values of $\sum_{n=1}^{\infty} a_n e^{-\lambda_n^2 t_D} U_o(\lambda_n)$ for $t_D = K_2\Delta t, 2K_2\Delta t, 3K_2\Delta t, \ldots, 31K_2\Delta t$, where $K_2 = 0.35 \times 10^{-5}$/ second and $\Delta t = 0.606 \times 10^6$ seconds, were obtained by interpolation between the values listed in Table XII. The resulting interpolated values were then employed as the A_j terms in Equation (IV-28), where

$$A_j = \sum_{n=1}^{\infty} a_n e^{-\lambda_n^2 j \Delta t_D} U_o(\lambda_n) \qquad \text{(IV-29)}$$

For each of several assumed 'gas loss' values, where

'gas loss' = inventory gas content (from Table XI)

- effective gas content,

the gas in place values given in Table XI were reduced by the assumed 'gas loss'. The resulting effective gas in place values were employed

TABLE XII

$\bar{P}_{2(1,t_D)}$ AS A FUNCTION OF DIMENSIONLESS TIME t_D

FOR AQUIFER STORAGE RESERVOIR E

Assumed $r_{D_e} = 10$

t_D	$\bar{P}_{2(1,t_D)} = \sum_{n=1}^{\infty} a_n e^{-\lambda_n^2 t_D} U_o(\lambda_n) = A_j$
0	- 16
2	- 4.954
4	- 3.518
6	- 2.762
8	- 2.280
10	- 1.937
12	- 1.674
14	- 1.463
16	- 1.286
18	- 1.134
20	- 1.003
22	- .888
24	- .787
26	- .698
28	- .618
30	- .549
32	- .487
34	- .432
36	- .383
38	- .340
40	- .301
42	- .267
44	- .237
46	- .210
48	- .187
50	- .166
52	- .147
54	- .130
56	- .116
58	- .102
60	- .091
62	- .081

in Equation (IV-28) to calculate the predicted pressures, P_j ($j = 1, 2, 3, \ldots, 31$), for sufficiently many assumed K_3 values to fix a minimum on a plot of DEV vs K_3. A constant K_2 value of 0.35×10^{-5} was employed throughout these calculations, which were performed by the IBM 650 computer. The resulting DEV values are listed in Table XIII as a function of K_3 for assumed 'gas loss' values of 11, 12, and 13 billion standard cubic feet. DEV is plotted vs K_3 in Figure 30 with the 'gas loss' value as a parameter. The reservoir E predicted pressures, for assumed 'gas loss' and K_3 values of 12 M^3 cf and 0.43×10^{-5} psia/ft.^{3}, respectively, are listed in Table XI and are compared graphically to the observed pressures in Figure 31.

The predicted reservoir E pressures were also calculated with the term $\overline{P}_{2(1,t_D)}$ ignored, i.e., with all the A_j terms in Equation (IV-28) set equal to 0. This neglect of $\overline{P}_{2(1,t_D)}$ reduces (IV-28) to the predictive Equation (III-22), which was developed for the case of a uniform (constant) initial pressure throughout the aquifer. A 'gas loss' of 11 billion standard cubic feet was assumed and the predicted pressures P_j ($j = 1, 2, 3, \ldots, 31$) were calculated from (IV-28) for sufficiently many assumed K_3 values to fix a minimum on a plot of DEV vs K_3. The resulting DEV values are listed in Table XIII and are plotted vs K_3 in Figure 30. The predicted pressures obtained are graphically compared with the observed reservoir E pressures in Figure 31 and are listed in Table XI.

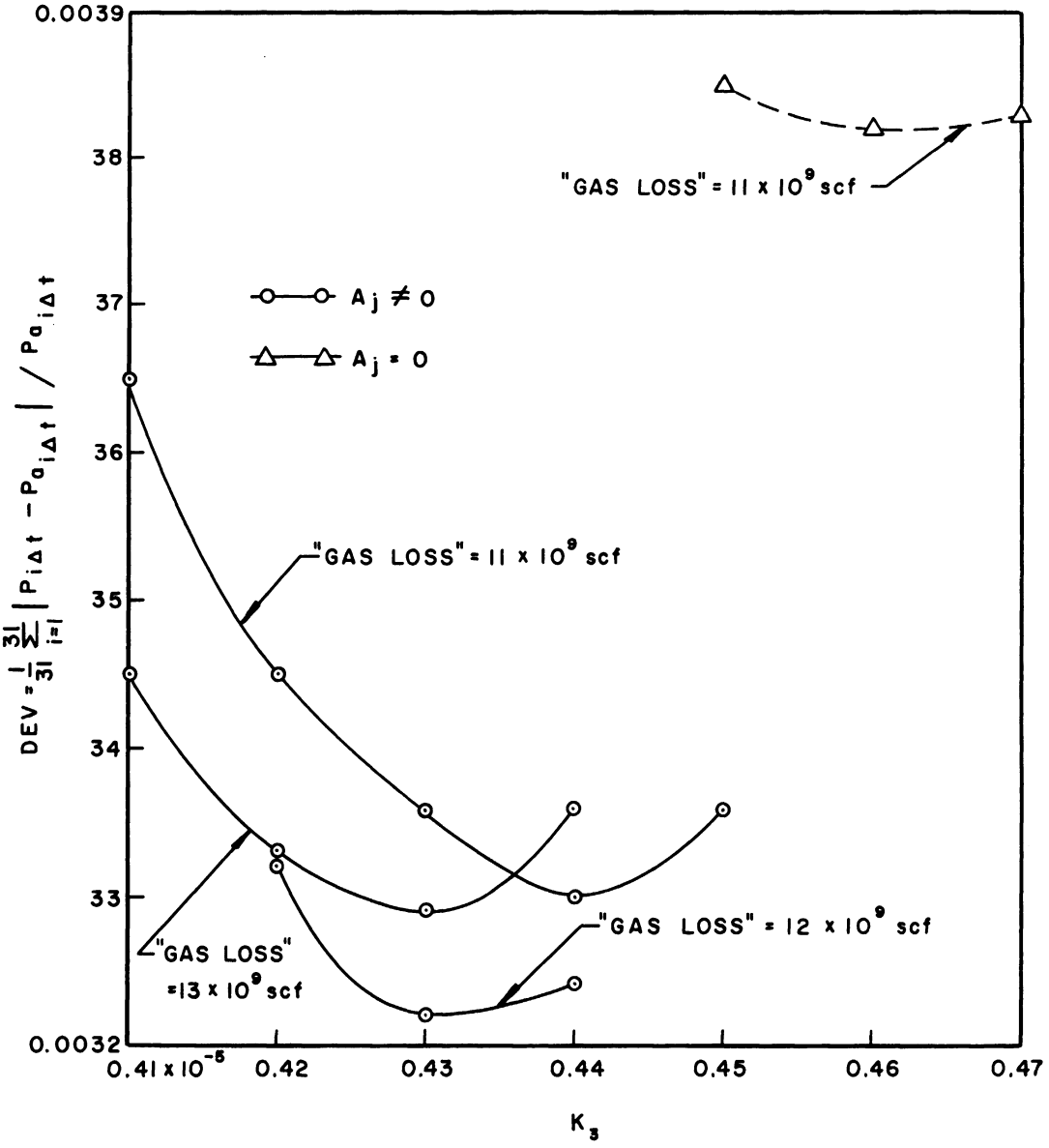

Effect of Assumed K_3 and "Gas Loss" Values on DEV Value for Aquifer Storage Reservoir E.

Figure 30

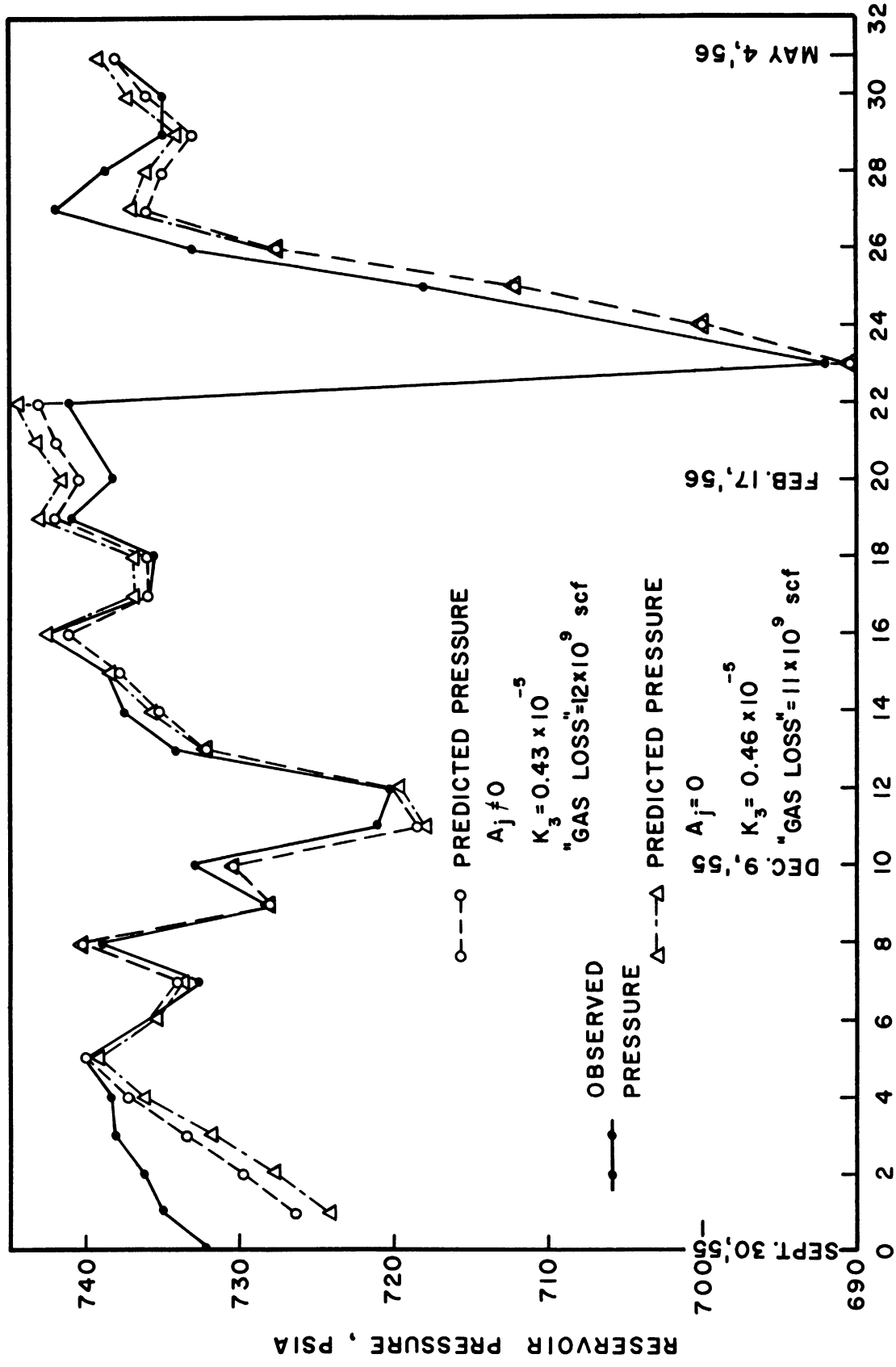

Figure 31. Comparison Between Aquifer Storage Reservoir E Observed and Predicted Pressures for Period September 30, 1955 - May 5, 1956.

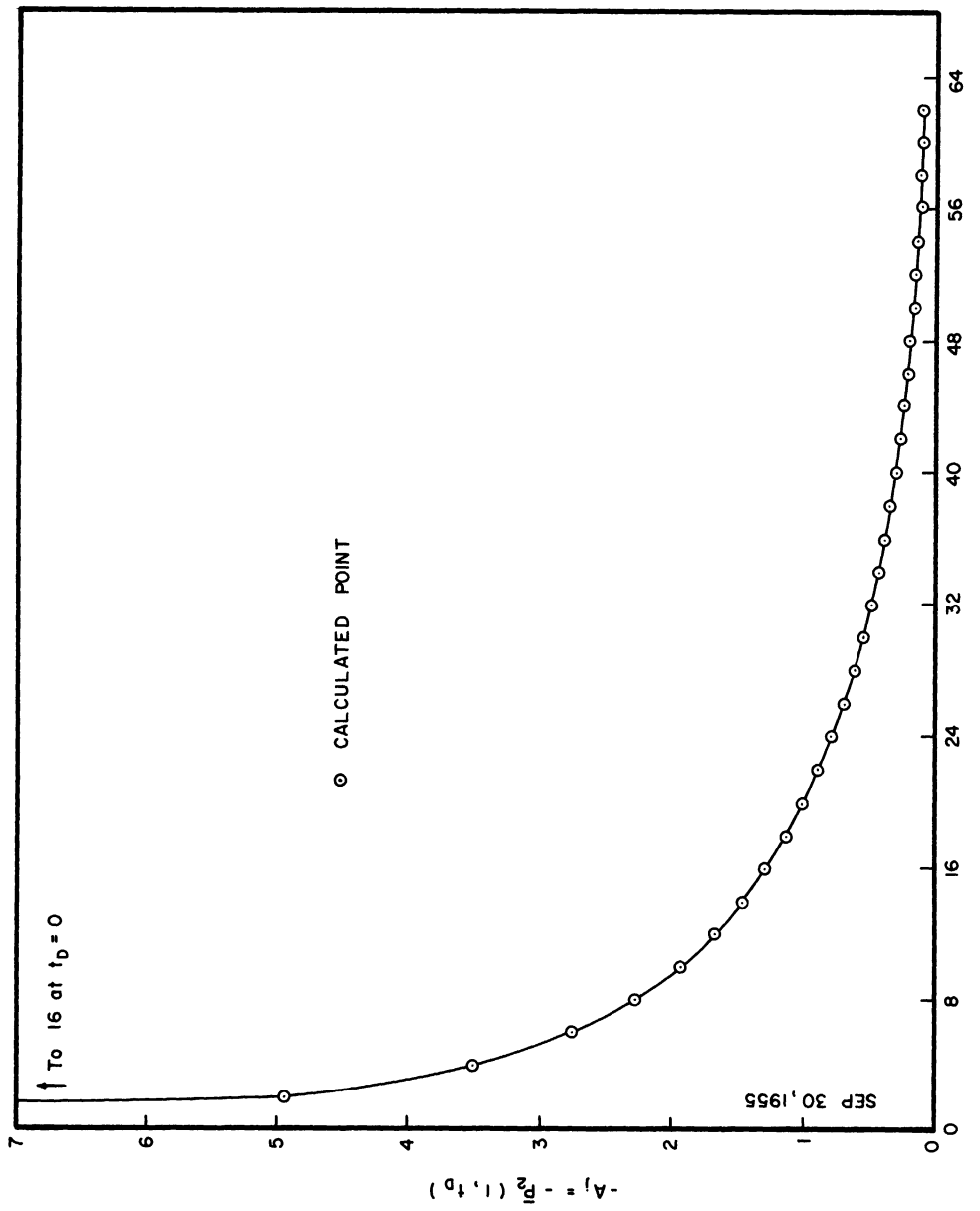

A_j vs. Dimensionless Time for Aquifer Storage Reservoir E.

Figure 32

TABLE XIII

DEV AS A FUNCTION OF ASSUMED "GAS LOSS" AND

K_3 VALUES FOR AQUIFER STORAGE RESERVOIR E

$K_2 = k/\mu\phi c r_b^2 = 0.35 \times 10^{-5}$ 1/seconds
$K = -.0001565$/Psia
Δt = 1 week = $.606 \times 10^6$ seconds
T = Gas Field Formation Temperature = 70°F
P_o = 715 Psia

Results for $A_j \neq 0$			Results for $A_j = 0$	
			Assumed "Gas Loss" = 11 M^3cf (@ 60°F & 14.65 psia)	
Assumed "Gas Loss" M^3cf (@ 60°F & 14.65 psia)	Assumed K_3 Value	DEV	Assumed K_3 Value	DEV
11	$.41 \times 10^{-5}$	.00365	$.45 \times 10^{-5}$	.00385
11	.42	.00345	$.46 \times 10^{-3}$	.00382
11	.43	.00336	$.47 \times 10^{-5}$	.00383
11	.44	.00330		
11	.45	.00336		
12	$.42 \times 10^{-5}$	.00332		
12	.43	.00322		
12	.44	.00324		
13	$.41 \times 10^{-5}$	.00345		
13	.42	.00333		
13	.43	.00329		
13	.44	.00336		

The results listed in Table XIII show that inclusion in Equation (IV-28) of the pressure drop term accounting for the aquifer initial pressure distribution, $\overline{P}_{2(1,t_D)}$, results in nearly a 16% decrease in the average fractional deviation (DEV) between the observed and predicted pressures (from 0.00382 to 0.00322 for an assumed 'gas loss' of 12 billion standard cubic feet). The definite minimums in the curves of DEV vs K_3 in Figure 30 show that a minimum DEV value serves as a good criteria for choice of the K_3 value when K_2 is fixed.

The above described Method A of treating cases involving a non-uniform initial aquifer pressure distribution may prove impractical in several respects. First, the value of r_{D_e} must be known or assumed and this value is, in general, unknown. Second, the calculation of the term $\overline{P}_{2(1,t_D)}$, required in application of Method A, is very lengthy since the roots λ_n of Equation (IV-25) must first be calculated, and the $a_n, U_o(\lambda_n)$, and $e^{-\lambda_n^2 t_D}$ values must then be determined and inserted into Equation (IV-24) in order to determine $\overline{P}_{2(1,t_D)}$. The practicality of Method A is further restricted by the requirement that the initial aquifer pressure distribution be known. Gas storage reservoir-aquifer systems may or may not have a sufficient number of aquifer observation wells to allow determination of this initial distribution.

3. Application to Aquifer Storage Reservoir E - Method B

The alternative Method B now presented requires neither qualitative nor quantitative knowledge of the initial pressure distribution and requires no specification of the value of r_{D_e}.

This method does require knowledge of the K_2, K_3, and P_o (where P_o is the constant aquifer pressure approaced at large radial distances from the gas reservoir) values. The K_2 ($= \frac{k}{\mu\phi c r_b^2}$) and K_3 ($= \frac{\mu}{2\pi hk\Delta t}$) values can be obtained from available data relating to the aquifer formation and water properties or from calculations similar to those described in Section III-C of this thesis.

The terms A_j, calculated above as $A_j = \sum_{n=1}^{\infty} a_n e^{-\lambda_n^2 j\Delta t_D} U_o(\lambda_n)$ can be calculated directly from field data by employing a rearranged form of Equation (IV-27)

$$A_j = P_o - P_{aj} - K_3 \sum_{i=0}^{i=j-1} (2V_{ai} - V_{a(i+1)} - V_{a(i-1)}) P((j-i)\Delta t_D) \quad \text{(IV-30)}$$

where P_{aj} = observed gas reservoir pressure at time $t = j\Delta t$, psia

V_{aj} = actual gas reservoir pore volume at time $t = i\Delta t$, $ft.^3$.

Suppose the predicted performance of a gas field is desired for a time period of (N-M) time increments, where M and N are both integers and $N > M$. Let M be such that 0 time is specified at M time increments prior to the beginning of the period for which the predicted performance is desired. If field data is available for the period from $t = 0$ to $t = M\Delta t$ then A_j can be calculated from Equation (IV-30) with $j = 1, 2, 3, \ldots, M$. Employing these A_j values for $j \leq M$, A_j values equal to 0 for $j > M$, and the projected gas in place schedule for the period from $t = (M+1)\Delta t$ to $t = N\Delta t$, one could then calculate P_j from Equation (IV-28) with $j = 1, 2, 3, \ldots, N$. However, the P_j values calculated for $j = 1, 2, 3, \ldots, M$, will simply be the P_{aj} values employed in calculating A_j from Equation (IV-30). Thus there is no need to calculate the terms A_j (from Equation IV-30) and P_j

(from IV-28) for j = 1, 2, 3, ..., M; the identical predicted pressures P_j (j = M+1, M+2, ..., N) will be obtained from (IV-28) by simply setting $P_j = P_{aj}$ and $V_i = V_{ai}$ for j or i < M, setting $A_j = 0$ for j > M, and beginning the calculations with j = M+1 in (IV-28). The approximation $A_j = 0$ for j > M will be valid in direct proportion to the value of $t_D = M\Delta t_D$ since

$$A_j = \sum_{n=1}^{\infty} a_n e^{-\lambda_n^2 j \Delta t_D} U_o(\lambda_n)$$

The method B outlined immediately above has been applied to gas storage reservoir E. The validity of the claim that the A_j values calculated from field data and Equation (IV-30) will decrease with increasing time was first tested. Pressure-injection data for the period September 1, 1956 - December 15, 1956, a time increment of three days, and K_2, K_3, and 'gas loss' values of .35 x 10^{-5}, 1.08 x 10^{-5}, and 12 M^3 cf, respectively, were employed in calculating A_j from Equation (IV-30). The resulting A_j values are listed in Table XIV with the gas field E data for the period September 1, 1956 - December 15, 1956. Figure 33 shows the decrease of A_j with increasing time.

Method B has been applied in calculating the predicted performance of aquifer storage reservoir E for the period December 18, 1956 - March 6, 1957. September 1, 1956 (36 three-day time increments prior to December 18, 1956) was specified as 0 time and the P_j and n_i values for j or i < 35 were taken from the data listed in Table XIV. The predicted P_j values were then calculated from Equation (IV-28) (with $A_j = 0$, $j \geq 36$) for j = 36, 37, ..., 62 (March 6, 1957). A three-day time increment and K_2 and 'gas loss'

Table XIV

SUMMARY OF RESERVOIR E DATA FOR PERIOD SEPTEMBER 1, 1956 - DECEMBER 15, 1956

Date	Observed Reservoir Pressure, Psia	Mcf Inventory Gas in Place (@ 14.65 psia & 60°F) (Includes Known 2.9475 M^3cf Vent Loss)	A_j Calculated from (IV-30) $K_2 = .35 \times 10^{-5}$ $K_3 = 1.08 \times 10^{-5}$ "Gas Loss" = 12 M^3cf $\Delta t = .25925 \times 10^6$ sec.
1956 Sept. 1	735	23,904,133	
Sept. 4	735	23,929,791	- 16.2
Sept. 7	734.2	23,946,195	- 14.0
Sept. 10	734.5	23,961,023	- 16.0
Sept. 13	735	23,981,894	- 16.2
Sept. 16	734.2	23,999,853	- 13.0
Sept. 19	734	24,016,902	- 13.4
Sept. 22	734	24,029,576	- 14.3
Sept. 25	734	24,073,009	- 9.8
Sept. 28	734	24,104,968	- 10.3
1956 Oct. 1	734	24,149,612	- 8.0
Oct. 4	735.2	24,202,403	- 9.6
Oct. 7	735.5	24,254,215	- 7.9
Oct. 10	736	24,299,321	- 9.1
Oct. 13	737	24,339,011	- 11.7
Oct. 16	736	24,363,984	- 8.9
Oct. 19	735.4	24,393,082	- 8.1
Oct. 22	735.3	24,426,468	- 8.1
Oct. 25	735.2	24,471,546	- 6.1
Oct. 28	735	24,515,877	- 5.2
Oct. 31	735.2	24,564,983	- 5.0
1956 Nov. 3	735.7	24,616,976	- 5.4
Nov. 6	736.2	24,664,850	- 6.3
Nov. 9	736	24,690,894	- 7.7
Nov. 12	735.8	24,735,508	- 5.1
Nov. 15	736.5	24,777,252	- 7.6
Nov. 18	736	24,807,763	- 6.3
Nov. 21	736	24,824,767	- 9.3
Nov. 24	733	24,831,932	- 1.7
Nov. 27	733.5	24,838,476	- 9.2
Nov. 30	733.5	24,879,548	- 4.4
1956 Dec. 3	734	24,928,980	- 4.1
Dec. 6	735.5	24,987,209	- 6.1
Dec. 9	734	25,001,096	- 4.2
Dec. 12	734.5	25,001,751	- 11.1
Dec. 15	732.5	25,021,261	- 2.2
Dec. 18	733	25,052,917	
Dec. 21	734.5	25,109,917	
Dec. 24	735	25,152,600	
Dec. 27	735.5	25,192,432	
Dec. 30	735.5	25,233,545	

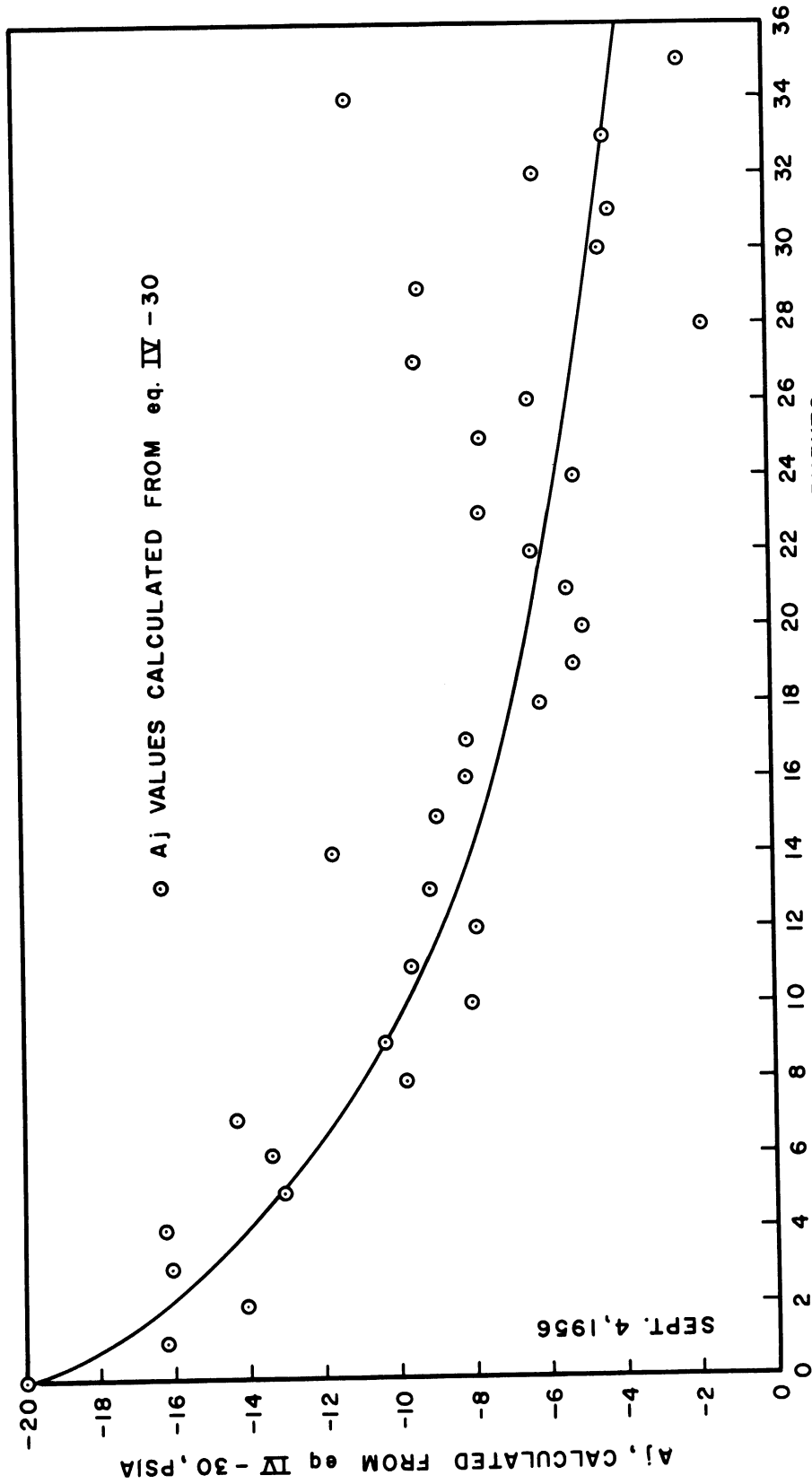

A_j vs. Time for Aquifer Storage Reservoir E, September 1, 1956 - December 15, 1956.

Figure 33

values of .35 x 10^{-5} and 12 M^3 cf, respectively, were employed in the calculations. The December 18, 1956 - March 6, 1957 gas in place data used in the calculations are listed in Table XV, along with the observed and predicted gas bubble pressures. The value of K_3 was varied until the value of DEV, defined in Equation (III-25) (with N = 62-35 = 27), passed through a minimum. The DEV values obtained are plotted versus K_3 in Figure 34 and the predicted reservoir E pressures are compared to the observed reservoir pressures in Figure 35.

The reservoir E predicted pressures for the December 18, 1956 - March 6, 1957 period were also calculated, ignoring the initial pressure distribution, from Equation (III-22). December 15, 1956 was specified as 0 time and a three-day time increment, and K_2 and 'gas loss' values of .35 x 10^{-5} and 12 M^3 cf, respectively, were used in the calculations. The K_3 value was varied until DEV, defined in (III-25) (with n = 27), passed through a minimum. DEV is plotted versus K_3 in Figure 34 and the predicted reservoir pressures calculated from (III-22) are listed in Table XV and plotted in Figure 35.

Figure 34 shows that use of method B yields significantly better agreement between the observed and predicted pressures than that obtained by ignoring the initial pressure distribution.

C. Treatment of the Moving Boundary Problem Encountered in Aquifer Storage Operations

As pointed out previously (Section I), the distinguishing characteristic of an 'aquifer storage' gas field is the growth of the field radius or

Table XV

SUMMARY OF RESERVOIR E OBSERVED

AND PREDICTED PERFORMANCE, DECEMBER 15, 1956 - MARCH 6, 1957

Date	Mcf Inventory Gas in Place (@ 60°F & 14.65 psia) (Includes Known 2.9475 Vent Loss)	Observed Reservoir Pressure, Psia	Predicted Pressure, Psia "Gas Loss" = 12 M^3cf $K_2 = .35 \times 10^{-5}$ Δt = 3 days = $.25925 \times 10^6$ sec. P_o = 715 Psia	
			From Method B ($K_3 = .63 \times 10^{-5}$)	Ignoring Initial Pressure Distribution ($K_3 = .55 \times 10^{-5}$)
1956 Dec. 15	25,021,261	732.5		
Dec. 18	25,052,917	733	728.5	725.7
Dec. 21	25,109,917	734.5	727.8	724.2
Dec. 24	25,152,600	735	727.1	723,2
Dec. 27	25,192,342	735.5	726.6	722.7
Dec. 30	25,233,545	735.5	726.3	722.4
1957 Jan. 2	25,164,139	731.5	722.1	718.5
Jan. 5	25,170,410	728.5	721.9	718.5
Jan. 8	25,211,675	733	722.9	719.6
Jan. 11	24,951,832	723	712.4	709.7
Jan. 14	24,409,203	713	694.1	692.7
Jan. 17	23,641,655	687.5	671.1	671.7
Jan. 20	23,746,900	688.3	688.5	689
Jan. 23	23,829,446	702.5	698.5	698.2
Jan. 26	23,606,157	700.5	692.5	692.8
Jan. 29	23,464,763	698	692	692.5
1957 Feb. 1	23,581,566	702	701.9	702
Feb. 4	23,813,816	718	713.1	712.4
Feb. 7	24,075,535	728.5	722.0	720.5
Feb. 10	24,129,902	729.5	720.6	718.9
Feb. 13	24,219,643	731	721.8	719.8
Feb. 16	24,307,362	733.5	722.8	720.7
Feb. 19	24,326,681	734.5	721.3	719.3
Feb. 22	24,405,428	733	722.7	720.6
Feb. 25	24,466,676	734	723.0	720.8
Feb. 28	24,503,658	733.5	722.4	720.3
1957 Mar. 3	24,560,432	732.8	722.9	720.7
Mar. 6	24,637,685	733	724.1	721.9

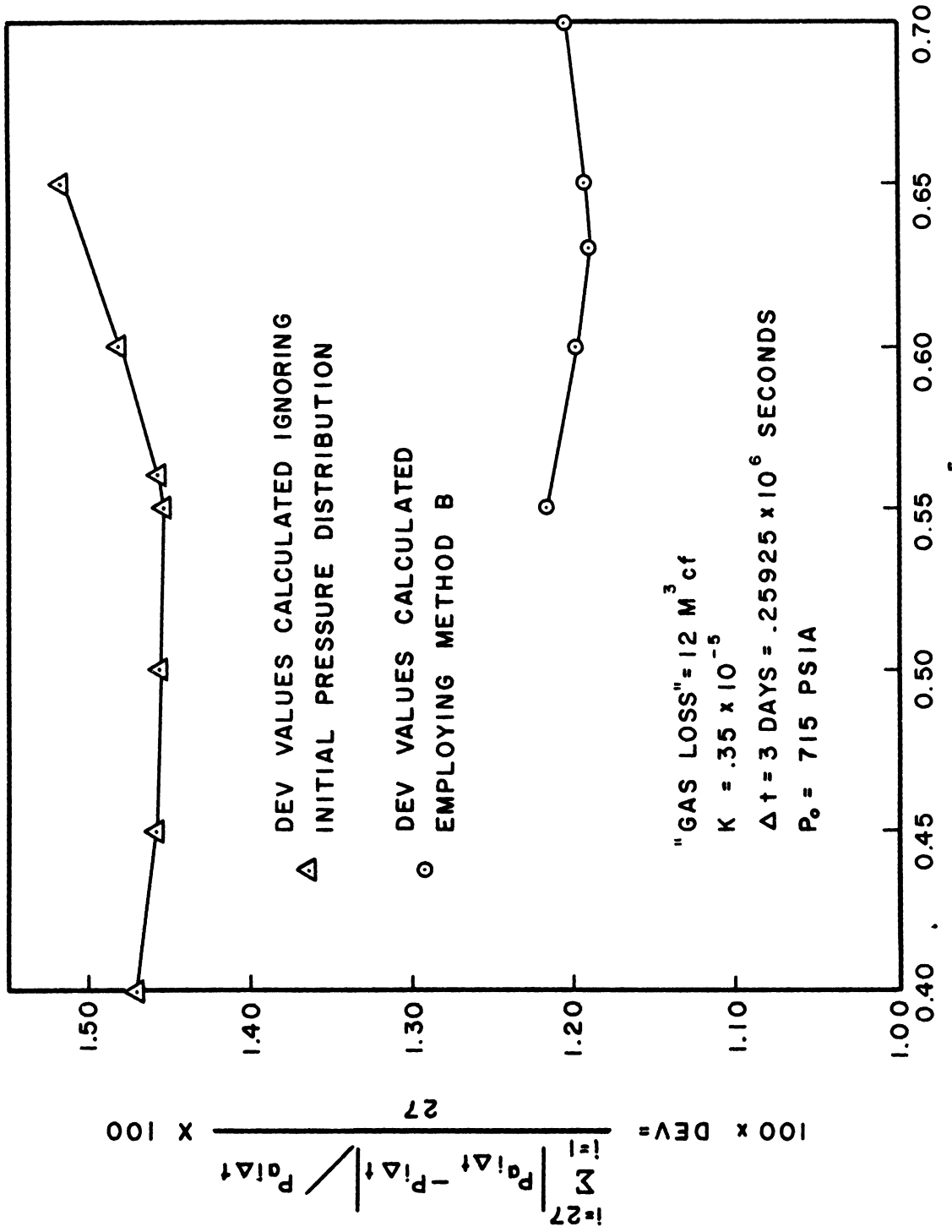

Figure 34. DEV vs. K_3 for Aquifer Storage Reservoir E, Period December 15, 1956 - March 6, 1957.

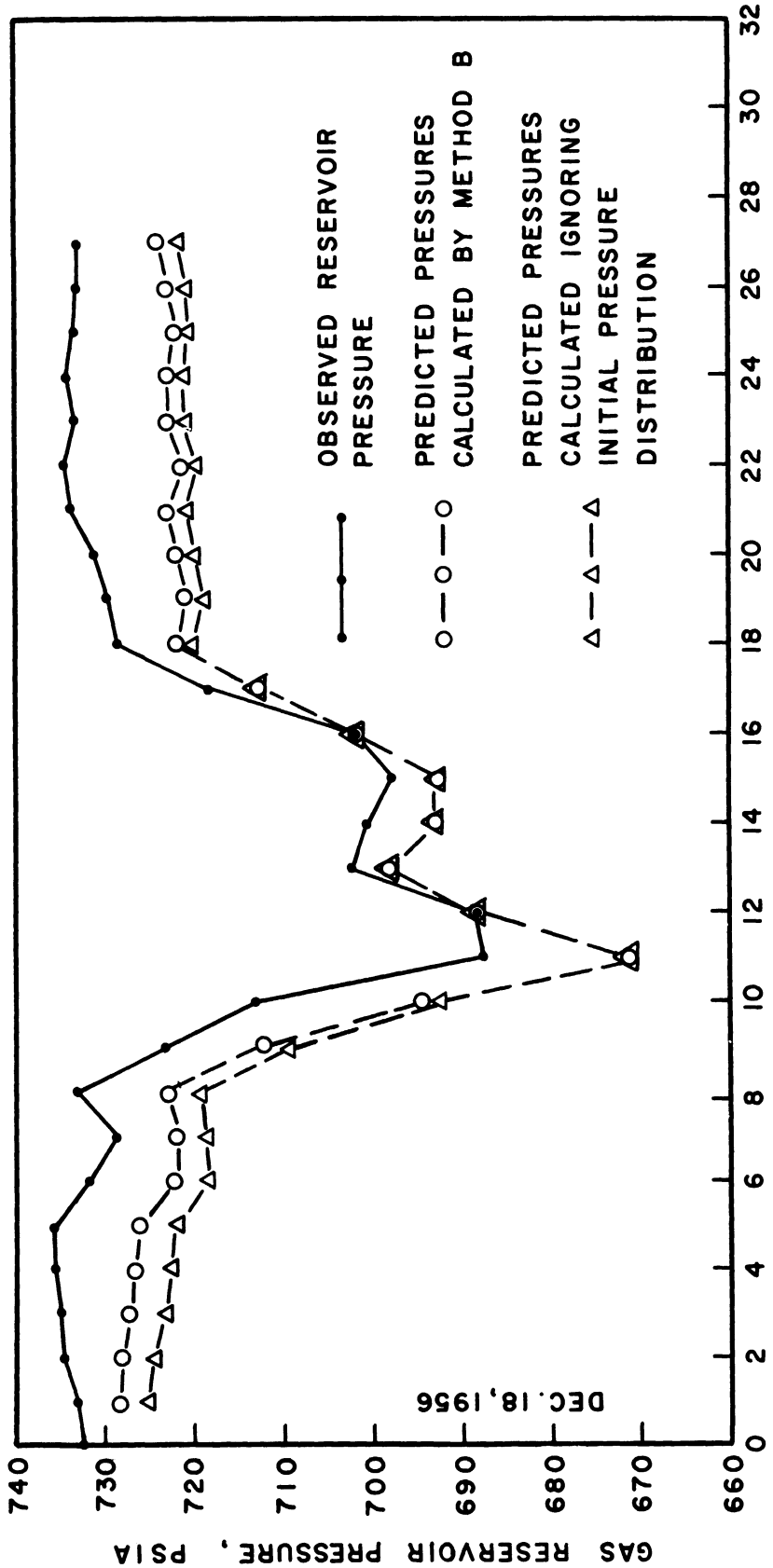

Figure 35. Comparison Between Aquifer Storage Reservoir E Observed and Predicted Pressures, December 15, 1956 - March 6, 1957.

volume with increasing time. The radius grows from a value of 0 at the time of initiation of the storage reservoir to values of several thousand feet. This increasing r_b (gas bubble radius) complicates the solution of the diffusivity Equation (III-5) since the term $K_2 = k/\mu\phi c r_b^2$ which appears in t_D ($t_D = K_2 t$) is no longer constant but is a function of time. The solution of Equation (III-5) for this case is commonly called a 'moving boundary problem'.

A general method of solving analytically a true moving boundary problem* has not been devised to date. The difficulty of solution lies in the fact that the diffusivity or governing differential equation cannot be solved until the time variation of the moving boundary position is known, but this boundary position is not known as a function of time until the differential equation has been solved. The literature[9] does contain analytical solutions to the diffusivity equation for cases involving moving line or moving point sources when the moving line or point position is known as a function of time. A numerical procedure[13] has also been presented for the solution of a liquid-liquid displacement problem in a square, where one liquid is injected at one corner and the other liquid is removed at an equal rate at the diagonally opposite corner. The moving source solutions are not applicable to the case considered here: the displacement or flow of a liquid away from a moving circular boundary at which a time-variant pressure is maintained. The numerical procedure can simulate only finite aquifers, entails a tremendous volume of calculations for an aquifer of reasonable extent (e.g. a ratio of 10 or greater between the aquifer exterior and interior radii), and is incapable of yielding general solutions applicable to any gas field.

* A 'true moving boundary problem' is one in which the movement of the boundary is not known *a priori* as a function of time.

The problem of predicting aquifer storage reservoir performance (during the initial growth stage of the gas bubble) is considered below from three points of view. First, the agreement between predicted and actual performance which can be obtained by ignoring the variation of r_b with time is determined. Second, an analytical approach to the moving boundary problem is developed and the resulting method is applied in a case study where the moving boundary position is known as a function of time. Third, the developed analytical approach to the moving boundary problem is employed in predicting the performance of an aquifer storage reservoir when the moving boundary position is not known a priori as a function of time.

The reader should recall that, as pointed out in Section IV-B, above, the difficulty presented by the growing r_b of an aquifer storage reservoir can be avoided entirely if the gas bubble is already grown and a prediction of future performance is desired. For, in this case, 0 time can be specified at a date when r_b has attained a relatively stable value and method B of Section IV-B can be employed to account for the non-uniform pressure distribution throughout the equifer at that date.

1. Prediction of Aquifer Storage Reservoir Behavior with r_b Assumed Constant

Calculations described in Section III-C of this thesis yielded the predicted performance of aquifer storage reservoir B for the period November 30, 1957 - July 5, 1958. The radius r_b was assumed constant in these calculations, i.e. the term $K_2 = k/\mu\phi c r_b^2$ was assumed to be independent of time. The calculations showed that no unique combination of K_3 and K_2 values resulted in best

agreement between predicted and actual performance but that this agreement improved as K_3 was decreased and K_2 increased. However, comparison between the predicted and actual pore volumes, plotted in Figures 21 and 22, shows that the agreement obtained is satisfactory for engineering purposes. The observation was made in Section III-C that the actual pressures in field B were increasing less rapidly than the predicted pressures; thus the question arises as to whether the discrepancy between the actual performance of field B and the predicted performance (predicted with the assumption of a constant r_b), for a time period starting from July 5, 1958, will become sufficiently large to invalidate the predicted performance for engineering purposes. In order to answer this question, the predicted performance of field B has been calculated from Equation (III-22) (which was derived from the assumption of a constant r_b) and compared to the actual performance over the period July 5, 1958 - November 29, 1958. A time increment of one week and K_3 and K_2 values of 2.3×10^{-5} and 1000, respectively, (the same values employed in calculating the results plotted in Figure 19) were used in the calculations. Gas in place and pressure data for the July 5, 1958 - November 29, 1958 period are listed in Table XVI. The gas in place data from Tables V and XVI were employed in calculating the predicted pressures from the variable-rate Equation (III-22). These predicted pressures and the gas in place data were then employed in Equation (III-20) to obtain the predicted pore volumes. The observed pressures (Tables V and XVI) and gas in place data were employed in

TABLE XVI

SUMMARY OF RESERVOIR B OBSERVED AND PREDICTED PERFORMANCE, JULY 5, 1958 - NOVEMBER 29, 1958

Date	MMcf Gas in Place* @ 60°F & 14.65 Psia	Reservoir Pressure,* Psia		Gas Bubble Pore Volume,* MMcf	
1958 July 5	1116.565d	1242.7d	1267.2p	10.88d	10.62p
July 12	1212.612d	1247 d	1276.6p	11.76d	11.53p
July 19	1300.974d	1242.6d	1278.5p	12.68d	12.24p
July 26	1394.177d	1244.6d	1282.7p	13.55d	13.06p
1958 Aug. 2	1492.338d	1244.1d	1288.4p	14.52d	13.90p
Aug. 9	1581.520d	1239.7d	1288.0p	15.42d	14.74p
Aug. 16	1979.101d	1241.3d	1292.0p	16.38d	15.59p
Aug. 23	1783.678d	1241.7d	1298.2p	17.30d	16.46p
Aug. 30	1861.472d	1231.4d	1291 p	18.30d	17.30p
1958 Sept. 6	1994.792d	1250 d	1309.5p	19.28d	18.21p
Sept. 13	2132.184d	1258.4d	1324.9p	20.35d	19.18p
Sept. 20	2257.872d	1258.4d	1331.9p	21.64d	20.18p
Sept. 27	2378.619d	1256.6d	1335.6p	22.80d	21.19p
1958 Oct. 4	2509.062d	1259.1d	1342.0p	24.06d	22.21p
Oct. 11	2642.448d	1259.9d	1348.0p	25.26d	23.26p
Oct. 18	2758.985d	1254.2d	1347.3p	26.42d	24.31p
Oct. 25	2877.581d	1249.6d	1347.6p	27.81d	25.34p
1958 Nov. 1	2997.308d	1251.4d	1348.2p	28.89d	26.38p
Nov. 8	3127.890d	1254.9d	1352.0p	30.09d	27.44p
Nov. 15	3233.416d	1253.5d	1347.9p	31.06d	28.47p
Nov. 22	3362.744d	1255.3d	1351.3p	32.31d	29.51p
Nov. 29	3419.731d	1228.6d	1334.6p	33.74d	30.49p

* "d" denotes quantity obtained from field data.

* "p" denotes quantity predicted for $K_3 = 2.3 \times 10^{-5}$, $K_2 = 1000$

Equation (III-20) to obtain the actual pore volumes. All the calculated quantities are tabulated in Table XVI; Figures 36 and 37 compare the actual and predicted pressures and actual and predicted pore volumes, respectively. The predicted pressures and pore volumes for the November 30, 1957 - July 5, 1958 period are identical to the predicted values tabulated in Table V and plotted in Figures 19 and 21. The value of DEV, calculated from Equation (III-25) (with N = 52 since there are 52 weeks between November 30, 1957 (initiation of reservoir B) and November 29, 1958), is 3.27%. That is, if one takes an average pressure of 1200 psia for field B over the first 52 weeks of operations then the average difference between the predicted (assuming a constant r_b) and observed pressure is .0327 x 1200 or 39.2 psia.

Figure 36 shows that a difference of 106 psia occurs between the predicted and observed field B pressures 52 weeks after initiation of the gas bubble. This error of 8.3% in the actual 1228 psia pressure invalidates the predicted pressure curve for engineering purposes. However, the predicted pore volume curve, shown in Figure 37, allows a useful estimation of the bubble size as a function of time. For example, suppose the operators of storage field B, after 2 or 3 weeks of gas injection, estimated the injection schedule for the first year of operations and wanted to know the period of time required to grow the bubble to a pore volume of 30 MMcf. The predictive method of calculation employed here would have given them an answer of $51\frac{1}{2}$ weeks, which Figure 37

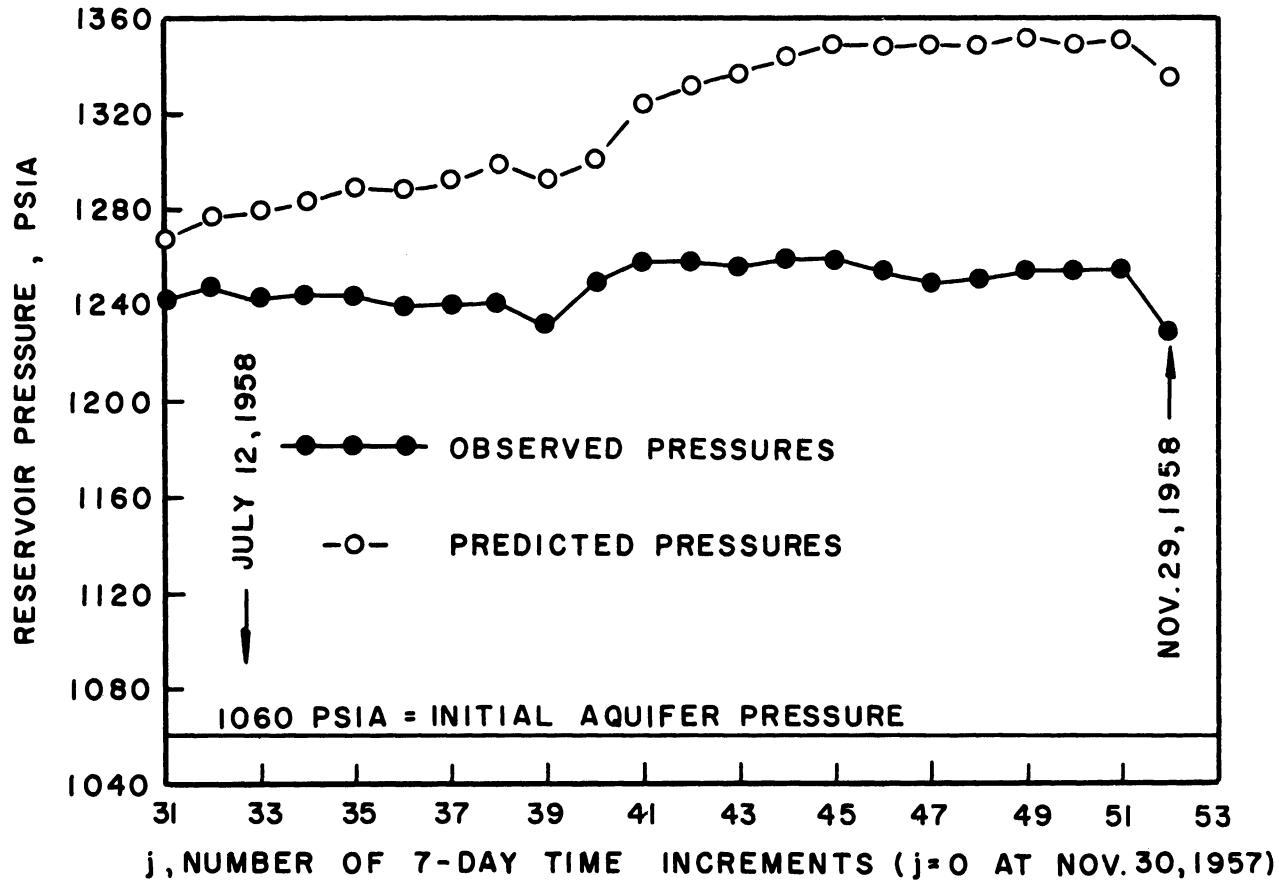

Figure 36. Comparison Between Aquifer Storage Reservoir B Predicted and Actual Pressures, July 5, 1958 - November 29, 1958.

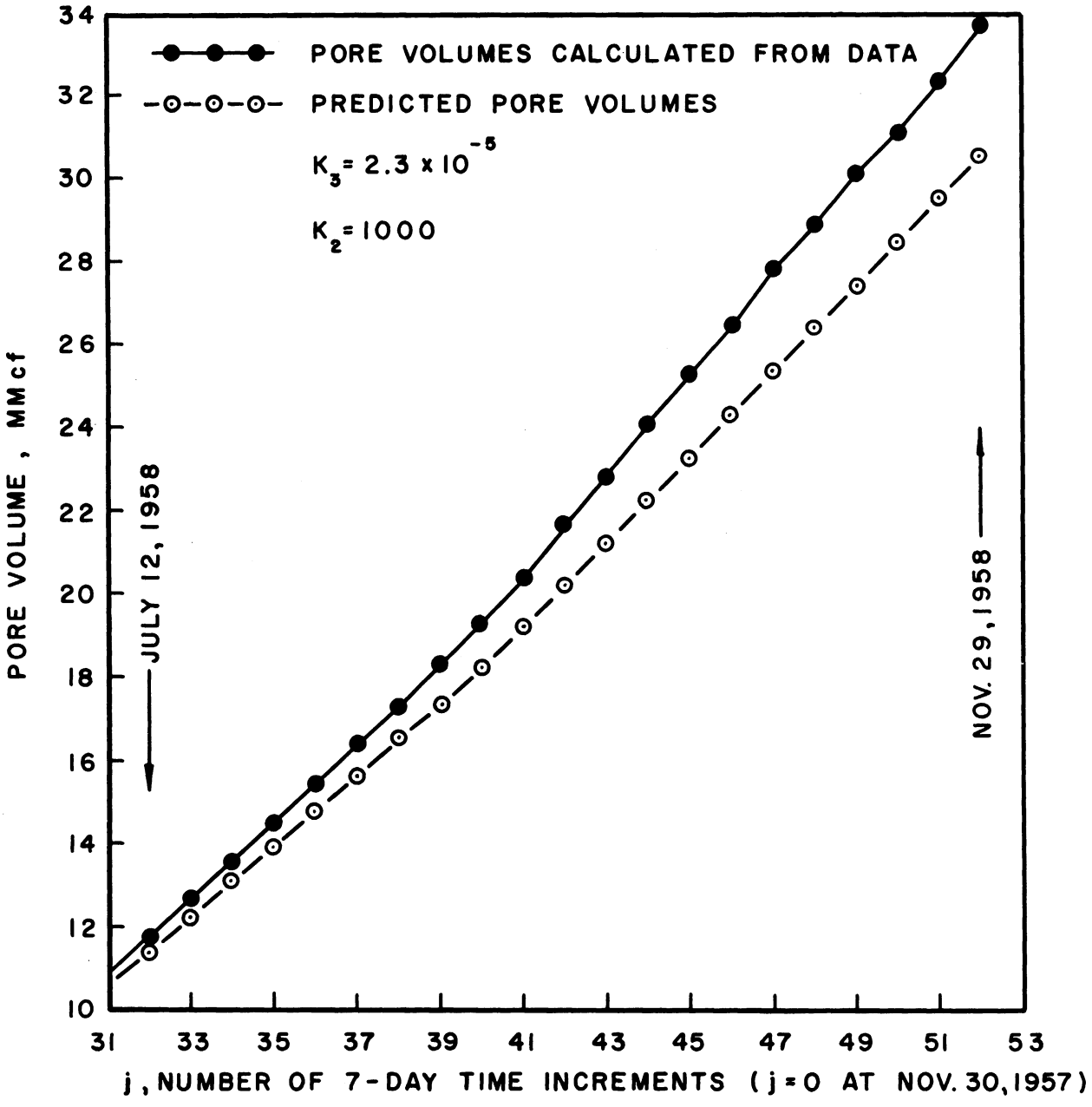

Figure 37. Comparison Between Aquifer Storage Reservoir B Predicted and Actual Pore Volumes, July 5, 1958 - November 29, 1958

shows is + $2\frac{1}{2}$ weeks in error. Thus the assumption of a constant r_b and use of the predictive equations developed in Section III-A provides a useful means of estimating the size of an aquifer storage reservoir as a function of time.

The discussion of field B in Section III-C-2 and in this section has attributed any gross difference between the actual and predicted performance to the increasing bubble radius. However, the observed difference, shown in Figures 36 and 37, can be attributed to two other factors. The first is leakage of gas through faults or permeable streaks in the field B cap rock. The effect of gas leakage would be that of decreasing the observed pressures (or increasing the pore volume, since $P \approx 1/V$, by the gas law) below the pressure corresponding to no leakage. Since Figure 36 shows that the actual pressure does fall below the predicted values, the possibility of gas leakage must be considered. The second factor is vertical pressure penetration into the aquifer formation. The predictive calculations assumed a circular disk flow model bounded on the top and bottom by impervious planes. However, a pressure test made in fall of 1958 indicated fluid pressure communication between the Mt. Simon and next lower formation, which had previously been considered separated by an impermeable shale streak. The effect of pressure communication to lower strata would be an increased pore volume growth rate since the water could recede in the vertical as well as horizontal directions. Since the actual growth rate exceeds the predicted rate, as shown in Figure 37, the possibility of vertical pressure penetration must also be

considered. The possibility of gas leakage and vertical pressure penetration is discussed further in Section IV-C-3, below.

An example is now presented of how the water influx calculations can provide information useful in the specification of gas injection and withdrawal during the growth of an aquifer storage reservoir. The Section III-A equations, derived from the assumption of a constant r_b, are employed in this example. The question considered is a very practical and important one concerning the effect of gas withdrawal during the initial growth stage of the gas bubble. The question is: what difference might be expected between the pore volumes and gas content of two aquifer storage reservoirs, separately grown in identical aquifer formations, at the end of a given number of years during which the first reservoir was grown under a constant bubble pressure and the second was grown under the same constant bubble pressure except during an annual 3 to 4 month gas withdrawal period? This question is of practical importance because storage field operators would like to compare the economics of withdrawing and selling gas from a reservoir as it is grown with the economics of withdrawing and selling gas only after the field is grown to the desired size.

Calculations have been performed to determine the aquifer storage reservoir performance effected by two different pressure schedules. The following reservoir properties were assumed:

infinite aquifer

P_o = 700 psia

$K_3 = 2.27 \times 10^{-5}$ psia/ft.^{3}

$K_2 = .89 \times 10^{-3}$ seconds^{-1}

along with a time increment of two weeks in calculating gas in place quantities from Equation (III-24) (when the pressure was specified) and in calculating pressures from Equation (III-22) (when the gas in place was specified).

The first case considered was the growth of the reservoir under a constant bubble pressure of 900 psia. The bubble pressure was increased in four 50 psia increments from 700 to 900 psia and was maintained at the latter value for 186 weeks. The predicted gas in place quantities were calculated from Equation (III-24) and were then employed in Equation (III-20) to yield the pore volumes. The specified pressure schedule and the calculated gas in place quantities and pore volumes are listed in Table XVII and plotted in Figure 38.

The second case treated was the growth of the reservoir at a constant bubble pressure of 900 psia, except during the last 12 weeks of each successive 48 week period when 20% of the current gas in place was withdrawn. Equations (III-22), (III-24), and (III-20) were again employed to calculate the pressure (when the gas in place was specified), the gas in place (when the pressure was specified) and the pore volumes. The calculated pore volumes and specified or calculated pressures and gas in place quantities and pore volumes are listed in Table XVII and plotted in Figure 38.

Table XVII

SUMMARY OF CALCULATED PERFORMANCE OF AQUIFER STORAGE RESERVOIR

WITH AND WITHOUT GAS WITHDRAWAL DURING THE GAS BUBBLE GROWTH STAGE

$K_3 = \mu/2\pi hk\Delta t = 2.27 \times 10^{-5}$ psia/ft^3
$K_2 = k/\mu\phi c r_b^2 = .89 \times 10^{-3}$ seconds^{-1}
Δt = 2 weeks
Case 1: Gas Bubble Grown at Constant 900 psia Pressure
Case 2: 20% of Current Gas in Place Withdrawn During Last 12 Weeks of Each 48 Week Period

j, Number of Two-Week Time Increments	Gas Bubble Pressure*, Psia		MMMcf Gas in Place*@ 14.65 Psia & 60°F		MMcf Gas Bubble Pore Volume	
	Case 1	Case 2	Case 1	Case 2	Case 1	Case 2
0	700	700	0	0	0	0
1	750s	750s	.034	.034	.605	.605
2	800s	800s	.108	.108	1.76	1.76
3	850s	850s	.226	.226	3.44	3.44
4	900s	900s	.395	.395	5.63	5.63
5	900s	900s	.541	.541	7.71	7.71
6			.682	.682	9.73	9.73
7			.821	.821	11.69	11.69
8			.956	.956	13.63	13.63
9			1.09	1.09	15.53	15.53
10			1.22	1.22	17.41	17.41
11			1.35	1.35	19.26	19.26
12			1.48	1.48	21.10	21.10
13			1.61	1.61	22.92	22.92
14			1.74	1.74	24.73	24.73
15			1.86	1.86	26.52	26.52
16			1.99	1.99	28.30	28.30
17			2.11	2.11	30.07	30.07
18			2.23	2.23	31.83	31.83
19		848.2	2.36	2.16s	33.58	32.96
20		808.1	2.48	2.09s	35.33	33.64
21		775.6	2.60	2.01s	37.06	33.99
22		748.5	2.72	1.94s	38.78	34.09
23		725.3	2.84	1.86s	40.50	33.96
24		705.1	2.96	1.79s	42.21	33.66
25		900s	3.08	2.51	43.91	35.77
26			3.20	2.65	45.61	37.71
27			3.32	2.78	47.30	39.58
28			3.44	2.91	48.99	41.40
29			3.56	3.03	50.67	43.19
30			3.67	3.16	52.34	44.96
31			3.79	3.28	54.01	46.71
32			3.91	3.40	55.68	48.45
33			4.02	3.52	57.34	50.17
34			4.14	3.64	58.99	51.88
35			4.26	3.76	60.64	53.58

Table XVII (CONT'D)

SUMMARY OF CALCULATED PERFORMANCE OF AQUIFER STORAGE RESERVOIR

WITH AND WITHOUT GAS WITHDRAWAL DURING THE GAS BUBBLE GROWTH STAGE

j, Number of Two-Week Time Increments	Gas Bubble Pressure*, Psia		MMMcf Gas in Place* @ 14.65 Psia & 60°F		MMcf Gas Bubble Pore Volume	
	Case 1	Case 2	Case 1	Case 2	Case 1	Case 2
36	900s	900s	4.37	3.88	62.29	55.28
37	900s	900s	4.49	4.00	63.93	56.96
38	900s	900s	4.60	4.12	65.57	58.64
39			4.72	4.23	67.21	60.32
40			4.83	4.35	68.84	61.98
41			4.95	4.47	70.47	63.64
42			5.06	4.58	72.09	65.30
43		860.7	5.17	4.43s	73.71	66.47
44		826.3	5.29	4.28s	75.33	67.27
45		795.6	5.40	4.12s	76.95	67.75
46		767.7	5.51	3.97s	78.56	67.95
47		742.0	5.63	3.82s	80.17	67.90
48		718.0	5.74	3.67s	81.77	67.63
49		900s	5.85	4.89	83.38	69.62
50			5.96	5.02	84.98	71.46
51			6.08	5.14	86.57	73.23
52			6.19	5.26	88.17	74.97
53			6.30	5.38	89.76	76.68
54			6.41	5.50	91.35	78.37
55			6.52	5.62	92.94	80.04
56			6.63	5.73	94.52	81.71
57			6.74	5.85	96.10	83.36
58			6.86	5.97	97.68	85.00
59			6.97	6.08	99.26	86.64
60			7.08	6.20	100.84	88.27
61			7.19	6.31	102.41	89.90
62			7.30	6.42	103.98	91.52
63			7.41	6.54	105.55	93.13
64			7.52	6.65	107.12	94.74
65			7.63	6.76	108.68	96.35
66			7.74	6.87	110.24	97.95
67		865.1	7.85	6.65s	111.80	99.13
68		833.2	7.96	6.42s	113.36	99.95
69		803.6	8.07	6.19s	114.92	100.47
70		775.8	8.17	5.96s	116.48	100.70
71		749.6	8.28	5.83s	118.03	100.68
72		724.7	8.39	5.50s	119.58	100.43
73		900s	8.50	7.18	121.13	102.36
74			8.61	7.31	122.68	104.14
75			8.72	7.43	124.23	105.86
76			8.83	7.55	125.77	107.55
77			8.94	7.66	127.31	109.21
78			9.04	7.78	128.85	110.85

Table XVII (CONT'D)

SUMMARY OF CALCULATED PERFORMANCE OF AQUIFER STORAGE RESERVOIR

WITH AND WITHOUT GAS WITHDRAWAL DURING THE GAS BUBBLE GROWTH STAGE

j, Number of Two-Week Time Increments	Gas Bubble Pressure*, Psia		MMcf Gas in Place*@ 14.65 Psia & 60°F		MMcf Gas Bubble Pore Volume	
	Case 1	Case 2	Case 1	Case 2	Case 1	Case 2
79	900s	900s	9.15	7.89	130.39	112.48
80			9.26	8.01	131.93	114.10
81			9.37	8.12	133.47	115.71
82			9.47	8.23	135.00	117.32
83			9.58	8.35	136.54	118.92
84			9.69	8.46	138.07	120.51
85			9.80	8.57	139.60	122.09
86			9.90	8.68	141.13	123.68
87			10.01	8.79	142.66	125.25
88			10.12	8.90	144.18	126.83
89			10.23	9.01	145.71	128.40
90			10.33	9.12	147.23	129.96
91		867.4	10.44	8.82s	148.75	131.96
92		836.8	10.55	8.51s	150.28	131.96
93		807.9	10.65	8.21s	151.80	132.49
94		780.3	10.76	7.90s	153.31	132.74
95		753.9	10.87	7.60s	154.83	132.73
96		728.4	10.97	7.30s	156.35	132.48

* "s", following number, denotes specified quantity

* Every number not followed by "s" was calculated from Equation (III-20), (III-22), or (III-24).

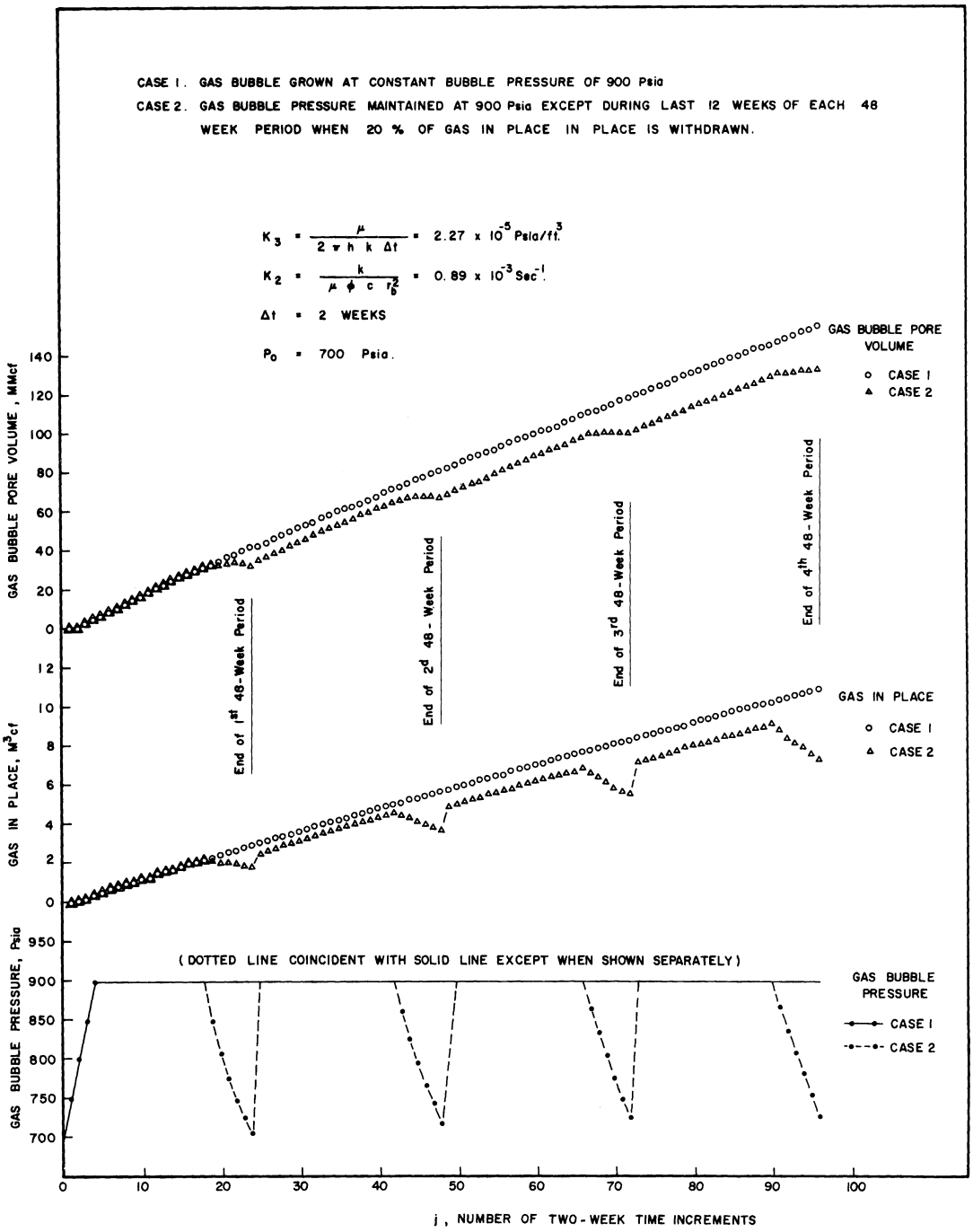

EFFECT OF GAS WITHDRAWAL DURING GROWTH ON PORE VOLUME & GAS CONTENT OF AQUIFER STORAGE RESERVOIR

Figure 38

The results listed in Table XVII show a gas in place difference between cases 1 and 2 of 1.21 M^3 cf (10.33 - 9.12 M^3 cf) at the end of 180 weeks of bubble growth. However, the cumulative gas withdrawn during the three withdrawal periods prior to the 180th week was 2.72 M^3 cf. Similarly, the difference between gas in place values at the end of 132 weeks is .87 M^3 cf although a cumulative 1.45 M^3 cf of gas was withdrawn (in case 2) prior to the 132nd week. Thus one can conclude (at least for the cases 1 and 2 considered here) that, at the end of a given gas injection season, the difference between the reservoir gas content obtained by continuous growth and the content obtained by interrupted injection of gas will be less than the cumulative gas withdrawn prior to the end of the given injection season.

2. Development of an Analytical Approach to the Moving Boundary Problem and Application to a Case Where r_b is Known as a Function of Time

As mentioned above, analytical solutions to the moving boundary problem, for cases where the position of the moving boundary is not known a priori as a function of time, have not been presented to date. A method is presented here which can be used in cases where r_b is known as a function of time. The usefulness of this method in cases where r_b is unknown a priori as a function of time is considered in Section IV-C-3 below.

The dimensionless time variable in the previously presented diffusivity Equation (III-5),

$$\frac{\partial^2 \bar{P}}{\partial r_D^2} + \frac{1}{r_D}\frac{\partial \bar{P}}{\partial r_D} = \frac{\partial \bar{P}}{\partial t_D} \qquad \text{(III-5)}$$

can be redefined in a manner which will take into account any arbitrary variation of r_b with time. t_D, as defined previously in this thesis, is related to t by

$$t_D = \frac{kt}{\mu\phi c r_b^2}$$

and $dt_D = k/\mu\phi c r_b^2 \; dt$. Now let τ_D be defined as

$$\tau_D = \frac{k}{\mu\phi c}\int_0^t \frac{dq}{r_b^2(q)} \qquad \text{(IV-31)}$$

where q is the dummy variable of integration, so that

$$d\tau_D = \frac{k}{\mu\phi c r_b^2(t)}\,dt = dt_D \qquad \text{(IV-32)}$$

Then Equation (III-5) becomes

$$\frac{\partial^2 \bar{P}}{\partial r_D^2} + \frac{1}{r_D}\frac{\partial \bar{P}}{\partial r_D} = \frac{\partial \bar{P}}{\partial \tau_D} \qquad \text{(IV-33)}$$

with τ_D defined by Equation (IV-31). The variation of r_b with time causes no difficulty with the boundary conditions Equation (III-6) or (III-7) since the conditions $\bar{P}_{(1,t_D)} = 1$ or $(\partial\bar{P}/\partial r_D)_{(1,t_D)} = 1$ spec the pressure and the pressure gradient at $r_D = r/r_b = 1$ and this r_D value is independent of the time varying r_b value.

Since the form of the diffusivity equation and its boundary conditions are unchanged by substituting τ_D for t_D, the tables of $\bar{Q}_{t_D}$ and $\underline{P}_{t_D}$ vs t_D, obtained by solution of the diffusivity equation for the conditions (III-6) and (III-7) and tabulated in the literature[1,2], can be interpreted as $\bar{Q}_{\tau_D}$ and $\underline{P}_{\tau_D}$ vs τ_D and can be applied in cases where r_b varies with time. The terms $\bar{Q}_{(j-i)\Delta t_D}$ and $\underline{P}_{(j-i)\Delta t_D}$ or $\bar{Q}_{j\Delta t_D - i\Delta t_D}$ and $\underline{P}_{j\Delta t_D - i\Delta t_D}$ in Equations

(III-21) and (III-22) must now be interpreted as $\bar{Q}_{\tau_{D_j}-\tau_{D_i}}$ and $\underline{P}_{\tau_{D_j}-\tau_{D_i}}$, where

$\bar{Q}_{\tau_{D_j}-\tau_{D_i}}$ = the dimensionless production quantity tabulated in the literature[1,2] vs. t_D, for $t_D = \tau_{D_j} - \tau_{D_i} = \frac{k}{\mu\phi c}\left[\int_0^{j\Delta t} \frac{dq}{r_b^2(q)} - \int_0^{i\Delta t} \frac{dq}{r_b^2(q)}\right]$

and $\underline{P}_{\tau_{D_j}-\tau_{D_i}}$ = the dimensionless pressure drop quantity tabulated in the literature[1,2] vs. t_D, for $t_D = \tau_{D_j}-\tau_{D_i}$.

The integral $\int_0^{j\Delta t} \frac{dq}{r_b^2(q)}$ can be evaluated approximately as

$$\int_0^{j\Delta t} \frac{dq}{r_b^2(q)} \cong \int_0^{(j-1)\Delta t} \frac{dq}{r_b^2(q)} + \frac{\Delta t}{2}\left[\frac{1}{r_b^2((j-1)\Delta t)} + \frac{1}{r_b^2(j\Delta t)}\right] \quad \text{(IV-34)}$$

where $\int_0^{\Delta t} \frac{dq}{r_b^2(q)}$ is obtained by setting r_b^2 equal to some assumed function of time for small time. For example, if r_b^2 is assumed proportional to $\sqrt{t}$ for small time, then

$$\int_0^{\Delta t} \frac{dq}{r_b^2(q)} = \int_0^{\Delta t} \frac{dq}{A\sqrt{q}} = \frac{2}{A}\sqrt{t}$$

where A is some constant. The value of A can be determined if r_b^2 is known at $t = \Delta t$ as $A = r^2_{b(\Delta t)}/\sqrt{\Delta t}$. If r_b^2 is assumed proportional to t^x for small time then x must be less than 1 for the integral $\int_0^{\Delta t} \frac{dq}{r_b^2(q)}$ to exist. In the present discussion, the value of r_b^2 at $t = j\Delta t$ ($j = 1, 2, 3, \ldots, N$) is assumed to be known from field data.

a. Application to Field B

The above outlined method of treating cases where r_b varies with time has been applied in determining the effective reservoir parameter values for aquifer storage reservoir B. Section III-C-2 describes the attempt to determine the field B

parameter values by calculations which employed equations derived from the assumption of a constant r_b. The result of this attempt was the conclusion that no unique combination of K_3 and K_2 values corresponded to best agreement between the actual and predicted performance of field B (over the November 30, 1957 - July 5, 1958 period) but that this agreement continuously improved as K_3 was decreased and K_2 was increased. The hypothesis was made that field B's nonconformance to the constant r_b assumption might be responsible for the failure to obtain a unique, optimum combination of K_3 and K_2 values. Thus application of the above outlined moving boundary theory should provide a test of this hypothesis.

The values of r_b^2 required in Equation (III-34), above, were obtained from field B's pressure-production data in the following manner. The relationship between r_b and y, where y is the vertical distance from the apex of the field B cap rock to the water level, was obtained from a contour map and is given in Equation (IV-35) below.

$$r_b = 200y \qquad \text{(IV-35)}$$

This relationship between r_b and y is shown in the idealized vertical cross-section of reservoir B, sketched in Figure 39. Since the volume of a right circular cone is $1/3\ \pi r^2 h$ or, in the terms employed here, $1/3\ \pi r_b^2 y$, the field B pore volume is related to r_b by the equation

$$V = \frac{1}{3}\phi\pi r_b^2 y = \frac{1}{3}\frac{\pi\phi r_b^3}{200} \qquad \text{(IV-36)}$$

or

$$r_b^2(t) = \left(\frac{600\,V_t}{\pi\phi}\right)^{2/3} \qquad \text{(IV-37)}$$

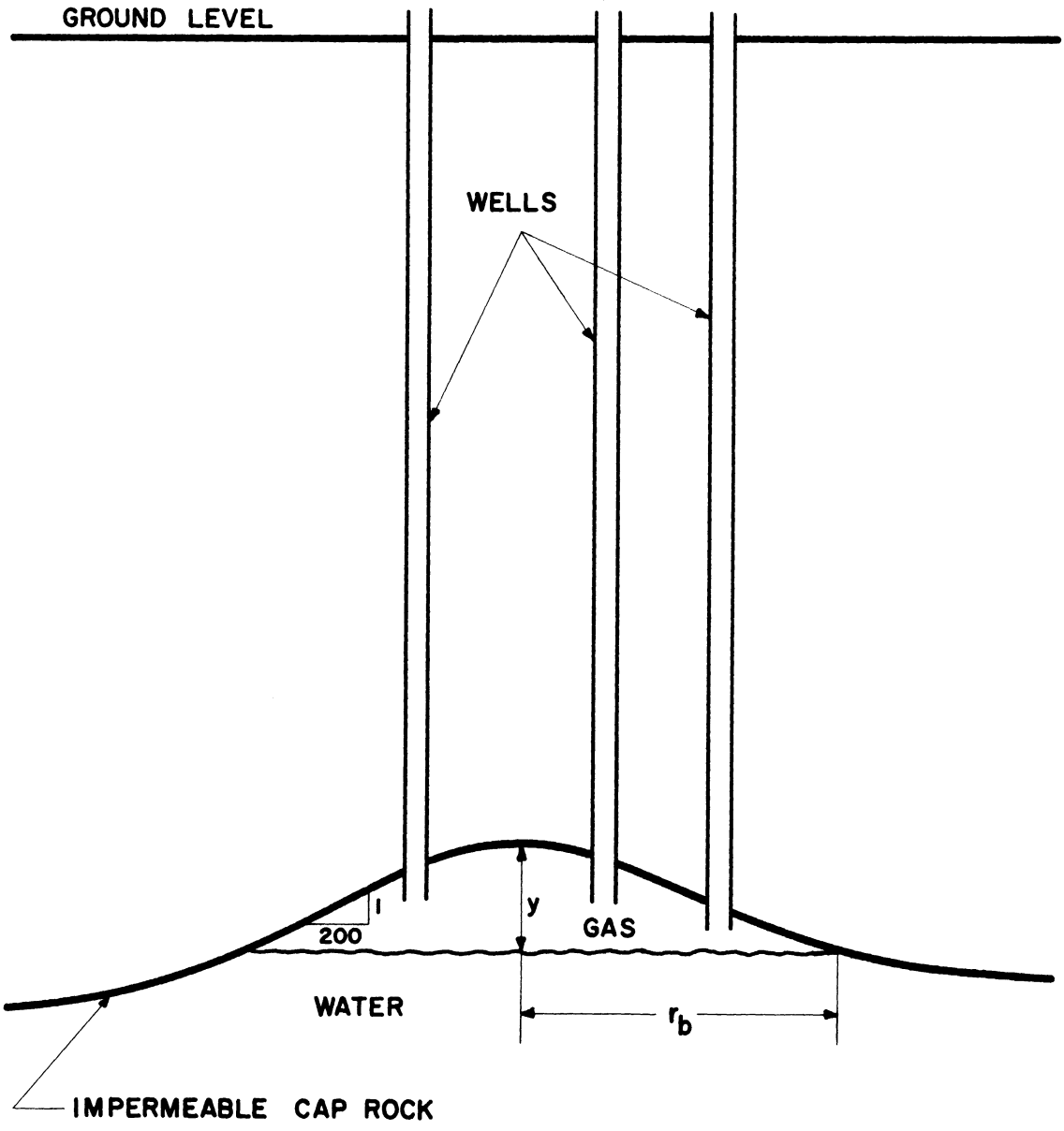

Figure 39. Relationship Between r_b and y (Distance of Water Level from Apex of Cap Rock) in Aquifer Storage Reservoir B.

Substituting V_t from Equation (III-20) into (IV-37), one obtains the following relationship between r_b^2 and n_t and P_t.

$$r_b^2 = \left(\frac{600RT}{\pi\phi}\right)^{2/3}\left[n_t\left(K + \frac{1}{P_t}\right)\right]^{2/3} \qquad \text{(IV-38)}$$

Equation (IV-38) now allows the calculation of r_b^2 from available pressure-production data (P_t and n_t). Insertion of r_b^2 from (IV-38) into (IV-31) yields

$$\tau_{D(t)} = \frac{k}{\mu\phi c}\left(\frac{\pi\phi}{600RT}\right)^{2/3}\int_0^t \frac{dt}{\left[n_t\left(K+\frac{1}{P_t}\right)\right]^{2/3}} \qquad \text{(IV-39)}$$

The value of $\tau_{D(t)}$ for $t = \Delta t$ (= one week = $.606 \times 10^6$ seconds) was obtained by assuming the field B pore volume directly proportional to time for small time. Thus

$$V_t = n_t RT\left(K + \frac{1}{P_t}\right) = Ct$$

where C is some constant, or

$$n_t\left(K + \frac{1}{P_t}\right) = At$$

where A is some constant to be determined from field data. The data listed in Table V give

$$n_{\Delta t} = \frac{5.092 \times 10^6 \text{ Scf}}{381 \text{ Scf/lb. mole}}$$

$$P_{\Delta t} = 1075 \text{ psia}$$

The value of K was obtained as - .000152 from compressibility data for the gas injected into field B. Thus

$$A = \frac{n_{\Delta t}\left(K + \frac{1}{P_{\Delta t}}\right)}{\Delta t} = \frac{\frac{5.092 \times 10^6}{381}\left(-.000152 + \frac{1}{1075}\right)}{.606 \times 10^6}$$

$$= 0.171 \times 10^{-4} \text{ lb.moles/psia-seconds}$$

and $n_t(K + 1/P_t) = .171 \times 10^{-4}t$ for $0 \leq t \leq \Delta t$. Inserting this expression for $n_t(K + 1/P_t)$ into Equation (IV-39) and integrating from $t = 0$ to $t = \Delta t$, one obtains

$$\tau_{D(\Delta t)} = \frac{k}{\mu\phi c}\left(\frac{\pi\phi}{600RT}\right)^{2/3} \times 3.78 \times 10^5 \qquad \text{(IV-40)}$$

The values of $\tau_{D_j} = \tau_{D_{(t = j\Delta t)}}$ ($j = 1, 2, 3, \ldots., N$, where N was taken as 31) are given by

$$\tau_{D_j} = \tau_{D_{j-1}} + K_2' \frac{\Delta t}{2}\left[\frac{1}{[n_{j-1}(K + \frac{1}{P_{j-1}})]^{2/3}} + \frac{1}{[n_j(K + \frac{1}{P_j})]^{2/3}}\right] \qquad \text{(IV-41)}$$

where

$$K_2' = \frac{k}{\mu\phi c}\left(\frac{\pi\phi}{600RT}\right)^{2/3}$$

and n_j and P_j are the actual (from data) pound moles gas in place and gas bubble pressure, respectively, at time $t = j\Delta t$.

The predicted field B pressures, for the 31 week period from November 30, 1957 to July 5, 1958, have been calculated from Equation (III-22). The n_t (gas in place) quantities required in this equation were obtained from the data listed in Table V. The term $\underline{P}_{(j-i)\Delta t_D}$ or $\underline{P}_{j\Delta t_D - i\Delta t_D}$ appearing in (III-22) was interpreted as $\underline{P}_{\tau_{D_j} - \tau_{D_i}}$, defined above; τ_{D_j} was calculated from Equation (IV-41) and the pressure and gas in place data listed in Table V. The predicted pressures P_j ($j = 1, 2, 3, \ldots., 31$) were calculated for various combination of K_3 ($= \mu/2\pi hk\Delta t$) and K_2' values, chosen as outlined in Section III-C-1. These pressures were then employed in calculating, for each combination of K_3 and K_2' values, the value of DEV, defined in Equation (III-25) (with N = 31). DEV is listed in Table XVIII and plotted vs K_3 with K_2' as a parameter in Figure 40. The predicted pressures and pore volumes, calculated

TABLE XVIII

DEV VALUES FOR RESERVOIR B, CALCULATED BY

MOVING BOUNDARY METHOD (SECTION IV-C-2)

$K_2' = (k/\mu\varphi c)(\pi\varphi/600RT)^{2/3}$

$K_3 = \mu/2\pi hk\Delta t$

$\Delta t = 7$ days $= .606 \times 10^6$ seconds

K_2'	K_3	DEV (in %)
7×10^{-6}	$.328 \times 10^{-3}$	1.627
7×10^{-6}	$.335 \times 10^{-3}$	1.593
7×10^{-6}	$.341 \times 10^{-3}$	1.568
7×10^{-6}	$.348 \times 10^{-3}$	1.583
7×10^{-5}	$.162 \times 10^{-3}$	1.549
7×10^{-5}	$.165 \times 10^{-3}$	1.515
7×10^{-5}	$.169 \times 10^{-3}$	1.512
7×10^{-5}	$.172 \times 10^{-3}$	1.536
7×10^{-4}	$.965 \times 10^{-4}$	1.531
7×10^{-4}	$.984 \times 10^{-4}$	1.482
7×10^{-4}	$.100 \times 10^{-3}$	1.453
7×10^{-4}	$.102 \times 10^{-3}$	1.465
7×10^{-3}	$.676 \times 10^{-4}$	1.532
7×10^{-3}	$.689 \times 10^{-4}$	1.482
7×10^{-3}	$.703 \times 10^{-4}$	1.472
7×10^{-3}	$.717 \times 10^{-4}$	1.480

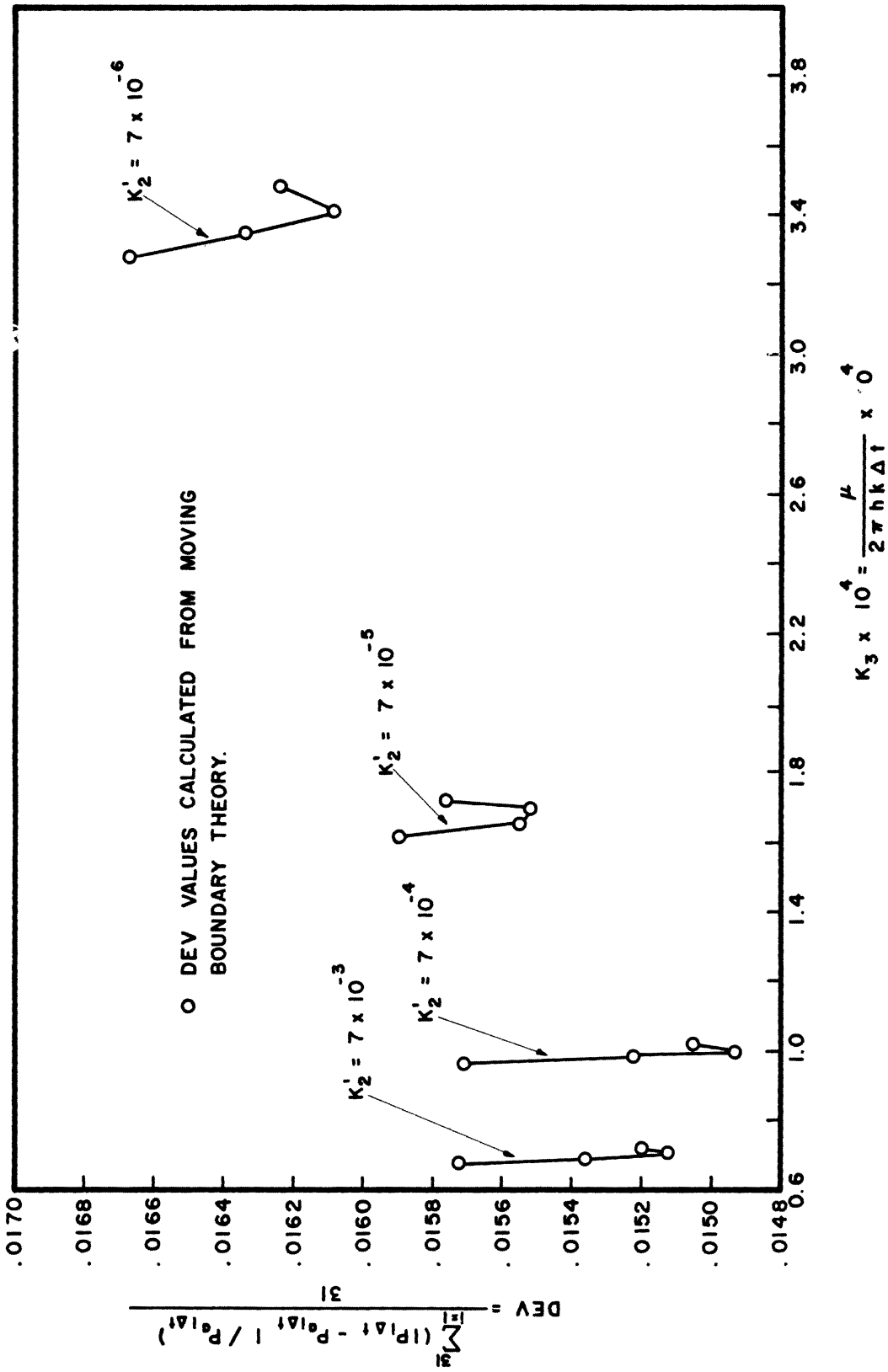

DEV vs K_3 for Aquifer Storage Field B.

Figure 40

for $K_3 = 1.0036 \times 10^{-4}$ and $K_2' = 7 \times 10^{-4}$ are listed in Table XIX and are compared to the actual pressures and volumes in Figures 41 and 42.

Figure 40 shows that the following unique combination of K_3 and K_2' values corresponds to best agreement between the field B actual and predicted performance:

$$\left.\begin{aligned} K_3 &= 1.0036 \times 10^{-4} = \frac{M}{2\pi h k \Delta t} \\ K_2' &= 7 \times 10^{-4} = \frac{k}{\mu \phi c}\left(\frac{\pi \phi}{600 RT}\right)^{2/3} \end{aligned}\right\} \qquad \text{(IV-42)}$$

Available field data yield

$h = 94'$

$k/\mu = 200 - 500$ millidarcys /centipoise

$\varphi = .16$

$RT = 5687$ psi - ft.^{3}/# mole

while a reasonable value of c, the sum of the aquifer water and formation compressibilities[23], is 7×10^{-6} vol./vol.-psia. Inserting the above values of c, φ, and RT into (IV-42) and considering h and k/μ as unknowns, one obtains

$h = 92.5'$

$k/\mu = 385$ millidarcys/centipoise

Thus use of the developed moving boundary theory in conjunction with the method of Section III-C-1 yields unique field B parameter values, which in turn yield formation permeability and thickness values in excellent agreement with those estimated from core analysis and field data. This fact, along with the fact that the method of Section III-C-1 yielded no unique combination of K_3 and K_2 values when equations derived from the assumption of a constant r_b were employed, indicate

Table XIX

RESERVOIR B PRESSURES AND PORE VOLUMES

PREDICTED BY MOVING BOUNDARY METHOD (SECTION IV-C-2),

NOVEMBER 30, 1957 - JULY 5, 1958

Date	Reservoir Pressure, psia		Reservoir Pore Volume, MMcf	
	Observed	Predicted*	Actual	Predicted*
1957 Nov. 30	1060		0	
Dec. 7	1075	1078.9	.059	.059
Dec. 14	1075.4	1075.7	.103	.103
Dec. 21	1088.2	1084.2	.180	.181
Dec. 28	1084.9	1080.5	.238	.239
1958 Jan. 4	1078.8	1070.7	.251	.253
Jan. 11	1093.2	1084.5	.333	.336
Jan. 18	1098.5	1091.4	.442	.446
Jan. 25	1100.7	1096.0	.568	.571
1958 Feb. 1	1206.9	1112.5	.702	.775
Feb. 8	1222.4	1151.2	1.09	1.174
Feb. 15	1103.9	1102.4	1.25	1.251
Feb. 22	1088.5	1087.3	1.27	1.272
1958 Mar. 1	1193.3	1135.1	1.50	1.598
Mar. 8	1204.6	1158.6	1.93	2.028
Mar. 15	1202.8	1167.7	2.39	2.478
Mar. 22	1166.8	1144.3	2.68	2.745
Mar. 29	1203.6	1176.3	3.15	3.239
1958 Apr. 5	1202.4	1182.8	3.67	3.741
Apr. 12	1191.4	1179.3	4.14	4.191
Apr. 19	1201.7	1191.3	4.67	4.717
Apr. 26	1145	1169.3	5.18	5.052
1958 May 3	1143.2	1155.0	5.37	5.303
May 10	1181.2	1181.8	5.79	5.785
May 17	1193.4	1193.2	6.32	6.322
May 24	1180.8	1186.6	6.82	6.776
May 31	1194.7	1195.4	7.30	7.297
1958 June 7	1208.8	1208.7	7.90	7.903
June 14	1207	1214.5	8.59	8.522
June 21	1190.3	1223.8	9.51	9.192
June 28	1238.9	1242.1	10.02	9.987
1958 July 5	1242.7	1250.0	10.88	10.799

* Predicted for $K_2' = (k/\mu\phi\vartheta)(\pi\phi/600RT)^{2/3} = 7 \times 10^{-4}$

$K_3 = \mu/2\pi hk\Delta t = 1.0036 \times 10^{-4}$

$\Delta t = 7$ days $= .606 \times 10^6$ seconds

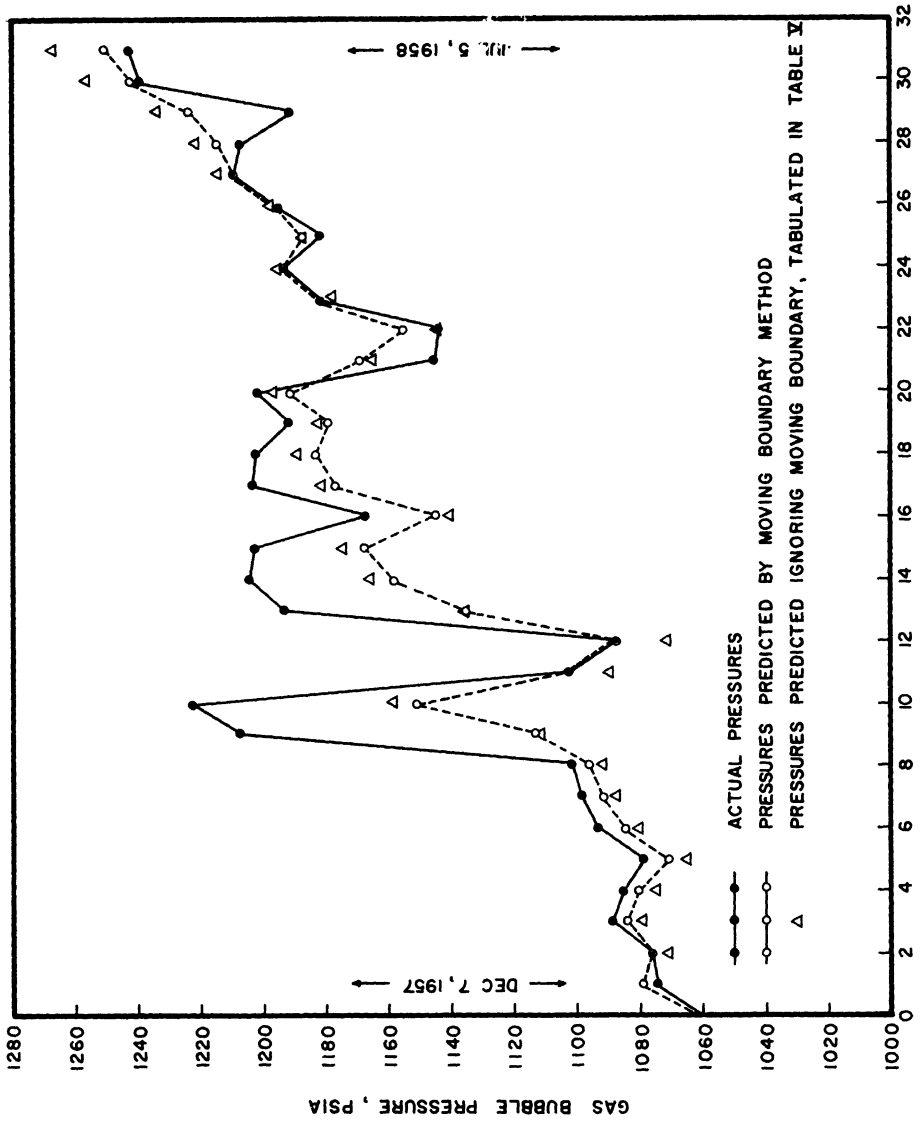

Comparison Between Field B Actual Pressures and Pressures Predicted by Moving Boundary Method, November 30, 1957 - July 5, 1958.

Figure 41

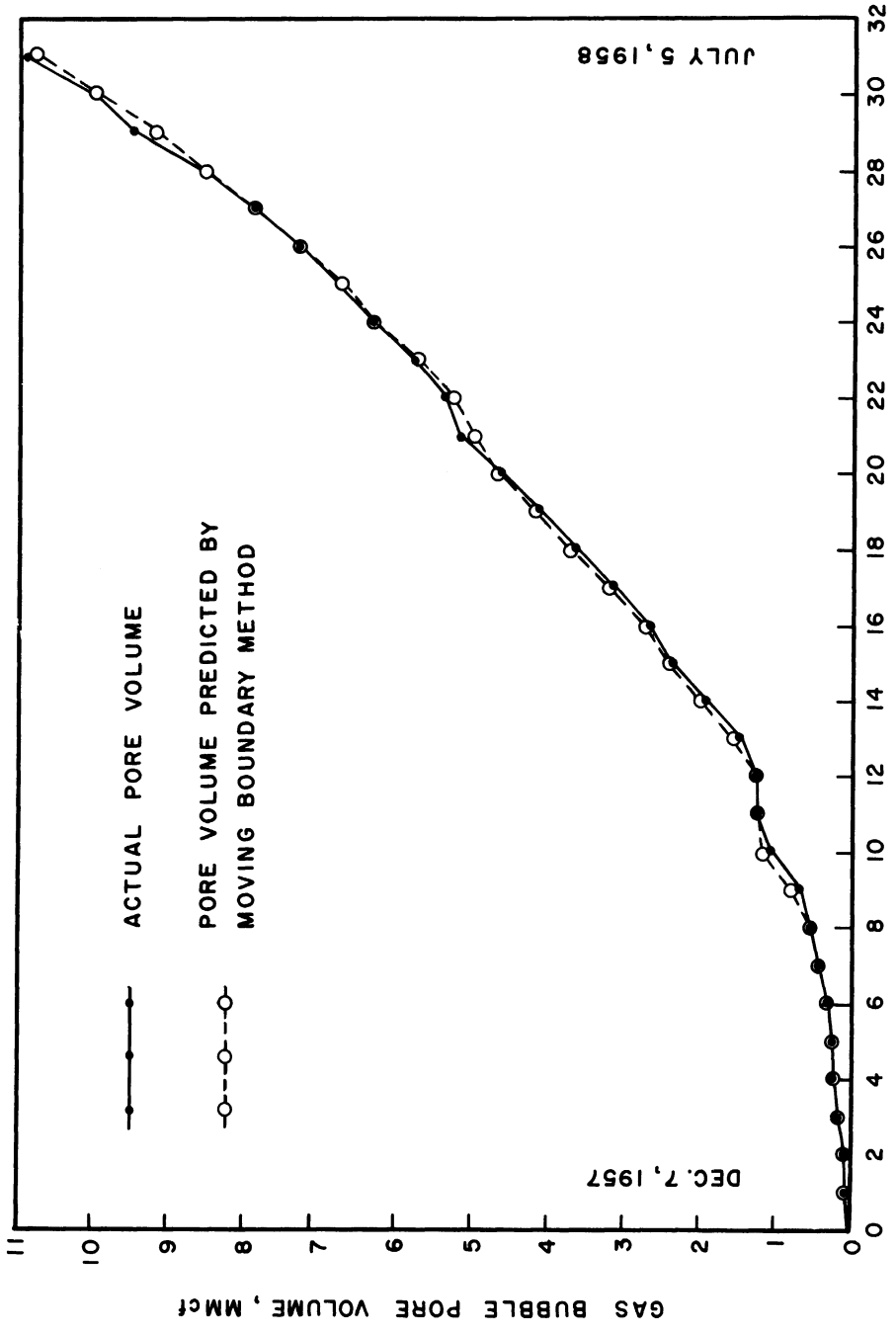

Comparison Between Field B Actual Pore Volumes and Pore Volumes Predicted by Moving Boundary Method, November 30, 1957 - July 5, 1958.

Figure 42

the validity and usefulness of the moving boundary method developed. The usefulness of this method is further indicated by the fact that the minimum DEV value obtained by the calculations described in this section was 1.45% (see Figure 40) whereas the minimum DEV obtained in Section III-C-2 ('constant r_b' treatment) was 1.63%. That is, the moving boundary treatment of field B presented in this section increased the agreement between predicted and actual performance 11% above the agreement obtained in Section III-C-2.

Figure 41 also shows the field B pressures (listed in Table V) predicted by assuming a constant r_b, as described in Section III-C-2. This figure shows the dampening effect on the rate of pressure increase effected by taking the moving boundary into account. That is, the 'moving boundary pressures' are initially somewhat higher, on the average, than the 'constant r_b pressures' but are considerably lower after 31 weeks of bubble growth.

3. Application of Moving Boundary Method to the Case Where r_b is Unknown as a Function of Time

The analytical approach to the moving boundary problem, developed in Section IV-C-2, above, is employed here in treatment of a case where r_b is unknown *a priori* as a function of time. Description and application is given of a trial and error method in which an assumed position of the moving boundary at time step j is employed in calculating P_j and P_j is then used to establish a more accurate position of the boundary. The gas in place schedule is considered specified and the pressures and pore volumes are considered unknown in the developments below.

The method developed in Section IV-C-2, above, involves replacement of the term $\underline{P}_{(j-i)\Delta t_D}$ in Equations (III-16a) or (III-22) by $\underline{P}_{\tau_{D_j}-\tau_{D_i}}$, where τ_{D_j} is given by Equation (IV-41). Thus Equation (III-22) becomes

$$P_j = \frac{-K_6'' + \sqrt{K_6''^2 + K_7'}}{2} \qquad \text{(IV-43)}$$

where K_6'' and K_7' are the same as K_6 and K_7 given on page 22, with $\underline{P}_{\Delta t_D}$ and $\underline{P}_{(j-i)\Delta t_D}$ replaced by $\underline{P}_{\tau_{D_j}-\tau_{D_{j-i}}}$ and $\underline{P}_{\tau_{D_j}-\tau_{D_i}}$, respectively. Equation (IV-43) allows an iterative procedure in which 1) a P_j value is assumed and employed in calculating τ_{D_j} from (IV-41), 2) a new P_j is then calculated from (IV-43), 3) the new P_j is employed to yield a new τ_{D_j}, from (IV-41), 4) etc., until successive values of P_j, calculated from (IV-43), are sufficiently close to one another. This iterative procedure has proven convergent in the application to field B, described below.

The field B gas in place data tabulated in Tables V and XVI and K_2', K_3 values of 7×10^{-4} and 1.0036×10^{-4}, respectively (the optimum combination found in Section IV-C-2, above), have been employed in calculating P_j by iterative solution of (IV-43) for $j = 1,2,3, \ldots, 52$. These P_j were then employed in Equation (III-20) to yield the predicted pore volumes and in Equation (III-25) to yield DEV. A τ_{D_1} value of $3.78 \times 10^5 K_2'$, developed in Section IV-C-2, was assumed. The calculations were programmed in the FORTRAN code and carried out by an IBM 704 computer.

The calculated pressures and pore volumes are listed in Table XX. Figures 43 and 44 compare these predicted quantities to the actual field performance. Figure 43 also shows the

TABLE XX

FIELD B PRESSURES AND PORE VOLUMES PREDICTED BY

MOVING BOUNDARY METHOD OF SECTION IV-C-3

Date		Reservoir Pressure*, Psia		Reservoir Pore Volume*, MMcf	
1957	Nov. 30	1060d		0	
	Dec. 7	1075d	1078p	.059d	.059p
	Dec. 14	1075.4d	1075.6p	.1025d	.1025p
	Dec. 21	1088.2d	1084.1p	.180d	.181p
	Dec. 28	1084.9d	1080.5p	.238d	.239p
1958	Jan. 4	1078.8d	1070.7p	.251d	.253p
	Jan. 11	1093.2d	1084.4p	.333d	.336p
	Jan. 18	1098.5d	1091.3p	.442d	.446p
	Jan. 25	1100.7d	1095.9p	.568d	.571p
1958	Feb. 1	1206.9d	1112.1p	.702d	.775p
	Feb. 8	1222.4d	1150.2p	1.09d	1.18p
	Feb. 15	1103.9d	1101.9p	1.25d	1.25p
	Feb. 22	1088.5d	1086.9p	1.27d	1.27p
1958	Mar. 1	1193.3d	1134.5p	1.50d	1.60p
	Mar. 8	1204.6d	1157.7p	1.93d	2.03p
	Mar. 15	1202.8d	1166.8p	2.39d	2.48p
	Mar. 22	1166.8d	1143.6p	2.68d	2.75p
	Mar. 29	1203.6d	1175.5p	3.15d	3.24p
1958	Apr. 5	1202.4d	1181.9p	3.67d	3.74p
	Apr. 12	1191.4d	1178.5p	4.14d	4.19p
	Apr. 19	1201.7d	1190.3p	4.67d	4.72p
	Apr. 26	1145d	1168.5p	5.18d	5.06p
1958	May. 3	1143.2d	1154.3p	5.37d	5.31p
	May 10	1181.2d	1181.0p	5.79d	5.79p
	May 17	1193.4d	1192.4p	6.32d	6.33p
	May 24	1180.8d	1185.8p	6.82d	6.78p
	May 31	1194.7d	1194.6p	7.30d	7.30p
1958	June 7	1208.8d	1207.9p	7.90d	7.91p
	June 14	1207d	1213.6p	8.59d	8.53p
	June 21	1190.3d	1223.0p	9.51d	9.20p
	June 28	1238.9d	1241.3p	10.02d	9.99p
1958	July 5	1242.7d	1249.3p	10.88d	10.81p
	July 12	1247d	1257.0p	11.76d	11.65p
	July 19	1242.6d	1259.2p	12.68d	12.47p
	July 26	1244.6d	1263.6p	13.55d	13.31p
1958	Aug. 2	1244.1d	1269.1p	14.52d	14.17p
	Aug. 9	1269.7d	1269.7p	15.42d	15.00p
	Aug. 16	1241.3d	1274.0p	16.38d	15.86p
	Aug. 23	1241.7d	1279.7p	17.30d	16.76p
	Aug. 30	1231.4d	1274.7p	18.30d	17.57p

TABLE XX (CONT'D)

FIELD B PRESSURES AND PORE VOLUMES PREDICTED BY

MOVING BOUNDARY METHOD OF SECTION IV-C-3

Date		Reservoir Pressure*, Psia		Reservoir Pore Volume*, MMcf	
1958	Sept. 6	1050d	1290p	19.28d	18.55p
	Sept. 13	1258.4d	1302.7p	20.35d	19.59p
	Sept. 20	1258.4d	1308.0p	21.64d	20.64p
	Sept. 27	1256.6d	1311.0p	22.80d	21.68p
1958	Oct. 4	1259.1d	1316.5p	24.06d	22.75p
	Oct. 11	1259.9d	1321.8p	25.26d	23.85p
	Oct. 18	1254.2d	1321.6p	26.42d	24.90p
	Oct. 25	1249.6d	1322.6p	27.81d	25.95p
1958	Nov. 1	1251.4d	1324.0p	28.89d	26.99p
	Nov. 8	1254.9d	1327.9p	30.09d	28.06p
	Nov. 15	1253.5d	1325.3p	31.06d	29.08p
	Nov. 22	1255.3d	1329.1p	32.31d	30.14p
	Nov. 29	1228.6d	1316.1p	33.74d	31.03p

* "d" denotes number obtained from field data.

* "p" denotes predicted quantity

$$K_2' = 7 \times 10^{-4}$$

$$K_3 = 1.0036 \times 10^{-4}$$

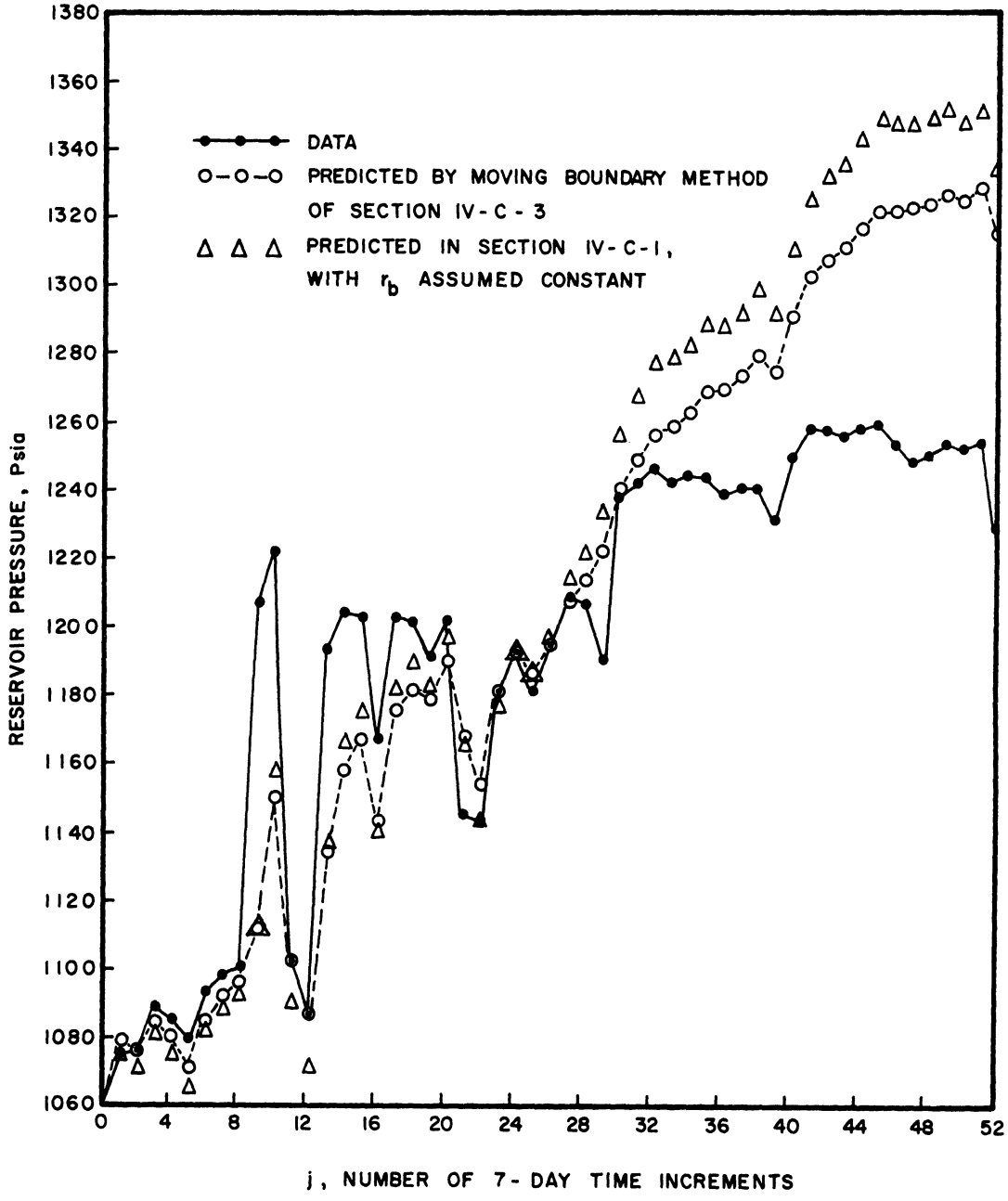

Comparison Between Field B Observed Pressures and Pressures Predicted by Moving Boundary Method of Section IV-C-3.

Figure 43

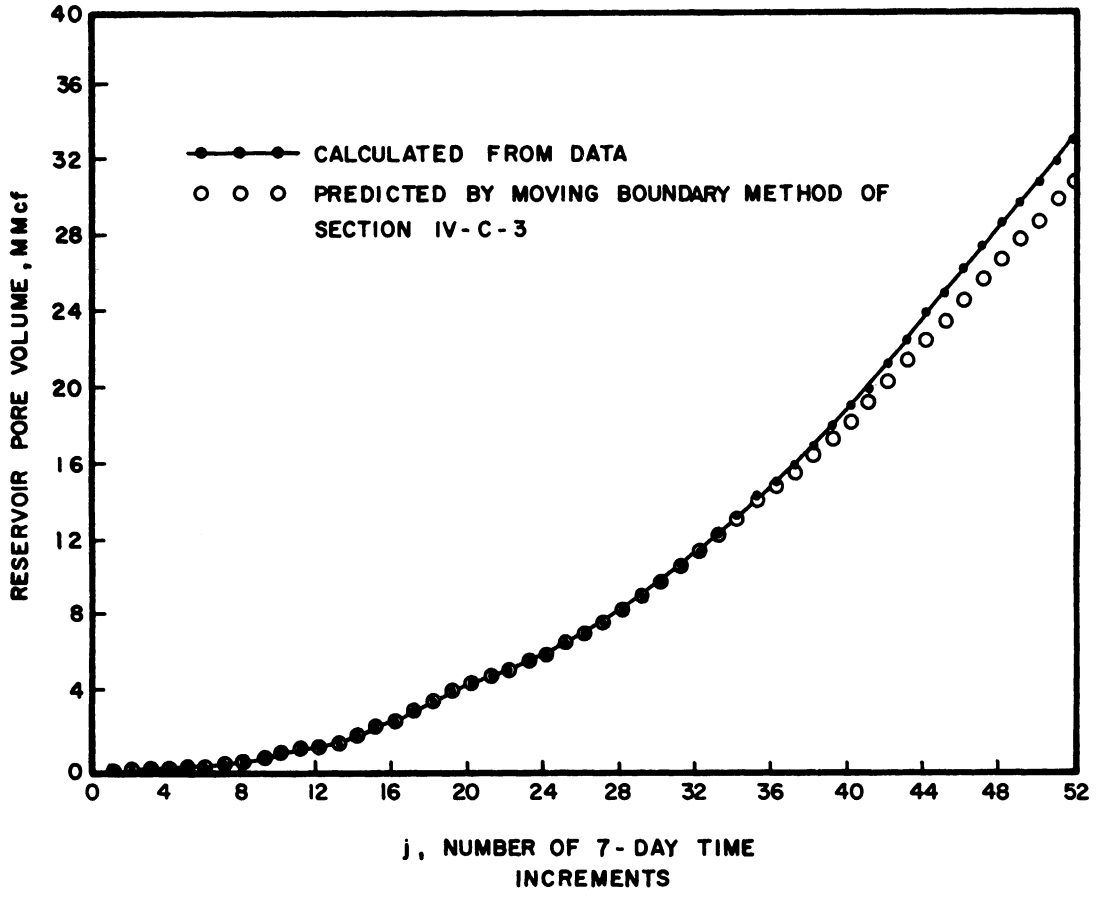

Comparison Between Field B Actual Pore Volumes and Pore Volumes Predicted by Moving Boundary Method of Section IV-C-3.

Figure 44

predicted pressures calculated with the assumption of a constant r_b, as described in Section IV-C-1. This figure reveals that the pressures calculated from Equation (IV-43) are, in general, in considerably better agreement with the observed pressures than are those calculated with the assumption of a constant r_b. As mentioned previously (Section IV-C-1), a DEV value of 3.27% was obtained for the latter calculated pressures. However, a DEV of 2.47% was calculated by inserting the pressures from Equation (IV-43) into Equation (III-25). Thus the moving boundary method described here resulted in a 24.4% (100 x (3.27 - 2.47)/ 3.27) decrease in the average difference between predicted and observed pressure.

The calculations described in Section IV-C-1 yielded the field B performance predicted with the assumption of a constant gas field radius. The results (Figure 36 or 43) show that the predicted pressures steadily increased after the 31st time increment (July 5, 1958) while the observed field pressures remained relatively constant. This systematic divergence between the predicted and observed field performances was discussed at the end of Section IV-C-1. Three possible causes of this divergence were cited: 1) a growing gas bubble radius, 2) gas leakage through the reservoir cap rock, 3) vertical pressure penetration into lower formations. The results obtained in this section (see Figure 43) reveal that the divergence between predicted and actual field performances was caused partly, but not wholly, by failure to take into account the growing gas bubble radius. After the 31st time increment, the pressures predicted here by the moving boundary method increase above

the observed pressures in much the same manner, but not to as great an extent, as the pressures predicted with the assumption of a constant r_b. The increase is too definite and systematic, however, to be considered as a random divergence about the observed performance. Thus one or both of the two other factors of gas leakage and vertical pressure penetration, which as pointed out previously would cause a systematic increase of the predicted above the observed pressures, must be held accountable for the divergence obtained. As mentioned in Section IV-C-1, data have been obtained which indicate pressure communication between the field B aquifer formation and lower formations. Since no physical evidence exists to support the possibility of gas leakage, the leveling out of the field B pressure after July 5 (31st time increment) is considered here to indicate the vertical displacement of water from the neighborhood of the gas bubble into lower formations.

V. CONCLUSIONS AND SUMMARY

(1) Solutions to the diffusivity equation, given in the literature[1], have been combined with the gas law and a material balance relation to give predictive equations which allow calculation of gas storage reservoir performance. The reservoir pressure can be calculated for any time-variant gas in place schedule or the gas in place can be calculated for any time-variant pressure schedule. Several assumptions concerning the geometry and physical characteristics of the reservoir-aquifer systems were necessary in the formulation of the predictive equations. The time necessary for manual execution of the calculations, which arise in application of these equations in an actual case study, is in general so large that use of a digital computer is almost mandatory. All of the calculations described in this thesis, involving use of these equations, were programmed in the IT compiler language and carried out by the IBM 650 digital computer or were programmed in the FORTRAN compiler code and carried out by the IBM 704 digital machine.

(2) The predictive equations have been employed in calculating the performance of several gas storage reservoirs. The agreement obtained between the actual and predicted performances is considered to be, with the exception of one case, more than adequate for engineering purposes; this fact indicates that the assumptions made in developing the predictive equations are in general valid for gas storage reservoirs.

(3) The utility of the developed equations and methods of calculation is evidenced by the better understanding of reservoir behavior obtained by their use. The pore volume variation of a gas storage reservoir was calculated for various different idealized pressure cycles. The

results show that a pressure cycle having an equal number of pound days above and below the initial pressure will result in a slowly growing or shrinking reservoir, according to whether the storage cycle is begun with gas production or gas injection. The results also revealed that identical gas field pressure cycles can result in greatly different yearly average reservoir volumes, depending upon whether storage operations are begun upon discovery or after a period of production and, if begun upon discovery, whether with gas injection or withdrawal.

(4) Consideration has been given to the problem of determining the effective reservoir parameter values. These parameters appear in the predictive equations as simple functions of reservoir physical constants such as porosity and permeability. Their 'effective' values are defined as those which result in best agreement between predicted and actual field performance over a time period for which field pressure-production data are available. A computational method of determining these effective parameters is described and applied to an actual aquifer storage reservoir. The values obtained are in excellent agreement with the values estimated from laboratory and geological data.

(5) The assumption of negligible vertical flow effects, made in this research, is in general valid for oil and gas reservoirs. Exceptions to this assumption have been considered in the development of an analytical solution to the diffusivity equation for the case of a storage reservoir situated on top of a very thick aquifer formation. Dimensionless flow or pressure drop quantities, similar to those presented by Van Everdingen and Hurst for the case of negligible vertical flow effects, can be obtained by numerical evaluation of the integral form of this analytical solution.

(6) A numerical method of solving the diffusivity equation in elliptic coordinates has been developed and employed to calculate the performance of a storage reservoir having an elliptic areal boundary. The results indicate that significant error in the calculated reservoir performance can be incurred at small and intermediate dimensionless time values ($t_D < 200$) by approximating the elliptic boundary as an equal area circle and employing the radial flow equations. The error decreases with increasing time. This result is of importance because water influx calculations reported in the literature, as well as those described in this thesis, invariably approximate the reservoir boundary by a circle. In most cases, however, the boundary can be more accurately approximated by an ellipse.

(7) A method of treating pressure interference between two or more reservoirs situated on a common aquifer is described and applied in an actual case study. The actual performances of the two reservoirs involved are duplicated closely by the performances predicted by the interference method. The interference method has been found to be considerably more accurate than the predictive method (ignoring interference effects) developed earlier in the thesis.

(8) Two methods have been given here for predicting reservoir behavior when the initial aquifer pressure in a non-uniform function of the radius. The first method requires quantitative knowledge of the initial pressure distribution and of the position of the aquifer exterior boundary. This method has been applied to a reservoir-aquifer system in which the initial pressure distribution was a known function of radius.

The agreement obtained between the actual and calculated field performances is significantly better than that achieved by ignoring the initial pressure distribution.

The second method requires knowledge of neither the initial pressure distribution nor of the position of the aquifer exterior boundary. The method does, however, require field pressure-production data over some time period. The second method again results in better agreement between the actual and predicted performances than that obtained by ignoring the initial pressure distribution. The first method is considered impractical since the initial pressure distribution and exterior radius are seldom known in actual case studies.

(9) The moving boundary problem encountered in aquifer storage operations has been described and treated. An aquifer storage reservoir is created by injecting gas into a water-bearing formation originally containing no gas. Thus its bubble radius increases from zero to values of several thousand feet as the reservoir is grown. When this increasing radius is assumed constant, the method of determining the effective reservoir parameter values is shown to yield no unique combination of values corresponding to best agreement between calculated and actual performance. However, when the moving boundary method developed is employed, a unique combination is obtained which yields aquifer permeability and thickness values in excellent agreement with those estimated from laboratory and geological data.

In summary, analytical methods have been developed for the treatment of the general problem of predicting gas storage reservoir performance. The investigation indicated that several special cases had

to be considered separately. The predictive accuracy of the developed theory has been critically examined through application in actual field studies. The results indicate that both the accuracy and applicability are more than adequate for present engineering needs. Through the theory and the applications, a substantially better understanding of gas storage reservoir performance has been obtained.

The ultimate goal of ability to predict the performance of any storage reservoir, on the other hand, has not been accomplished. Theory must be developed for several additional problems and must be evaluated by application in actual case studies. The following items are recommended for future study:

(a) An analytical solution to the diffusivity equation for the case of the vertical flow model has been developed and presented in the form of an infinite integral. This integral should be numerically evaluated and the results should be applied, as described in the thesis, in calculating the performance of an actual gas storage reservoir situated on top of a very thick aquifer. This predicted performance should then be compared with the actual field performance and with that predicted by the method (given in this thesis) developed from the assumption of negligible vertical flow effects. These comparisons should allow evaluation of the usefulness of the solutions obtained for the vertical flow model case.

(b) The diffusivity equation in elliptic coordinates should be solved analytically for the case of an infinite aquifer.

Dimensionless production and/or pressure-drop quantities should be numerically determined from the analytical solution and tabulated as a function of dimensionless time. The procedure detailed in the thesis should then be employed to compare the performance of an elliptically shaped reservoir with the performance calculated by approximating the field boundary as an equivalent circle and employing the radial flow equations. If the performances are significantly different then the dimensionless production and/or pressure-drop quantities for the elliptic flow case should be calculated and tabulated for ellipses of several eccentricities in the range 0-1.

(c) The effect of relative saturation on aquifer formation permeability and thus on the performance of the gas reservoir should be investigated. During the initial growth stage of an aquifer storage reservoir, the water is pushed outward into a formation essentially 100% saturated with water. Thus the permeability to water flow during this stage should be that corresponding to 100% saturation. During the first gas production cycle, however, the water moves back into a formation having a significant gas saturation. This partial water saturation will result in a permeability to water flow lower than that corresponding to 100% water saturation. This variation of permeability with time could be treated in much the same manner as the

time-variation of the gas bubble radius was treated in the moving boundary analysis, described in the thesis. Comparison of the observed performance of an actual gas reservoir with the performances predicted by ignoring and including relative saturation effects might allow conclusions concerning the importance of these effects in aquifer water flow.

APPENDIX I

IBM 650 IT COMPILER PROGRAM

The IBM 650 IT compiler program herein described effects the solution of Equation (III-21), below, as shown in the following block diagram.

$$P_j = \frac{k_4 + \sqrt{k_4^2 + k_5}}{2} \qquad \text{(III-21)}$$

The output or results from the program consist of the predicted reservoir (bottom-hole, psia) pressure and the predicted gas bubble pore volume at time $t = \Delta t, 2\Delta t, 3\Delta t, \ldots, N\Delta t$, where N is the total number of time increments specified. The only required input to the program is the gas storage reservoir production-injection schedule, certain physical constants representing the aquifer fluid and formation properties, and dimensionless production quantites, $\overline{Q}_{t_D}$, available from Van Everdingen and Hurst's 1949 paper[1] or Chatas' 1953 paper[2]. The latter reference is recommended in preference to the former since it contains more values of $\overline{Q}_{t_D}$. Values of $\overline{Q}_{t_D}$ are tabulated vs t_D for finite aquifers of various r_e/r_b ratios (where r_e is the radius of the aquifer exterior boundary and r_b is the gas field radius) as well as for 'infinite' aquifers.

A. Program Listing and Information Necessary for Compiling

Program Language: Perlis IT compiler for IBM 650 (1-pass, Michigan - October, 1958)

Packages and Suboutines Required: Compiler Package #1, square root subroutine

BLOCK DIAGRAM

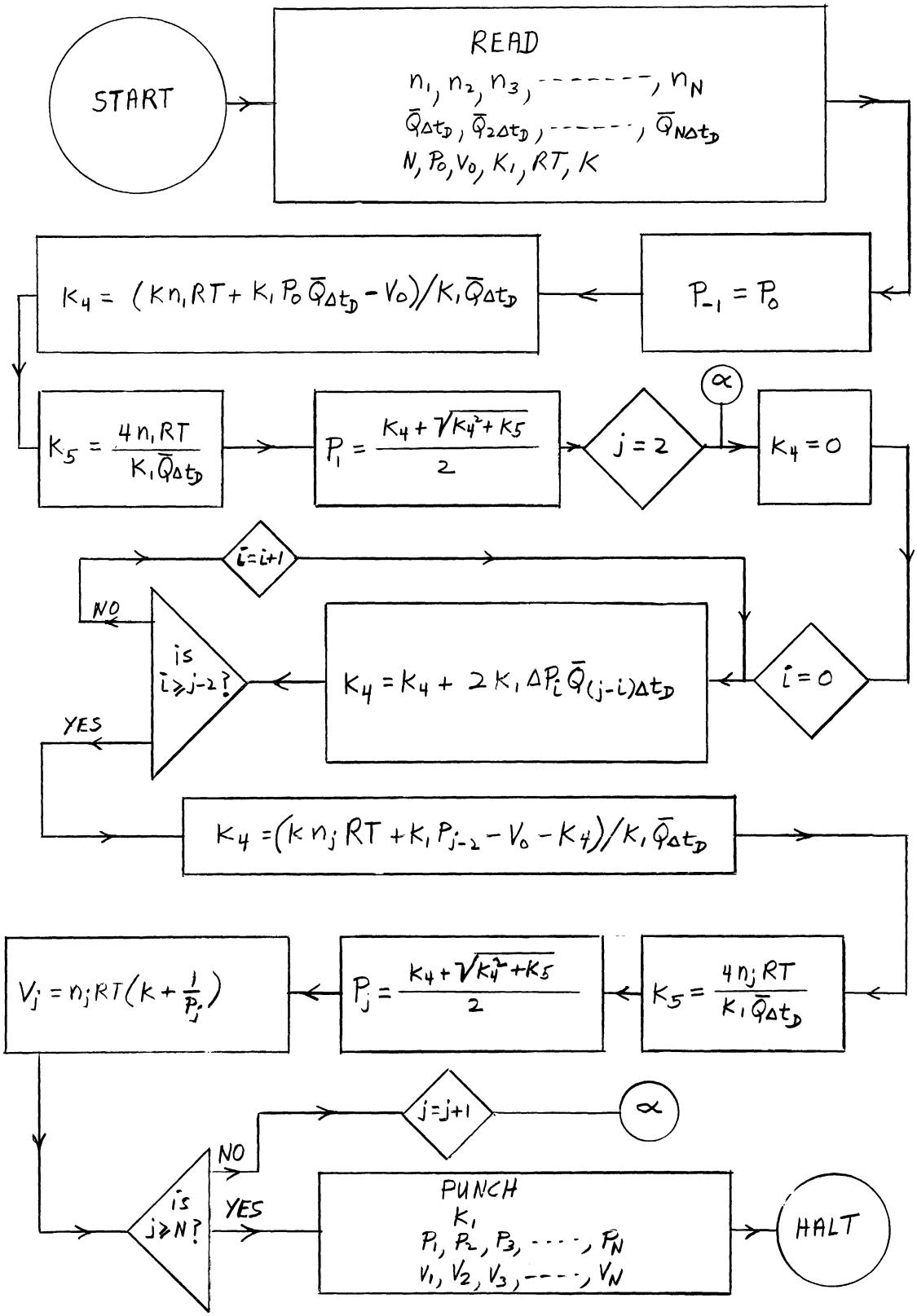

Header Card Data: n_I = 11, reservation for compiler 'I' variables

n_Y = 700, reservation for compiler 'Y' variables

n_C = 365, reservation for compiler 'C' variables

n_S = 5, number of numbered program statements

n_A = 50, greater than number of absolute constants assigned by program

n_E = 350, reservation of machine locations for package and square root extension.

Program Statements:

```
0:  READ       F

0:  C357 Z 6J2832 x C351 x C351 x C352 x C353 x C354  F

0:  C358 Z J5 x C357  F

0:  C359 Z LL C356 x C1 x C355 RS C358 x Y350 x Y1 RD C358
    x Y1  F

0:  C360 Z 8J x C1 x C355 D C357 x Y1  F

0:  Y351 Z J5 x C359 SQ20EKL C360 S C359 x C359 RQ  F

0:  3KI1K2K1KI10K  F

1:  C359 Z 0J  F

0:  2KI2K0K1KI1M2K  F

2:  C359 Z C359S C358 x YLI1MI2R x YL351SI2RMYL349SI2R  F

0:  C359 Z LLC356 x CI1 x C355RMC361MC359SC358 x YL348SI1R
    x Y1RDC358 x Y1  F

0:  C360 Z L8J x CI1 x C355DC357 x Y1RSC359 x C359  F

3:  YL350SI1R Z J5 x C359SQ20EKC360Q  F

0:  5KI1K1K1KI10K  F

4:  YI1 Z CI1 x C355 x C356S1JDYL350SI1R  F

5:  TYL350SI1R TYI1 TC351 TC353 TC354  F

0:  H    FF
```

B. Required Input or Data for Program

Compiler Variable Name	Physical Quantity
C361	V_o, initial pore volume of gas bubble, $ft.^3$.
I10	N, an even integer, ≤ 348; the number of time increments desired. If calculations are to be performed for a period of 5 years and a time increment of one month is specified, then $N = \frac{5(12)}{1} = 60$.
C1, C2, ..., CN	$n_1, n_2, \ldots, n_N$, the number of pound moles of gas in place in the bubble at time $t = \Delta t, 2\Delta t, \ldots, N\Delta t$.
Y350, Y349	P_o, initial gas bubble and aquifer pressure, psia
Y1, Y2, ..., YN	$\bar{Q}_{\Delta t_D}, Q_{2\Delta t_D}, \ldots, Q_{N\Delta t_D}$ dimensionless production quantities corresponding to dimensionless time, $t_D = \frac{k\Delta t}{\mu\varphi c r_b^2}, \frac{2k\Delta t}{\mu\varphi c r_b^2}, \ldots, \frac{kN\Delta t}{\mu\varphi c r_b^2}$
C356	K, constant in equation $z = 1+KP$, to be determined from compressibility data for gas in question
C355	RT; R, gas constant, = 10.73 psia - $ft^3/°R$ - # mole, T = average gas bubble temperature, °R
C354	c, sum of aquifer fluid and aquifer rock compressibilities, 1/psia
C353	h, thickness of aquifer formation, ft.
C352	φ, porosity of aquifer and gas sand
C351	r_b, radius of gas bubble, = interior radius of aquifer, ft.

C. Output or Results from Program

Compiler Variable Name	Physical Quantity
Y351, Y352, ..., Y(350 + N)	Gas reservoir (bottom-hole) pressure, psia, at times t = Δt, $2\Delta t$, ..., $N\Delta t$.
Y1, Y2, ..., YN	Gas bubble pore volume, $ft.^3$, at times t = Δt, $2\Delta t$, $3\Delta t$, ..., $N\Delta t$.
C351, C353, C354	r_b, h, and c as fed in as data

APPENDIX II

SOLUTION OF DIFFUSIVITY EQUATION GOVERNING PRESSURE DISTRIBUTION IN VERTICAL PRESSURE PENETRATION FLOW MODEL

The diffusivity equation and the corresponding boundary conditions governing the aquifer water flow in the vertical pressure penetration model appear as in Equations (1), (2), (3), and (4) below.

$$\frac{\partial^2 \bar{P}}{\partial r_D^2} + \frac{1}{r_D}\frac{\partial \bar{P}}{\partial r_D} + \frac{\partial^2 \bar{P}}{\partial y^2} = \frac{\partial \bar{P}}{\partial t_D} \tag{1}$$

$$\left(\frac{\partial \bar{P}}{\partial y}\right)_{y=M} = 0 \tag{2}$$

$$\left(\frac{\partial \bar{P}}{\partial y}\right)_{y=0} = f(r_D)\begin{cases} 0 & 1 < r_D < \infty \\ -1 & 0 \le r_D \le 1 \end{cases} \tag{3}$$

$$\bar{P}(r_D, y, 0) = 0 \tag{4}$$

where $M = h/r_b\sqrt{k_R}$

The condition given in Equation (3) specifies an infinite aquifer; replacement of Equation (3) by a condition simulating a finite aquifer actually simplifies somewhat the process of solution of Equation (1). Taking the Hankel transform with respect to r_D of both sides of Equation (1), one obtains an equation in y, t_D, and parameter of the Hankel transform, η:

$$\frac{\partial^2 \gamma(\eta, y, t_D)}{\partial y^2} - \eta^2 \gamma(\eta, y, t_D) = \frac{\partial \gamma(\eta, y, t_D)}{\partial t_D} \tag{5}$$

where $\gamma(\eta,y,t_D) = \int_0^\infty r_D \bar{P}(r_D,y,t_D)\, J_o(\eta r_D)dr_D$ = Hankel transform of $\bar{P}(r_D,y,t_D)$ and the Hankel transform of $\left(\frac{\partial^2 \bar{P}}{\partial r_D^2} + \frac{1}{r_D}\frac{\partial \bar{P}}{\partial r_D}\right)$

$$= \int_o^\infty r_D\left(\frac{\partial^2 \bar{P}}{\partial r_D^2} + \frac{1}{r_D}\frac{\partial \bar{P}}{\partial r_D}\right) J_o(r_D \eta)\, dr_D = -\eta^2 \gamma(\eta, y, t_D).$$

Equation (5) can be solved by the method of separation of variables; γ is assumed equal to $Y\theta$ where Y is a function of y only and θ is a function of t_D only. Equation (5) then becomes

$$\frac{Y''}{Y} - \eta^2 = \frac{\theta'}{\theta} = -\lambda^2 \tag{6}$$

where λ^2 is a constant since the left side is a function of y only and the right side is a function of t_D only.

For $\lambda = 0$,

$Y_{(y)} = A \cosh \eta y + B \sinh \eta y$; $\Theta = 1$, or only other real constant

and for $\lambda \neq 0$,

$$Y_{(y)} = C \cos \sqrt{\lambda^2-\eta^2}\, y + D \sin \sqrt{\lambda^2-\eta^2}\, y \quad ; \quad \Theta = e^{-\lambda^2 t_D} \quad ,$$

where A, B, C, and D are constants to be determined from the initial and boundary conditions. Setting $\gamma = Y\Theta = A \cosh \eta y + B \sinh \eta y + [\cos \sqrt{\lambda^2-\eta^2}\, y + D \sin \sqrt{\lambda^2-\eta^2}\, y]\, e^{-\lambda^2 t_D}$, one finds that

$$\left(\frac{\partial \gamma}{\partial y}\right)_{y=0} = B\eta + D\sqrt{\lambda^2-\eta^2}\, e^{-\lambda^2 t_D}$$

But $(\partial\gamma/\partial y)_{y=0} = \bar{f}(\eta)$, where $\bar{f}(\eta)$ is the Hankel transform of $f(r_D)$, from Equation (3); therefore

$$B\eta + D\sqrt{\lambda^2-\eta^2}\, e^{-\lambda^2 t_D} = \bar{f}(\eta) = \int_0^\infty x f(x) J_0(\eta x)\, dx = -\int_0^1 x J_0(\eta x)\, dx = -\frac{J_1(\eta)}{\eta} \quad (7)$$

The equalities $D = 0$

$$B = -J_1(\eta)/\eta^2$$

must hold if Equation (7) is to be satisfied for all t_D and η. Inserting these values of D and B into the expression for γ, one obtains

$$\gamma(\eta, y, t_D) = A\cosh(\eta y) - \frac{J_1(\eta)}{\eta^2}\sinh(\eta y) + C\cos\sqrt{\lambda^2-\eta^2}\, y\, e^{-\lambda^2 t_D} \quad (8)$$

Now, since $(\partial\gamma/\partial y)_{y=M} = 0$, where

$$M = h/r_b \sqrt{k_R} \quad \text{by definition,}$$

one finds

$$\left(\frac{\partial \gamma}{\partial y}\right)_{y=M} = A\eta \sinh M\eta - \frac{J_1(\eta)}{\eta}\cosh M\eta - C\sqrt{\lambda^2-\eta^2}\sin(\sqrt{\lambda^2-\eta^2}\, M)e^{-\lambda^2 t_D} = 0 \quad (9)$$

and $\sin\sqrt{\lambda^2-\eta^2}\,M$ must = 0, or

$$\sqrt{\lambda^2-\eta^2} = m\pi/M = \alpha_m, \text{ by definition,}$$

$$\text{and } \lambda^2 = \eta^2 + \alpha_m^2$$

Also, from Equation (9),

$$A = \frac{J_1(\eta)}{\eta^2}\coth(M\eta)$$

Inserting the values of $\sqrt{\lambda^2-\eta^2}$ and A into Equation (8), one obtains

$$\gamma(\eta,y,t_D) = \frac{J_1(\eta)}{\eta^2}\left[\coth(M\eta)\cosh(\eta y) - \sinh(\eta y)\right] + C\cos(\alpha_m y)e^{-\lambda^2 t_D}$$
$$= \frac{J_1(\eta)}{\eta^2}\left[\frac{\cosh(\eta(M-y))}{\sinh(M\eta)}\right] + C\cos(\alpha_m y)e^{-\lambda^2 t_D} \qquad (10)$$

A sum of terms of the form $C_m \cos\alpha_m y e^{-\lambda_m^2 t_D}$ will be required in order to satisfy the initial condition, Equation (4). Thus

$$\gamma(\eta,y,0) = 0 = \frac{J_1(\eta)}{\eta^2}\left(\frac{\cosh\eta(M-y)}{\sinh(M\eta)}\right) + \sum_{m=0}^{\infty} C_m\cos\alpha_m y$$

or

$$\sum_{m=0}^{\infty} C_m\cos\alpha_m y = -\frac{J_1(\eta)}{\eta^2}\,\frac{\cosh\eta(M-y)}{\sinh M\eta}$$

The terms $\cos\alpha_m y$ are orthogonal over the interval (0,M), where $\alpha_m = m\pi/M$, and by multiplying both sides of Equation (11) by $\cos\alpha_m y$ and integrating over y from 0 to M, one finds

$$C_m\int_0^M \cos^2(\alpha_m y)\,dy = -\frac{J_1(\eta)}{\eta^2}\int_0^M \cosh\eta(M-y)\cos(\alpha_m y)\,dy$$

or, performing the indicated integrations,

$$C_m = \frac{-2J_1(\eta)}{(\alpha_m^2+\eta^2)M\eta} \qquad (11)$$

and

$$C_0 = -\frac{J_1(\eta)}{\eta^3 M} \qquad (12)$$

Thus the expression for $\gamma(\eta,0,t_D)$ now becomes

$$\gamma(\eta,0,t_D) = \frac{J_1(\eta)}{\eta^2}\coth(M\eta) - \frac{J_1(\eta)}{\eta^3 M}e^{-\eta^2 t_D} - \frac{2J_1(\eta)}{M\eta}\sum_{m=1}^{\infty}\frac{e^{-(\eta^2+\alpha_m^2)t_D}}{\alpha_m^2+\eta^2} \qquad (13)$$

and since the inverse Hankel transform of $\bar{g}(\eta)$ (where $\bar{g}(\eta)$ is the Hankel

transform of $g(r_D)$ is $\int_0^\infty \eta\, \bar{g}(\eta)\, J_{o(r_D\eta)}\, d\eta$, the solution for $\bar{P}_{(r_D,0,t_D)}$ is

$$\bar{P}(r_D,0,t_D) = \int_0^\infty \frac{J_1(\eta)}{\eta}\left[\coth M\eta - e^{-\eta^2 t_D}\cdot\frac{1}{M\eta} - \frac{2\eta}{M}\cdot \sum_{m=1}^{\infty}\frac{e^{-(\eta^2+\alpha_m^2)t_D}}{\eta^2+\alpha_m^2}\right] J_0(r_D\eta)\, d\eta \qquad (14)$$

APPENDIX III

ROUND-OFF AND TRUNCATION ERRORS ARISING IN THE NUMERICAL SOLUTION OF THE DIFFUSIVITY EQUATION IN ELLIPTIC COORDINATES

An estimated limit on the round-off error is obtained here by determining the maximum round-off error in the asymptotic (or large time) $\overline{Q}_{t_{DE}}$ and assuming this maximum is not exceeded in any smaller $\overline{Q}_{t_{DE}}$ values. For example, if a maximum round-off error of 0.3% occurs in the value of $\overline{Q}_{t_{DE}}$ at the 600th time step, then this assumption would place an upper limit of 0.3% on the round-off error in $\overline{Q}_{t_{DE}}$ at any time step prior to the 600th. A maximum round-off error in the asymptotic or steady-state, machine-calculated $\overline{Q}_{t_{DE}}$ value is determined as follows.

The machine-calculated $\overline{Q}_{t_{DE}}$ (for $\Delta u = .08$, $\Delta v = .098175$, Δt_{DE} given on page 103) reaches an asymptotic value of 35.15587 as shown in Table VII. The actual or true asymptotic $\overline{Q}_{t_{DE}}$ can be readily calculated from a simple material balance and can be compared to the machine value of 35.15587. For at steady-state (large dimensionless time), the pressure drop attains a uniform value of 1 throughout the elliptic cylinder flow model. Thus, since the initial pressure drop was 0, the total volumetric expansion of the water in the flow model (at steady-state) must be equal to the total original volume of water multiplied by the compressibility and the pressure drop of 1. But this volume of expansion must be equal to the asymptotic or final value of Q_{tE}, the cumulative water influx into the elliptic sink, since the water can only expand into the inner sink (the exterior boundary impervious). Thus one has

$$1 \cdot c \cdot [h\phi(\pi a_e b_e - \pi a_i b_i)] = (Q_{tE})_{asymptotic} = 4h\phi c f^2 \cdot 1 \cdot (\overline{Q}_{t_{DE}})_{asymptotic}$$

or

$$(\overline{Q}_{t_{DE}})_{asymptotic} = \frac{(\pi a_e b_e - \pi a_i b_i)}{4f^2}$$

But $\pi a_e b_e$ is the area encompassed by the exterior elliptic boundary which is

101.3 times the area ($\pi a_i b_i$) within the inner elliptic boundary, which is, in turn,

$$\pi a_i b_i = \pi f^2 \cosh u_b \sinh u_b = \pi f^2 \cosh(.4) \sinh(.4) = .445\pi f^2$$

Therefore

$$(\bar{Q}_{t_{DE}})_{asymptotic} = \frac{100.3\,\pi\,(.445)}{4} = 35.151;$$

since the asymptotic machine solution for $\bar{Q}_{t_{DE}}$ is 35.15587, the difference between the two values due to truncation and round-off error is .0048.. Since the truncation error analysis developed below places a maximum error of .06 in $(\bar{Q}_{DE})_{asymptotic}$ (see Table IX) due to truncation error, an upper limit on the round-off error is (35.15587 + .06) - 35.151 or .065. This latter figure represents .185% of 35.15587 and an upper limit on the round-off error in $\bar{Q}_{t_{DE}}$ will be assumed to be .185 % for all t_{DE}.

The following truncation error analysis is based on a method described by Scarborough[22]. Inclusion in Equations (III-90) and (III-91) of the lowest order Taylor series derivatives ignored in obtaining the finite difference forms of the derivatives $\partial^2\bar{P}/\partial u$, $\partial\bar{P}/\partial v^2$, and $\partial\bar{P}/\partial t_{DE}$ would result in the following term added to the right side of the equations:

$$-\frac{(\Delta u)^2}{12}\frac{\partial^4\bar{P}}{\partial u^4} - R\frac{(\Delta v)^2}{12}\frac{\partial^4\bar{P}}{\partial v^4} + f_{m,n}\frac{\Delta t_{DE}}{2}\frac{\partial^2\bar{P}}{\partial t_{DE}^2}$$

The total truncation error in $\bar{P}_{m,n,i}$ is therefore the sum of the integrals of these terms; this sum can be written

$$A(\Delta u)^2 + B(\Delta v)^2 + C\Delta t_{DE},$$

where A, B, and C are numbers which may be dependent upon m, n, and i. Thus if the true solution is denoted by $\bar{P}^*_{m,n,i}$ and the machine solution by $\bar{P}_{m,n,i}$, then

$$\bar{P}^*_{m,n,i} - \bar{P}_{m,n,i} = A(\Delta u)^2 + B(\Delta v)^2 + C\Delta t_{DE} \qquad (1)$$

We now proceed to deduce the truncation error in $\bar{Q}_{t_{DE}}$ from this form of the truncation error in $\bar{P}_{m,n,i}$. If $\bar{q}^{**}$ denotes the value of $\int_0^{\frac{\pi}{2}} \left(\frac{\partial \bar{P}^*}{\partial u}\right)_{u=u_b} dv$ and $\bar{q}^{*}$ denotes the value of $\int_0^{\frac{\pi}{2}} \left(\frac{\partial \bar{P}}{\partial u}\right)_{u=u_b} dv$, then

$$\bar{q}^{**} - \bar{q}^{*} = \int_0^{\frac{\pi}{2}} \left[\frac{\partial \bar{P}}{\partial u} + (\Delta u)^2 \frac{\partial A}{\partial u} + (\Delta v)^2 \frac{\partial B}{\partial u} + \Delta t_{DE} \frac{\partial C}{\partial u} \right]_{u=u_b} dv - \int_0^{\frac{\pi}{2}} \left(\frac{\partial \bar{P}}{\partial u}\right)_{u_b} dv \tag{2}$$

$$= A^{(1)}(\Delta u)^2 + B^{(1)}(\Delta v)^2 + C^{(1)} \Delta t_{DE}$$

where

$$A^{(1)} = \int_0^{\frac{\pi}{2}} \left(\frac{\partial A}{\partial u}\right)_{u_b} dv$$

$$B^{(1)} = \int_0^{\frac{\pi}{2}} \left(\frac{\partial B}{\partial u}\right)_{u_b} dv$$

and

$$C^{(1)} = \int_0^{\frac{\pi}{2}} \left(\frac{\partial C}{\partial u}\right)_{u_b} dv$$

If $\bar{q}$ denotes the value of $\int_0^{\frac{\pi}{2}} \left(\frac{\partial \bar{P}}{\partial u}\right)_{u_b} dv$ as determined by the Simpson's integration (Equation III-112), then

$$\bar{q}^{*} - \bar{q} = D \Delta v \tag{3}$$

since the numerical integration introduces an error term proportional to Δv. Adding Equation (2) to Equation (3), one obtains

$$\bar{q}^{**} - \bar{q} = A^{(1)}(\Delta u)^2 + B^{(1)}(\Delta v)^2 + C^{(1)} \Delta t_{DE} + D \Delta v \tag{4}$$

which is the expression for the difference between the true and machine values of $\bar{q}$.

The same procedure employed in obtaining $\bar{q}^{**} - \bar{q}$ can be employed to obtain

$$\bar{Q}_{t_{DE}}^{**} - \bar{Q}_{t_{DE}} = A^{(2)}(\Delta u)^2 + (B^{(2)} \Delta v + D^{(1)}) \Delta v + (C^{(2)} + E) \Delta t_{DE} \tag{5}$$

where $\bar{Q}_{t_{DE}}^{**} = \int_0^{t_{DE}} \bar{q}^{**} \, dt_{DE}$

and $\bar{Q}_{t_{DE}}$ = the value of $\int_0^{t_{DE}} \bar{q} \, dt_{DE}$ as determined from Simpsons's integration (Equation III-114).

Rewriting Equation (5), and assuming the term $D^{(1)}\Delta v$ to dominate the term $B^{(2)}\Delta v^2$, one obtains

$$\bar{Q}^{**}_{t_{DE}} - \bar{Q}_{t_{DE}} = F(\Delta u)^2 + G(\Delta v) + H(\Delta t_{DE}) \qquad (6)$$

which is an expression for the difference between the true and machine solutions due to truncation error alone.

REFERENCES

1. Van Everdingen, A. F. and Hurst, W., "The Application of the Laplace Transformation to Flow Problems in Reservoirs", Journal of Petroleum Technology, Dec., 1949.

2. Chatas, A. T., "A Practical Treatment of Nonsteady-State Flow Problems in Reservoir Systems", The Petroleum Engineer, May, 1953.

3. Katz, D. L., Tek, M. R. and Coats, K. H., "The Effect of Unsteady State Aquifer Motion on the Size of an Adjacent Gas Storage Reservoir", Paper #1114G presented at 33rd Annual Fall Meeting of AIME, October, 1958.

4. Katz, D. L., Vary, J. A. and Elenbaas, J. R., "Design of Gas Storage Fields", Paper #1059G presented at 33rd Annual AIME Fall Meeting, October, 1958.

5. Schilthuis, R. J. and Hurst, W., "Variations in Reservoir Pressure in the East Texas Field", Petroleum Trans. A.I.M.E. Vol. 114, p 164, (1935).

6. Mortada, M., "A Practical Method for Treating Oilfield Interference in Water-Drive Reservoirs", AIME Petroleum Transactions, Vol. 204, 1955.

7. Warren, J. E., "The Unsteady-State Behavior of Linear Gas-Storage Reservoirs", The Petroleum Engineer, November, 1956.

8. Muskat, M., The Flow of Homogeneous Fluids Through Porous Media, J. W. Edwards, Inc., 1946.

9. Carslaw, H. S. and Jaeger, J. C., Conduction of Heat in Solids, Oxford at the Clarendon Press, 1947.

10. Churchill, R. V., Modern Operational Mathematics in Engineering, McGraw-Hill, 1944.

11. Woods, R. W. and Muskat, M., "An Analysis of Material Balance Calculations" Petroleum Trans. Vol. 160, 1945.

12. Sneddon, I. N., Fourier Transforms, McGraw-Hill, 1951.

13. Douglas, J., Garder, A. O. and Peaceman, D. W., "Numerical Solution of a Two-Dimensional Moving Boundary Problem", presented at the June 19-21 Houston Meeting of the Association for Computing Machinery.

14. Whittaker, E. T. and Watson, G. N., A Course of Modern Analysis, Cambridge University Press, 1952.

15. Morse, P. M. and Feshbach, H., Methods of Theoretical Physics, McGraw-Hill, 1953.

16. Margenau, H. and Murphy, G. M., The Mathematics of Physics and Chemistry, Van Nostrand, 1956.

17. Douglas, J. and Peaceman, D. W., "Numerical Solution of Two-dimensional Heat-flow Problems", AIChE Journal, December, 1955.

18. Bruce, G. H., Peaceman, D. W., Rachford, H. H. and Rice, J. D., "Calculations of Unsteady-State Gas Flow Through Porous Media", Petroleum Transactions, AIME, Vol. 198, 1953.

19. Mickley, H. S., Sherwood, T. K. and Reed, C. E., Applied Mathematics in Chemical Engineering, McGraw-Hill, 1957.

20. Peaceman, D. W. and Rachford, H. H., J. Ind. Appl. Math., 3, 28, (1955).

21. Richtmyer, R. D., Difference Methods for Initial-Value Problems, Interscience Publishers, 1957.

22. Scarborough, J. B., Numerical Mathematical Analysis, The Johns Hopkins Press, 1950.

23. Hall, H. N., "Compressibility of Reservoir Rocks", Journal of Petroleum Technology, January, 1953.

UNIVERSITY OF MICHIGAN
3 9015 02827 3970